

DEVELOPMENT OF A CONSTRAINED LAYER SURFACE DAMPING  
TREATMENT WITH OPTIMIZED SPACER GEOMETRY FOR PLATES

A THESIS SUBMITTED TO  
THE GRADUATE SCHOOL OF NATURAL AND APPLIED SCIENCES  
OF  
MIDDLE EAST TECHNICAL UNIVERSITY

BY

BARKAN ULUBALCI

IN PARTIAL FULFILLMENT OF THE REQUIREMENTS  
FOR  
THE DEGREE OF MASTER OF SCIENCE  
IN  
MECHANICAL ENGINEERING

DECEMBER 2019



Approval of the thesis:

**DEVELOPMENT OF A CONSTRAINED LAYER SURFACE DAMPING  
TREATMENT WITH OPTIMIZED SPACER GEOMETRY FOR PLATES**

submitted by **BARKAN ULUBALCI** in partial fulfillment of the requirements for the degree of **Master of Science in Mechanical Engineering Department, Middle East Technical University** by,

Prof. Dr. Halil Kalıpçılar  
Dean, Graduate School of **Natural and Applied Sciences**

\_\_\_\_\_

Prof. Dr. M. A. Sahir Arıkan  
Head of Department, **Mechanical Engineering**

\_\_\_\_\_

Assist. Prof. Dr. Gökhan Osman Özgen  
Supervisor, **Mechanical Engineering, METU**

\_\_\_\_\_

**Examining Committee Members:**

Prof. Dr. F. Suat Kadiođlu  
Mechanical Engineering Dept., METU

\_\_\_\_\_

Assist. Prof. Dr. Gökhan Osman Özgen  
Mechanical Engineering, METU

\_\_\_\_\_

Prof. Dr. Serkan Dađ  
Mechanical Engineering Dept., METU

\_\_\_\_\_

Assoc. Prof. Dr. Demirkan Çöker  
Aerospace Engineering Dept., METU

\_\_\_\_\_

Assist. Prof. Dr. Selçuk Himmetođlu  
Mechanical Engineering Dept., Hacettepe University

\_\_\_\_\_

Date: 06.12.2019

**I hereby declare that all information in this document has been obtained and presented in accordance with academic rules and ethical conduct. I also declare that, as required by these rules and conduct, I have fully cited and referenced all material and results that are not original to this work.**

Name, Surname: Barkan Ulubalcı

Signature:

## **ABSTRACT**

### **DEVELOPMENT OF A CONSTRAINED LAYER SURFACE DAMPING TREATMENT WITH OPTIMIZED SPACER GEOMETRY FOR PLATES**

Ulubalcı, Barkan  
Master of Science, Mechanical Engineering  
Supervisor: Assist. Prof. Dr. Gökhan Osman Özgen

December 2019, 169 pages

For aviation applications, the noise and vibration cancellation is so important that there are many damping methods and applications used in the field. In military configurations the weight and the visual elegance is not so important that even a blanket may solve the problem. In civil configurations, on the other hand, there should be a lightweight solution for vibration damping. For this reason, since shell structures are widely used on aerospace applications, it is common to use surface damping solutions on aircrafts. Because, surface damping treatments are generally used on shell structures, such as plates and beams, where transverse vibrations problems are critical and resonant frequency vibrations are dominant in a wide broadband due to low thickness. In this thesis study, different novel designs for surface damping treatments are studied and compared by means of their effectiveness. A fuselage like structure is designed and validated by finite element modelling and by experimental results in order to estimate the damping solution effect on application point. Furthermore, due to broadband random vibrations induced on fuselage geometry, a metric is suggested considering the loading condition in order to estimate damping effectiveness. In literature it is seen that in order to increase damping performance, a layer with reduced density and elastic modulus, a spacer layer, is added to the surface damping treatments. By this spacer layer addition, the viscoelastic layer can be shifted away

from neutral axis which increases the induced shear strain hence damping performance. Due to high performance low additional weight, standoff damping treatment, a slotted and a sophisticated version of space layered surface damping treatments, is generally used in aerospace structures. With the help of literature and previously optimized spacer geometries for beams, six novel designs are suggested through finite element models and their damping effectiveness are compared with commonly used configurations and adapted versions.

Keywords: Constrained layer damping, stand-off layer damping, plate vibrations, viscoelasticity, finite element method, free-layer damping, acoustic vibrations, damping

## ÖZ

### **OPTİMİZE EDİLMİŞ ARA LEVHA GEOMETRİSİ KULLANARAK UÇAK GÖVDESİ TARZI PLAKALAR İÇİN KONTROLLÜ YÜZEY TİTREŞİM SÖNÜMLEYİCİ GELİŞTİRME**

Ulubalcı, Barkan  
Yüksek Lisans, Makina Mühendisliği  
Tez Danışmanı: Dr. Öğr. Üyesi Gökhan Osman Özgen

Aralık 2019, 169 sayfa

Havacılık sektöründe gürültü ve titreşim sönümlenme çok önemlidir ve sönümlenmeyi sağlamak için bir çok metot kullanılmaktadır. Askeri konfigürasyonlarda ağırlık ve görsellik çok önemli olmadığı için bu sönümlenme bir battaniye ile de yapılabilir. Sivil konfigürasyonlar da ise bu çözümlerin hafif olması çok önemlidir. Bu sebeple kabuksu yapılar havacılık sanayide çok tercih edildiğinden, yüzey sönümlenme teknikleri bu sektörde sıklıkla kullanılmaktadır. Yüzey titreşim sönümlenme teknikleri genellikle ince kalınlık kaynaklı geniş frekans aralığındaki enine titreşim sonucu titreşim problemlerinin kabuksu yapılarda, çubuk ve plaka, giderilmesi için kullanılan çözüm uygulamalarıdır. Bu çalışmada, rezonans kaynaklı titreşim problemlerinin giderilmesinde kullanılan farklı yüzey titreşimleri sönümlenme tekniklerin özgün tasarımları üzerine çalışılmış ve performans etkileri sunulmuştur. Bu sebeple, bu çalışmada sönümlenme etkisinin gerçek kullanım alanındaki etkisini sunabilmek adına gövde kabuğu tipinde bir temsili yapı tasarlanıp sonlu eleman modeli ve testler ile doğrulanmıştır. Ek olarak, gövde tipi yapılara etki eden rasgele titreşimlerden dolayı titreşim sönümlenmeyi ölçmek adına yükleme koşullarını göz eden bir metrik öne sunulmuştur. Literatürde görüldüğü üzere, yüzey sönümlenme teknikleri arasına ara katman, daha az yoğunlukta ve daha elastik, eklenerek viskoelastik katman doğal

eksenden daha çok uzaklaştırılarak sönümlenme katmanı içerisinde oluşan yırtılma stresinde artış sağlanabilmektedir. Bu artış doğal olarak malzeme içerisinde gerçekleşen sönümlenme performansının artışına sebep olmaktadır. Bu uygulamanın daha gelişmiş bir versiyonu olan gözenekli ara katman yapıları havacılık sektöründe performans ağırlık oranının yüksek olması sebebiyle tercih edilmektedir. Literatür sonuçları ve daha önceden çubuksu yapılar için optimize edilmiş ara katman tasarımları incelenerek bunların plaka yapılarına adaptasyonu yapılmış altı özgün tasarımın sonlu elemanlar modeli kullanılarak modellenmesi ve sönümlenme performanslarının hâlihazırda kullanılan versiyonlarla kıyaslaması yapılmıştır.

Anahtar Kelimeler: Kontrollü yüzey sönümlenme, ara katmanlı sönümlenme, plaka titreşimi, viskoelastisite, sonlu elemanlar metodu, serbest yüzey sönümlenme, akustik titreşim, sönümlenme

To my family present and future ...

## ACKNOWLEDGEMENTS

I would like to thank my supervisor, Asst. Prof. Dr. Gökhan O. Özgen for his supervision, help and guidance from the beginning to end of this dissertation.

Special thanks to my close friend, Gülce Öztürk for her endless support and motivation throughout this study. I would not have been able to complete without her endless support and patience throughout this dissertation.

I want to thank my friends, Hasan Can Özden and Bahar Özden for their support and encouragement throughout this study.

I also would like to express my thanks to my coworkers, Burak Rodoplu, Onur Özaydın and Veysel Yalın Öztürk and my manager Şiar Deniz Yavuz for their support and encouragement throughout this study.

I also would like to thank my supervisor, Asst. Prof. Dr. Gökhan O. Özgen and METU Mechanical Engineering Department technical staff Ufuk Cengizel for their help throughout the manufacturing of the prototypes and experimental studies carried out in this study.

Finally, I would like to thank my family, Asuman Ulubalcı, Eyüp Celalettin Ulubalcı for being always there for me. They always support, encourage and motivate me no matter what and helped me to achieve the completion of this thesis study.

## TABLE OF CONTENTS

ABSTRACT .....	v
ÖZ .....	vii
ACKNOWLEDGEMENTS .....	x
TABLE OF CONTENTS .....	xi
LIST OF TABLES .....	xiv
LIST OF FIGURES .....	xvi
LIST OF ABBREVIATIONS .....	xxiii
LIST OF SYMBOLS .....	xxv
CHAPTERS	
1. INTRODUCTION .....	1
1.1. Introduction .....	1
1.2. Background and Motivation .....	3
1.3. Objective of the Thesis .....	4
1.4. Scope of the Thesis .....	4
1.5. Outline of the Thesis .....	5
2. LITERATURE SURVEY .....	7
2.1. Viscoelastic Materials .....	7
2.1.1. Viscoelastic Material Models .....	11
2.1.1.1. Fractional Derivative Model .....	13
2.2. Surface Damping Treatment Methods .....	15
2.2.1. Free Layer Damping Treatment .....	15
2.2.2. Constrained Layer Damping Treatment .....	16

2.2.3. Constrained Layer Damping Treatment with Spacer Layer.....	16
2.2.4. Standoff Layer Damping Treatment (Slotted Spacer Design) .....	17
2.3. Literature Survey.....	18
3. DESIGN AND DEVELOPMENT OF REPRESENTATIVE FUSELAGE GEOMETRY .....	25
3.1. Theoretical Background of Riveted Joints.....	26
3.1.1. Lap Joints .....	26
3.1.2. Butt Joints.....	27
3.1.3. Riveted Connection Modelling Types.....	27
3.2. Generating the Fuselage FE Model.....	30
3.2.1. Defining Materials.....	31
3.2.2. Meshing Parts .....	35
3.2.3. Defining Riveted Joints .....	39
3.3. Validation of Fuselage Geometry .....	43
3.3.1. Finite Element Results.....	44
3.3.2. Experimental Results.....	48
3.4. Generating the Surface Damping Treated Fuselage FEM .....	54
3.4.1. Defining Viscoelastic Material Properties .....	54
4. VALIDATION AND INTEGRATION OF VISCOELASTIC MATERIAL ....	59
4.1. Validation and Integration of Viscoelastic Material.....	59
4.1.1. Defining and Assigning VEM Properties.....	59
4.1.2. Verification of Reference Constrained Layer Beam .....	59
5. DEVELOPMENT AND VERIFICATION OF DAMPING TREATMENT ....	81
5.1. Metrics for Quantifying the Damping Performance of the Treatment.....	81

5.2. Baseline Geometry Selection .....	86
5.3. Optimized Spacer Geometry Modeling.....	107
5.3.1. Optimized Spacer Geometry Using Literature Knowledge .....	107
5.3.2. Optimized Spacer Geometry Using Novel Designs for Beams .....	120
5.3.2.1. Enhanced Genetic Algorithm Solution Targeting Low Frequency Modes Results of Eyyüpoğlu [8].....	120
5.3.2.2. Global Response Surface Method Targeting Low Frequency Modes Results of Sun [7].....	122
5.3.2.3. Spacer Design Using Topology Results of Sun [7] .....	124
5.3.2.4. Finite Element Results of the Novel Designs .....	128
5.3.2.5. Comparison of the Novel Designs .....	137
5.4. Experimental Results of the Designed Surface Damping Treatments .....	143
5.4.1. Comparison of the Experimental and Simulation Results of the Designed Surface Damping Treatments .....	153
6. CONCLUSION AND FUTURE WORK .....	157
6.1. Conclusion.....	157
6.2. Future Work .....	158
REFERENCES.....	159
A. DIN-LN-9415 [41].....	165
B. DIN-LN-9414 [42].....	167
C. DIN-LN-9411 [43].....	169

## LIST OF TABLES

### TABLES

Table 3.1. Part Attributes and Dimensions .....	26
Table 3.2. Material Properties .....	31
Table 3.3. Mesh Comparison Table.....	39
Table 3.4. FEM Modal Results.....	46
Table 3.5. FEM Modal Results in target range Corrected .....	47
Table 3.6. Impact Locations for Roving Hammer Test and Eigenvector Locations .	47
Table 3.7. Experiment Modal Results .....	48
Table 4.1. Reference CLD Properties.....	60
Table 4.2. Free-Free Boundary Condition Modal Values using 0 Hz Material properties .....	67
Table 4.3. Free-Free Boundary Condition Modal Values after iterations .....	67
Table 4.4. Simply Supported - Simply Supported Boundary Condition Modal Values using 0 Hz Material properties .....	68
Table 4.5. Simply Supported - Simply Supported Boundary Condition Modal Values after iterations .....	68
Table 5.1. Dimensions of Layers.....	88
Table 5.2. Additional Mass with respect to Configurations .....	89
Table 5.3. Additional Mass with respect to Configurations .....	91
Table 5.4. Input point 10 Output point 7 damping Ratios .....	93
Table 5.5. Input point 10 Output point 16 damping Ratios .....	95
Table 5.6. Input point 10 Output point 7 damping Ratios .....	101
Table 5.7. Input point 10 Output point 16 damping Ratios .....	102
Table 5.8. Additional Mass with respect to Configurations .....	108
Table 5.9. Additional Mass with respect to Configurations .....	109
Table 5.10. Input point 10 Output point 7 damping Ratios .....	115

Table 5.11. Input point 10 Output point 16 damping Ratios .....	117
Table 5.12. Designed Solution Parameters .....	127
Table 5.13. Damping Ratio Comparison for Point 7 .....	134
Table 5.14. Damping Ratio Comparison for Point 16 .....	135
Table 5.15. Calculated Experimental Damping Ratios .....	152
Table 5.16. dB Band Power Reductions on full Frequency Range.....	155

## LIST OF FIGURES

### FIGURES

Figure 1.1. Visual presentation of constrained layer damping treatment with uniform spacer geometry .....	2
Figure 2.1. Elastic Modulus and loss factor change vs temperature for Viscoelastic Materials [50].....	8
Figure 2.2. Complex Modulus and Loss Factor vs Frequency for Plastic and Elastomeric Materials [1] .....	8
Figure 2.3. Complex Shear Modulus and Loss Factor vs Frequency and Temperature [51].....	9
Figure 2.4. Viscoelastic Complex Material Chains Visualization [50] .....	9
Figure 2.5. Damping Comparison for Structural Alloys, High Damping Alloys and Viscoelastic Materials for Different Strain Amplitude [50] .....	10
Figure 2.6. Master Modulus and Loss Factor Curves Formed by Shift Factors [1] ..	14
Figure 2.7. Free Layer Surface Damping Treatment .....	15
Figure 2.8. Constrained Layer Surface Damping Treatment.....	16
Figure 2.9. Constrained Layer Surface Damping Treatment with Uniform Layer ...	17
Figure 2.10. Standoff Layer Surface Damping Treatment (Slotted Spacer) .....	17
Figure 3.1. Rivet Modelling [31] .....	28
Figure 3.2. Solid Model .....	30
Figure 3.3. Shell Model .....	31
Figure 3.4. Material Definition in ABAQUS .....	33
Figure 3.5. Section Definition Dialog box in ABAQUS .....	33
Figure 3.6. Section Material Definition in ABAQUS .....	34
Figure 3.7. Section Assignment on to Parts in ABAQUS .....	34
Figure 3.8. Mesh types in ABAQUS [9] .....	36
Figure 3.9. Meshed Fuselage Geometry .....	37

Figure 3.10. Analytical Solution of a Free-Free Plate [45].....	37
Figure 3.11. Mesh Comparison Mesh Types Shell-Solid Quad-Solid Tet .....	38
Figure 3.12. Creating Connector Section in ABAQUS .....	40
Figure 3.13. Fastener definition in ABAQUS.....	42
Figure 3.14. Fastener definition in ABAQUS rivet top and bottom centers.....	42
Figure 3.15. Fastener definition in ABAQUS connected nodes .....	43
Figure 3.16. MAC Comparison of FEM and Experimental Results .....	45
Figure 3.17. Eigenvector locations that are used in MAC .....	45
Figure 3.18. FRF Results for Impact Location 10 Output Locations 7 and 16.....	46
Figure 3.19. METU Experiment Bare Plate Accelerometer and Impact Locations...	49
Figure 3.20. Accelerometer points selection for best outputs .....	49
Figure 3.21. Accelerometer that is used in experiment.....	50
Figure 3.22. Impact hammer used in experiment.....	50
Figure 3.23. METU Experiment Mode Shape I.....	51
Figure 3.24. METU Experiment Mode Shape II .....	51
Figure 3.25. METU Experiment Mode Shape III .....	52
Figure 3.26. METU Experiment Mode Shape IV .....	52
Figure 3.27. FEM vs Experimental FRF Results Impact Location 10 Output Location 7.....	53
Figure 3.28. FEM vs Experimental FRF Results Impact Location 10 Output Location 16.....	53
Figure 3.29. ABAQUS Viscoelastic Material Definition I.....	56
Figure 3.30. ABAQUS Viscoelastic Material Definition II.....	56
Figure 3.31. ABAQUS Viscoelastic Material Definition III .....	57
Figure 3.32. ABAQUS Viscoelastic Material Definition IV .....	57
Figure 3.33. ABAQUS Viscoelastic Material Definition V .....	58
Figure 4.1. Simply Supported Reference Beam FEM .....	61
Figure 4.2. Modal Analysis settings using 0 Hz material properties for initial mode frequencies .....	62

Figure 4.3. Modal Analysis normalization settings using 0 Hz material properties for initial mode frequencies..... 62

Figure 4.4. Complex Mode analysis settings for first mode using material properties calculated at initial guess found by Step-1 ..... 63

Figure 4.5. Complex Mode analysis settings for second mode using material properties calculated at initial guess found by Step-1 V ..... 63

Figure 4.6. Complex Mode analysis settings for third mode using material properties calculated at initial guess found by Step-1 ..... 64

Figure 4.7. Complex Mode analysis settings for fourth mode using material properties calculated at initial guess found by Step-1 ..... 64

Figure 4.8. Complex Mode analysis settings for fifth mode using material properties calculated at initial guess found by Step-1 ..... 65

Figure 4.9. Mode shapes of beam under transverse vibration [45] ..... 66

Figure 4.10. Modal Parameters for Beam under transverse vibration [45] ..... 66

Figure 4.11. MAC Plot for Simply Supported- Simply Supported Beam ..... 69

Figure 4.12. Direct point FRF  $x=0.1L$  Simply Supported- Simply Supported Beam 69

Figure 4.13. Analytical First mode for Simply Supported- Simply Supported Beam ..... 70

Figure 4.14. ABAQUS First mode for Simply Supported- Simply Supported Beam ..... 70

Figure 4.15. Analytical Second mode for Simply Supported- Simply Supported Beam ..... 71

Figure 4.16. ABAQUS Second mode for Simply Supported- Simply Supported Beam ..... 71

Figure 4.17. Analytical Third mode for Simply Supported- Simply Supported Beam ..... 72

Figure 4.18. ABAQUS Third mode for Simply Supported- Simply Supported Beam ..... 72

Figure 4.19. Analytical Fourth mode for Simply Supported- Simply Supported Beam ..... 73

Figure 4.20. ABAQUS Fourth mode for Simply Supported- Simply Supported Beam ABAQUS .....	73
Figure 4.21. Analytical Fifth mode for Simply Supported- Simply Supported Beam .....	74
Figure 4.22. ABAQUS Fifth mode for Simply Supported- Simply Supported Beam .....	74
Figure 4.23. MAC Plot for Free-Free Case.....	75
Figure 4.24. Analytical First mode for Free-Free Beam.....	76
Figure 4.25. ABAQUS First mode for Free-Free Beam .....	76
Figure 4.26. Analytical Second mode for Free-Free Beam .....	77
Figure 4.27. ABAQUS Second mode for Free-Free Beam.....	77
Figure 4.28. Analytical Third mode for Free-Free Beam .....	78
Figure 4.29. ABAQUS Third mode for Free-Free Beam.....	78
Figure 4.30. Analytical Fourth mode for Free-Free Beam.....	79
Figure 4.31. ABAQUS Fourth mode for Free-Free Beam.....	79
Figure 4.32. Analytical Fifth mode for Free-Free Beam .....	80
Figure 4.33. ABAQUS Fifth mode for Free-Free Beam.....	80
Figure 5.1. MIL-STD-810G Category 14 Rotary Wing Aircraft-Helicopter Vibration Curve [47] .....	82
Figure 5.2. FRF Result for Undamped Fuselage Geometry .....	83
Figure 5.3. Single and Double Constraining Layer Solutions .....	86
Figure 5.4. Triple Constraining Layer Solution.....	87
Figure 5.5. Standoff Layer Solution.....	87
Figure 5.6. 75, 45 and 30 Percent Coverage Areas.....	90
Figure 5.7. Orientation and Location of Damping Treatment .....	91
Figure 5.8. Bare Plate vs Single, Double and Triple CLDs Point 7.....	92
Figure 5.9. Bare Plate vs Single, Double and Triple CLDs Point 16.....	93
Figure 5.10. Full Octave Band dB Band Power Reduction Point 7.....	96
Figure 5.11. Full Octave Band dB Band Power Reduction Point 16.....	96
Figure 5.12. 1/3 Octave Band dB Band Power Reduction Point 7 .....	97

Figure 5.13. 1/3 Octave Band dB Band Power Reduction Point 16.....	97
Figure 5.14. 1/10 Octave Band dB Band Power Reduction Point 7.....	98
Figure 5.15. 1/10 Octave Band dB Band Power Reduction Point 16.....	98
Figure 5.16. Narrow Octave Band dB Band Power Reduction Point 7.....	99
Figure 5.17. Narrow Octave Band dB Band Power Reduction Point 16.....	99
Figure 5.18. Bare Plate vs Triple CLD vs Uniform Spacer Point 7 .....	100
Figure 5.19. Bare Plate vs Triple CLD vs Uniform Spacer Point 16 .....	101
Figure 5.20. Full Octave Band dB Band Power Reduction Point 7 .....	103
Figure 5.21. Full Octave Band dB Band Power Reduction Point 16 .....	104
Figure 5.22. 1/3 Octave Band dB Band Power Reduction Point 7.....	104
Figure 5.23. 1/3 Octave Band dB Band Power Reduction Point 16.....	105
Figure 5.24. 1/10 Octave Band dB Band Power Reduction Point 7.....	105
Figure 5.25. 1/10 Octave Band dB Band Power Reduction Point 16.....	106
Figure 5.26. Narrow Octave Band dB Band Power Reduction Point 7.....	106
Figure 5.27. Narrow Octave Band dB Band Power Reduction Point 16.....	107
Figure 5.28. 15mm Periodic Slotted Spacer Design for equal and twice tower length .....	108
Figure 5.29. Uniform vs Slotted Spacers Point 7 .....	110
Figure 5.30. Uniform vs Slotted Spacers Point 16 .....	110
Figure 5.31. Full Octave Band dB Band Power Reduction Point 7 .....	111
Figure 5.32. Full Octave Band dB Band Power Reduction Point 16 .....	111
Figure 5.33. 1/3 Octave Band dB Band Power Reduction Point 7.....	112
Figure 5.34. 1/3 Octave Band dB Band Power Reduction Point 16.....	112
Figure 5.35. 1/10 Octave Band dB Band Power Reduction Point 7.....	113
Figure 5.36. 1/10 Octave Band dB Band Power Reduction Point 16.....	113
Figure 5.37. Narrow Octave Band dB Band Power Reduction Point 7.....	114
Figure 5.38. Narrow Octave Band dB Band Power Reduction Point 16.....	114
Figure 5.39. Enhanced Genetic Algorithm Material Distribution Optimized for First Three Mode [8].....	120

Figure 5.40. Enhanced Genetic Algorithm Material Distribution Double Cantilevered Beam .....	121
Figure 5.41. Enhanced Genetic Algorithm Material Distribution Double Cantilevered Beam 100mm coverage.....	121
Figure 5.42. Enhanced Genetic Algorithm Material Distribution Double Cantilevered Beam 100mm coverage Designed Part and Mesh Generated .....	122
Figure 5.43. GRSM Optimum Solution for 250mm Cantilevered Beam [7].....	123
Figure 5.44. GRSM Optimum Solution for 250mm Cantilevered Beam .....	124
Figure 5.45. Topology Optimization Results for Cantilevered Beam suggested by Sun [7] .....	125
Figure 5.46. Topology Optimization Adapted Suggested Solutions Side View.....	126
Figure 5.47. Topology Optimization Adapted Suggested Solutions Isometric View .....	126
Figure 5.48. FRF Results for Novel Results Point 7.....	129
Figure 5.49. FRF Results for Novel Results Point 16.....	129
Figure 5.50. Full Octave Band dB Band Power Reduction Point 7.....	130
Figure 5.51. Full Octave Band dB Band Power Reduction Point 16.....	130
Figure 5.52. 1/3 Octave Band dB Band Power Reduction Point 7 .....	131
Figure 5.53. 1/3 Octave Band dB Band Power Reduction Point 16 .....	131
Figure 5.54. 1/10 Octave Band dB Band Power Reduction Point 7 .....	132
Figure 5.55. 1/10 Octave Band dB Band Power Reduction Point 16 .....	132
Figure 5.56. Narrow Octave Band dB Band Power Reduction Point 7 .....	133
Figure 5.57. Narrow Octave Band dB Band Power Reduction Point 16.....	133
Figure 5.58. FRF Results for Best Novel Results Point 7.....	138
Figure 5.59. FRF Results for Best Novel Results Point 16.....	138
Figure 5.60. Full Octave Band dB Band Power Reduction Point 7.....	139
Figure 5.61. Full Octave Band dB Band Power Reduction Point 16.....	139
Figure 5.62. 1/3 Octave Band dB Band Power Reduction Point 7 .....	140
Figure 5.63. 1/3 Octave Band dB Band Power Reduction Point 16 .....	140
Figure 5.64. 1/10 Octave Band dB Band Power Reduction Point 7 .....	141

Figure 5.65. 1/10 Octave Band dB Band Power Reduction Point 16.....	141
Figure 5.66. Narrow Octave Band dB Band Power Reduction Point 7.....	142
Figure 5.67. Narrow Octave Band dB Band Power Reduction Point 16.....	142
Figure 5.68. Constrained Layer Damping Treatment Patches.....	143
Figure 5.69. Uniform Spacer Layer Manufactured .....	144
Figure 5.70. Standoff Layer Damping Treatment (Slotted Spacer).....	144
Figure 5.71. Experimental Setup for Fuselage Geometry .....	145
Figure 5.72. Bare Fuselage Experimental Setup .....	146
Figure 5.73. Multiple Constrained Layer Experimental Setup.....	147
Figure 5.74. FRF Results for Experimental Results Point 7.....	148
Figure 5.75. Full Octave Scale dB Band Power Reduction Results .....	148
Figure 5.76. Full Octave Scale dB Band Power Results .....	149
Figure 5.77. 1/3 Octave Scale dB Band Power Reduction Results .....	149
Figure 5.78. 1/3 Octave Scale dB Band Power Results.....	150
Figure 5.79. 1/10 Octave Scale dB Band Power Reduction Results .....	150
Figure 5.80. 1/10 Octave Scale dB Band Power Results.....	151
Figure 5.81. Narrow dB Band Power Reduction Results .....	151
Figure 5.82. Narrow dB Band Power Results.....	152
Figure 5.83. FRF Results Comparison for Experimental vs Simulation Results Point 7 .....	154
Figure 5.84. FRF Results Comparison for Multilayer CLDs Experimental vs Simulation Results Point 7.....	154
Figure 5.85. FRF Results Comparison of TCLD vs Uniform Spacer Experimental vs Simulation Results Point 7.....	155

## LIST OF ABBREVIATIONS

### ABBREVIATIONS

<i>ACLD</i>	Active Constrained Layer Damping
<i>ADF</i>	Anelastic Displacement Fields
<i>CAD</i>	Computer Aided Drawing
<i>CMA</i>	Complex Modulus Approach
<i>CL</i>	Constrained Layer
<i>CLD</i>	Constrained Layer Damping
<i>DFR</i>	Direct Frequency Response
$E^*$	Complex Elastic Modulus
ESO	Evolutionary Structural Optimization
<i>FEM</i>	Finite Element Model
<i>FE</i>	Finite Element
<i>FLD</i>	Free Layer Damping
<i>FRF</i>	Frequency Response Function
$G^*$	Complex Shear Modulus
<i>GHM</i>	Golla-Hughes-McTavish
<i>ICE</i>	Iterative Complex Eigensolution
<i>IMSE</i>	Iterative Modal Strain Energy
<i>MSE</i>	Model Strain Energy

*PCL* Passive Constrained Layer

*PCLD* Passive Constrained Layer Damping

*PSOL* Passive Standoff Layer

*SED* Strain Energy Distribution

*SOL* Stand-Off Layer

*SOLD* Stand-Off Layer Damping

*SSOL* Slotted Stand-off Layer

*VEM* Viscoelastic Material

*VIP* Very Important Person

## LIST OF SYMBOLS

### SYMBOLS

$\alpha(T)$  Temperature Shift Factor

$\omega_n$  Natural Frequency

$f_r$  Reduced Frequency

$\varepsilon$  Strain

$\sigma$  Bending Stress

$\tau$  Shear Stress

$\Phi$  Shear Strain

$\psi$  Phase Lag



# CHAPTER 1

## INTRODUCTION

### 1.1. Introduction

Surface damping treatment applications are mostly used on sheet metal structures in order to decrease the vibratory motions or acoustic noise generated due to resonant frequency problems. Since sheet metals are highly responsive to transverse vibrations, the application of the surface damping treatments on to these structures helps to decrease resonant peaks and noise generated by excessive vibration. For this reason, surface damping solutions are usually preferred in aerospace applications to reduce broadband input effects and to control acoustic noise level transferred into cabin. These surface damping treatment solutions utilize a highly viscoelastic layer, with low stiffness and long material chains, to dissipate the vibratory motion of the base structure as heat. There are several types of applications and they are briefly introduced below.

The most basic version of the surface damping solutions is free layer surface damping (FLD) treatment. The bending motion of the base beam or plate is transferred to viscoelastic layer which in fact damped in this layer. After detailed inspections it is seen that the performance can be increased by adding a stiff constraining layer on the top of the viscoelastic layer in order to force the damping layer deforming in the shear mode instead of bending mode. This method provides induced larger deformations between molecular chains of viscoelastic material. This effective application is called constrained layer damping (CLD) treatment.

With increasing competitiveness in aerospace industry, companies seek for lightest solutions in their aircraft to increase efficient flight hour and comfort while minimizing flight cost and maintenance cost. This need, forced engineers to further

increase the effectiveness of CLD treatments. Since CLD applications efficiency is related to shear stress occur in viscoelastic layer, a spacer layer made from more flexible and low density material is used to increase damping performance by increasing the shear deformations by further shifting the damping layer out of neutral axis. However, since aerospace applications are weight critical, every additional weight costs money, which in fact turns engineers to seek a better proposal than uniform spacer layers.

The standoff layer damping treatment (SOLD) is a special version of uniform spacer used CLD where the spacer layer is slotted to increase the neutral axis shift with same additional mass on to base structure. Figure 1.1 shows a standoff layer damping treatment with uniform spacer geometry in un-deformed and deformed shape for illustration.

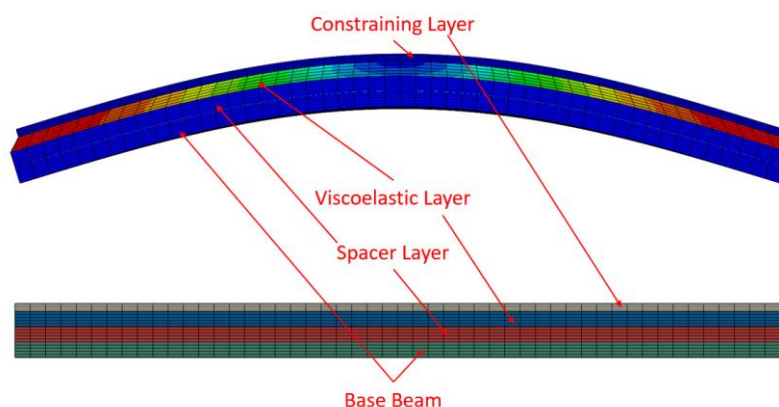


Figure 1.1. Visual presentation of constrained layer damping treatment with uniform spacer geometry

For a standoff layer to be effective as much as possible, it is important to develop a spacer geometry that does not limit the shear deformation and vibratory motion of viscoelastic layer. As a result, an ideal spacer geometry should have zero bending stiffness to transfer the vibratory motions to damping layer, while having infinite shear stiffness not to deform with viscoelastic layer and limit the induced shear strains.

In this study, different than literature, a new damping estimation technique is suggested using random input & output relations considering fuselage loadings to simulate broadband damping effect. Furthermore, several spacer geometries are designed by adapting beam optimized spacer geometries and parametrizing the commonly used slotted designs in different tower to slot ratios.

## **1.2. Background and Motivation**

In aerospace applications, where sheet metal materials are commonly used, structures are subjected to both sinusoidal and random input due to rotary motion of engines and environmental and aerodynamic loads. Since sheet metals are thin walled structures, they are highly sensitive to transverse vibration problems. These wide ranged loading on fuselage, commonly up to 4000 Hz, creates a resonant frequency problems because the fuselage itself is responsive to this kind of loading. If this vibratory motion is not damped, it can decrease the fatigue life of aircraft and passenger comfort.

In literature, there exist optimization of surface damping treatments and spacer geometries; however, for plates there is only partial coverage and CLD treatment studies on plates. Although there exist some studies that utilize fuselage like structure, there is no detailed information about it. This gap in literature is used as motivation in this study to develop and validate a fuselage geometry where an adequate damping solution can be simulated.

Furthermore, the use of special designed spacer layer with different shapes can affect the damping performance drastically, where in this study it is intended to use beam optimized spacer geometries in order to suggest a new design for fuselage geometry. The design of a spacer layer mainly focus on optimized solutions and parametric design alterations on already used off the shelf solution in aerospace applications.

Lastly, in literature it is seen that the damping is estimated only using modal identification methods, generally half power picking method, but not considering the loading condition of the structure itself. Since these geometries are used to damp wide frequency resonance problems, we see a need of a new metric for estimation of damping performance.

### **1.3. Objective of the Thesis**

The main aim of the study is to develop and suggest several possible standoff layer damping treatments for a fuselage like structure utilizing a plate-adapted solution of previously optimized spacer geometry for beams. After developing possible solutions, the performance characteristics will be modelled through finite element simulations including new designed and validated fuselage like structure throughout this study as the vibrating base structure rather than bare plate and present the damping estimation using new metric defined. The damping estimation metric for broadband vibration effect is also suggested alongside with modal identification methods to estimate increase in passenger comfort due to noise.

### **1.4. Scope of the Thesis**

Throughout the study, scaled down fuselage like structure is also designed and validated in order to demonstrate real life applications. A new damping estimation technique is suggested and used to represent the performance of the designed damping solutions along with modal identification methods. In this thesis, several spacer geometries will be developed and finite element models will be used to simulate the performance characteristics of these standoff layer damping treatments on a fuselage like structure. Analyses were performed using ABAQUS [9]. The viscoelastic material properties were implemented as user inputs through software as temperature and frequency dependent material data.

Damping performance and frequency shift analysis are also performed in finite element modelling up to 600 Hz and the results were compared through experiments for best possible solutions regarding the finite element model results. The reason of limiting the interested frequency up to 600Hz is that with increasing frequency spectrum the computational cost and time increases highly and due to boundary conditions first non-rigid ten modes can be visible up to 600Hz.

### **1.5. Outline of the Thesis**

The structure of the thesis can be seen in the following statements. Chapter 2 will give theoretical background information about previous studies and knowhow used in analyses along with literature survey. In Chapter 3, design and development studies carried out for fuselage geometry, validation and viscoelastic layer inclusion on to fuselage is explained. In Chapter 4, reference standoff layer damping treated structure finite element modelling was performed. In Chapter 5, developed optimized spacer geometries were included in finite element model and damping performance was simulated using finite element modeling. In addition, experimental verification studies and comparison between simulations and experimental results will be given. In the last chapter, conclusion of the study and future work will be given.



## CHAPTER 2

### LITERATURE SURVEY

#### 2.1. Viscoelastic Materials

Viscoelastic products are materials that has both viscous and elastic behavior characteristics and change its mechanical properties, such as elastic modulus and loss factor, with temperature and frequency. The stress and the stress rate applied to these materials affects the strain occurs inside of the viscoelastic material, which in turn changes the nature of the problem. These materials have four basic regions called as “Glassy”, “Transition”, “Rubbery” and “Flow” regions [1]. All these regions have their own characteristics, which shall be considered in design phase for maximum efficiency. In “Glassy Region” VEM has the highest elastic modulus that is decreasing slowly with low damping coefficients; in “Rubbery Region” material has stable elastic modulus and loss factor but the values are lower than the required values mostly. However, the “Transition” has the highest loss factor value but both elastic modulus and loss factor is not stable in this region. The trend of modulus is drastic decrease with temperature increase where the trend of loss factor is drastic increase and then drastic decrease until rubberlike region. This region is the mostly used region in applications. As seen on Figure 2.2, as frequency increases modulus tends to increase where loss factor has same characteristics as in temperature where a peak is observed after an increase and a sudden decrease at Transition-Glassy region interface point.

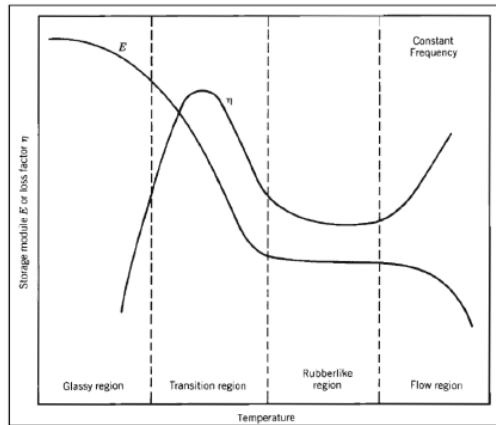


Figure 2.1. Elastic Modulus and loss factor change vs temperature for Viscoelastic Materials [50]

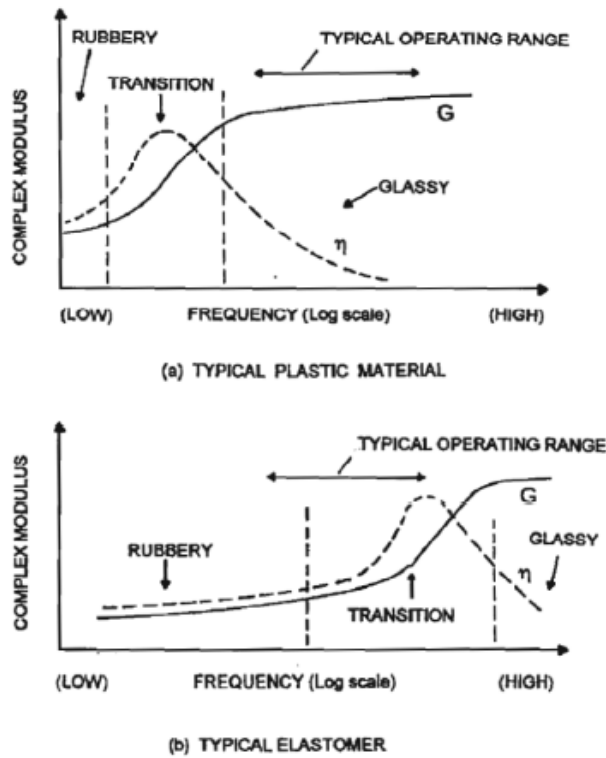


Figure 2.2. Complex Modulus and Loss Factor vs Frequency for Plastic and Elastomeric Materials [1]

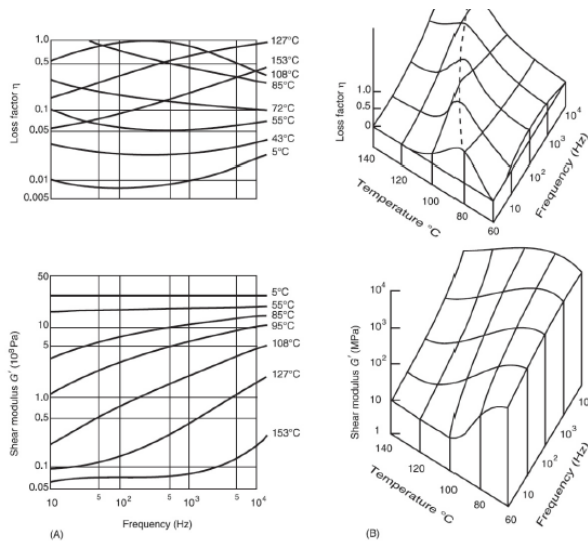


Figure 2.3. Complex Shear Modulus and Loss Factor vs Frequency and Temperature [51]

Due to low density and high loss factors compared to plastic materials, these materials are highly desired in daily life especially in aerospace and car industry where every weight counts. These materials are different from elastics in terms of molecular base. The difference from elastic materials is that, viscoelastic products are made of long and complex chains, which makes it hard to model them analytically shown in Figure 2.4. Due to that, they tend to have more damping capacity with same strain values compared to elastic materials as shown in Figure 2.5.

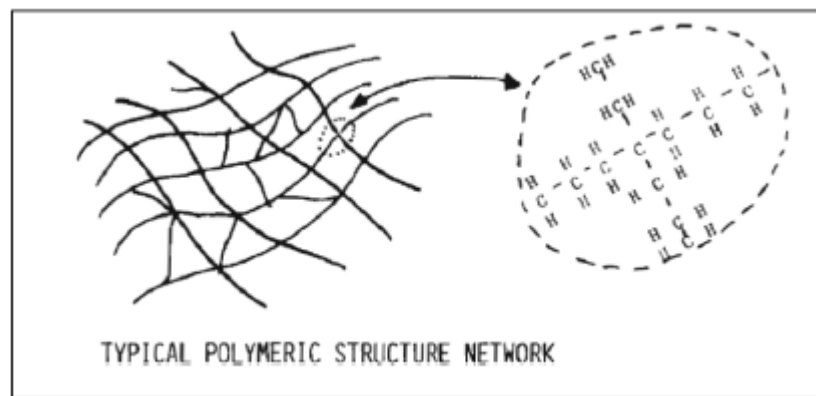


Figure 2.4. Viscoelastic Complex Material Chains Visualization [50]

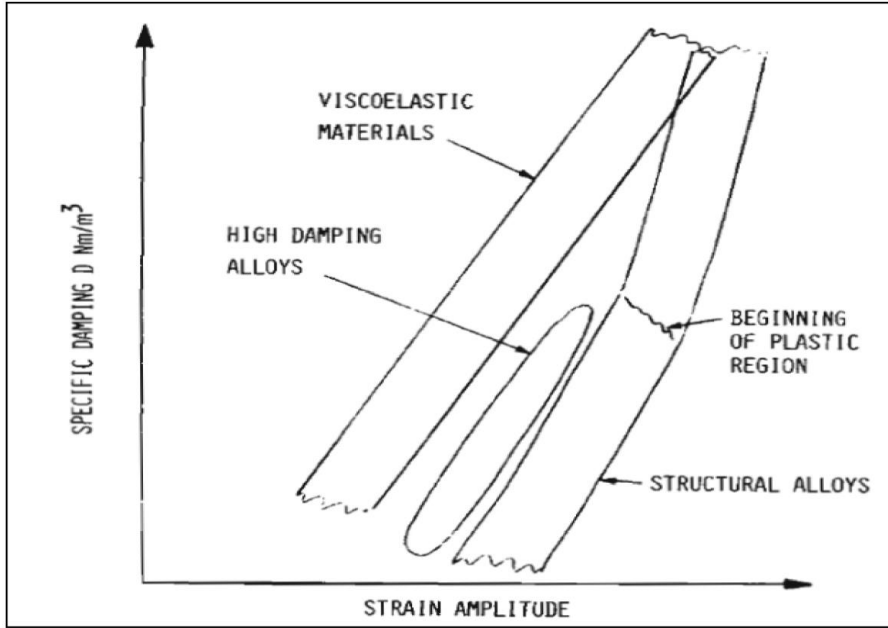


Figure 2.5. Damping Comparison for Structural Alloys, High Damping Alloys and Viscoelastic Materials for Different Strain Amplitude [50]

The viscoelastic materials due to frequency and temperature dependency, cannot be represented by linear material models as metals. In order to relate stress strain relation for viscoelastic materials, one can use standard linear viscoelastic constitutive relation for uniaxial state of stress by [38];

$$\sigma(t) + \sum_{k=1}^K b_k \frac{d^k \sigma}{dt^k} = E_0 \varepsilon(t) + \sum_{j=1}^J E_j \frac{d^j \varepsilon}{dt^j} \quad (1)$$

For harmonic excitation analysis, stress and strain can be defined as  $\sigma(t) = \sigma_0 e^{i\omega t}$ ,  $\varepsilon(t) = \varepsilon_0 e^{i\omega t}$ . Substituting these relations on to constitutive equation gives;

$$\sigma_0 = \frac{\varepsilon_0 [E_0 + \sum_{j=1}^J E_j (i\omega)^j]}{1 + \sum_{k=1}^K b_k (i\omega)^k} = \frac{\varepsilon_0 E_0 [1 + \sum_{j=1}^J a_j (i\omega)^j]}{1 + \sum_{k=1}^K b_k (i\omega)^k} \quad (2)$$

This relation can be expressed in a more compact way as follows;

$$\sigma_0 = (E' + iE'')\varepsilon_0 \quad (3)$$

Where  $E'$  and  $E''$  are storage and loss modulus respectively. For metals  $E'$  is constant where  $E''$  is weak; but for viscoelastic materials both moduli are frequency dependent. For harmonic response, strain and stress amplitude relation than can be expressed with frequency dependent complex modulus  $\tilde{E}^*(j\omega)$  defined as;

$$\sigma_0 = \tilde{E}^*(j\omega)\varepsilon_0 = ((E'(\omega) + jE''(\omega))\varepsilon_0 \quad (4)$$

Which gives;

$$\tilde{E}^*(i\omega) = E'(\omega)[1 + j\eta(\omega)] \quad (5)$$

Where the loss factor term  $\eta(\omega)$  is defined as

$$\eta(\omega) = \frac{E''(\omega)}{E'(\omega)} \quad (6)$$

### 2.1.1. Viscoelastic Material Models

In order to represent the damping and elastic characteristics of the material, viscous damper and spring element combinations were used to simulate the behavior of VEMs. These models use serial and parallel configurations of spring and viscous elements to define simple or complex material behavior depending on the application.

From basic to complex the models are as follows;

- Maxwell
- Voight
- Standard Linear Solid Model
- Generalized Maxwell
- Fractional Derivative Model

The Maxwell model is as mentioned the simplest model to represent viscoelastic materials. Consists of linear spring and damper configuration. Where Voight model consists of spring and damper element connected in parallel. The advantage of Voight compared to Maxwell is that the Voight model can simulate the creep behavior better. A further growth model is standard linear solid model where a serial connected spring and damper is connected to spring element in parallel. This model gives user the ability to represent the steady state behavior; however, at some points can behave very divergent. The most complex modelling among them is the generalized Maxwell model where standard linear solid model is expanded by infinite parallel connected configurations to single spring element. The advantage of this model is that, even with ten elements and with moderate computational effort, one can simulate the behavior with good approximation.

Although above mentioned models are used to model the viscoelastic materials in time domain with good approximations, they cannot be used to model the viscoelastic material in frequency domain. Due to ease of use and less computational effort needed a fractional derivative model in frequency domain is generated. This model is used in most of the experimental and finite element solutions and can model the real behavior of the viscoelastic layer with less error.

### 2.1.1.1. Fractional Derivative Model

Other than the previous mentioned models, a frequency domain modelling technique called Fractional Derivative model can be used to model viscoelastic parameters especially for damping treatment calculations. This model is used to predict and formulate material properties to fit experimental results with less parameters and computational requirements. The model that is used in this study is a version of fractional derivative model and material properties is as given below [40];

$$\tilde{E}^* = E(1 + i\eta) = \frac{a_1 + b_1(i\omega_R)^{\beta_1}}{1 + c_1(i\omega_R)^{\alpha_1}} \quad (7)$$

Where;

$\omega_R = \omega\alpha(T)$ ,  $\alpha(T) = \text{Temperature shift factor}$

$a_1 = \text{Low frequency storage modulus or rubbery storage modulus}$

$\alpha_1, \beta_1 = \text{Transition slope}$

$b_1, c_1 = \text{Glassy region storage modulus constants}$

As seen from above figure there exists a temperature shift coefficient which plays a role in defining temperature dependent material properties in fractional derivative model that makes easy using this model in finite element and experimental studies.

This material definition is done with defining a new variable called reduced frequency where temperature and frequency effects are combined in to single variable. This I done by measuring the complex modulus at any defined frequency  $f_0$ , and any reference temperature selected  $T_0$ , are identical to the values at any other frequency  $f_1$  at different temperature  $T_1$  given below;

$$\tilde{E}^*(f_0, T_0) = E^*(f_1 \cdot \alpha(T_1)) \quad (8)$$

Since in every equation one point is fixed, the measured complex modulus data is shifted along frequency axis to create a complex modulus graph. The axis where each curve is slid is called the reduced frequency axis.  $\alpha(T_0)$  is unity and other  $\alpha(T_i)$  values will generate master modulus and loss factor curves given as below. Once these curves are formed, by curve fitting process each  $\alpha(T)$  can be calculated.

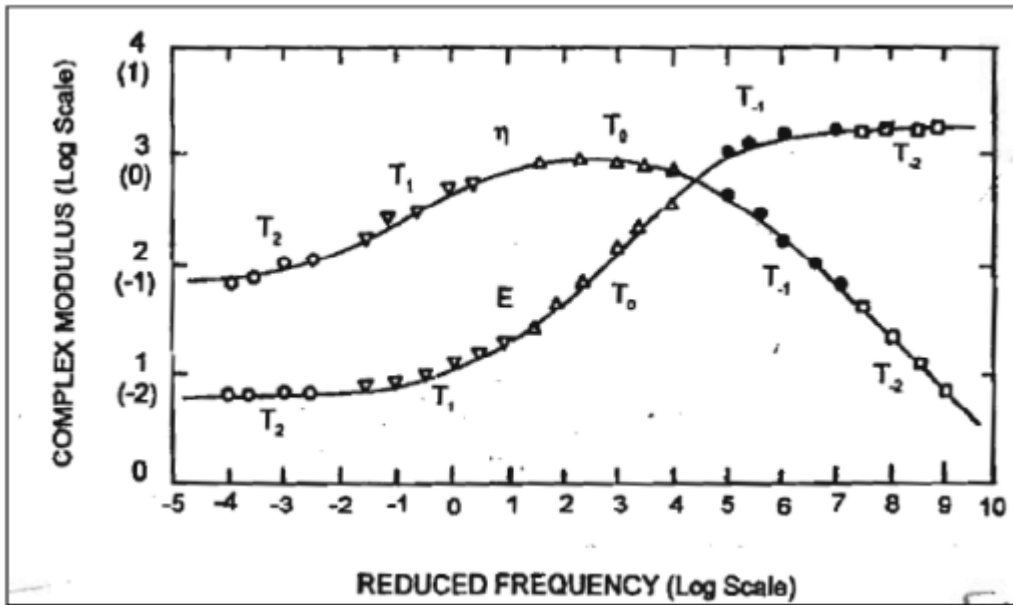


Figure 2.6. Master Modulus and Loss Factor Curves Formed by Shift Factors [1]

There are two methods to define the temperature shift factor.

- The William-Landel –Ferry (WLF) shift factor equation

$$\log[\alpha(T)] = -C_1 \frac{(T - T_0)}{(B_1 + T - T_0)} \quad (9)$$

Where  $B_1$  and  $C_1$  are constants and  $T_0$  is the reference temperature (all temperatures must be in absolute degree  $K^\circ$ )

- The Arrhenius shift factor equation (linear)

In many cases  $\log[\alpha(T)]$  vs  $1/T$  is a straight line and can be represented by;

$$\log[\alpha(T)] = T_A \left( \frac{1}{T} - \frac{1}{T_0} \right) \quad (10)$$

Where  $T_0$  is an arbitrary reference temperature (all temperatures must be in absolute degree  $K^\circ$ )

## 2.2. Surface Damping Treatment Methods

In this chapter surface damping methods will be explained in detail. There are four types of surface damping methods used in literature. The basic visual expressions are as given below sections.

### 2.2.1. Free Layer Damping Treatment

This method consists of bare plate or beam with viscoelastic material combination only. It utilizes the bending vibratory motion due to resonant frequencies occur on base structure. A figure that shows FLD treatment is given below.

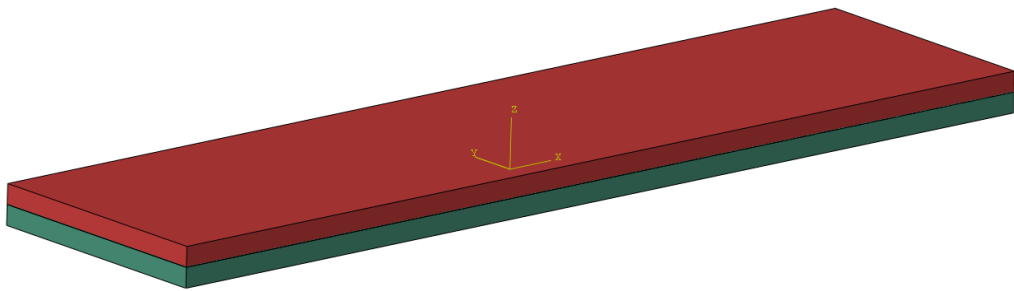


Figure 2.7. Free Layer Surface Damping Treatment

### 2.2.2. Constrained Layer Damping Treatment

Due to need of increasing damping performance it is found that a constraining layer can force viscoelastic material to deform in shear mode instead of bending. Due to higher shear strains occur in damping layer increased heat dissipation between viscoelastic material chains occur. A figure that shows CLD treatment is given below.

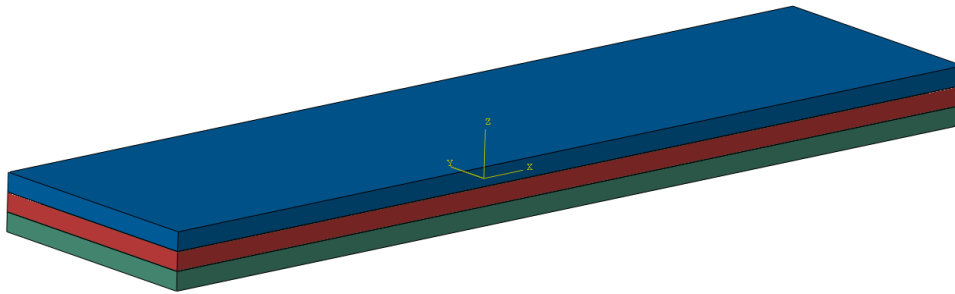


Figure 2.8. Constrained Layer Surface Damping Treatment

### 2.2.3. Constrained Layer Damping Treatment with Spacer Layer

A more advanced method of CLD treatments is to use a low density elastic layer to shift damping layer out of neutral axis to induce much more shear stress. This layer is called spacer layer in literature and increases the damping performance in a cost of additional mass.

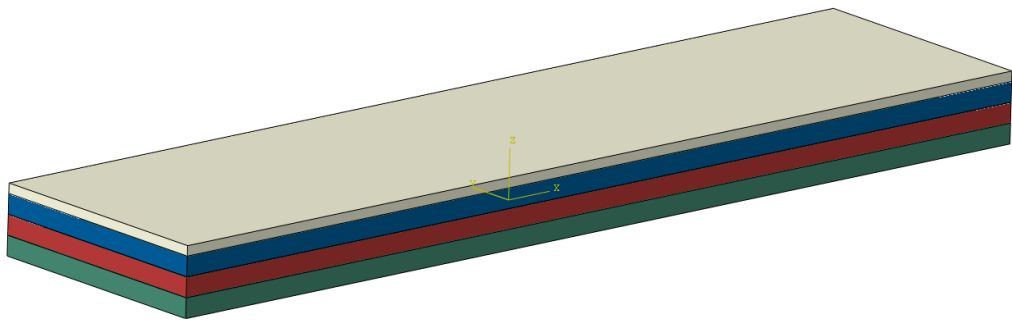


Figure 2.9. Constrained Layer Surface Damping Treatment with Uniform Layer

#### 2.2.4. Standoff Layer Damping Treatment (Slotted Spacer Design)

Due to additional mass of spacer layer, in weight critical application such as aerospace industry applications, a weight optimized solutions should be utilized. Slots cut through spacer layer can decrease weight while maintaining the neutral axis shift same; but also can increase neutral axis shift with same additional mass. This type of solutions are commonly used in aircraft due to performance vs additional mass ratio and widely studied in literature as will be mentioned in the following section. A simple model for a slotted design can be seen in Figure 2.10 which is given below.

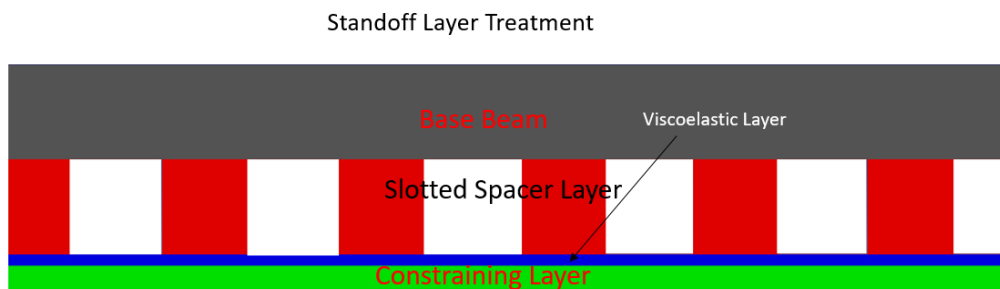


Figure 2.10. Standoff Layer Surface Damping Treatment (Slotted Spacer)

### 2.3. Literature Survey

The vibration and acoustic comfort for thin-walled structures are highly of concern in civil and aerospace applications. One of the most effective way to control the vibration amplitudes and noise due to acoustic radiation is using constrained layer dampers (CLD) [1,10,11, 12]. The energy of vibrating base structure is dissipated by means of shear strains induced in viscoelastic layer of CLD application. Bending motions of the vibrating base structure tends to deform the viscoelastic material (VEM) and constraining layer. Since the constraining layer is stiffer than VEM layer, the strain difference between constrained layer (CL) and base beam, enforces the VEM to deform in shear mode rather than bending mode as it is in free-layer surface damping treatments. The shear strains, the vibratory energy is converted to heat energy which is dissipated. The strain difference between the CLD and free layer damping (FLD) is remarkable, which increases the damping capability of application in return of additional mass.

Early works focused on passive configurations where the constraining layers are commonly made of metals similar to base structure. Kerwin [13] developed a simplified theory to calculate the loss factor of a plate with passive constrained layer damping (PCLD) treatment. Same year Whittier [14], found that addition of a layer called spacer between VEM and base structure increases the effectiveness by shifting away the viscoelastic layer from neutral axis which increases the induces shear strain. This study, which will trigger the optimization studies in later years when the reduced weight and effectiveness will play an important role on designs especially in automotive and aerospace industry, has an important role in later studies.

Later, several studies have been published related to formulations and techniques to model the VEM and to predict the dissipation of CLD treatments for vibrating structures [15–20]. Active constrained layer damping (ACLD) [19, 21-23], which replaces the passive constraining layer above the VEM with active piezoelectric layer, is recently receive attention to be used in several applications and indicate its

considerable enhancement of the low frequency damping performance yet is still expensive and complicated to replace PCLD treatment in industry.

In today's world, PCLD patches are used in oil pans, valve covers, engine covers, door and floor panels and brake insulators etc. to resolve resonant vibration and noise problems [11]. The most critical thing that should be considered using the PCLD is the addition of mass while keeping the damping performance as high as possible. Recently, several studies have been published related to optimization of PCLD usage and stand-off layer damping (SOLD) treatments. Garrison et al. [24] carried out a parametric study to optimize location, coverage and thickness of damping layer of a PCLD treatment with spacer. Their study showed that using SOLD with less area coverage can ensure same amount of damping effectiveness with less added weight. Several configurations such as partial coverage with full length strip from edges with different locations, centered partial and full coverage and offset in different directions from edges. It is found out that a thin strip in the direction of the length of the plate placed a little off-centered supplied the best configuration for wide range of frequencies.

Masti and Sainsbury [25] conducted a study for cylindrical shell structures with partially covered standoff constrained layer damping treatment having different boundary conditions. Their study showed that, locating the patches where the modal strain energy distributions (SED) are high could provide better results instead of full coverage applications with reduced weight of the application. The weight of the spacer layer is limited to 4 percent of the base structure and clamped-clamped along with simply supported condition is modelled analytically for finite element model (FEM) and validated in the study for the first five mode of structure. The numerical results show that instead of increasing the local coverage area increasing the thickness of the patch advance the effectiveness of the application.

Chen and Huang [26] carried out a topology optimization study in order to locate the optimal location of CLD. The mathematical model uses energy approach for

optimization purpose along with an objective function including structural damping ratios, resonant frequencies' shift, and CLD thickness. The simulated results show that the best solution is when the constraining layer thickness is twice of the viscoelastic layer thickness.

Trindade [23] conducted a modal selective hybrid method, which utilizes active and passive combinations for beams. Clamped-clamped aluminum beam with different configurations of standoff treatment with piezoelectric actuators have been considered for both geometric and topology optimizations. Genetic algorithm combined with multiobjective optimization strategy is utilized for the survival of the fittest theory applied for a set of variables in a narrow frequency range. The main objective of the study is to find the maximum overall damping while minimizing mass added on to system. Two times state space modal reduction is applied in order to calculate the passive-active control response. Other than viscoelastic damping, %0.1 viscous damping is added to system to include other type of damping effects. The no active control, active-direct active, active-passive standoff layer and active-passive constrained layer treatments were of concern. It is also found that the contribution of passive components in the best solutions are higher compared to active parts and in case of a malfunction of active components, the system is still well damped.

In 2009, Lepoittevin and Kress [12] investigated the effect of segmentation of the constraining layer to damping performance with their finite element model. They considered two dimensional cantilever beam as base structure and use modal strain energy (MSE) to calculate the modal loss factors. This study aims to locate the cut for optimum damping performance for a defined frequency range. By the cuts induced in constraining layer strain energy on VEM increases which is due to the edge effect. The outcomes of the study are, a good solution can be obtained with this model if; oscillations are harmonic, there is low structural damping in system and the frequency dependence of storage modulus of VEM is not effecting the system much. In addition,

since bending motion of the system decreases shear deformation, a cut should be placed where high bending is observed to increase effectiveness.

Kim et al. [27] studied maximizing the modal loss factor with maximum allowable volume of damping material for a quarter cylindrical shell structure using topology optimization. Their study compares topology optimization with two other methods namely mode shape based evolutionary structural optimization (ESO) and strain energy based strain energy distribution (SED) methods. The viscoelastic material is modeled using complex modulus definition in their numerical model for finite element analysis considering first four modes and up to 500 Hz. In addition, they have validated their models and results. The optimized solution provides 61.14 percent higher modal loss factors; however, the SED can be used as a startup point for initial layout distribution since it gives closer values and layouts to optimized solution.

Kang et al. [28] carried out a study in order to find the optimal distribution of damping layer for shell structures under harmonic excitation and different boundary conditions using topology optimization. They used complex modal superposition along with reduced state approach in order to calculate the response of the system due to non-proportional damping of VEM layer. They only considered the steady state response in their study and used Rayleigh damping coefficient for modelling the viscoelastic material. Zheng et al. [29] also carried a similar study to [28]; however, the difference is that the layout is not damping layer but constrained layer. As it is in [28], Zheng et al. [29] also used solid isotropic material penalization along with method of moving asymptotes [30] in their finite element model. They modelled the base structure and constraining layer as shell elements where the VEM is modelled with eight nodal solid element. They only considered first three modes in their topology optimization process, which is up to 130 Hz.

Yellin et al. [2-4], started carrying out studies in order to represent the stand-off layer damping treatment applications for Euler-Bernoulli beams and experimental validation studies. In 1998, an analytical approach for a passive stand-off layer

damping treatment for Euler-Bernoulli beams is suggested [2, 4]. By modelling the spacer layer as Timoshenko beam, an analytical model has been generated by Yellin et al. and the results for the first two modes were promising because the passive standoff layer (PSOL) treatment nearly doubled the damping factor when compared to CLD treatments. In order to validate the model two special cases are considered; first is zero spacer thickness which leads to passive constrained layer (PCL) treatment and the second is that the assumption of ideal spacer properties as an input to analytical model. After these special cases it is found that the analytical model for PSOL gives exactly same result with PCL when the stand-off layer thickness is given as zero and the ideal stand-off layer properties is valid for this case with the material and thicknesses used in this study. It is also found that, when the shear stiffness of stand-off layer does not affect the system after some point and the shear modulus of the viscoelastic layer dominates the damping parameter. In addition, since the bending stiffness of the base beam is relatively much higher than the spacer layer assuming stand-off layer has negligible bending stiffness is valid in this study.

After validating her analytical model, Yellin et al. experimentally compared the analytical model with experimental results [3, 4]. Instead of using a solid spacer layer without internal damping parameters, a relatively stiffer viscoelastic material, which also has internal damping characteristics, has been used in this study in order to increase the damping performance and compare the PCL and PSOL effectiveness. At first 1.02 mm thick base beam is used; however, coherence values were low for the first two modes due to minimal clipping. After increasing the base structure thickness to 2.29 mm preferable results has been obtained.

In 2000, with the help of previously proven methods [4], Yellin et al. [5] carried out a new study with the purpose of finding an analytical approach to find the frequency response function of a slotted stand-off layer treated Euler-Bernoulli beam. This study showed that with the increasing number of slots ideal spacer geometry assumption can be achieved due to two reasons. Firstly, increased number of slots increases the

discontinuity in the spacer layer, which reduces bending stiffness while not affecting shear stiffness much. Secondly, increasing slots reduces weight, which reduces the total weight of the system.

Using the results of [2-5], Yellin et al. modeled the slotted stand-off layer damping treated beam in FEM and compared the results with the experimental values [6]. This study showed that slotted spacer layer assumptions should be different than PSOL treatment assumptions. A four layered beam theory gave inconsistent results when compared with experimental results. After seeing that the trend and values are inconsistent, Yellin included the epoxy layer in to the FEM and carried out the numerical procedure to see if results are changed. After including the epoxy layer and thickness effect, the results were closer to experimental values; however, the trend was not yet achieved. With a six-layer beam theory, the contact cement layer between spacer and vem layer interface is modelled. Still not enough so physical and visual investigations showed that there exists a delamination with increasing the number of slots in geometry due to improper bonding region in real life. After making some assumptions for delamination, such as decreasing the elastic modulus as half and decreasing the bonding region length in FEM, preferable results were obtained. This study showed that while using SSOL bonding regions should be included in FEM and PSOL assumptions such as ideal bonding regions and no-delamination assumptions are not valid for all cases.

In 2016, as a master's degree thesis Sun [7] and Eyyüpoğlu [8] studied on a novel spacer geometry that is optimized for beams using topology and geometric algorithms with the help of previously carried out studies [2-6]. The main objectives of these studies are to design a spacer geometry that can sufficiently transfer the vibratory motion of the base structure to VEM without resisting and limiting it too much while sufficiently shifting the VEM away from neutral axis. The edge effect and partial treatment is also considered in optimization process. The outcomes of these two thesis

studies will be used in the further analysis in this study in order to be adapted to be applicable to plate structures such as aerospace or automotive bodies.

However, in order to model the aerospace or automotive shell bodies a FEM that can simulate the riveted connection between thin walled plates is needed. Several studies are carried out [33-36] for both aerospace and automotive applications and finite element modeling techniques are evolved for riveted connections. Shell and solid modelling techniques are studied in these studies and pros and cons of both technique is deeply investigated. A FEM implementation and experimental validation of viscoelastic material is also studies by Vasques et al. [31-32] in year 2010. Different FE implementation techniques of VEM modelling such as Golla-Hughes-McTavish (GHM), anelastic displacement fields (ADF) model and direct frequency response (DFR) which is based on the complex modulus approach (CMA), iterative modal strain energy (IMSE) and an approach based on an iterative complex eigensolution (ICE) is considered.

The detailed inspection of studies carried out until now, it is seen that there exists a high potential of developing a surface damping solution for a plate that has better performance than commercial used solutions and already suggested applications. In addition, the suggested metric for estimating the broadband dampening effect of the application using random input output system approach is not used before and can be used to represent the amount of increase in passenger comfort. Furthermore, there exist studies about topology and genetic algorithm optimizations for beams, yet for plates the suggested solutions are only for partial free layer and CLD coverages. Our suggested solutions based on previous optimized spacer geometries can be used for increasing damping performance on fuselage structures. Lastly, a fast prototype 3D printing method is used for spacer manufacturing which can bring fast and responsive solutions in aerospace applications for resonant frequency vibrations.

## CHAPTER 3

### DESIGN AND DEVELOPMENT OF REPRESENTATIVE FUSELAGE GEOMETRY

This study involves real life application simulation so in order to do that a representative fuselage geometry is designed and validated first to show damping performance of a novel standoff layer design for plates. In finite element model, first fuselage geometry needed to be represented. For generating CAD geometry, CATIA V5R22 software [44] is used as in aerospace industry. The sheet metal models were used in designing the stringers and C-frame of the fuselage. For fuselage parts commonly used aerospace structures and extrusion parts were selected. Given below stringer, C-frame and L-bracket extrusion designs shown in **Appendices A, B and C**. For outer skin plate to represent fuselage skin, square aluminum plate is chosen. Part dimensions and material information is given in below Table 3.1. For finite element modeling ABAQUS v6.14 [9] is used since nonlinear solvers of ABAQUS is more powerful compared to competitors and readily available software to use in aerospace industry. In analysis's performed, first frequency (modal) analysis is performed and then for fuselage validation steady-state direct analysis is performed for FRF extraction. For SOLD analysis, a complex frequency analysis step is also added for complex mode shape and natural frequency foundation.

Table 3.1. Part Attributes and Dimensions

	Length (mm)	Width (mm)	Depth (mm)	Thickness (mm)	Material	Temper
Stringer	260	30	25	1	AL 2024	T3
C-Frame	300	20	40	1.6	AL 2024	T3
L- Bracket	15	15	15	1	AL 2024	T3
Skin	300	300	-	1	AL 2024	T3

### 3.1. Theoretical Background of Riveted Joints

Amongst all joints, for sheet metal structures riveted joints are the most commonly used due to its ease of application and low weight. Aerospace and automotive industry uses riveted joints in fuselage, chassis and equipment installation frames. Although there are two main types of rivet joints, there exist several applications of these types differing how the sheet metals combined and whether rivet head is flat or left as spherical. All joints given in this section can be of two types named Lap or Butt joints.

#### 3.1.1. Lap Joints

This method is used when transferring the load in serial or stabilizing another part. This is the most common version used since there is no additional support plates other than load carrying plates, which reduced the added mass to system. In fuselage structures, grift sheet metal that overlap each other is used with this method to distribute the aerodynamic loads of outer skin. This joint type is the type used in this study to join fuselage like structure where the frames and stringers are connected to outer skin plate. Since no aerodynamic effects are of interest universal round (button) head is used.

### **3.1.2. Butt Joints**

This method used to transfer load from one structure to other by support plates which can carry more load but includes more mass to system. Main load carrying plates are placed butt to butt and connected to each other by riveted connection through other plate. Each support plate is called strap, because the main jobs is to tie plates each other. This method is commonly used in inner surfaces where there is no flat surface requirement and more load carry capacity is needed.

### **3.1.3. Riveted Connection Modelling Types**

In literature, there exist several modelling techniques depending which analysis will be performed, how complex load transfer is and whether or not the nonlinear effects of riveted joints are intended to be included. The easiest and most commonly used on solid structures is that coupling of the rivet holes to act together when the main concern is not around holes but the structure itself. Same procedure can be performed on sheet structures bonding the lap region to transfer load when the desired region to be inspected is not around rivets.

However, when the rivet locations and effects are important, rivet modelling techniques have an important role on analysis. For FEM, one can model the rivets in analysis such as Atre [36]; or model it as a beam element attached to node regions in the vicinity of fastener radius in FEM such as [33, 34]. If the model desired is small and has small numbers of rivets in it modelling it with solid element in solid model defining frictional and hard surface contact to simulate plastic deformation of rivet is the best solution to model riveted connections. However, considering an airplane, helicopter or even car chassis where the number of rivets are in the order of hundreds or even thousands modelling 2mm diameter rivets in solid elements with fine mesh creates high computational time and sources to be performed. At this point, beam elements that have stiffness have an important role to define riveted connections.

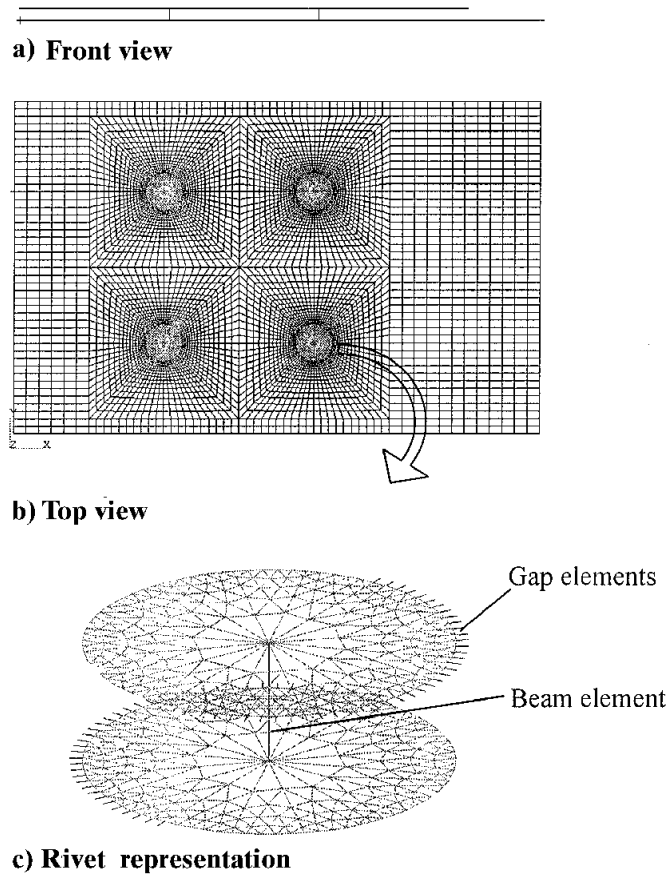


Figure 3.1. Rivet Modelling [31]

One of the most commonly used method in aerospace industry similar to Xiong and Bedair [31], is HUTH method. In HUTH method depending on the material types and row number stiffness value of the single rivet connection changes and can be assigned to beam element in fastener definition in FE software. Below is the HUTH formula given in Eq.22 and Eq.23 for non-axial and axial stiffness values.

$$f_{nonaxial} = \left( \frac{t_1 + t_2}{2d} \right)^a \frac{b}{n} \left( \frac{1}{t_1 E_1} + \frac{1}{nt_2 E_2} + \frac{1}{2t_1 E_f} + \frac{1}{2nt_2 E_f} \right) \quad (11)$$

$$f_a = \left( \frac{A_f E_f}{t_1 + t_2} \right) \quad (12)$$

Where;

$t_1 = 1^{st}$  layer thickness

$t_2 = 2^{nd}$  layer thickness

$d =$  Diameter of the rivet

$a =$  Joint coefficient depending on the material , 2/5 of metallic

$b =$  Joint coefficient depending on the material , 2.2 of metallic

$n =$  Rivet row

$E_1 = 1^{st}$  layer Youngs Modulus

$E_2 = 2^{nd}$  layer Youngs Modulus

$E_f =$  Fastener Youngs Modulus

$A_f =$  Fastener Area

As mentioned above, due to its low weight to load carrying capacity through shell structures, riveted joints are commonly used on fuselage and skin panels in industry. By using the riveted connection techniques above mentioned, it is decided to use lap joints with stiffness beam element to represent the riveted connections of the representative fuselage geometry. For stiffness beam model, above mentioned HUTH model, which is given name after its founder, is used that is commonly used in aerospace applications to define structural body joints.

### 3.2. Generating the Fuselage FE Model

The designed CAD model is imported in to ABAQUS software using step files. Below in Figure 3.2 and Figure 3.3 imported geometry can be seen. Both solid and shell models were generated but shell modelling technique is used for computational ease and convergence achieved after validation process for fuselage geometry. In ABAQUS software, after importing the geometry model is completed steps in the given order below,

- Defining Material
- Assigning Material Sections
- Meshing the Parts
- Creating Assembly
- Creating Steps (Solver Requests)
- Constraints (Tie, Coupling)
- Loads and BC's

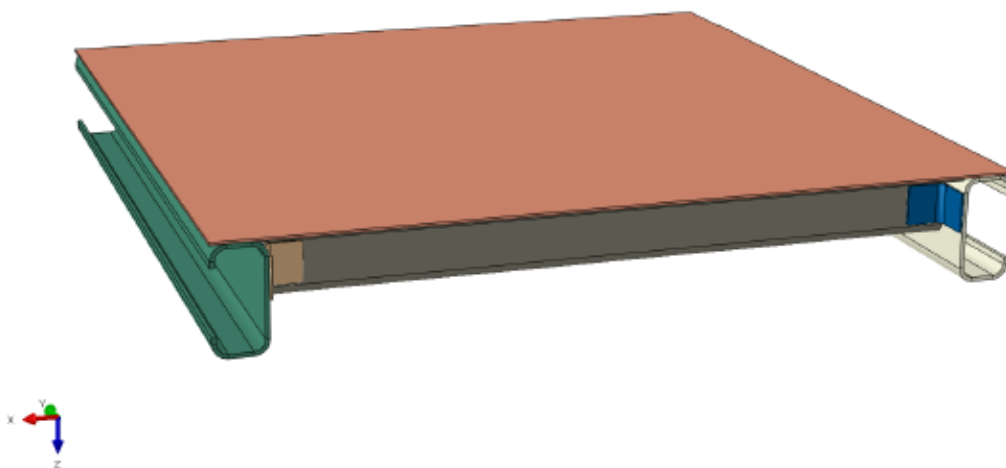


Figure 3.2. Solid Model

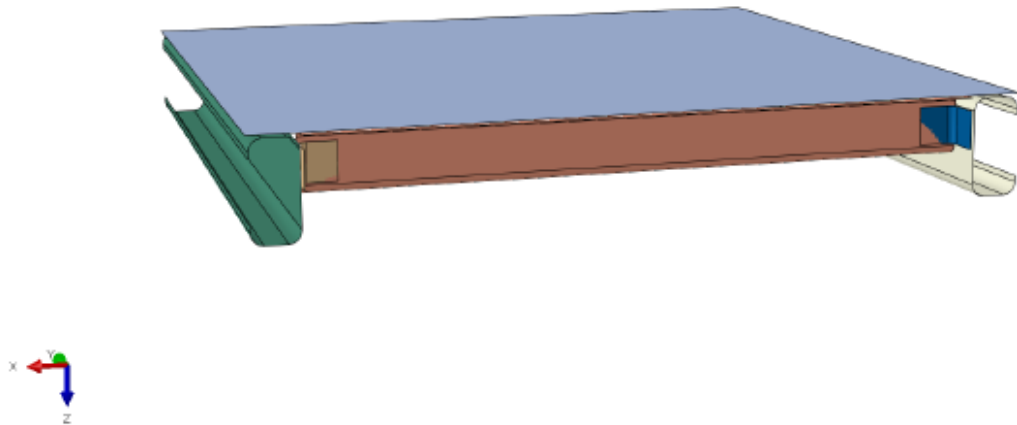


Figure 3.3. Shell Model

### 3.2.1. Defining Materials

In ABAQUS there is no material library and no default units. Due to that every material needs to be calculated according to imported geometry in the convenient units. This study uses mm, N, tons, MPa, sec, Hz as the units for analysis. By these units the acceleration obtained by FRF is  $\text{mm/s}^2$ . Below given in Table 3.2, material properties defined in ABAQUS GUI is shown with their units

Table 3.2. Material Properties

	Aluminum 2024 T3	ISD-112
Density ( $\text{tons/mm}^3$ )	2770	1040
Damping (Structural)	0.005	0.005
Elastic Modulus (Mpa)	70000	2400
Poisson's Ratio	0.33	0.49

In order to define these properties, in ABAQUS first material needs to be created. The shell definition and solid material definition differs when assigning the material so only shell material assignment is represented. Firstly, to create a material designer needs to open material dialog box by double clicking material under design FEM tree. After opening the dialog box desired material properties need to be added under material simply general density, mechanical elastic properties containing elastic modulus and poisson's ratio and mechanical damping. Below assigning process is summarized in Figure 3.4. After creating the material, shell section needs to be created for assignment on to parts. This process is done similar to material creation but under FEM tree section dialog box is opened. In dialog box, desired section type is selected and section name is given.

After approving selections new dialog box is opened giving opportunity to set shell thickness and material selection for the section. After these selections are performed one needs to go under parts to assign these sections on to parts. While doing that, dialog box asks whether the section is assigned as mid plane or top, bottom plane. Generally mid plane assignment is performed in aerospace industry and all imported geometry is designed as mid surface geometries. The section creation and section assignment is shown in Figure 3.5, Figure 3.6, Figure 3.7 representatively. These steps are repeated for each material. For shell structures that have same materials but different thicknesses, different sections need to be created different from solid sections. In solid sections, for each material one section is enough since thickness information is on part rather than sections. After material definition is performed for each part meshing can be performed for each part as described in next section.

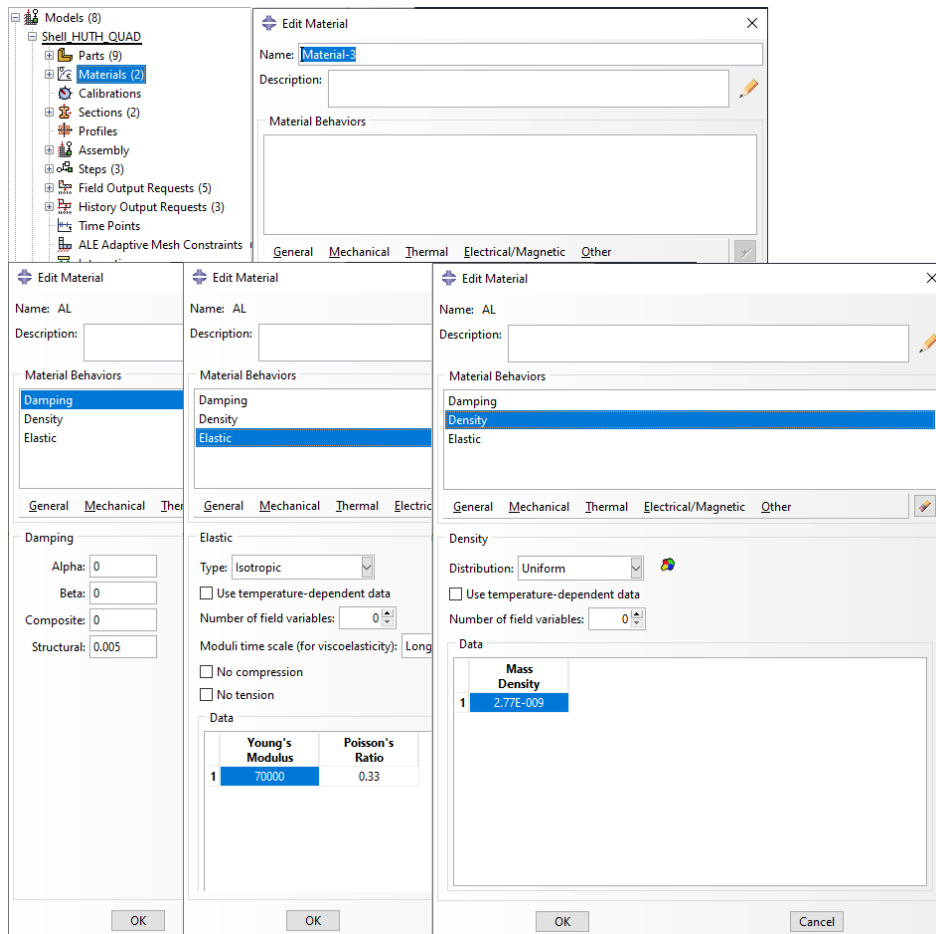


Figure 3.4. Material Definition in ABAQUS

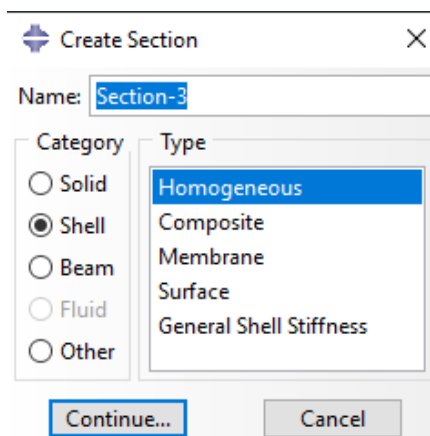


Figure 3.5. Section Definition Dialog box in ABAQUS

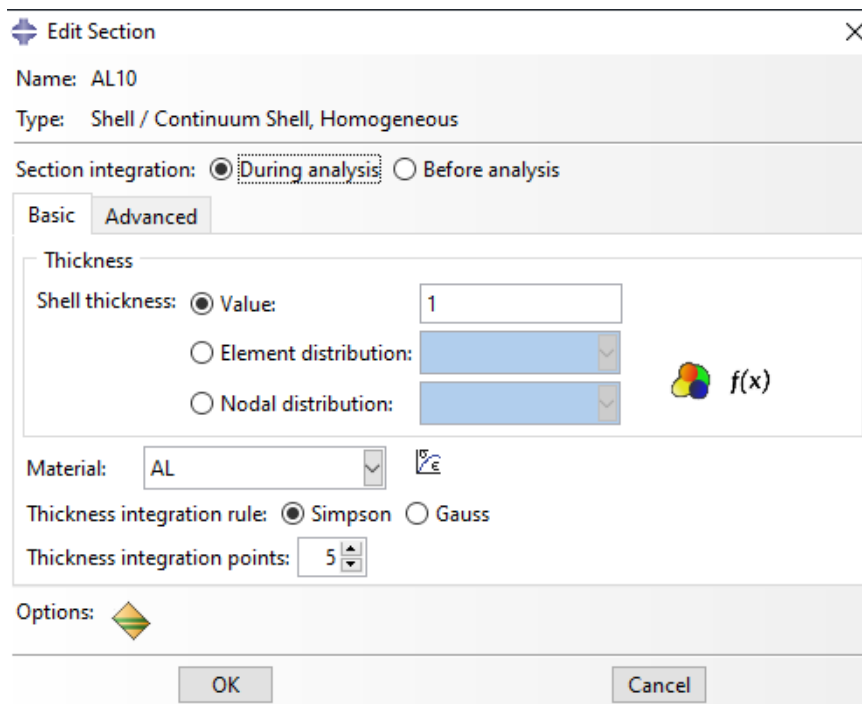


Figure 3.6. Section Material Definition in ABAQUS

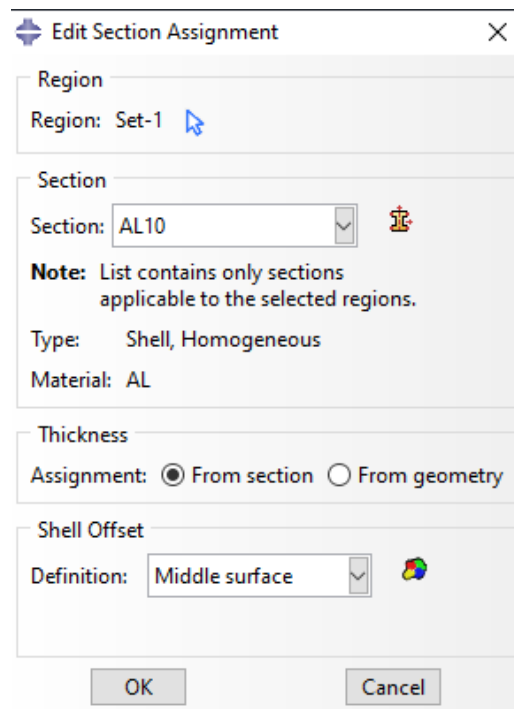


Figure 3.7. Section Assignment on to Parts in ABAQUS

### 3.2.2. Meshing Parts

After assigning related material properties to parts, second step in FEM is to mesh the parts. In this study, it is desired to have part dependent mesh in order to update the mesh and connections easily after changing the part dimensions or shape. For fuselage assembly, linear quadrilateral mesh (S4R) with 3mm mesh seed is used. In Figure 3.8 ABAQUS mesh types can be seen. For L-brackets [43], mesh seed is selected as 1.5mm for at least 10 elements in width of the part. These settings are applied under part attributes and whole domain is selected as mesh target. While selecting the mesh domain it is important to assign global settings as structured quadrilateral instead of quadrilateral dominant in order to mesh mapped structure for part. In order to achieve mapped structured quad mesh, the rivet holes are sewed in shell body before import process. In Figure 3.9 the meshed assembly can be seen. The mesh of this type S4R is selected with testing of a free-free plate harmonic analysis with performance and converge analysis. The outer skin plate is meshed with different solid and shell elements and compared with analytical results. The fastest and closest results were obtained with S4R for thin shell metal parts and to represent the fuselage geometry this mesh was selected to be used. The analytical results of the plate is given in Eq.24 as given in [45]. Mode shapes and modal parameters for analytical solution is given in Figure 3.10. The comparison of meshes and their results were given in Figure 3.11 and Table 3.3. Mesh Comparison Table. Among all possible mesh types the S4R was the fastest and most convergent with thirteen minutes of computational time. D3D20R and D3D10 was also close to analytical solutions; however, their computational times were long such as 660 minutes and 70 minutes respectively. In the light of these results, S4R was chosen for fuselage geometry in the future analysis purposes.

$$f_{ij} = \frac{\lambda_{ij}^2}{2\pi a^2} \left[ \frac{Eh^3}{12\gamma(1-\nu^2)} \right]^{\frac{1}{2}} ; \quad i = 1,2,3 \dots ; j = 1,2,3 \dots \quad (13)$$

Where;

$a = \text{Width of plate}$

$b = \text{Length of plate}$

$f_{ij} = \text{Natural Frequency of } ij^{\text{th}} \text{ mode}$

$E = \text{Elastic Modulus of plate}$

$\nu = \text{Poisson's Ratio of plate}$

$h = \text{Thickness of plate}$

$\gamma = \text{Density of plate}$

$\lambda_{ij}^2 = \text{Boundary Condition Mode Square}$

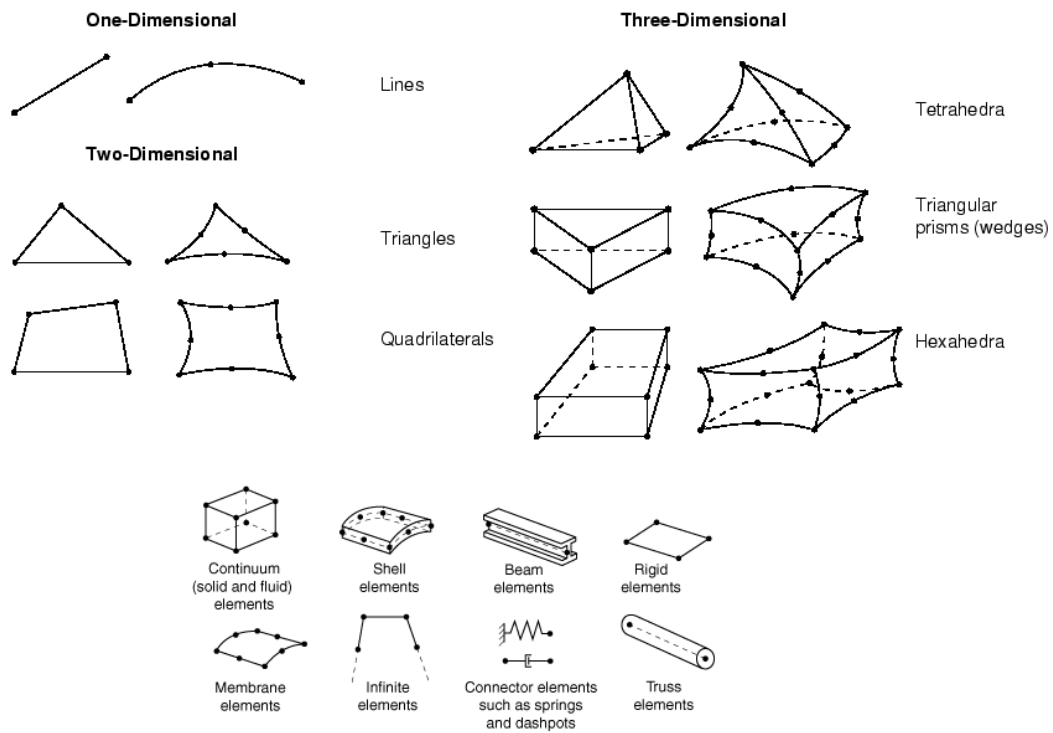


Figure 3.8. Mesh types in ABAQUS [9]

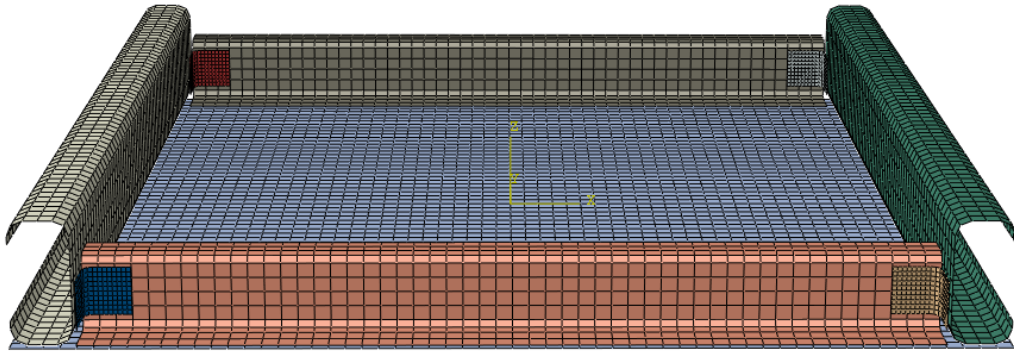
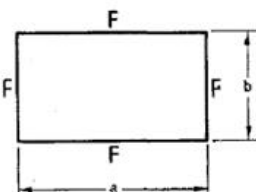
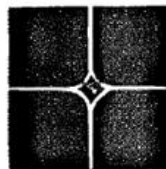


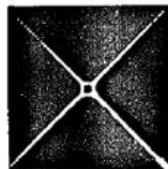
Figure 3.9. Meshed Fuselage Geometry

Description	$\lambda_{ij}^2$ and (ij)					
	Mode Sequence					
1. Free-Free - Free-Free						
	$\frac{a}{b}$	1	2	3	4	5
	0.4	3.483 (13)	5.288 (22)	9.622 (14)	11.44 (23)	18.79 (15)
	2/3	8.946 (22)	9.602 (13)	20.74 (23)	22.35 (31)	25.87 (16)
	1.0	13.49 (22)	19.79 (13)	24.43 (31)	35.02 (32)	61.53 (41)
	1.5	20.13 (22)	21.60 (31)	46.65 (32)	50.29 (13)	58.20 (41)
	2.5	21.04 (31)	33.05 (22)	60.14 (41)	71.48 (32)	117.5 (51)
						119.4 (42)

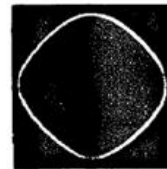
$\nu = 0.3$ ; (ij) = (11), (12), (21) are rigid body modes. Also see Ref. 11-82.



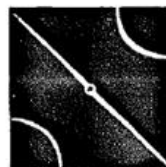
$i = 2, j = 2$   
 $\lambda_{22}^2 = 13.49$



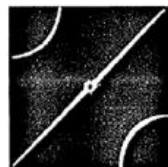
$i = 1, j = 3$   
 $\lambda_{13}^2 = 19.79$



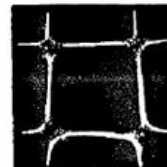
$i = 3, j = 1$   
 $\lambda_{31}^2 = 24.43$



$i = 3, j = 2$   
 $\lambda_{32}^2 = 35.02$



$i = 2, j = 3$   
 $\lambda_{23}^2 = 35.02$



$i = 4, j = 1$   
 $\lambda_{41}^2 = 61.53$

Figure 3.10. Analytical Solution of a Free-Free Plate [45]

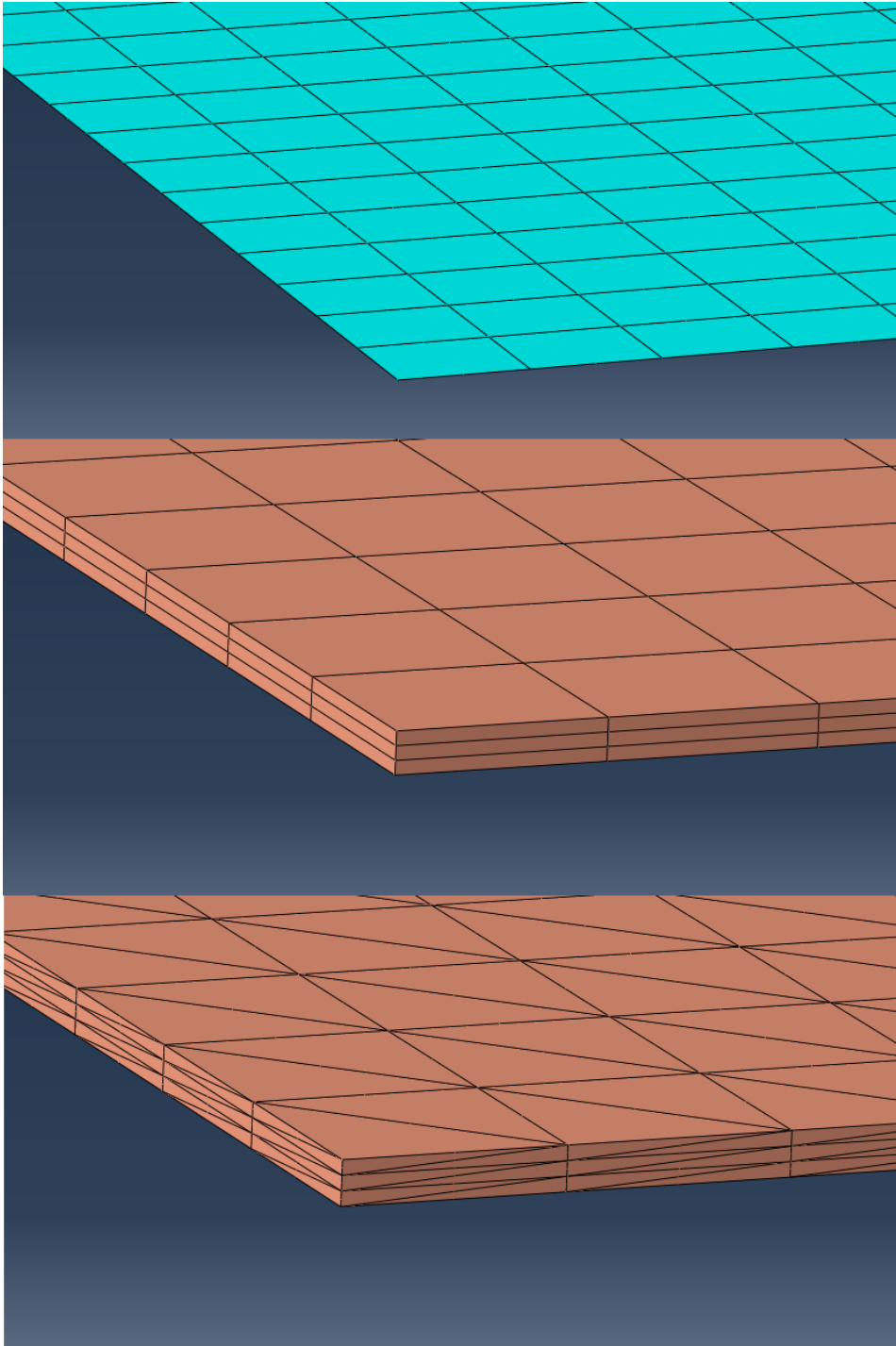


Figure 3.11. Mesh Comparison Mesh Types Shell-Solid Quad-Solid Tet

Table 3.3. Mesh Comparison Table

Analytical Model		Shell Model (S4R)		Solid Hex Linear (D3D8R)		Solid Hex Quadratic (D3D20R)		Solid Tetrahedron Linear (D3D4)		Solid Tetrahedron Quadratic (D3D10)	
Mode Number	Frequency (Hz)	Mode Number	Frequency (Hz)	Mode Number	Frequency (Hz)	Mode Number	Frequency (Hz)	Mode Number	Frequency (Hz)	Mode Number	Frequency (Hz)
1	0	1	0	1	0	1	0.05	1	0	1	0
2	0	2	0	2	0	2	0.05	2	0.01	2	0
3	0	3	0	3	0.01	3	0.05	3	0.01	3	0
4	0	4	0	4	0.01	4	0.11	4	0.01	4	0
5	0	5	0	5	0.01	5	0.12	5	0.01	5	0
6	0	6	0	6	0.02	6	0.12	6	0.01	6	0
7	36.9	7	38 (%3)	7	58.6 (%59)	7	38.1 (%3)	7	329.6 (%792)	7	39.4 (%7)
8	54.2	8	56.3 (%4)	8	70.5 (%30)	8	56.1 (%3)	8	347.9 (%542)	8	67.9 (%5)
9	66.9	9	67.1 (%0)	9	176.7 (%164)	9	67.1 (%0)	9	906.3 (%1255)	9	67.9 (%2)
10	95.9	10	95.8 (%0)	10	186.4 (%94)	10	95.7 (%0)	10	950.1 (%891)	10	97.9 (%2)
11	95.9	11	96.2 (%0)	11	318.3 (%232)	11	96.2 (%0)	11	989.9 (%932)	11	99 (%3)
12	168.5	12	167.4 (%1)	12	332.9 (%98)	12	167 (%1)	12	-	12	170.5 (%1)

### 3.2.3. Defining Riveted Joints

The later step in modelling is to create an assembly from parts and then define the riveted joints. The parts under the parts module in ABAQUS cannot be used unless they are defined under assembly module. This can be done double clicking the assembly and selecting representative parts. After the related parts are imported under assembly their positional constraints should be checked and after corrected all positional constraints should be converted as deleted in order to analysis to be performed. The connections between parts will be defined under constraints module later if needed.

For riveted joints, as explained before beam elements with stiffness in every degree of freedom shall be defined and assigned as a fastener in assembly module in a similar way as Xiong and Bedair [31]. To define a beam element, under connector sections

basic connector with Cartesian-Cardan coordinate system shall be selected. In the opened dialog box elastic behavior with six degrees of freedom is selected and calculated material properties with HUTH method is entered under related axis properties. The most important thing while defining the connector is that defining the axes considering the rivet coordinate system. Due to all rivet axes are located in z-direction in assembly of this study, axial material properties are entered to D33 and D66 respectively as given in Figure 3.12.

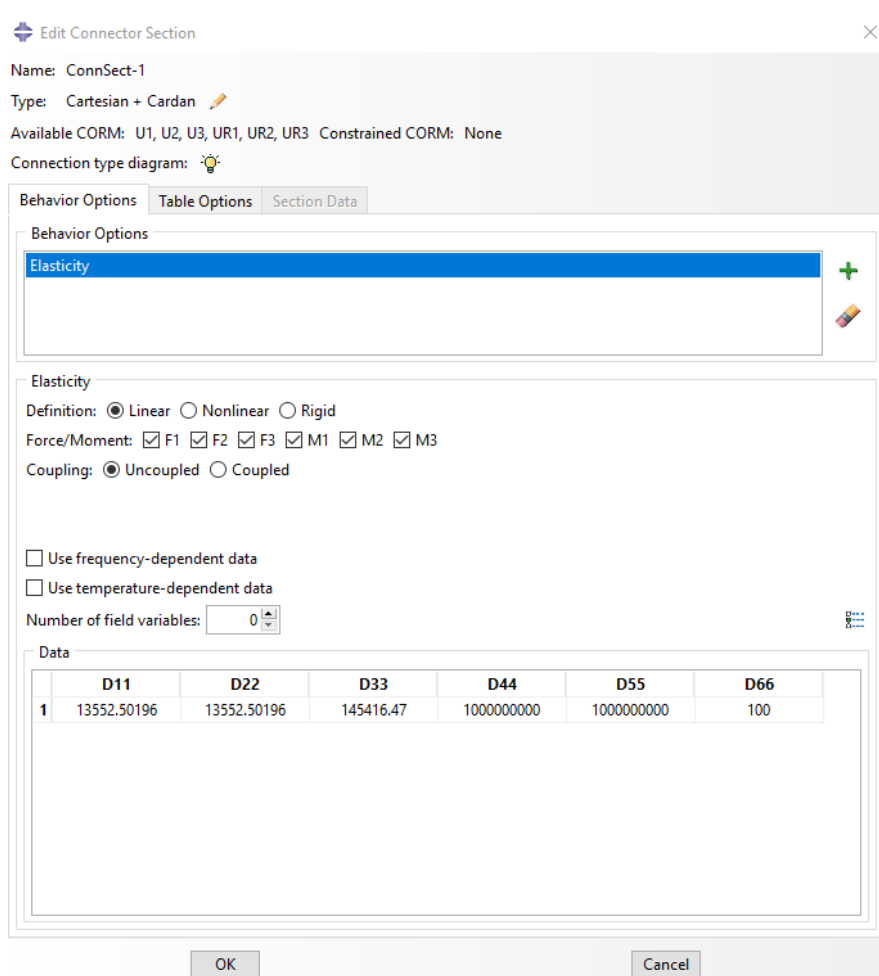


Figure 3.12. Creating Connector Section in ABAQUS

This process defines a connector section to be assigned for fasteners or connectors. To be able to define a connector as in [31], in ABAQUS attachment points and attachment lines needs to be generated to define each rivet body. To define them, in assembly module a datum point is created for each rivet head center. And to create a rivet body, attachment lines are created along direction of rivet axis using only rivet head center point. This method creates both rivet axis and rivet bottom center attachment point in the process. After creating attachment lines, the defined connector section is defined for each line created as shown in Figure 3.13 under fastener definition dialog box. the rivet head radius and axis propagation method with respect to coordinate system shall be defined while defining riveted joints. The weighting method is selected as uniform since every rivet carries the load equally in its own axis along rivet head to rivet bottom. Also it is an important parameter to define the rivet mass per each rivet under fastener definition since faulty values under that gives divergent results from the real case. The defined HUTH method rivets are shown in Figure 3.14 and Figure 3.15. Figure 3.14 shows the rivet head center and bottom center representatively and Figure 3.15 shows the connected nodes in the vicinity of fastener radius.

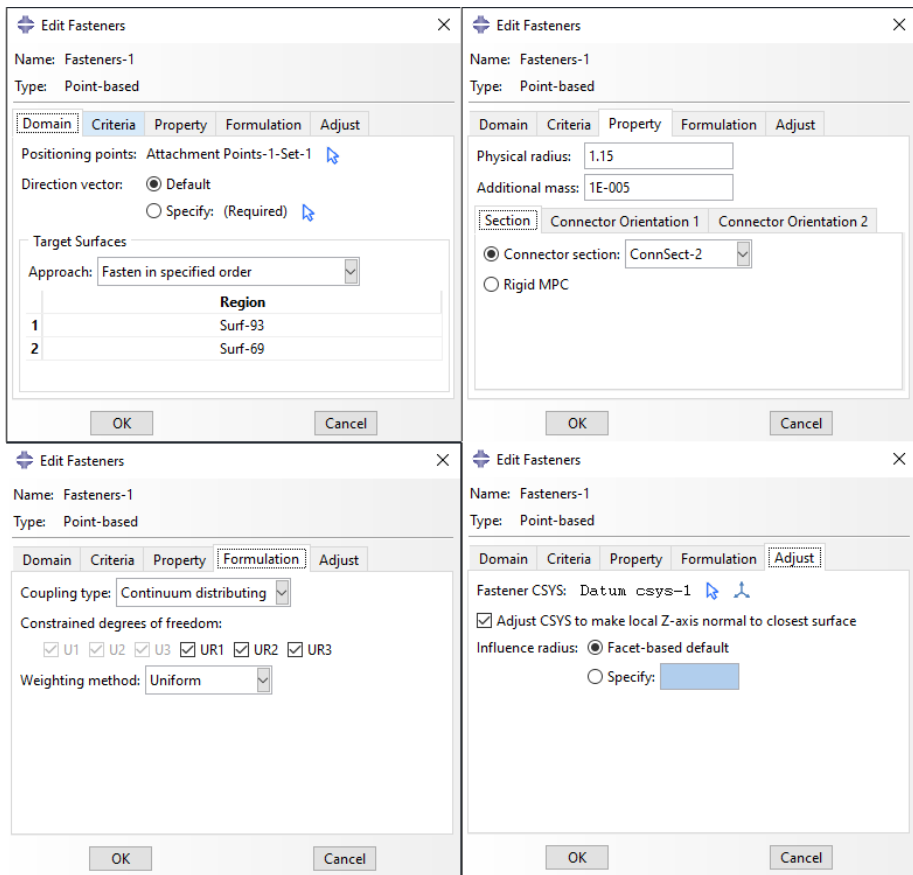


Figure 3.13. Fastener definition in ABAQUS

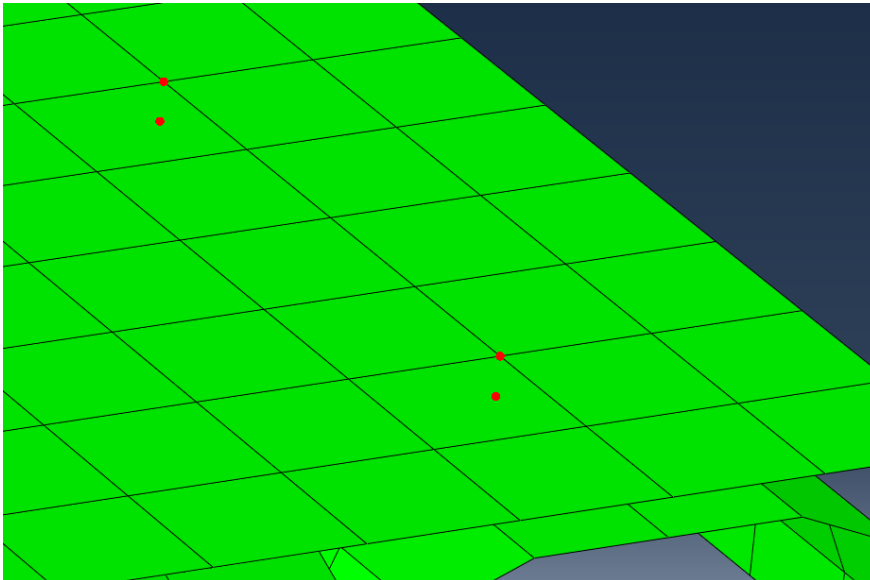


Figure 3.14. Fastener definition in ABAQUS rivet top and bottom centers

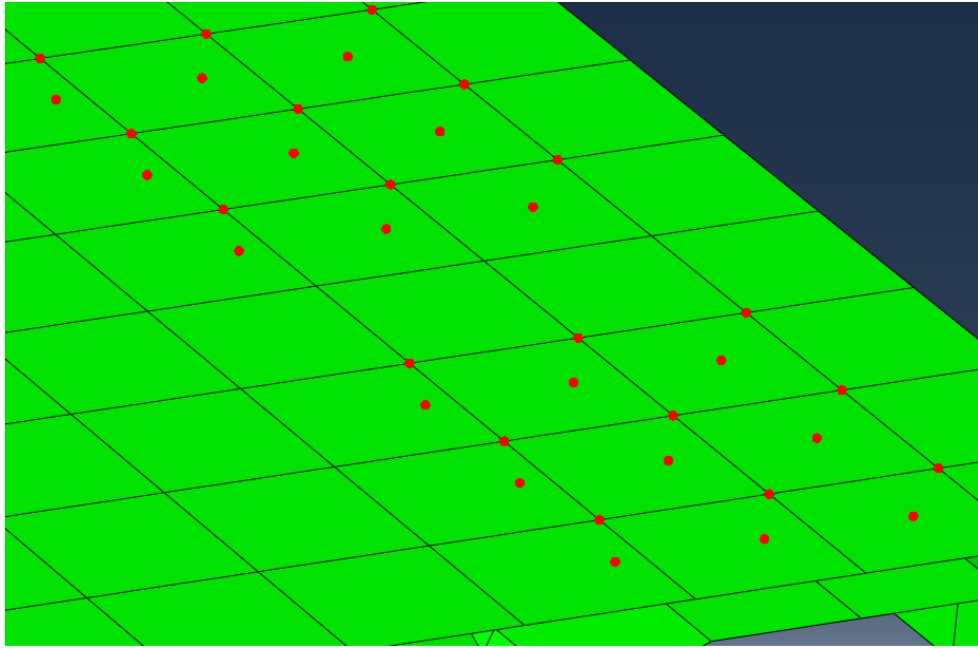


Figure 3.15. Fastener definition in ABAQUS connected nodes

### 3.3. Validation of Fuselage Geometry

In order to use the designed fuselage geometry, first it is needed to validate the finite element model of the bare fuselage geometry without any damping treatment. Since there exist sixty-four riveted joints between nine parts there exist lots of nonlinearities due to riveted joints and appropriate finite element model has to be generated to simulate the damping performance in the future analysis that has to be done. The finite element model of fuselage geometry first tried with tie command for interacting parts, which acts as a glue command in ABAQUS, but the results of the tie command are not satisfactory enough and a further simulation of riveted joints were needed to be implemented in to the model. As explained before in chapter four, HUTH modelling of riveted joints were utilized for better convergence between experimental and finite element results. After creating the finite element model as described in chapter four, the results were obtained as given in the following sub chapter. The rivet mass added, interaction surface partitions and additional accelerometer mass influence radius were changed until a good convergence has obtained through out the process. Only the final results were given for finite element model since there exists lots of trials and errors

throughout the beginning and the best convergence is obtained with normal hard contact interaction definition along with HUTH modelling with very low additional mass for rivets. The additional mass of the rivets are 0.1 grams for each rivet.

### **3.3.1. Finite Element Results**

This section briefly summarizes the HUTH solution for fuselage geometry with above mentioned analysis steps. To validate the fuselage geometry two accelerometer is placed in analysis as reference points with the influence radius of accelerometer radius to simulate the effects. Also additional inertial mass is assigned to these points since accelerometer and cables attached has a finite mass contributing to the system. Below, finite element results can be found that are used to be compared with the test results. The mode shapes and natural frequencies are compared through modal assurance criteria (MAC) and two cross point frequency response functions (FRFs) were compared since for damping FRF comparison will be used to measure damping performance through half power bandwidth method.

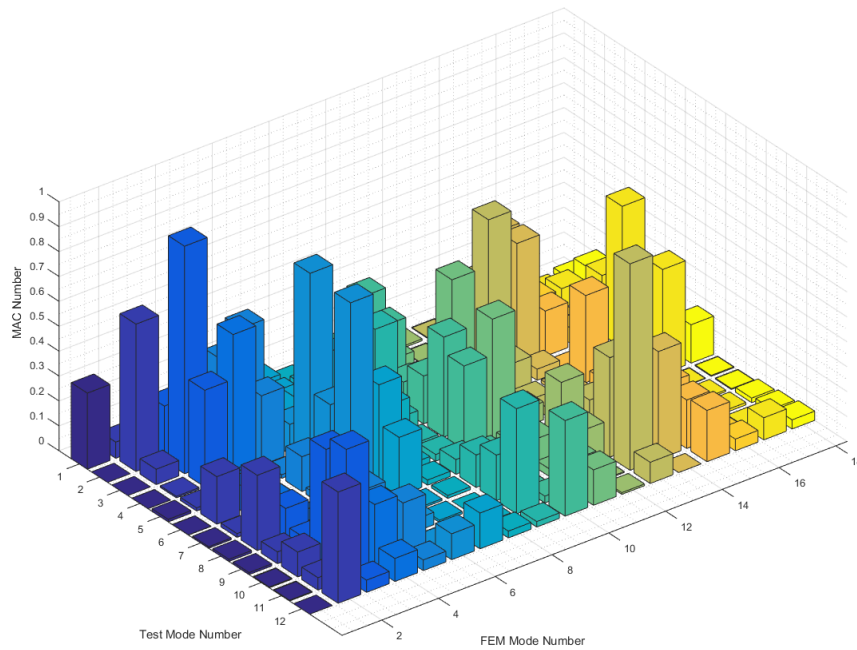


Figure 3.16. MAC Comparison of FEM and Experimental Results

In order to get the best output from accelerometers and excite the system with impact hammer possible areas were tried as seen from Figure 3.17. These points are also used for eigenvector extraction.

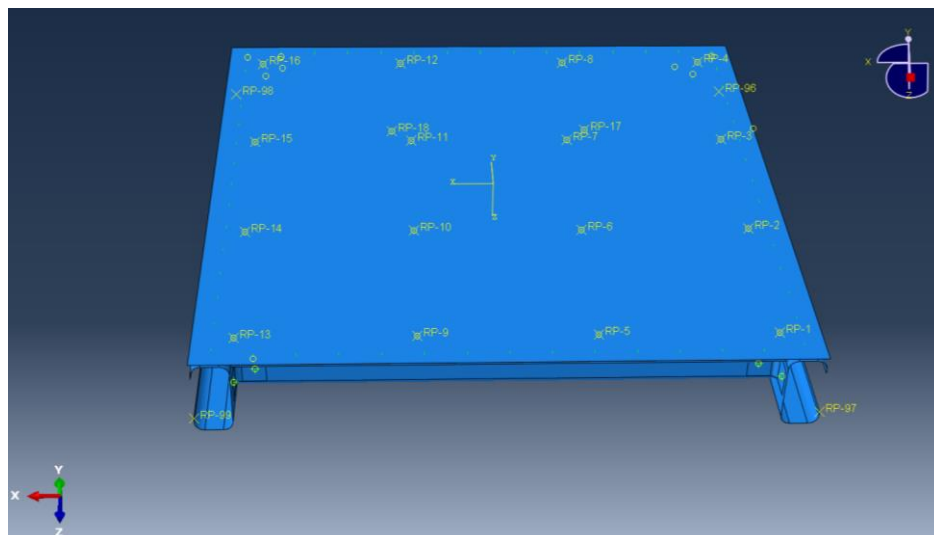


Figure 3.17. Eigenvector locations that are used in MAC

In experiment it is found that for cross point FRF extraction, it is best to excite the system from point 10 and get outputs from 7-16 from the locations shown in Figure 3.17.

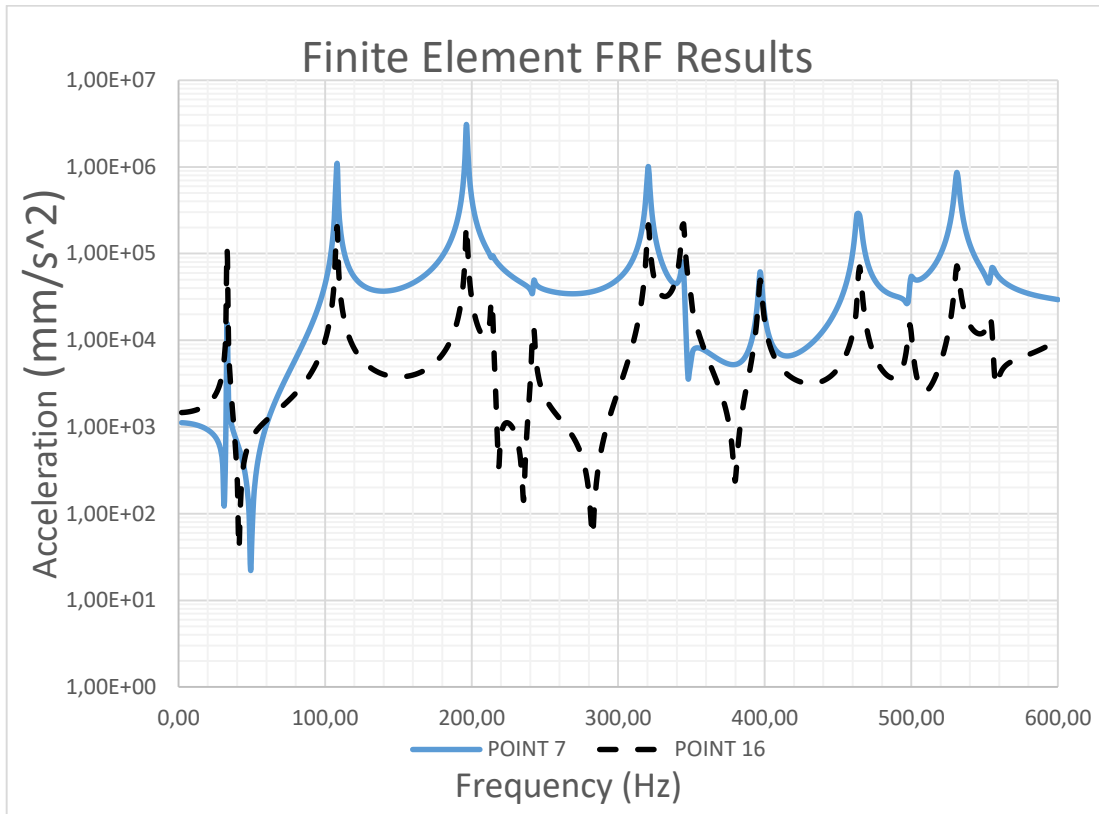


Figure 3.18. FRF Results for Impact Location 10 Output Locations 7 and 16

Table 3.4. FEM Modal Results

	Mode 1 (Hz)	Mode 2	Mode 3	Mode 4	Mode 5	Mode 6
Natural Frequency (Hz)	0	0	0	0	0	0
	Mode 7	Mode 8	Mode 9	Mode 10	Mode 11	Mode 12
Natural Frequency (Hz)	33.0904	107.853	196.464	213.791	241.949	320.417
	Mode 13	Mode 14	Mode 15	Mode 16	Mode 17	Mode 18
Natural Frequency (Hz)	344.168	350.219	396.854	463.234	464.656	499

However, MAC results show that there exist pseudo modes in FEM that are not caught by experiment or due to FEM related issues and the representative modal values corrected are as follows in the target range.

Table 3.5. FEM Modal Results in target range Corrected

	Mode 1 (Hz)	Mode 2	Mode 3	Mode 4	Mode 5	Mode 6
Natural Frequency (Hz)	0	0	0	0	0	0
	Mode 7	Mode 8	Mode 9	Mode 10	Mode 11	Mode 12
Natural Frequency (Hz)	33.0904	107.853	196.464	213.791	320.417	344.168

Table 3.6. Impact Locations for Roving Hammer Test and Eigenvector Locations

Point Number	X-Coordinate	Y-Coordinate
Pt 1	20	20
Pt 2	20	106.666
Pt 3	20	193.332
Pt 4	20	280
Pt 5	106.666	20
Pt 6	106.666	106.666
Pt 7	106.666	193.332
Pt 8	101.566	280
Pt 9	193.332	20
Pt 10	193.332	106.666
Pt 11	193.332	193.332
Pt 12	198.432	280
Pt 13	280	20
Pt 14	280	106.666
Pt 15	280	193.332
Pt 16	280	280

### 3.3.2. Experimental Results

In order to use the FEM generated for fuselage geometry for damping analysis, the model should be validated because the geometry is a new design and to be sure that the dynamic behavior is estimated correctly. A roving hammer test is found to be best suitable test method to achieve the mode shapes and modal parameters for the geometry with low additional mass. The test was performed as same as in finite element model as free-free condition by using soft sponges under corners of the frames as shown in Figure 3.19. The mode shapes; only first four non-rigid modes, and natural frequencies of the test results were given in following figures and Table 3.7. Experiment Modal Results. The experimental test was performed in METU Mechanical Engineering B Block Automotive Laboratory with the help of Asst. Prof. Dr. Gökhan O. Özgen. Figure 3.21 and Figure 3.22 shows the piezo accelerometer and impact hammer used in the experimental studies. Between Figure 3.23 and Figure 3.26 mode shape results are given after extraction of eigenvectors. The frequency response function results for both simulation and experiments are given in Figure 3.27 and Figure 3.28 respectively.

Table 3.7. Experiment Modal Results

	Mode 1 (Hz)	Mode 2	Mode 3	Mode 4	Mode 5	Mode 6
Natural Frequency (Hz)	0	0	0	0	0	0
	Mode 7	Mode 8	Mode 9	Mode 10	Mode 11	Mode 12
Natural Frequency (Hz)	30.6	120	212	232	326	341
	Mode 13	Mode 14	Mode 15	Mode 16	Mode 17	Mode 18
Natural Frequency (Hz)	378	423	510	519	555	651

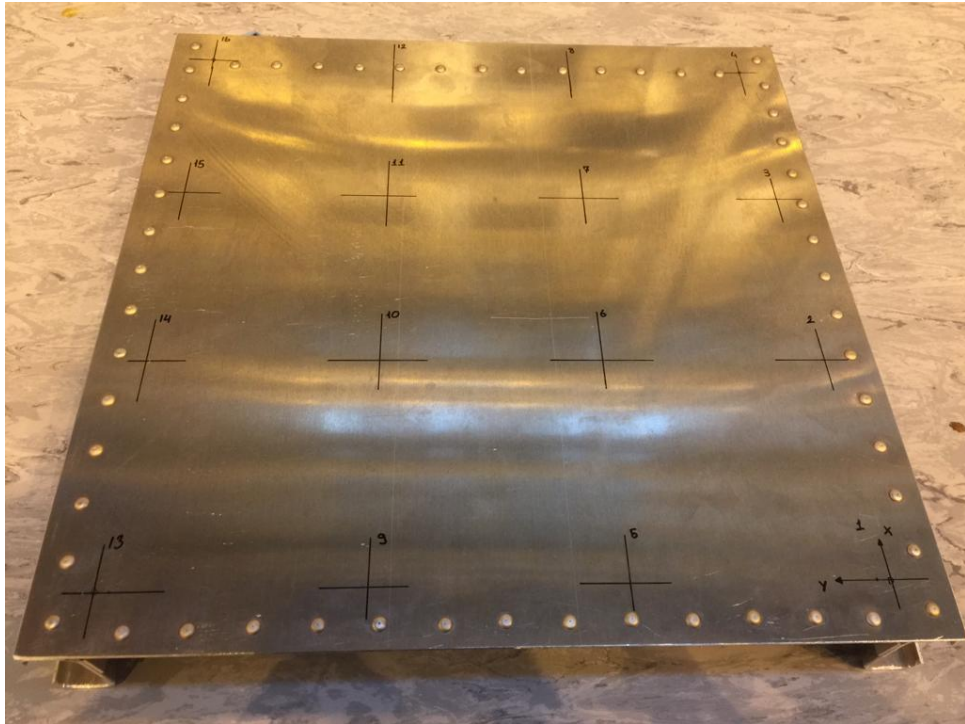


Figure 3.19. METU Experiment Bare Plate Accelerometer and Impact Locations

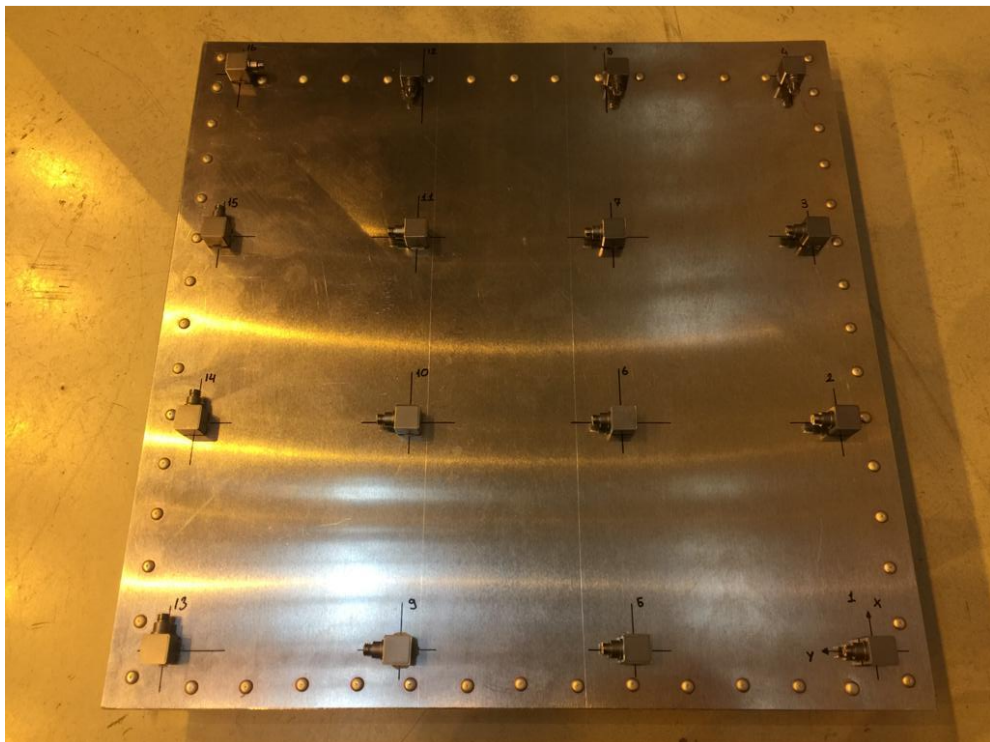


Figure 3.20. Accelerometer points selection for best outputs

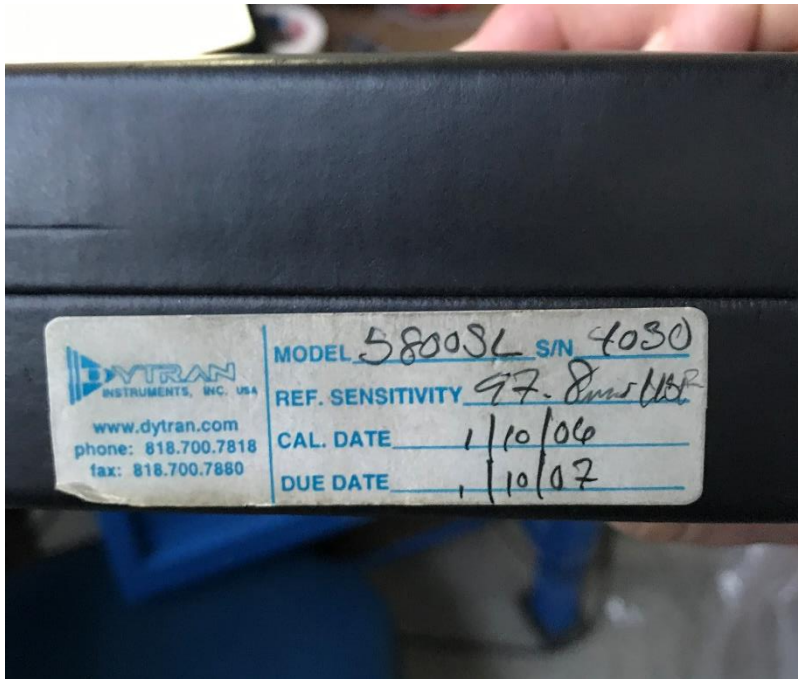


Figure 3.21. Accelerometer that is used in experiment



Figure 3.22. Impact hammer used in experiment

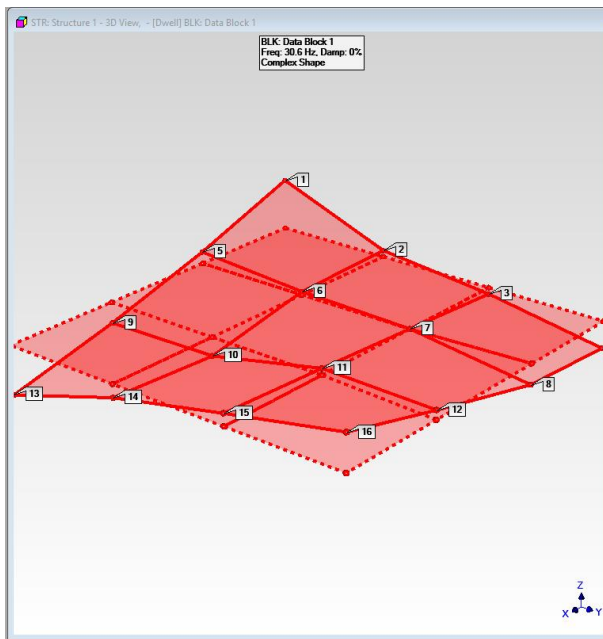


Figure 3.23. METU Experiment Mode Shape I

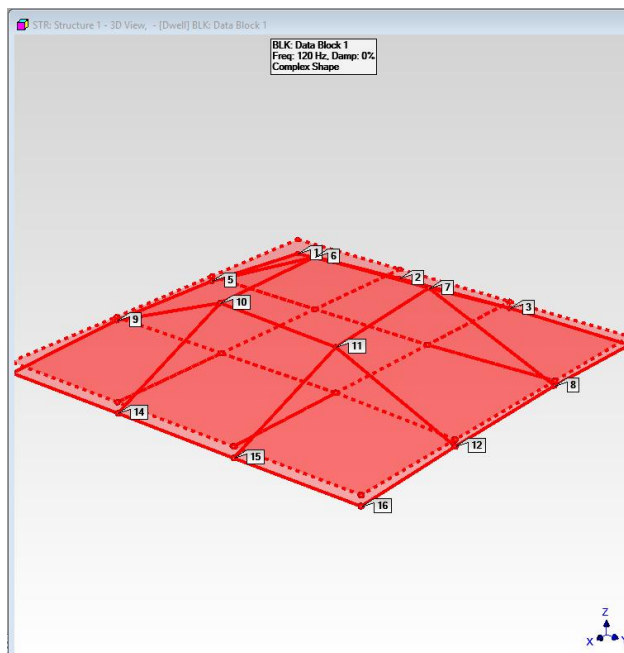


Figure 3.24. METU Experiment Mode Shape II

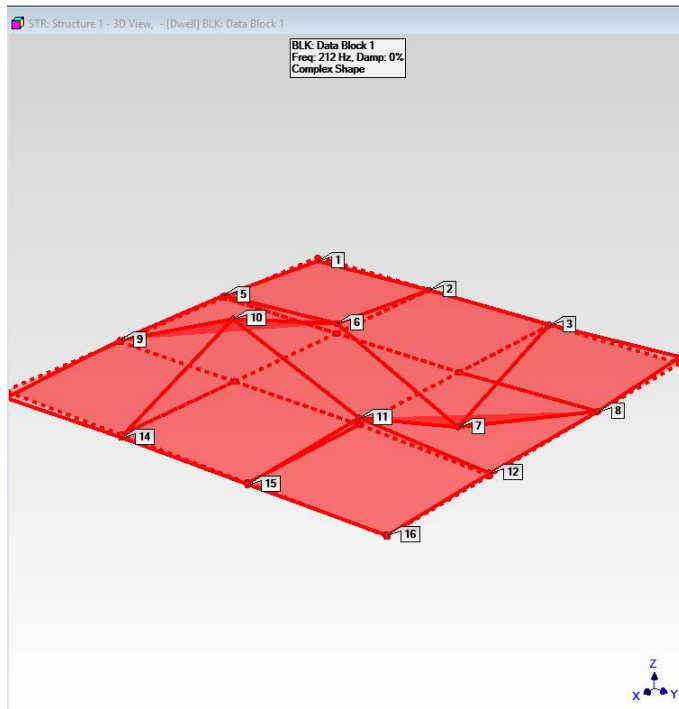


Figure 3.25. METU Experiment Mode Shape III

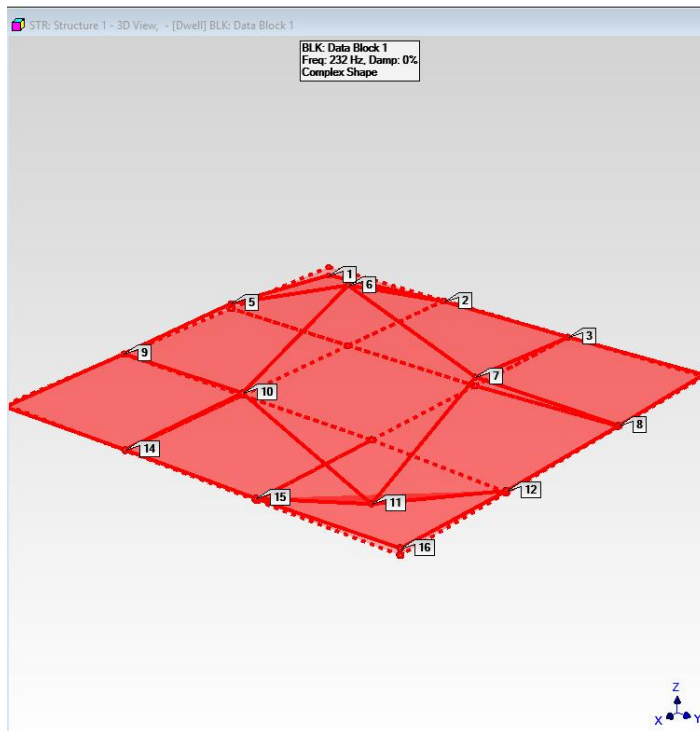


Figure 3.26. METU Experiment Mode Shape IV

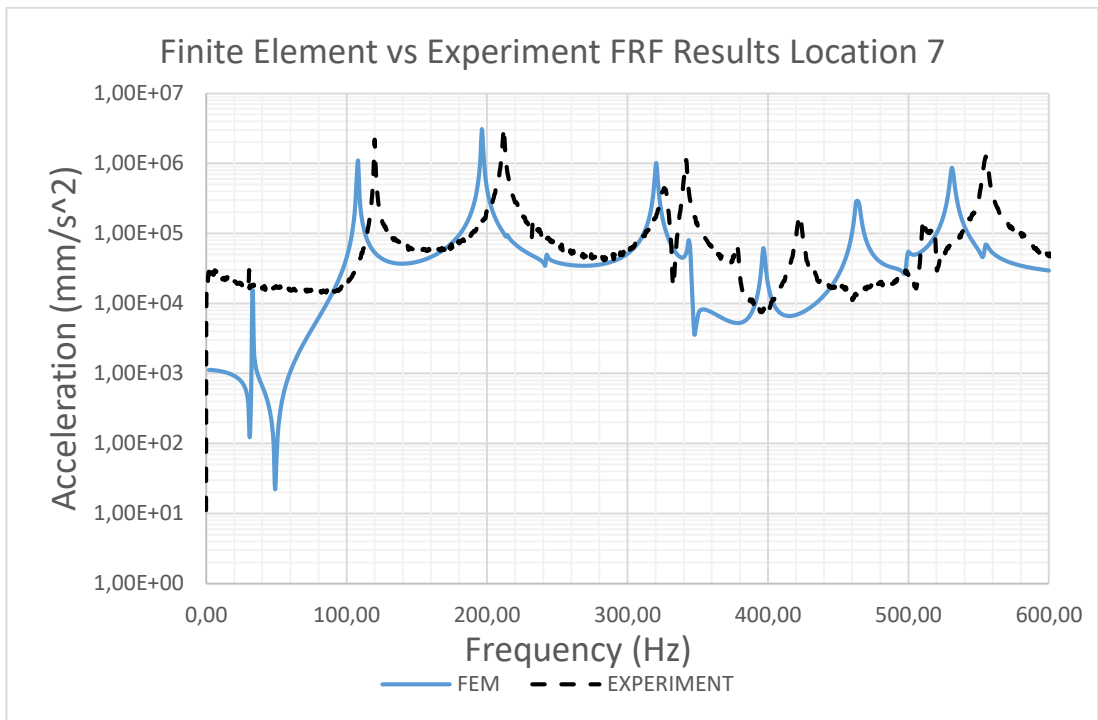


Figure 3.27. FEM vs Experimental FRF Results Impact Location 10 Output Location 7

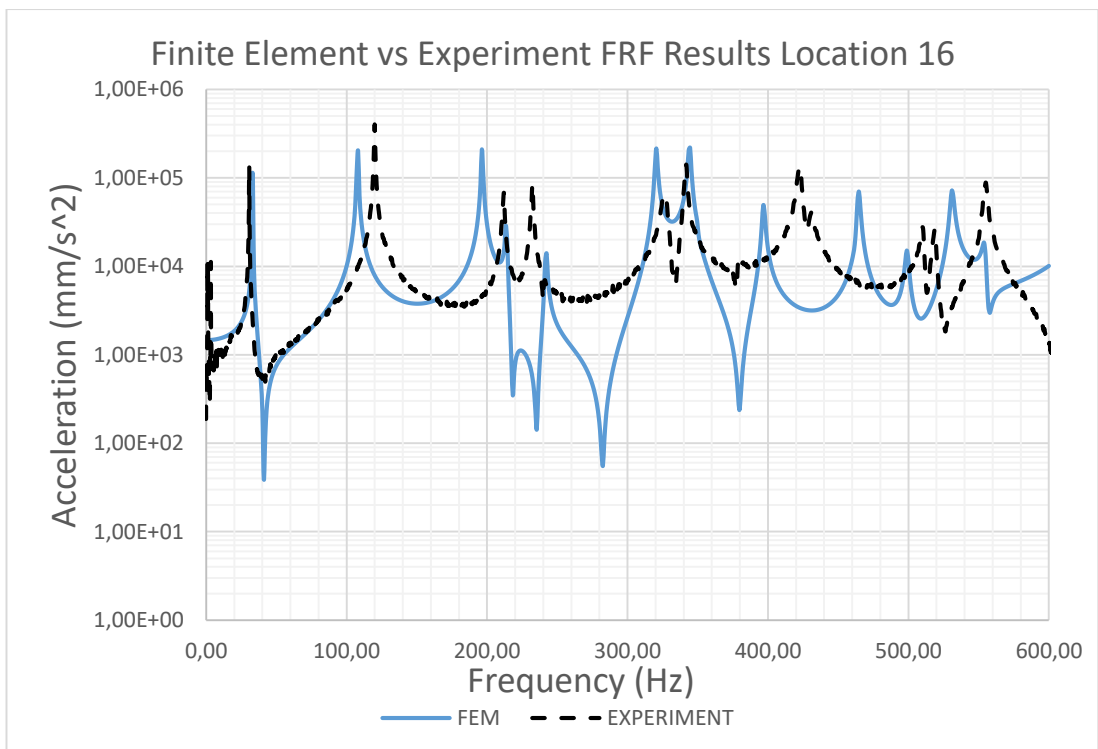


Figure 3.28. FEM vs Experimental FRF Results Impact Location 10 Output Location 16

### 3.4. Generating the Surface Damping Treated Fuselage FEM

For the damped fuselage FEM, all procedures until now is repeated for fuselage part. For the constrained layer and stand-off layer definitions are similar for material definition. The difference between two models is related with viscoelastic material definition which is explained in the following section in a detailed way. The definition of a viscoelastic material in ABAUS has its own way and one must be careful while defining it. The formations taken from [9] is given below and entered accordingly under material definition interface.

#### 3.4.1. Defining Viscoelastic Material Properties

As defined in previous chapters, viscoelastic materials have both temperature and frequency dependent material properties. ABAQUS has an option to define these properties with ease under software interface. To be able to define viscoelastic material properties, the first step is to calculate the properties with the given Eq.14 using the parameters given in [40] for ISD-112. MATLAB software is used for convenience to calculate properties. Once complex shear modulus is calculated with Eq.14 given the real and complex parts of it has to be converted in to the form that ABAQUS can read it. This conversion is performed by the given formulas below Eq.15 through Eq.18. Due to our analysis type bulk modulus terms can be ignored while material definition process.

$$G^* = G(1 + i\eta) = G_e + \frac{G_1}{1 + c_1 \left(i \frac{f_r}{f_1}\right)^{-\alpha_1} + \left(i \frac{f_r}{f_1}\right)^{-\beta_1}} \quad (14)$$

Where;

$$G_e = 0.4307 \text{ MPa}$$

$$G_1 = 1200 \text{ MPa}$$

$$f_1 = 0.1543 \times 10^7 \text{ Hz}$$

$$\alpha_1 = 0.18$$

$$\beta_1 = 0.6847$$

$$c_1 = 3.241$$

$f_r = \text{reduced frequency} = f * \alpha(T)$ ,  $\alpha(T) = \text{Temperature shift factor}$

$$\omega R(g^*) = \frac{G_l}{G_\infty} \quad (15)$$

$$\omega I(g^*) = 1 - \frac{G_s}{G_\infty} \quad (16)$$

$$\omega R(k^*) = \frac{K_l}{K_\infty} \quad (17)$$

$$\omega I(k^*) = 1 - \frac{K_s}{K_\infty} \quad (18)$$

Where;

$G_l = \text{Imaginary part of the complex Shear Modulus}$

$G_s = \text{Real part of the complex Shear Modulus}$

$G_\infty = \text{Long - term Shear Modulus (calculated at 0 Hz)}$

$K_l = \text{Imaginary part of the complex Bulk Modulus}$

$K_s = \text{Real part of the complex Bulk Modulus}$

$K_\infty = \text{Long - term Bulk Modulus (calculated at 0 Hz)}$

The calculated properties are entered through interface as shown in Figure 3.29 through Figure 3.33. For elastic modulus under elasticity definition elastic modulus calculated based on long-term shear modulus is entered since ABAQUS calculates  $G_{\infty}$  from the entered value.

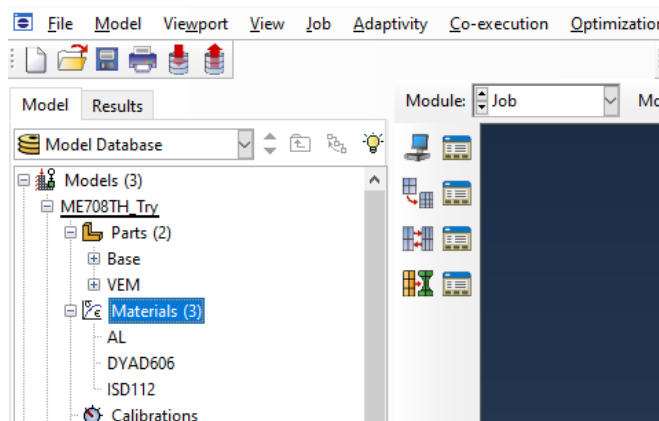


Figure 3.29. ABAQUS Viscoelastic Material Definition I

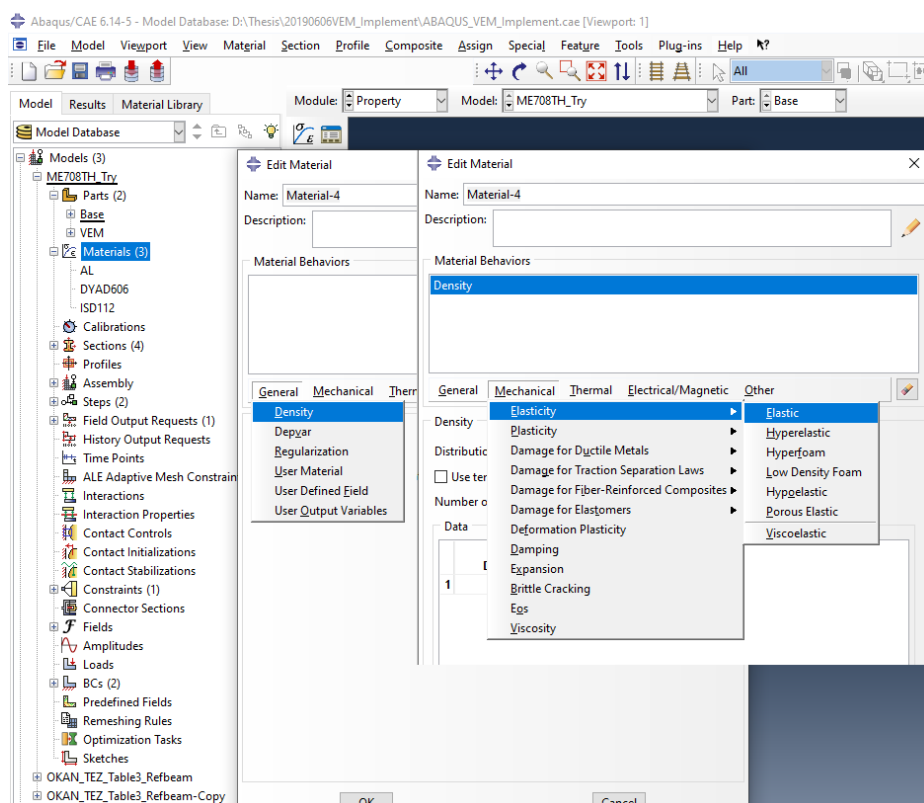


Figure 3.30. ABAQUS Viscoelastic Material Definition II

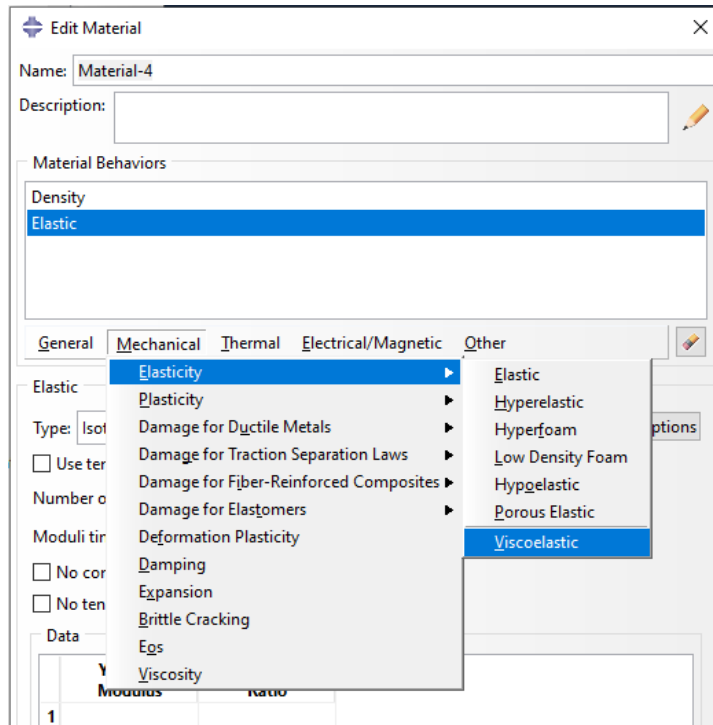


Figure 3.31. ABAQUS Viscoelastic Material Definition III

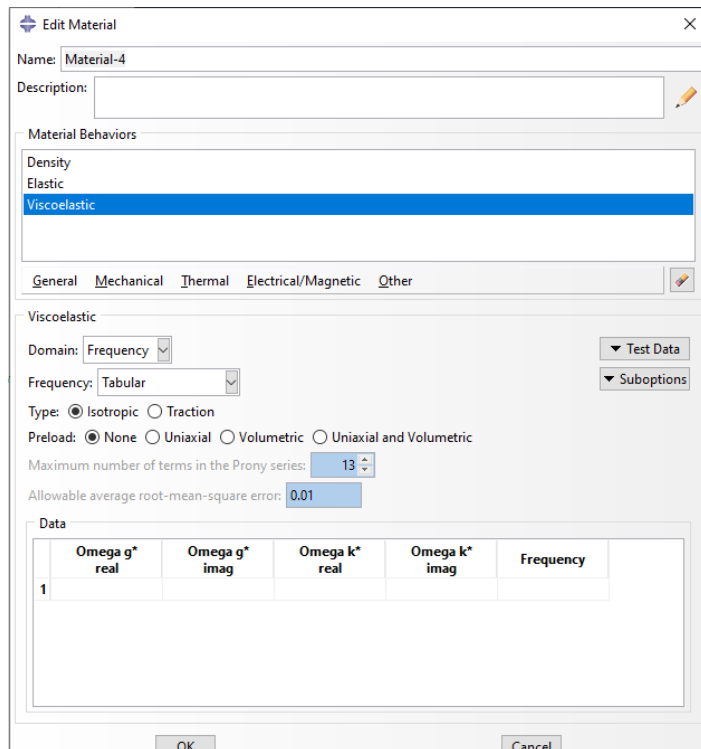


Figure 3.32. ABAQUS Viscoelastic Material Definition IV

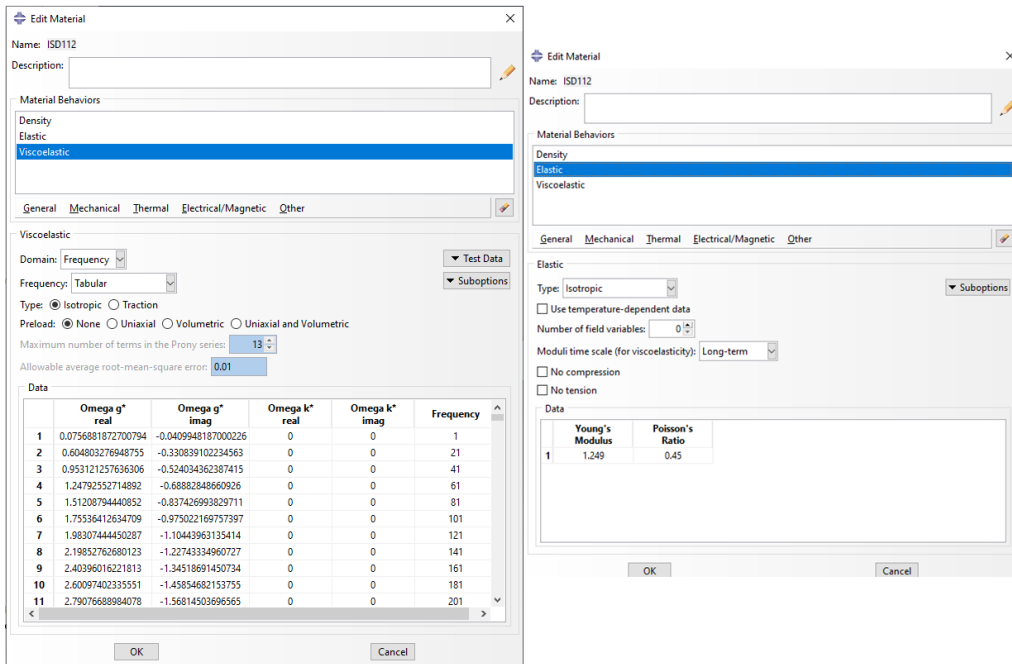


Figure 3.33. ABAQUS Viscoelastic Material Definition V

## CHAPTER 4

### VALIDATION AND INTEGRATION OF VISCOELASTIC MATERIAL

#### 4.1. Validation and Integration of Viscoelastic Material

In this chapter, verification of defined viscoelastic materials in a simpler FEM model on a simpler geometry is summarized. The purpose is to verify the finite element model definitions of complex material properties on a simple constrained layer treated beam on a reference study before applying on to the fuselage geometry. The finite element results were compared with analytical results and represented in the following sub chapters.

##### 4.1.1. Defining and Assigning VEM Properties

As previously described in chapter 3.4.1, the viscoelastic material definition through ABAQUS user interface is simple yet has its own definition technique. The most important thing while assigning the material for VEM is to know the deformation technique. For free layer applications, where the main deformation type is bending moment rather than shear stress, one can also use shell material assignment to VEM layer if the shell assumption criteria is satisfied, that is the thickness to lateral length ratio has to be lower than  $\frac{1}{10}$ th of the lateral dimension. But if the model has constrained layer or stand-off layer treatments as in our case, shell modelling of VEM layer gave faulty results since shell model cannot imulate the shear deformations as desired. Due to that limitation one has to use solid model with at least 3 edge seed on solid thickness direction.

##### 4.1.2. Verification of Reference Constrained Layer Beam

In order to show the assignment of viscoelastic properties are correct a simple geometry consisting of a base beam, viscoelastic layer and a constraining layer has

selected from the study of Eyyüpoğlu [8], and the reference material and geometric properties are given in Table 4.1.

Table 4.1. Reference CLD Properties

<b>Property</b>	<b>Value</b>	<b>Unit</b>
Base Beam Thickness	1	Mm
Base Beam Modulus	70	GPa
Base Beam Density	2700	$kg/m^3$
Base Beam Poisson's Ratio	0.33	N/A
Base Beam Material	AL 2024 T3	N/A
VEM Thickness	0.127	mm
VEM Modulus	See Reference [40]	MPa
VEM Density	900	$kg/m^3$
Base Beam Poisson's Ratio	0.45	N/A
VEM Material	ISD-112	N/A
Length	150	mm
Width	12.7	mm
Constrained Layer Thickness	0.254	Mm
Constrained Layer Modulus	70	GPa
Constrained Layer Density	2700	$kg/m^3$
Constrained Layer Poisson's Ratio	0.33	N/A
Constrained Layer Material	AL 2024 T3	N/A

Using the above given properties FE model is created in ABAQUS and analytical model comparison is carried out using both ABAQUS and Matlab R2014b. For direct FRF comparison simply supported-simply supported case has selected due to ease of

the analytical representation and additional free-free case has selected for modal comparison. The created model can be seen in Figure 4.1. Since complex material is defined to VEM layer, the modal analysis has an iterative procedure for natural frequency extraction in both ABAQUS and Matlab. This iterative procedure is defined in ABAQUS through complex frequency analysis after normal frequency analysis, where one can define the frequency which the material properties needed to be calculated to search for a natural frequency in a user defined region. The representative figures showing the procedure is given in Figure 4.2 - Figure 4.7.

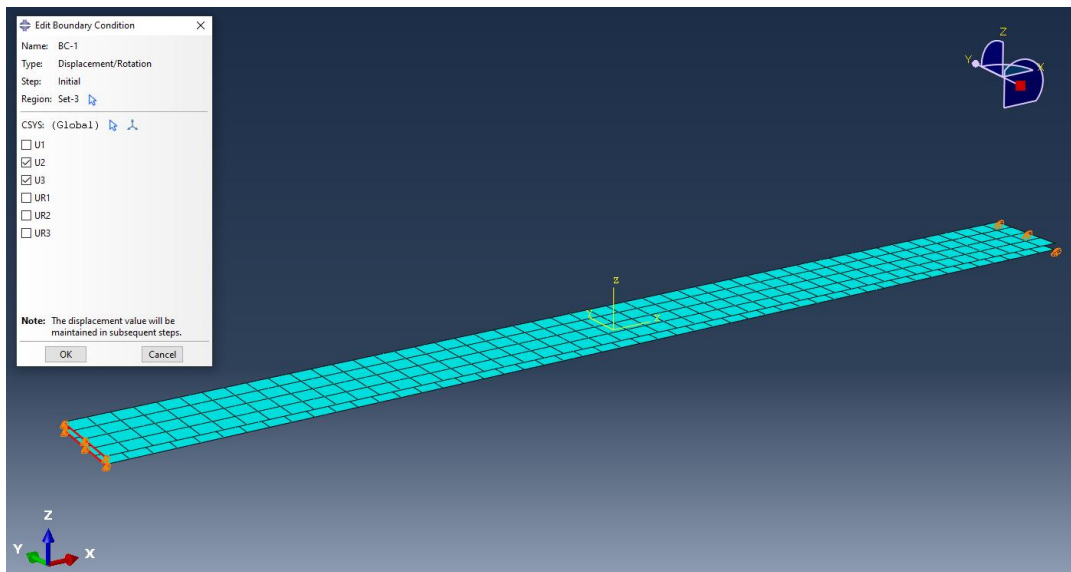


Figure 4.1. Simply Supported Reference Beam FEM

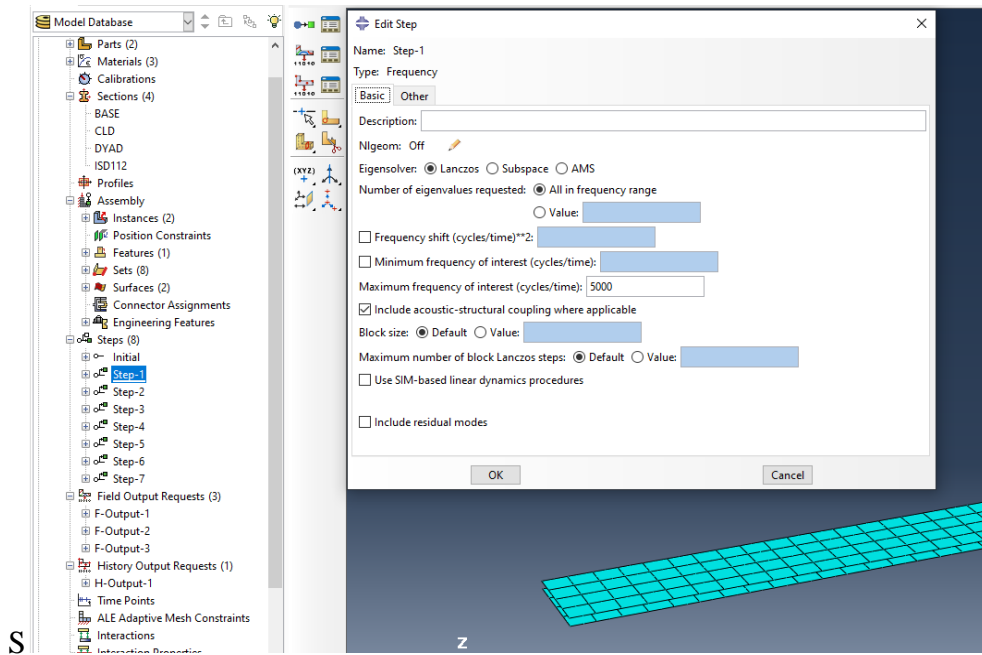


Figure 4.2. Modal Analysis settings using 0 Hz material properties for initial mode frequencies

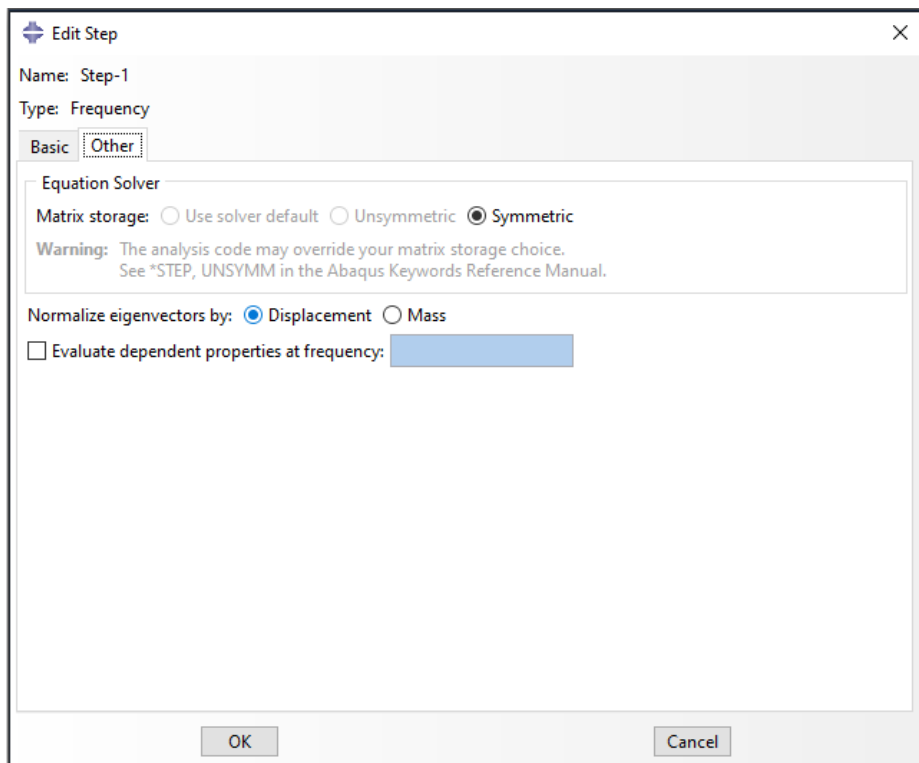


Figure 4.3. Modal Analysis normalization settings using 0 Hz material properties for initial mode frequencies

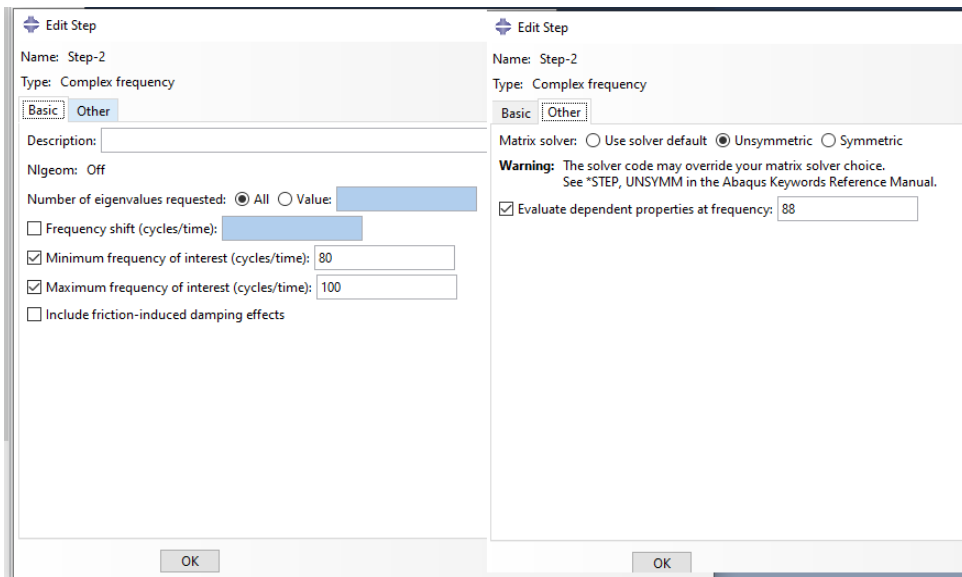


Figure 4.4. Complex Mode analysis settings for first mode using material properties calculated at initial guess found by Step-1

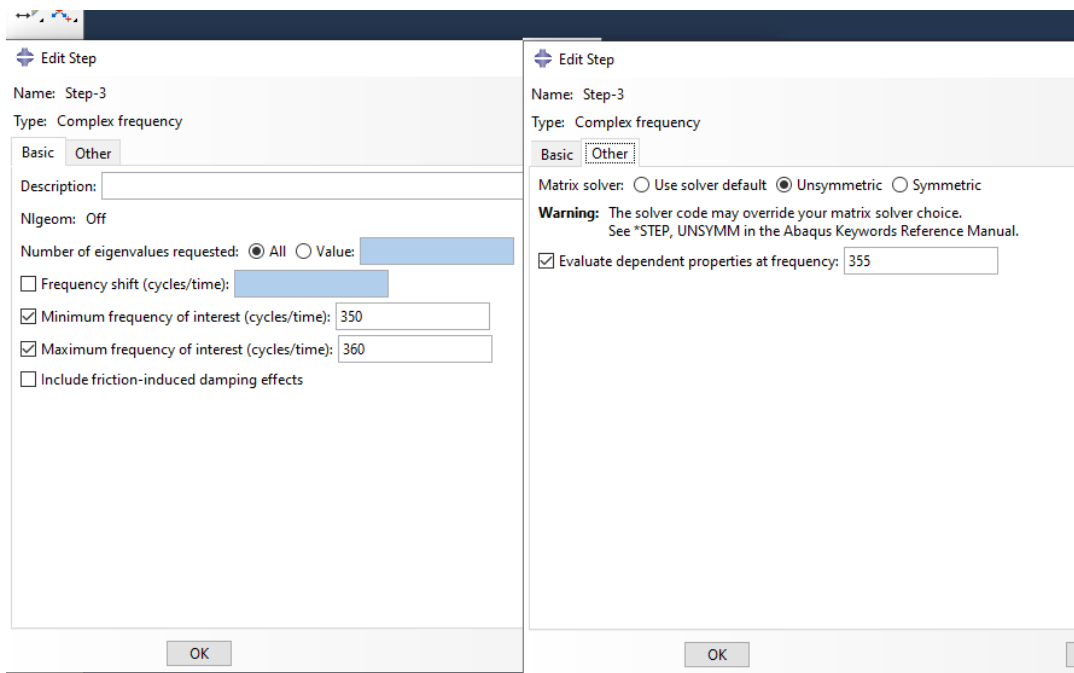


Figure 4.5. Complex Mode analysis settings for second mode using material properties calculated at initial guess found by Step-1V

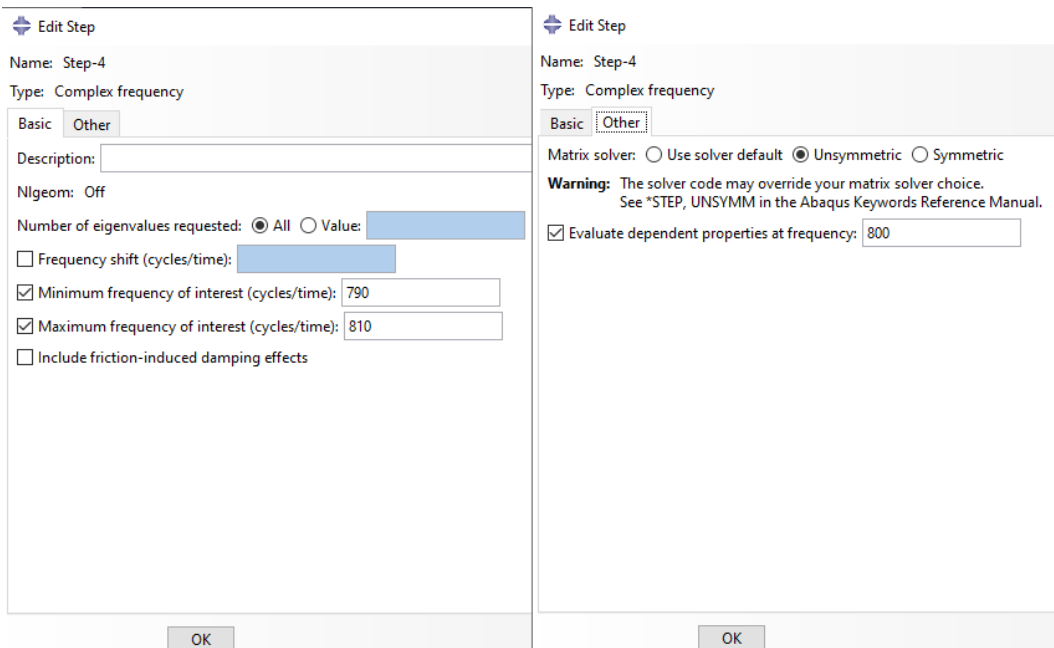


Figure 4.6. Complex Mode analysis settings for third mode using material properties calculated at initial guess found by Step-1

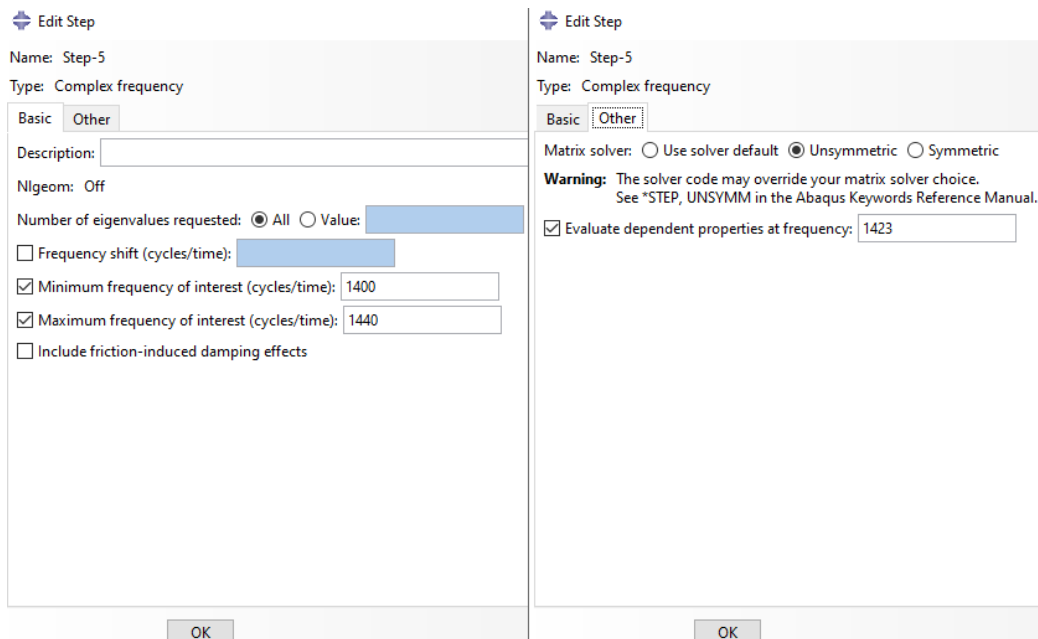


Figure 4.7. Complex Mode analysis settings for fourth mode using material properties calculated at initial guess found by Step-1

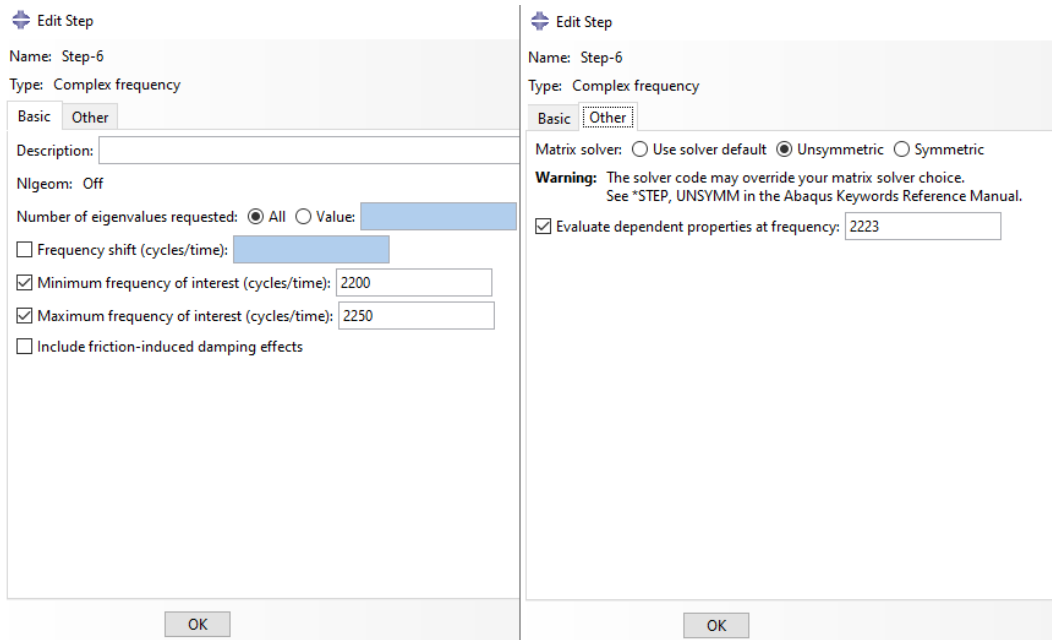


Figure 4.8. Complex Mode analysis settings for fifth mode using material properties calculated at initial guess found by Step-1

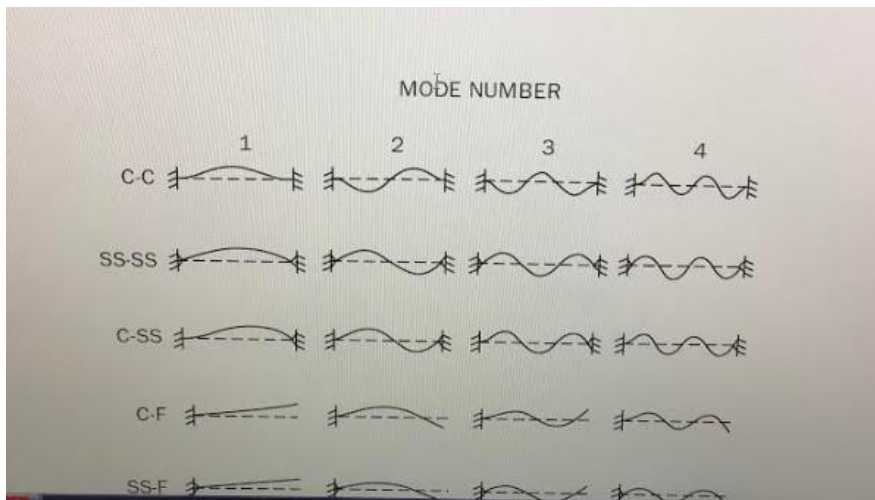


Figure 4.9. Mode shapes of beam under transverse vibration [45]

$m$	C-C	C-SS	C-F	SS-SS	SS-F	F-F
1	22.373	15.418	3.5160	9.8696	0	0
2	61.673	49.965	22.034	39.478	15.418	0
3	120.903	104.248	61.697	88.826	49.965	22.373
4	199.859	178.270	120.902	157.914	104.248	61.673
5	298.556	272.031	199.860	246.740	178.270	120.903
>5	$(2m + 1)^2 \pi^2 / 4$	$(4m + 1)^2 \pi^2 / 16$	$(2m - 1)^2 \pi^2 / 4$	$m^2 \pi^2$	$(4m - 3)^2 \pi^2 / 16$	$(2m - 3)^2 \pi^2 / 4$

**TABLE 4.1** Frequency Parameters  $\beta^2 = \omega l^2 \sqrt{\rho A / EI}$  for Beams

Figure 4.10. Modal Parameters for Beam under transverse vibration [45]

Using lecture notes of ME708 Vibration Control and Isolation Chapter 5 Free Layer Surface Damping Treatment notes, Matlab code is written for transverse beam vibration free layer damping treatment. From the below results it is shown that using solid material section with complex material definition has to be used and has good convergence to analytical results if complex frequency analysis and direct steady state frequency extraction is used for frequency response function.

Below are the results for each case and mode:

Table 4.2. Free-Free Boundary Condition Modal Values using 0 Hz Material properties

Mode Number	Analytical Model (Hz)	ABAQUS Finite Element Model (Hz)
1	293.3	249.36
2	747.3	611.60
3	1386.6	1162.2
4	2208.1	1892.5
5	3213.2	2811.4

Table 4.3. Free-Free Boundary Condition Modal Values after iterations

Mode Number	Analytical Model (Hz)	ABAQUS Finite Element Model (Hz)
1	293.3	296.52
2	747.3	738.97
3	1386.6	1381.6
4	2208.1	2204.8
5	3213.2	3224.6

Table 4.4. Simply Supported - Simply Supported Boundary Condition Modal Values using 0 Hz  
Material properties

Mode Number	Analytical Model (Hz)	ABAQUS Finite Element Model (Hz)
1	123.9	110.57
2	460.7	392.55
3	990.8	851.69
4	1709.3	1494
5	2614.8	2321.9

Table 4.5. Simply Supported - Simply Supported Boundary Condition Modal Values after iterations

Mode Number	Analytical Model (Hz)	ABAQUS Finite Element Model (Hz)
1	123.9	122.87
2	460.7	454.96
3	990.8	979.06
4	1709.3	1694.6
5	2614.8	2602.9

## Simply Supported- Simply Supported

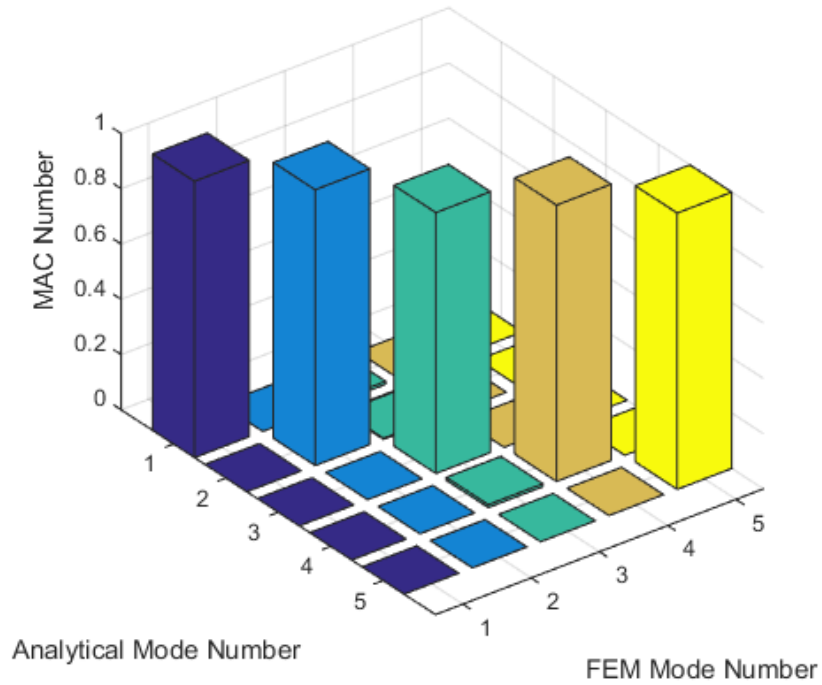


Figure 4.11. MAC Plot for Simply Supported- Simply Supported Beam

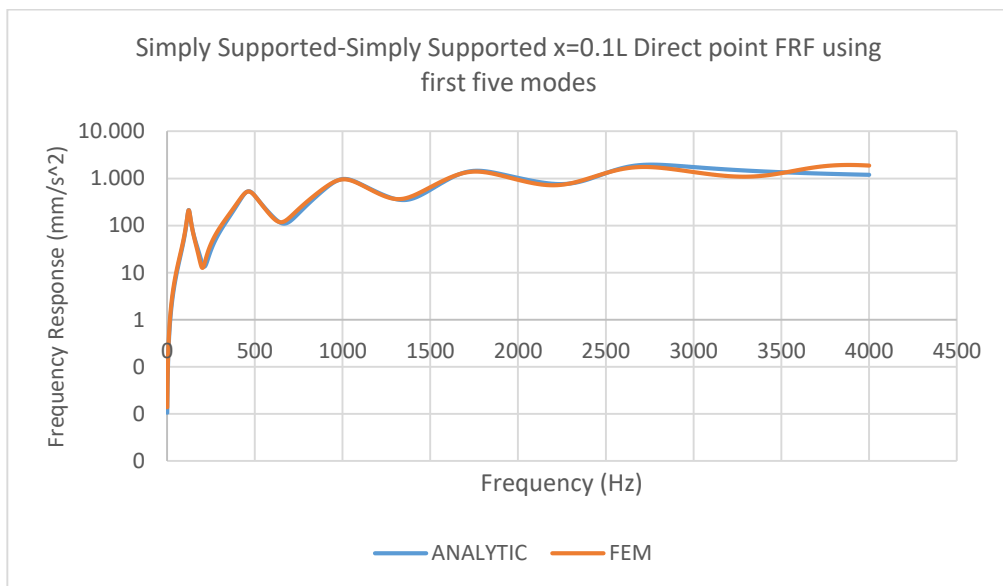


Figure 4.12. Direct point FRF x=0.1L Simply Supported- Simply Supported Beam

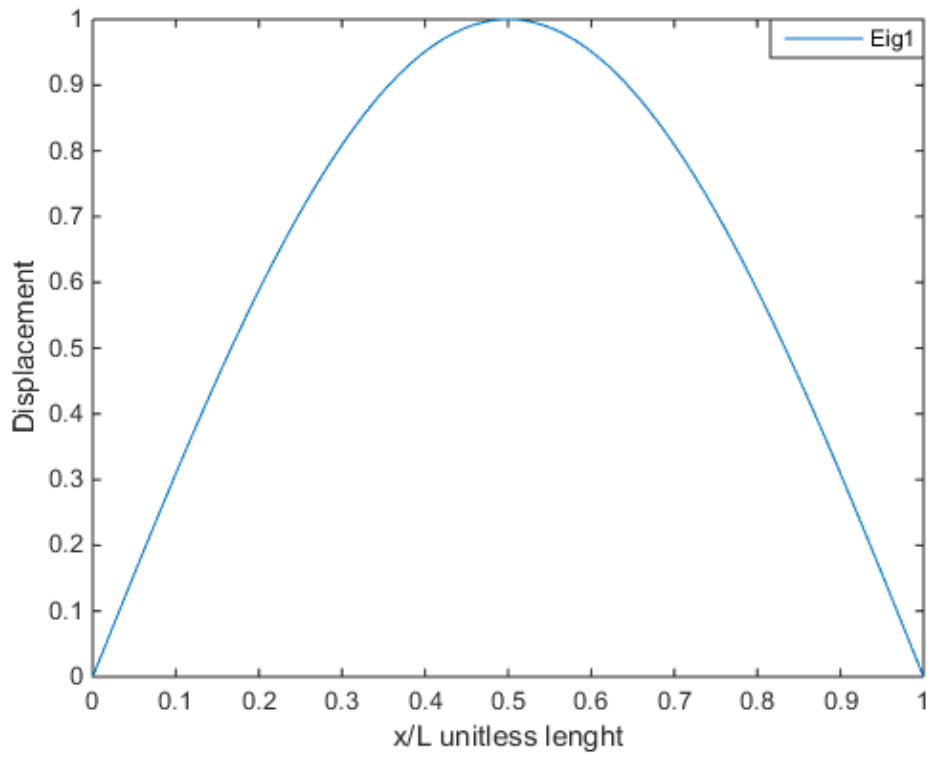


Figure 4.13. Analytical First mode for Simply Supported- Simply Supported Beam

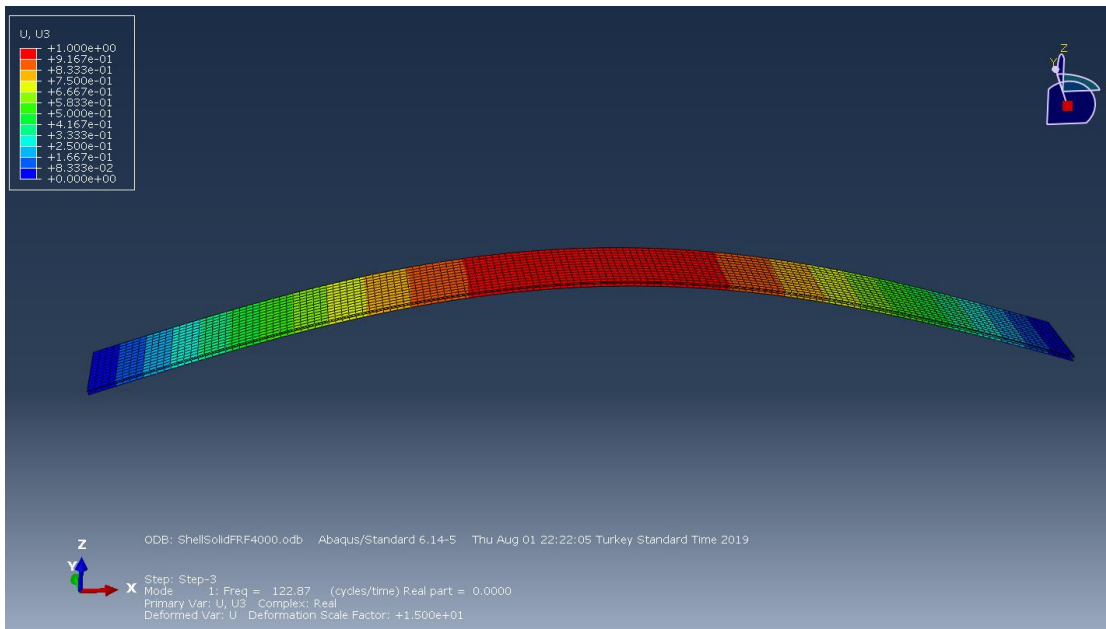


Figure 4.14. ABAQUS First mode for Simply Supported- Simply Supported Beam

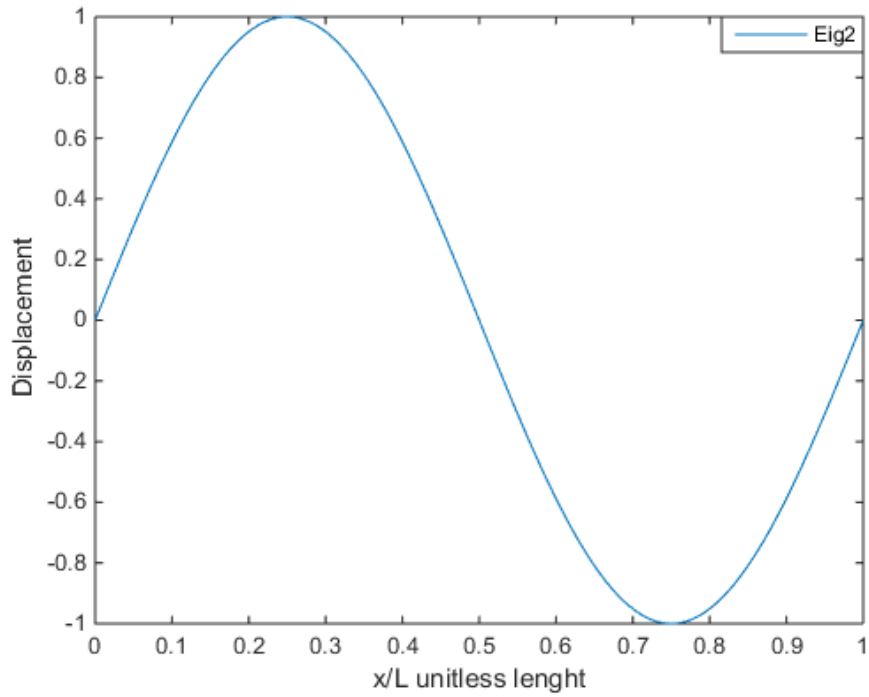


Figure 4.15. Analytical Second mode for Simply Supported- Simply Supported Beam

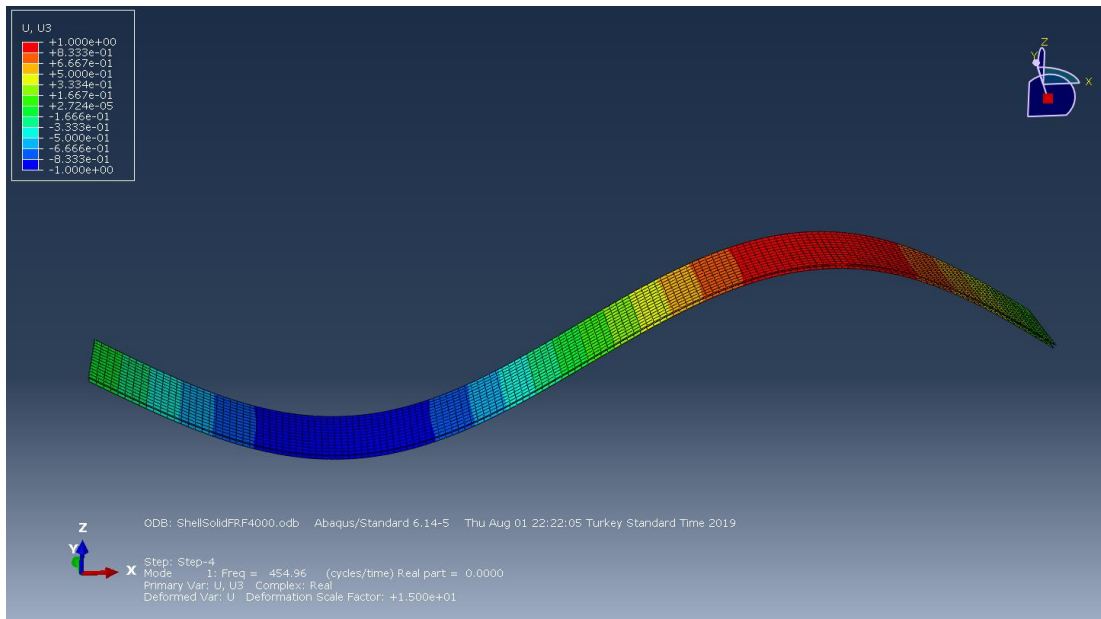


Figure 4.16. ABAQUS Second mode for Simply Supported- Simply Supported Beam

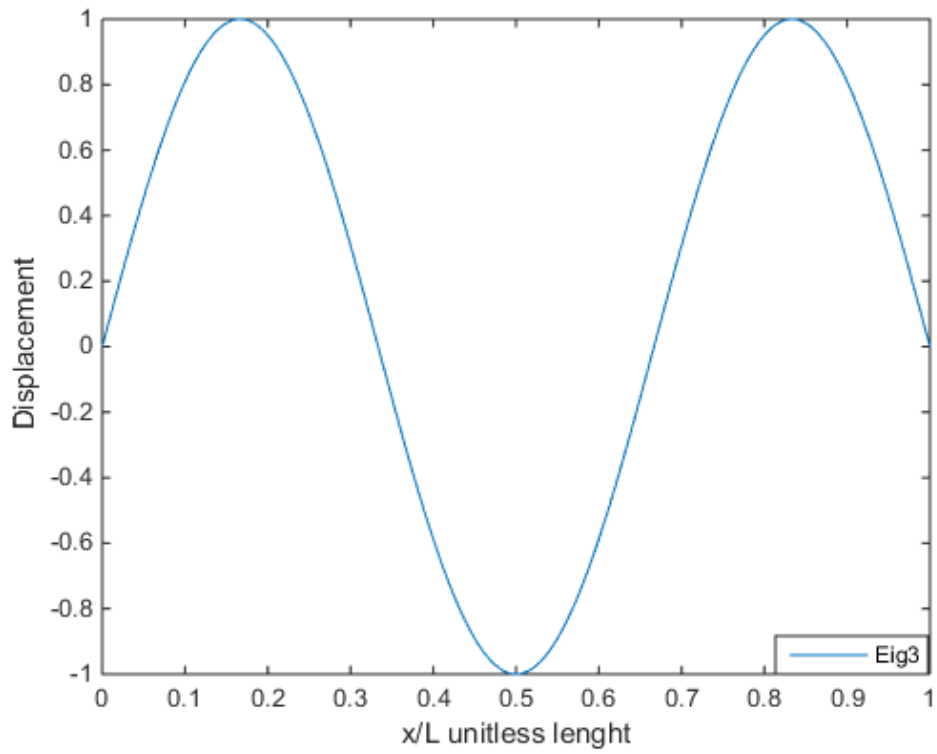


Figure 4.17. Analytical Third mode for Simply Supported- Simply Supported Beam

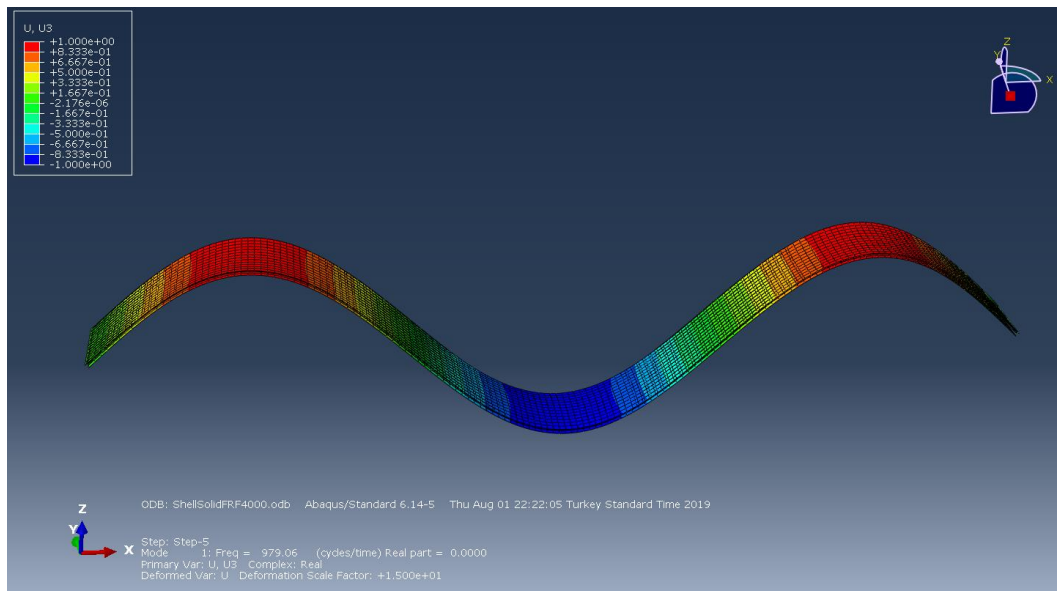


Figure 4.18. ABAQUS Third mode for Simply Supported- Simply Supported Beam

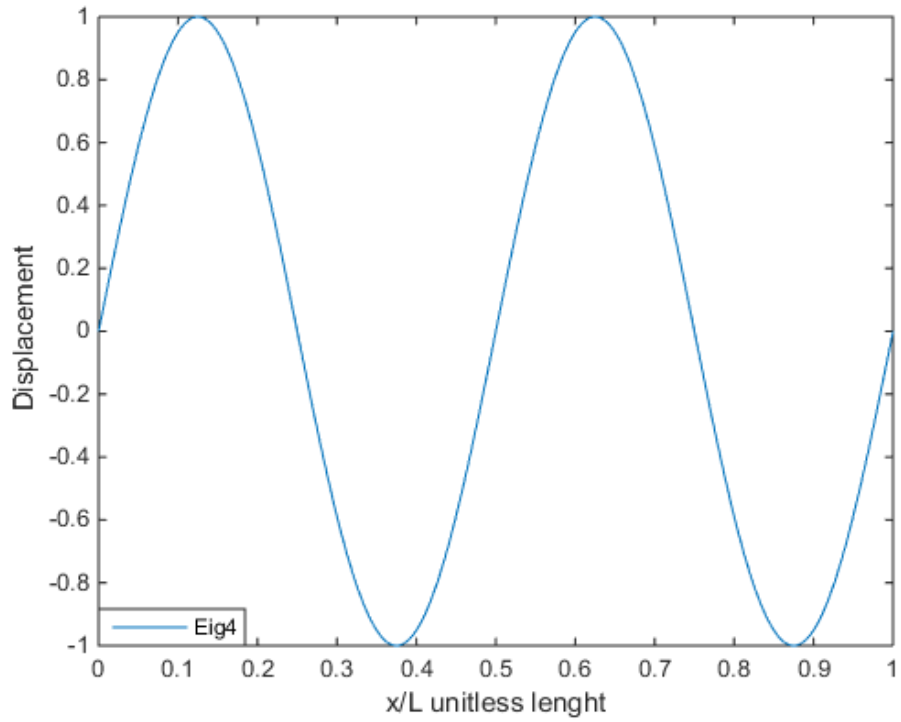


Figure 4.19. Analytical Fourth mode for Simply Supported- Simply Supported Beam

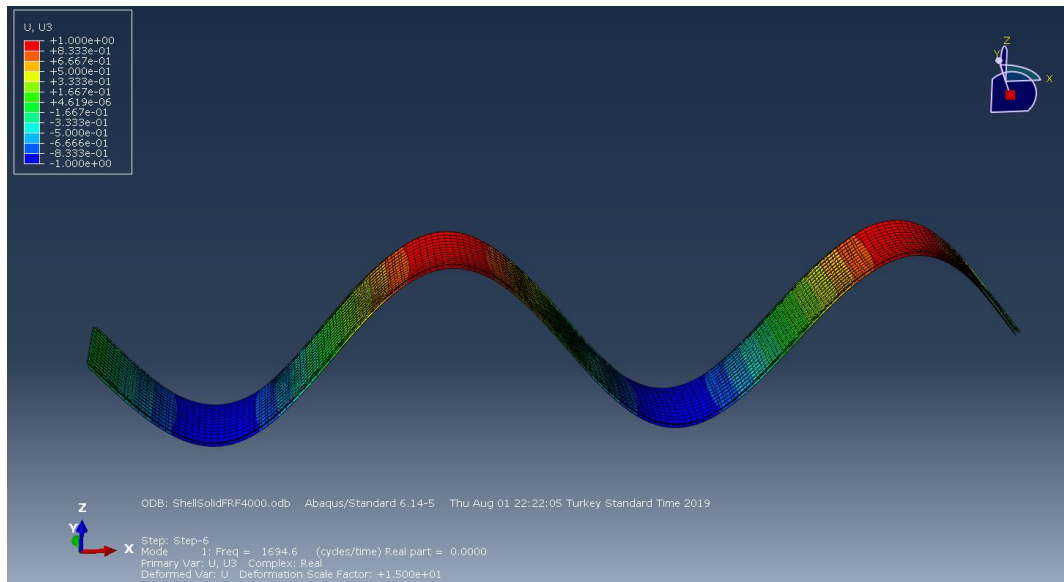


Figure 4.20. ABAQUS Fourth mode for Simply Supported- Simply Supported Beam ABAQUS

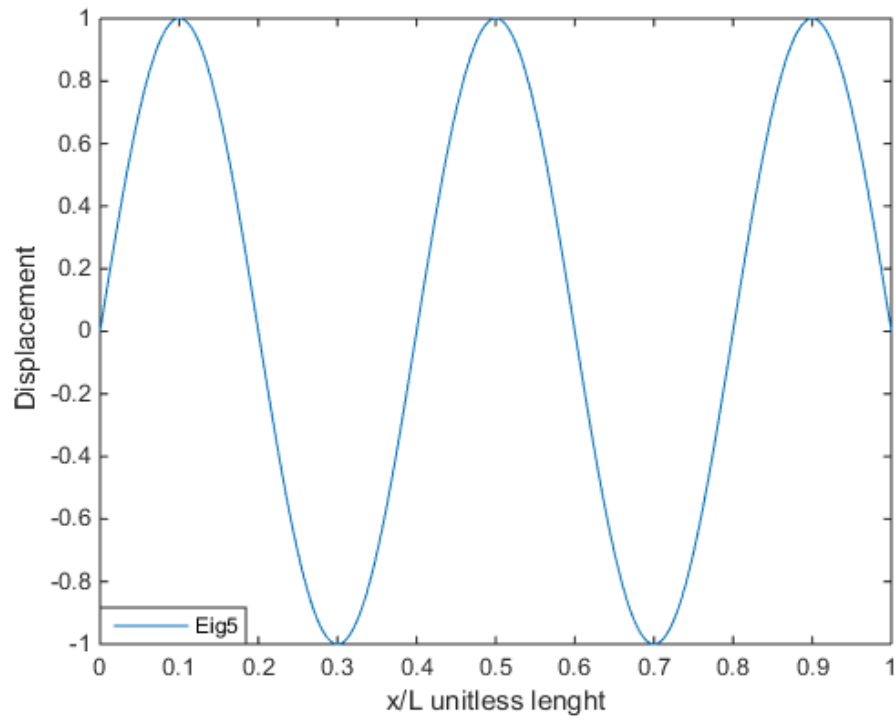


Figure 4.21. Analytical Fifth mode for Simply Supported- Simply Supported Beam

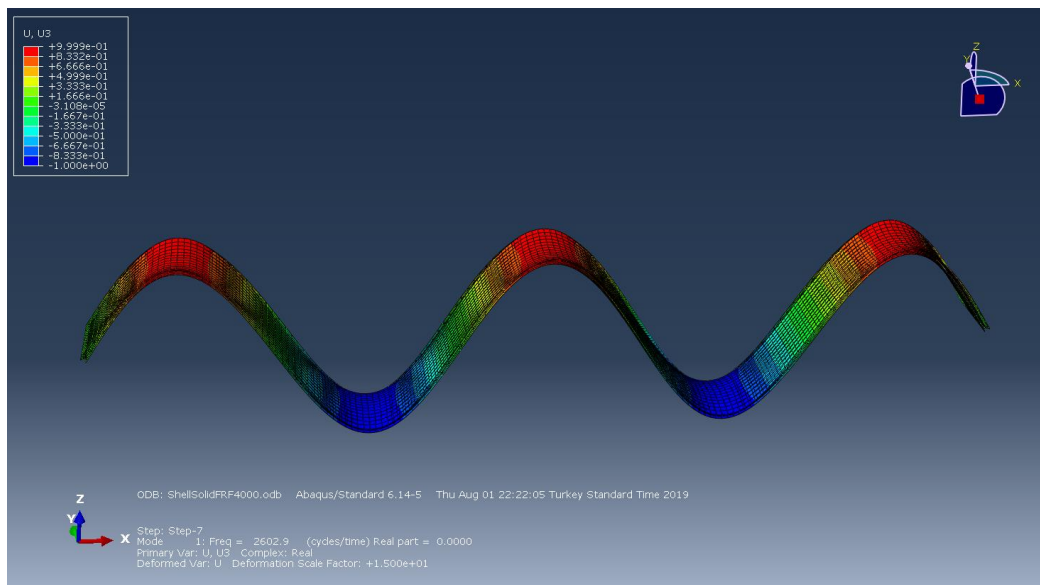


Figure 4.22. ABAQUS Fifth mode for Simply Supported- Simply Supported Beam

Free-Free:

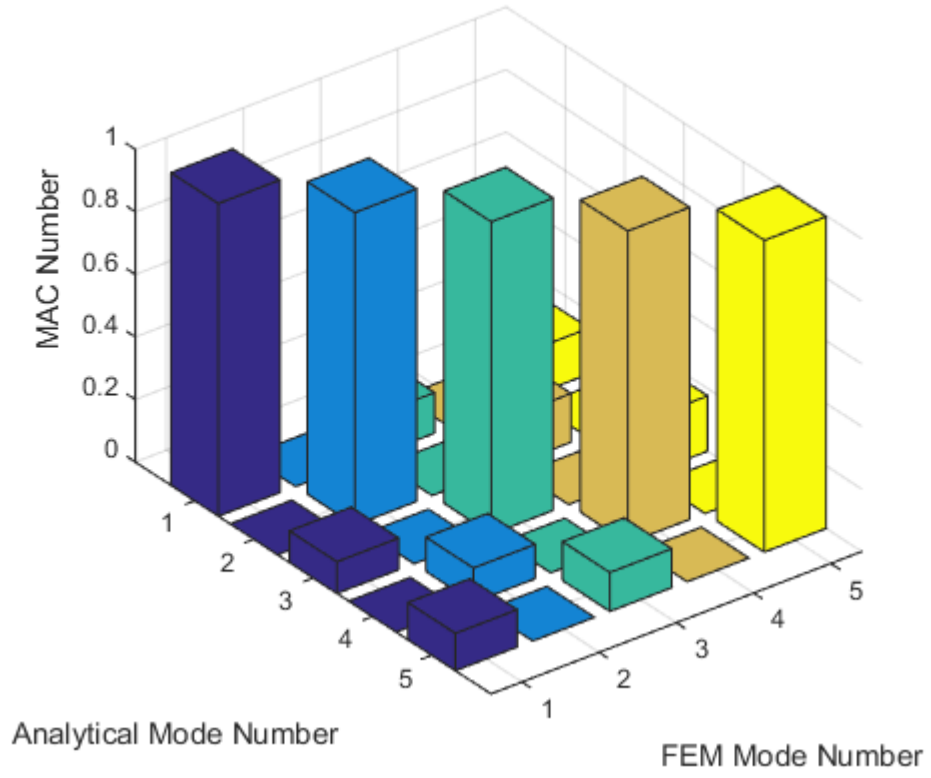


Figure 4.23. MAC Plot for Free-Free Case

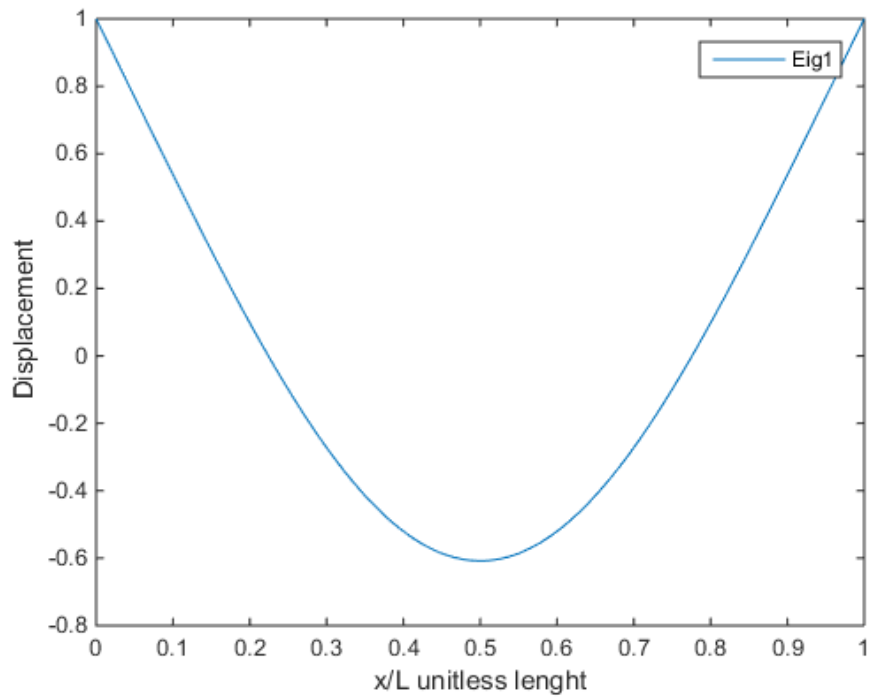


Figure 4.24. Analytical First mode for Free-Free Beam

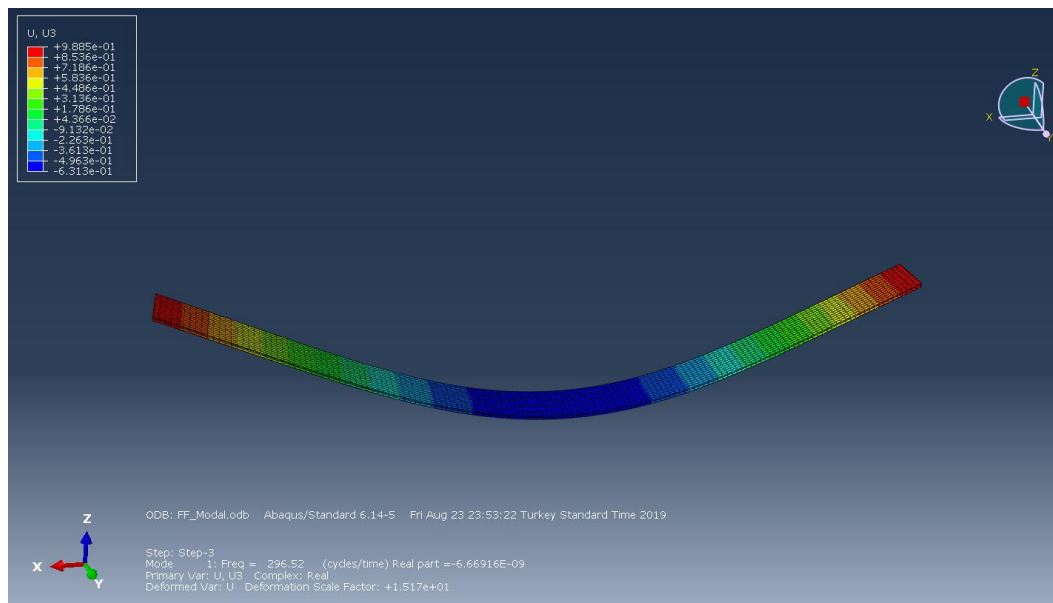


Figure 4.25. ABAQUS First mode for Free-Free Beam

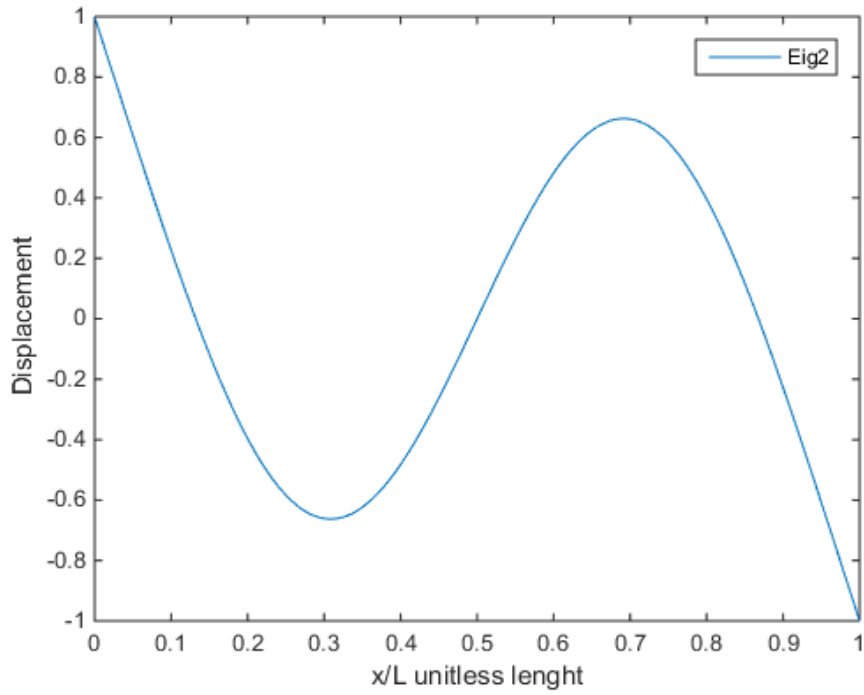


Figure 4.26. Analytical Second mode for Free-Free Beam

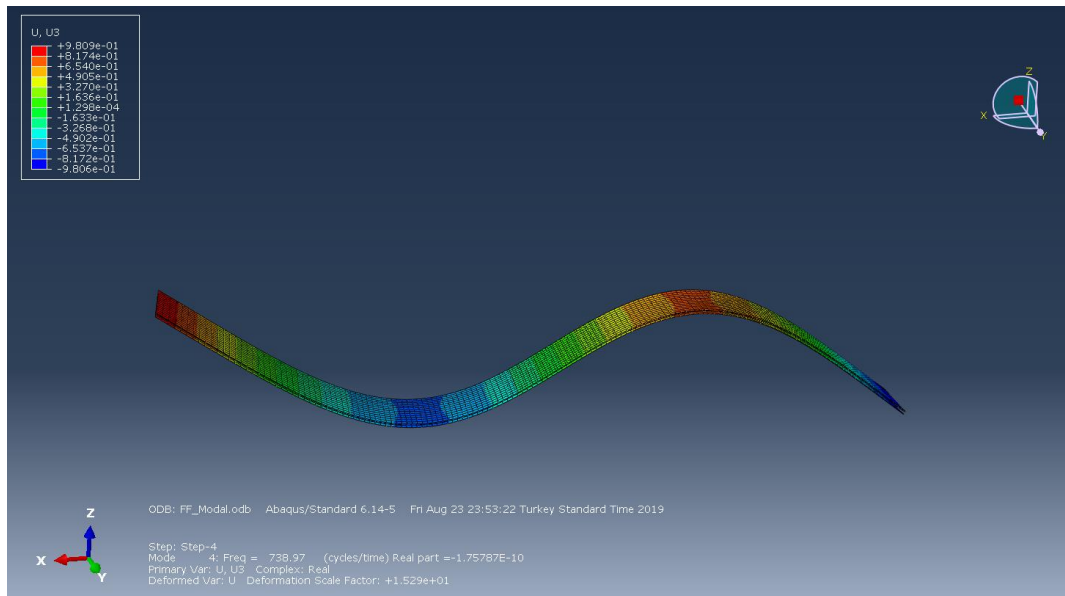


Figure 4.27. ABAQUS Second mode for Free-Free Beam

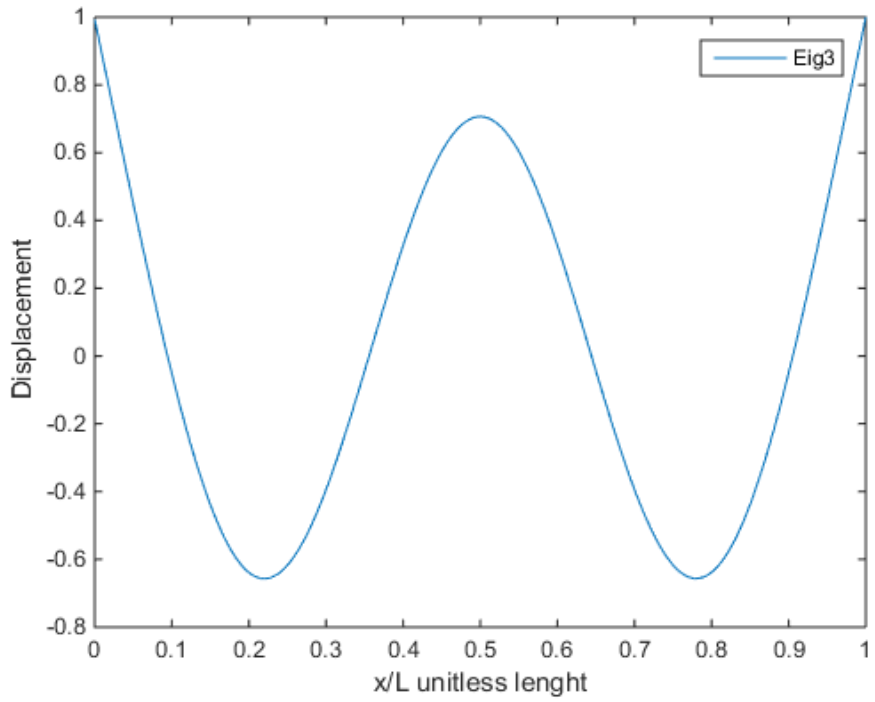


Figure 4.28. Analytical Third mode for Free-Free Beam

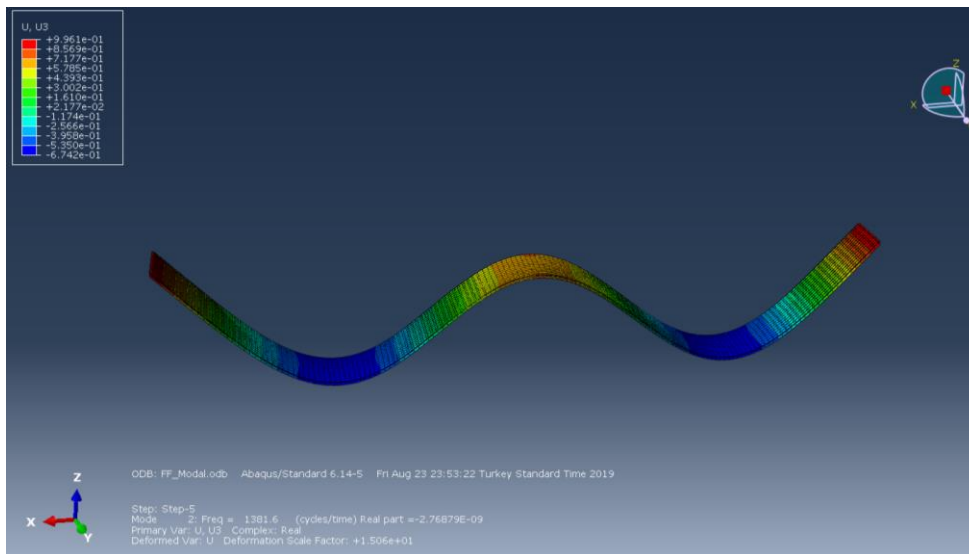


Figure 4.29. ABAQUS Third mode for Free-Free Beam

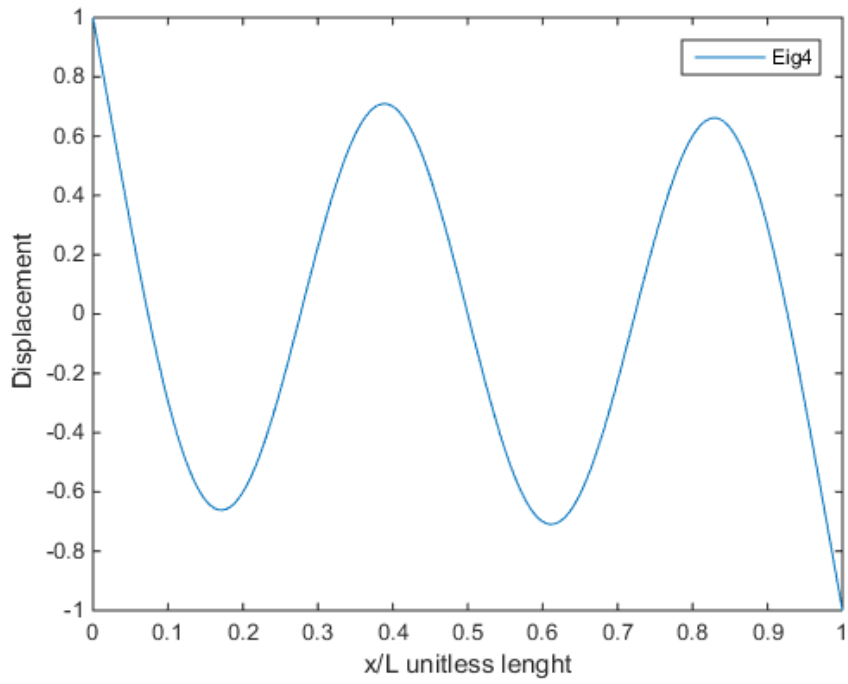


Figure 4.30. Analytical Fourth mode for Free-Free Beam

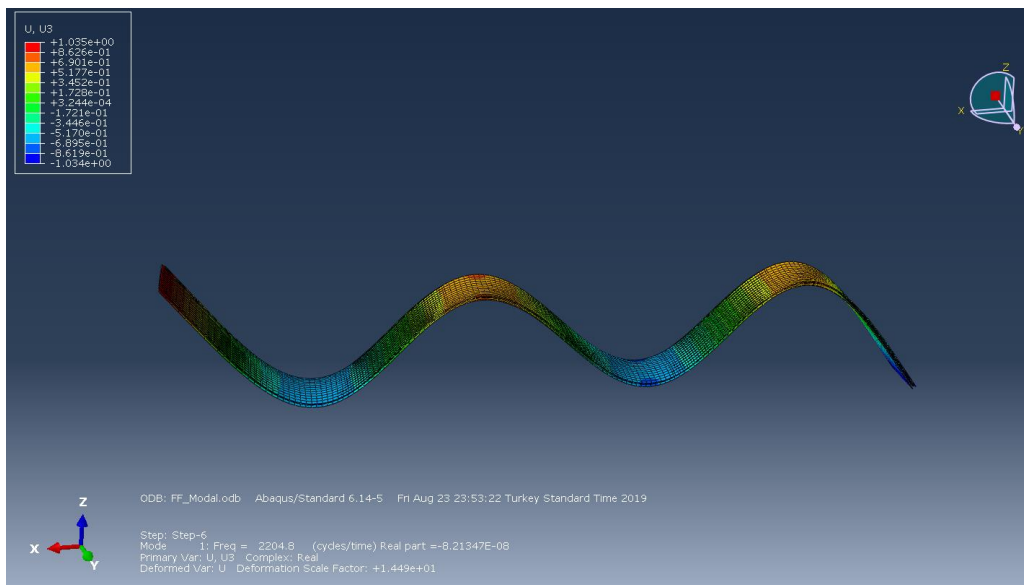


Figure 4.31. ABAQUS Fourth mode for Free-Free Beam

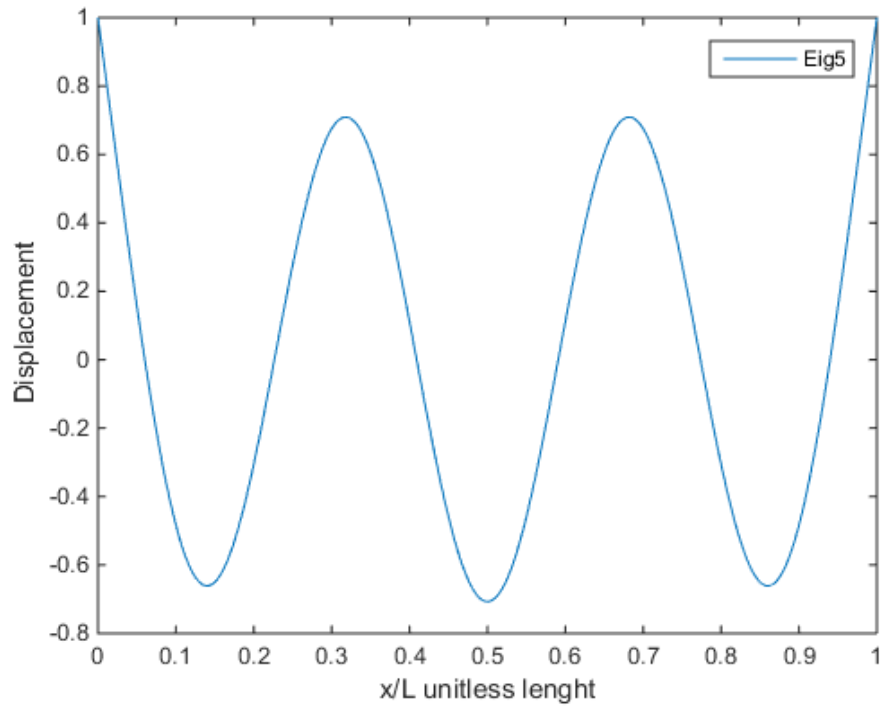


Figure 4.32. Analytical Fifth mode for Free-Free Beam

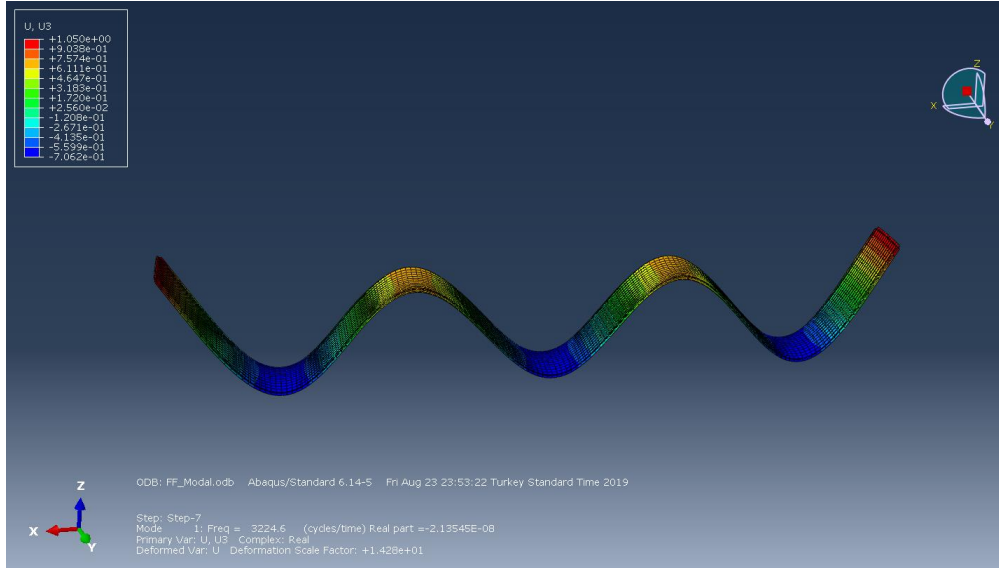


Figure 4.33. ABAQUS Fifth mode for Free-Free Beam

## CHAPTER 5

### DEVELOPMENT AND VERIFICATION OF DAMPING TREATMENT

The purpose of this study is to develop a standoff layer treatment with a novel spacer geometry for a plate that has improved damping performance with reduced weight or at equal weight. Sun [7] and Eyüpoğlu [8] has carried out a similar study in their thesis study in 2015 for beams. Their study has shown that there exists high potential of improvement in the spacer geometry for targeted modes and application. In order to develop a novel damping treatment for a fuselage like structure, one must define a reference damping solution that can be reached and applied by anyone in need without much effort using off the shelf products. For this purpose, in the following subchapters, a baseline definition study has been carried out in order to be compared with the new developed SOLD treatment. The most important thing while selecting the baseline damping solution is to have maximum damping performance with least additional mass without altering the dynamics of base platform largely. In order to define effective damping, the measurement of damping performance metrics is summarized in the subchapter following.

#### 5.1. Metrics for Quantifying the Damping Performance of the Treatment

In literature damping performance is commonly measured through modal identification methods and the most used method is the half power method for modal damping estimation of a system through FRF output obtained by either analytical or finite element method. Because of that the half power method will be used in order to estimate modal damping improvements of the damping treatment that is developed.

The designed system that the damping treatment will be applied is a compact fuselage like geometry that is manufactured to simulate the application performance of the damping treatments. In order to estimate the application performance of the damping

solution, one should consider the loading conditions of the fuselage for best estimate. The aerospace structures are under sinusoidal loads due to their rotary components such as motors, rotors and transmission and on top of that the outer shell of the vehicle is also under random loading due to flight loads and aerodynamic forces acting on fuselage. This loading condition is commonly called sine-on-random loading for structures and the equipment's that will be used on aerospace applications shall sustain its performance and life target under this type of vibratory test condition. The graph to simulate the loading condition is given in Figure 5.1 below.

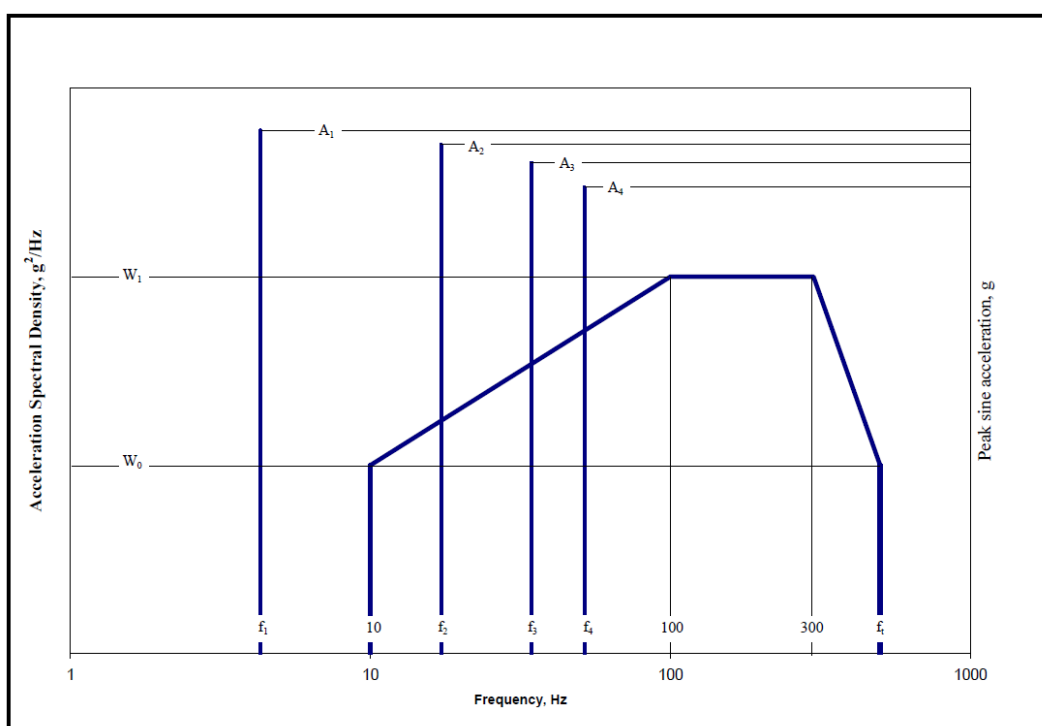


Figure 5.1. MIL-STD-810G Category 14 Rotary Wing Aircraft-Helicopter Vibration Curve [47]

Because of ease of computation time and first non-rigid ten mode limits, the finite element solution for damping performance estimation is limited between 0-600Hz span and the fuselage FRF graph is given in Figure 5.2.

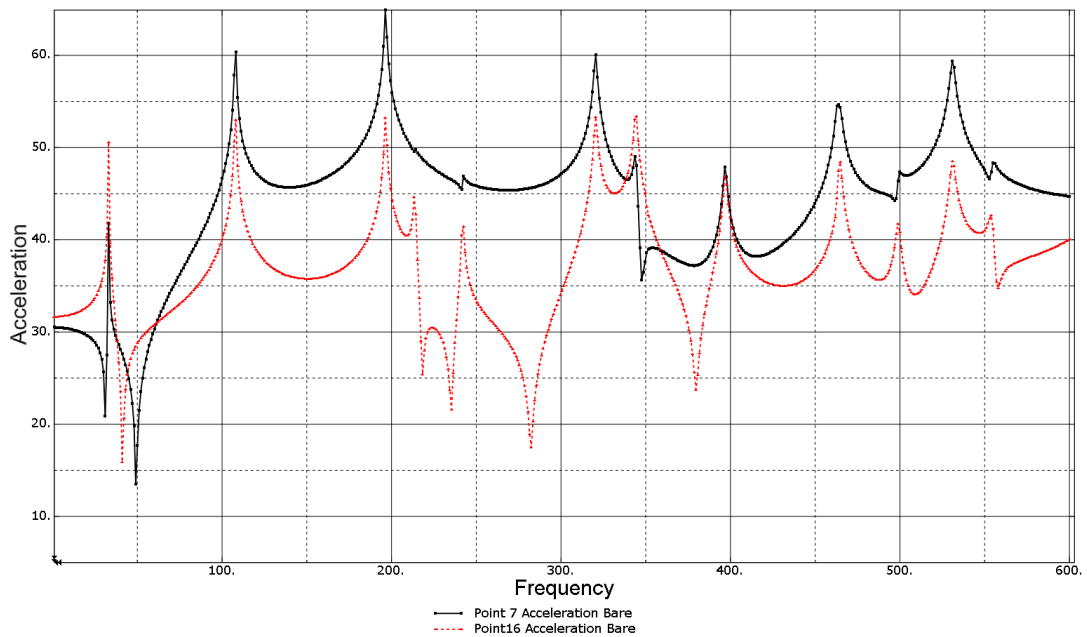


Figure 5.2. FRF Result for Undamped Fuselage Geometry

However, although the above mentioned test standard is applicable for both military and commercial vehicles, the human comfort in military conditions is only limited to pilots but not for crews. On the other hand, for special use aerospace aircrafts such as commercial airplanes and VIP helicopters, the comfort of the passenger is targeted to be maximized for competitiveness in the aircraft market. Due to that commercial aircrafts utilize damping treatment solutions on fuselage geometries in order to decrease the vibration induced acoustic noise transferred to passengers.

In order to estimate the damping treatment performance considering above mentioned design criteria, one should use a broadband damping effect estimation method which also takes in to account the loading conditions of the fuselage geometries. Since the loading o the fuselage geometry is random, as explained in the second paragraph in this chapter and aircraft standard [47] states, one should use single input single output random system formulations to relate the input to output of the system as such.

For a single input single output system with random vibration excitation, the output signal power spectral density (PSD) is related to random input as follows;

$$S_y(f) = \int_{-\infty}^{\infty} R_y(\tau) e^{-j2\pi f\tau} d\tau \quad (19)$$

$$\begin{aligned} \int_{-\infty}^{\infty} R_y(\tau) e^{-j2\pi f\tau} d\tau \\ = \int_{-\infty}^{\infty} e^{-j2\pi f\tau} d\tau \int_{-\infty}^{\infty} \int_{-\infty}^{\infty} R_x(\tau + \theta - \phi) h(\theta) h(\phi) d\theta d\phi \end{aligned} \quad (20)$$

Where;  $S_y$  is the output signal power spectral density,  $R_y$  is the random input and  $\tau$  is the time shift constant.

After some modifications;

$$S_y(f) = \int_{-\infty}^{\infty} h(\theta) e^{j2\pi f\theta} d\theta \int_{-\infty}^{\infty} h(\phi) e^{-j2\pi f\phi} d\phi \int_{-\infty}^{\infty} R_x(\tau + \theta - \phi) e^{-j2\pi f(\tau + \theta - \phi)} d\tau \quad (21)$$

$$S_y(f) = H^*(f) H(f) \int_{-\infty}^{\infty} R_x(\zeta) e^{-j2\pi f\zeta} d\zeta \quad (22)$$

$$S_y(f) = H^*(f) H(f) S_x(f) = |H(f)|^2 S_x(f) \quad (23)$$

Where  $H(f)$  is the frequency response function and  $S_x$  is the input signal power spectral density.

This equation means that for a single input single output system the output PSD is related to input PSD with a multiplier and that multiplier is the amplitude square of the frequency response function itself of the system. The mean square of the output signal PSD can be used to represent the power or energy of the output signal and can be calculated by the following equation;

$$E[y^2] = R_y(0) \int_{-\infty}^{\infty} \int_{-\infty}^{\infty} R_x(\theta - \phi) h(\theta)h(\phi)d\theta d\phi \quad (24)$$

$$E[y^2] = \int_{-\infty}^{\infty} S_y(f) df = \int_{-\infty}^{\infty} |H(f)|^2 S_x(f) df \quad (25)$$

Where  $E[y^2]$  is the total energy of the output signal for given input function.

These equations mean that for a known input PSD output signal power can be represented by the area under frequency response curve over a defined frequency band and is called band power throughout the study. By assuming unit input PSD the **Eq.25** gives;

$$E[y^2]_{band} = \int_{f_l}^{f_u} S_y(f) df = \sum_{f_l}^{f_u} |H(f)|^2 \quad (26)$$

By using octave band definitions one can define area under a defined frequency range with a single central frequency using trapezoidal rule over that area given as;

$$E[y^2]_{central} = \int_{f_l}^{f_u} S_y(f) df = \sum_{i=1}^n \frac{|H(f_i)|^2 + |H(f_{i+1})|^2}{2} \quad (27)$$

$= dB \text{ Band Power}$

Where, n is the number of frequencies depending on the selected octave band scale and the central frequency. After obtaining the mean square of a signal over a band, it is called a band power in this study and used to correlate the output signal power to FRF of the system assuming a unit input PSD. Since this calculated power is presented through dB scale it is called dB band power throughout the study. By subtracting the band power of the damped system and undamped system one obtains the amplitude power difference which is used to estimate the damping performance as follows;

$$dBReduction = dBBandPower_{DAMPED} - dBBandPower_{UNDAMPED} \quad (28)$$

This method is used in our study in order to estimate the vibratory energy reduction over a frequency band, in different octave bands, assuming unit input PSD for damped system and undamped system. The area under the frequency curve squared function is calculated using trapezoidal integration with unit frequency increment over desired octave band and the difference in the estimated output PSD values in the octave band.

## 5.2. Baseline Geometry Selection

Before developing a novel spacer for increased damping performance for plates an already used knowhow on literature is used to define a baseline damping solution to compare the effectiveness of the spacer designed. In order to do that, multiple constrained layer damping treatment solutions and equal weight spacer solutions in uniform condition and slotted configurations are used. Below the single, double, triple and uniform spacer geometry sections are shown with unscaled figures for visual representations only. Due to viscoelastic layers thickness it is exaggerated for it to be visible in cross section.

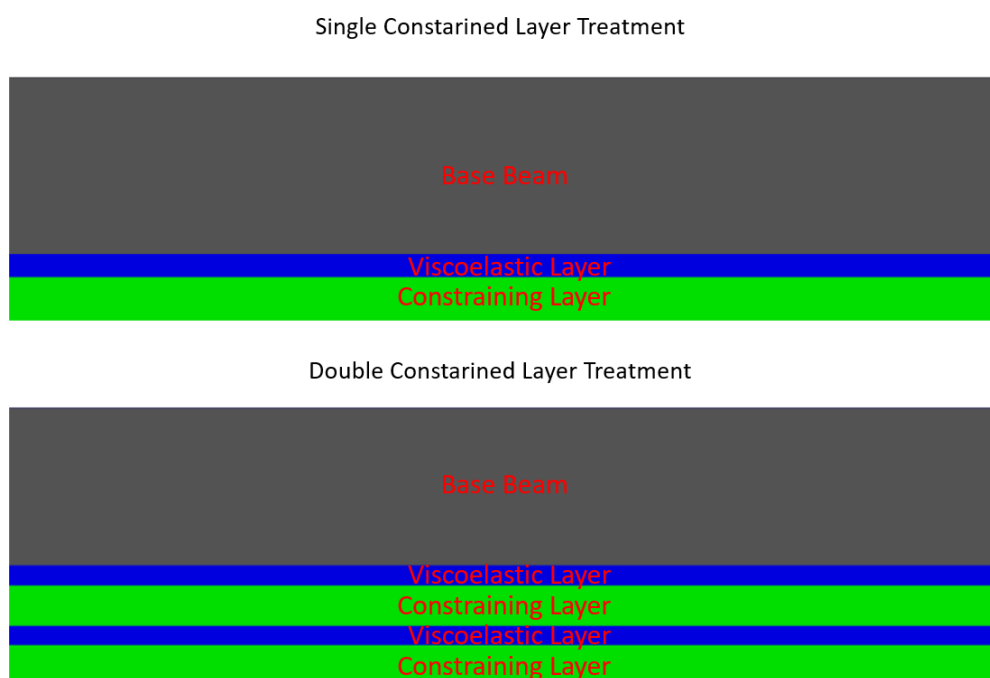


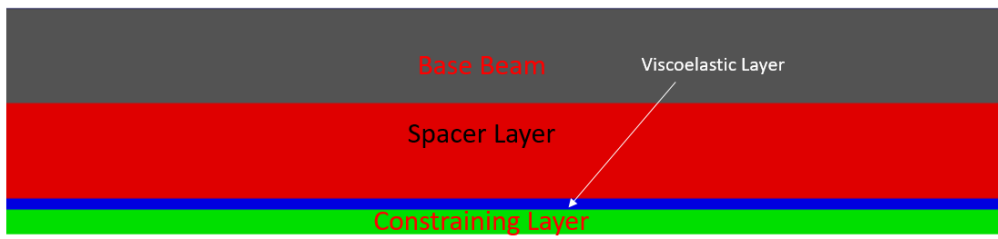
Figure 5.3. Single and Double Constraining Layer Solutions

Triple Constrained Layer Treatment



Figure 5.4. Triple Constraining Layer Solution

CLD with Spacer Layer Treatment



Standoff Layer Treatment

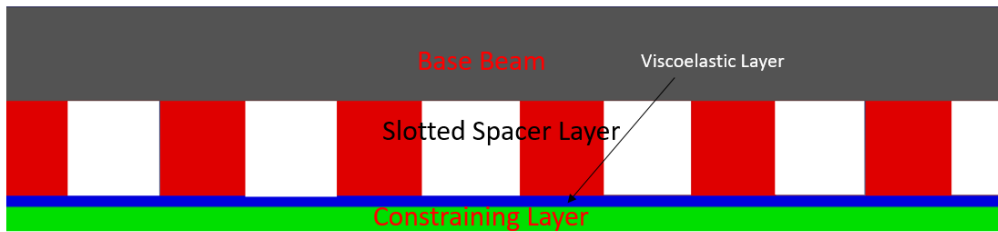


Figure 5.5. Standoff Layer Solution

Table 5.1. Dimensions of Layers

VEM Material	ISD-112
VEM Thickness	0.127 mm
Constraining Layer Material	AL 6061
Constraining Layer Thickness	0.254 mm

As an initial starting point the coverage are is selected to be %56.25 of the full outer plate which simulates the outer surface of fuselage geometry. However, since damping solution is applied in the inner surface of the fuselage, due to stringers and frames the area is restricted to 260mm x 260mm instead of 300mm x 300mm. The change in the effective length of the plate changes the starting coverage are from %56.25 to %75 of the effective space. The frequency response graphs show that the coverage are is large for the fuselage geometry and even with double constraining layer treatment, the damping solution exceed the %10 of the total weight of the fuselage geometry. Since aerospace applications are weight critical applications, the coverage are needed to be decreased for further studies. The initial tryout study weight comparison table is given below.

Table 5.2. Additional Mass with respect to Configurations

Configuration Number	Additional Mass (g)	Mass of Fuselage (g)	Additional Mass Percent (%)
No1 (Single CLD)	40.5	575	7%
No2 (Double CLD)	81	575	14%
No3 (0.5 Uniform SOLD Single CLD)	66.825	575	12%
No4 (0.5 Uniform SOLD Double CLD)	107.325	575	19%
No5 (1 Uniform SOLD Single CLD)	93.15	575	16%
No6 (1 Uniform SOLD Double CLD)	133.65	575	23%
No7 (2 Uniform SOLD Single CLD)	145.8	575	25%
No8 (2 Uniform SOLD Double CLD)	183.6	575	32%
No9 (3 Uniform SOLD Single CLD)	198.45	575	35%
No10 (3 Uniform SOLD Double CLD)	238.95	575	42%
No11 (5 Uniform SOLD Single CLD)	303.75	575	53%
No12 (5 Uniform SOLD Double CLD)	344.25	575	60%

As expected, addition of the spacer layer increased the damping performance of the system, however due to high additional mass to the system and due to high bending stiffness added on free region, increasing thickness in the central region of the fuselage, the dynamics of the fuselage is effected largely. Because of this the baseline study coverage are is planned to be changed. After detailed inspection of the applications in literature, it is found to be that the damping treatment applications are limited between %30-%45 of the effective area of the system. In following figures one can see the %75, %45 and %30 coverage representations of the fuselage geometry.

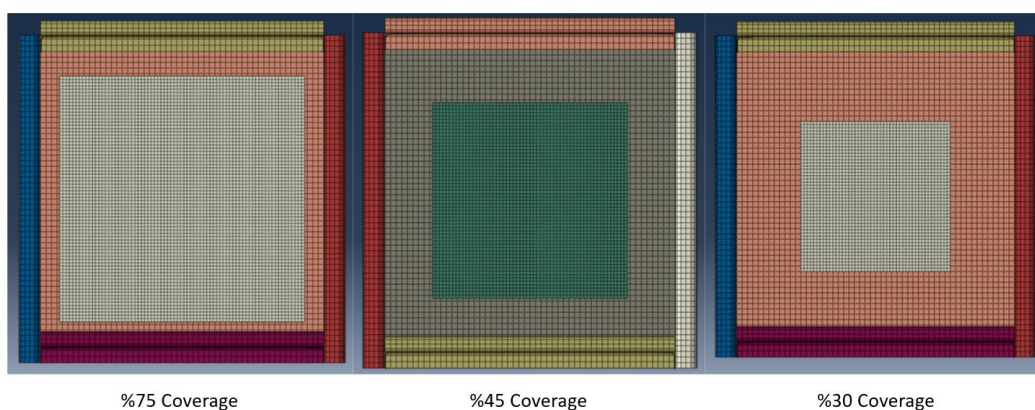


Figure 5.6. 75, 45 and 30 Percent Coverage Areas

Due to material limitation available the coverage area is decreased further to 15 percent, using 100mm by 100mm square region on central area, and the base layer configuration is increased to triple constrained layer condition. The CLD strip is 50mm width with more than 5m, the configuration distribution is selected as 50mm by 100mm strips side by side as shown in figure below.

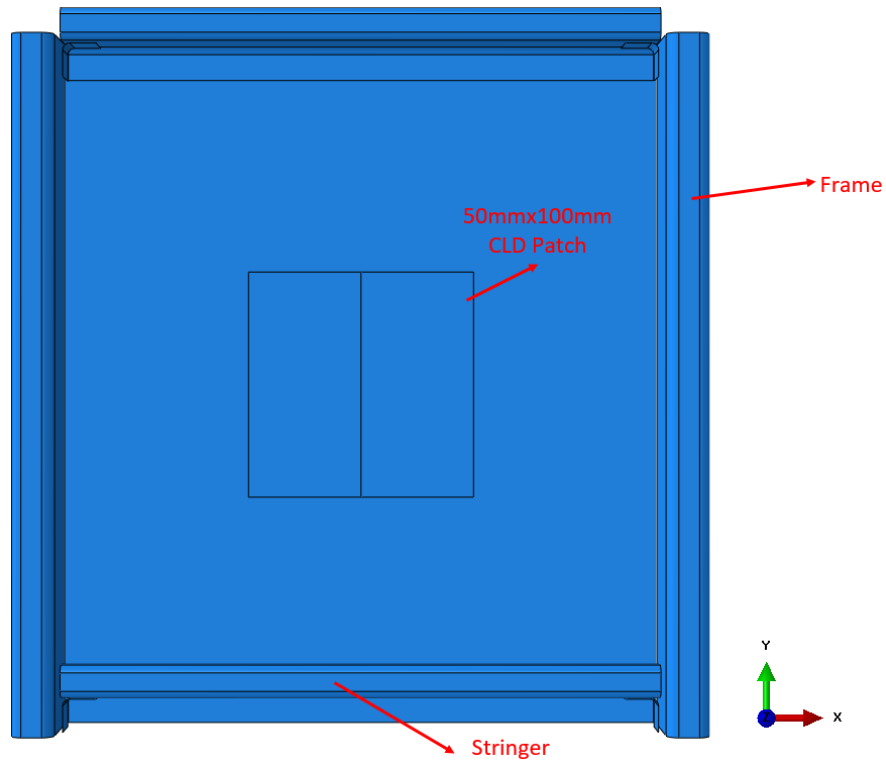


Figure 5.7. Orientation and Location of Damping Treatment

Furthermore, due to decreased area the additional weight limits are changed as given in below table.

Table 5.3. Additional Mass with respect to Configurations

Configuration	Weight Added (g)	Weight Added (%)	Thickness (mm)	Contact Area (mm <sup>2</sup> )	Contact Area Percent (%)
SCLD	8.001	1%	0.127+0.254	10000	100%
DCLD	16.002	3%	2x(0.127+0.254)	2x10000	200%
TCLD	24.003	4%	3x(0.127+0.254)	3x10000	300%
UNIFORM	23.8506	4%	1.524	10000	100%

For baseline selection single, double and triple constrained layer damping treatment is selected as off the shelf solutions and the weight limit of the triple constrained layer is used for standoff solutions. For state of art baseline solution uniform spacer with single constraining layer is used.

For above mentioned geometries the frequency response functions, damping ratios and band power reductions in full, 1/3, 1/10 and narrow octave band is given below. Although it is expected, also clearly seen from the below results that the best solution is the triple constrained layer damping solution between multiple constrained layer treatments due to high viscoelastic material in treatment and addition of spacer in to design increases damping performance.

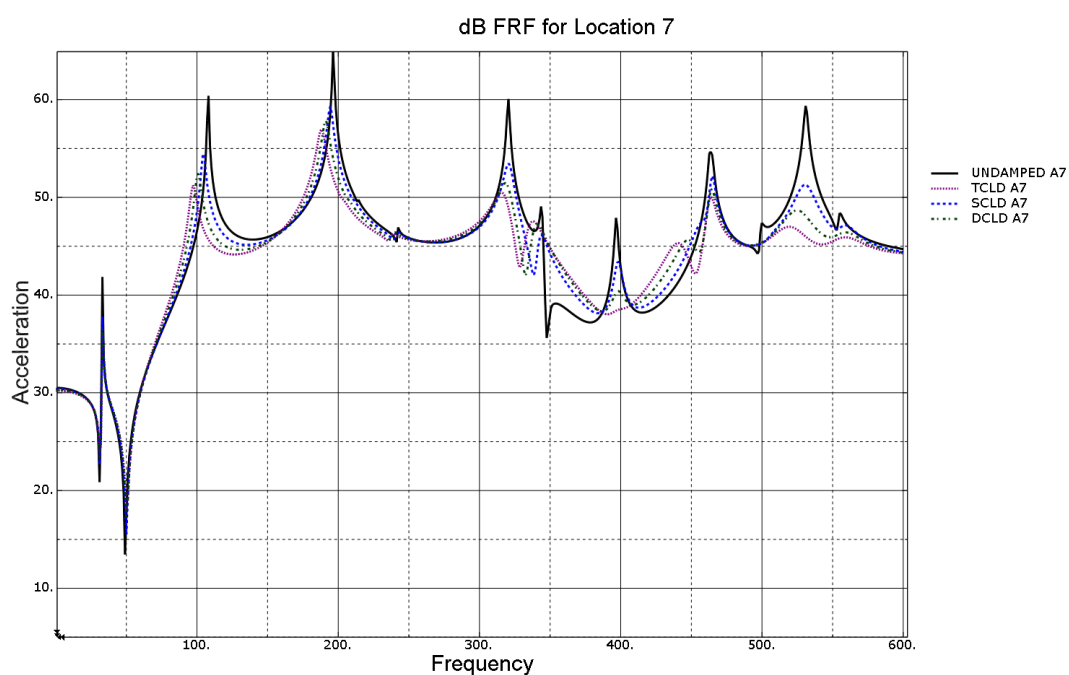


Figure 5.8. Bare Plate vs Single, Double and Triple CLDs Point 7

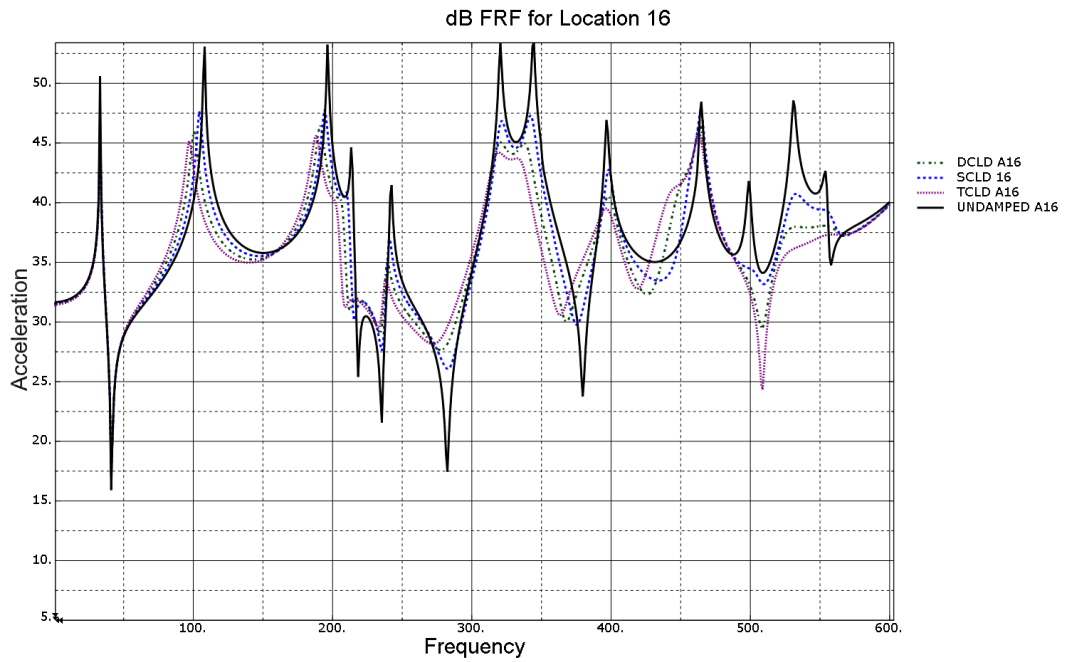


Figure 5.9. Bare Plate vs Single, Double and Triple CLDs Point 16

Table 5.4. Input point 10 Output point 7 damping Ratios

ACC7	Mode1 Damping Ratio	Frequency (Hz)	Mode2 Damping Ratio	Frequency (Hz)	Mode3 Damping Ratio	Frequency (Hz)
Bare	0.0098	33.06	0.0051	108.18	0.0028	196.33
SCDL	0.0119	33.06	0.0139	104.17	0.0091	194.32
DCDL	0.0139	33.06	0.0198	101.17	0.0123	191.32
TCDL	0.0172	33.06	0.0226	97.16	0.0147	188.31
ACC7	Mode4 Damping Ratio	Frequency (Hz)	Mode5 Damping Ratio	Frequency (Hz)	Mode6 Damping Ratio	Frequency (Hz)
Bare	0.0025	320.53	0.0037	343.57	0.0026	396.66
SCDL	0.0100	320.53	0.0110	343.57	0.0068	398.66
DCDL	0.0154	318.53	0.0145	340.57	N/A	398.66
TCDL	N/A	315.53	0.0177	337.56	N/A	N/A

ACC7	Mode7 Damping Ratio	Frequency (Hz)	Mode8 Damping Ratio	Frequency (Hz)	Mode9 Damping Ratio	Frequency (Hz)
Bare	N/A	N/A	0.0041	463.77	N/A	N/A
SCDL	N/A	N/A	0.0045	464.78	N/A	N/A
DCDL	N/A	N/A	0.0059	464.78	N/A	N/A
TCDL	0.0178	440.74	0.0069	463.77	N/A	N/A
ACC7	Mode10 Damping Ratio	Frequency (Hz)	Mode11 Damping Ratio	Frequency (Hz)	Mode12 Damping Ratio	Frequency (Hz)
Bare	0.0025	530.89	0.0012	554.93		
SCDL	0.0134	530.89	N/A	N/A		
DCDL	0.0218	524.88	N/A	553.92		
TCDL	N/A	518.87	N/A	558.93		

Table 5.5. Input point 10 Output point 16 damping Ratios

ACC16	Mode1 Damping Ratio	Frequency (Hz)	Mode2 Damping Ratio	Frequency (Hz)	Mode3 Damping Ratio	Frequency (Hz)
Bare	0.0097	33.06	0.0052	108.18	0.0028	196.33
SCDL	0.0111	33.06	0.0137	104.17	0.0091	194.32
DCDL	0.0120	33.06	0.0198	100.17	0.0124	191.32
TCDL	0.0129	33.06	0.0222	97.16	0.0148	188.31
ACC16	Mode4 Damping Ratio	Frequency (Hz)	Mode5 Damping Ratio	Frequency (Hz)	Mode6 Damping Ratio	Frequency (Hz)
Bare	0.0036	213.36	0.0038	242.40	0.0024	320.53
SCDL	N/A	N/A	0.0074	240.40	0.0280	321.54
DCDL	N/A	N/A	0.0677	239.40	N/A	320.53
TCDL	N/A	N/A	0.0130	238.40	N/A	319.53
ACC16	Mode7 Damping Ratio	Frequency (Hz)	Mode8 Damping Ratio	Frequency (Hz)	Mode9 Damping Ratio	Frequency (Hz)
Bare	0.0033	344.57	0.0026	396.66	0.0023	464.78
SCDL	0.0108	342.57	0.0064	398.66	0.0046	464.78
DCDL	N/A	337.56	0.0117	397.66	0.0058	463.77
TCDL	N/A	332.55	0.0161	396.66	0.0069	462.77
ACC16	Mode10 Damping Ratio	Frequency (Hz)	Mode11 Damping Ratio	Frequency (Hz)	Mode12 Damping Ratio	Frequency (Hz)
Bare	0.0026	498.83	0.0026	530.89	0.0042	553.92
SCDL	N/A	N/A	N/A	532.89	N/A	N/A
DCDL	N/A	N/A	N/A	N/A	N/A	N/A
TCDL	N/A	N/A	N/A	N/A	N/A	N/A

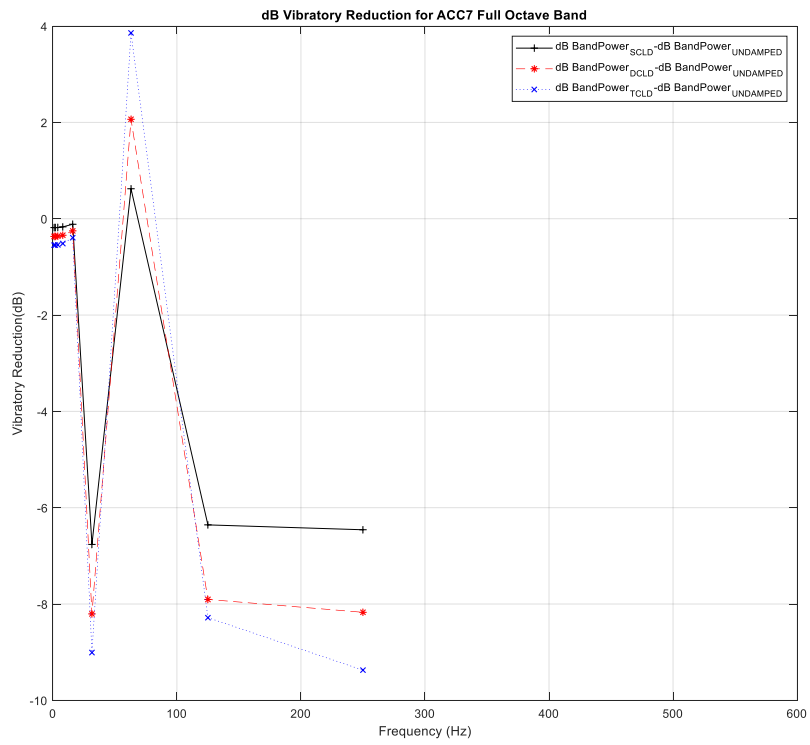


Figure 5.10. Full Octave Band dB Band Power Reduction Point 7

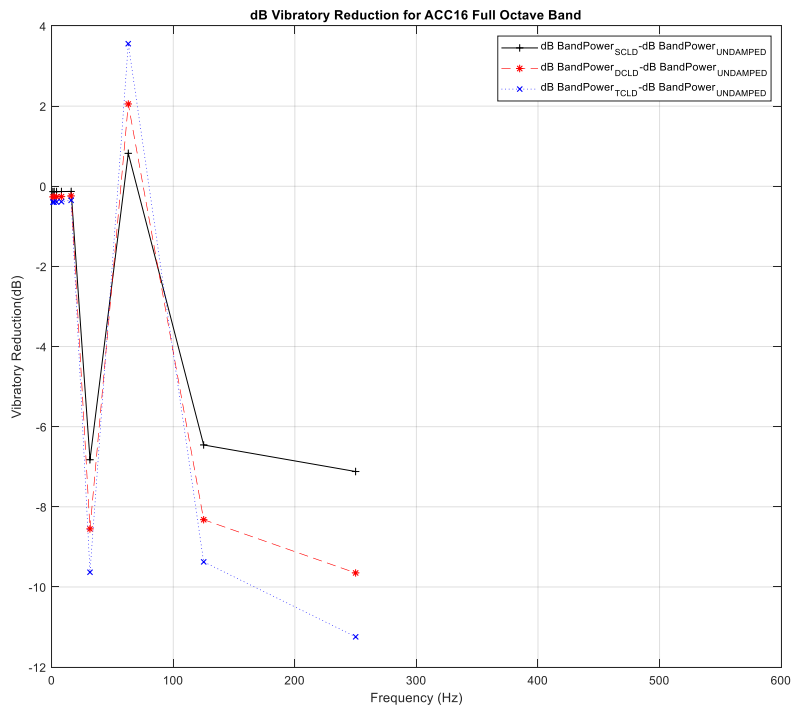


Figure 5.11. Full Octave Band dB Band Power Reduction Point 16

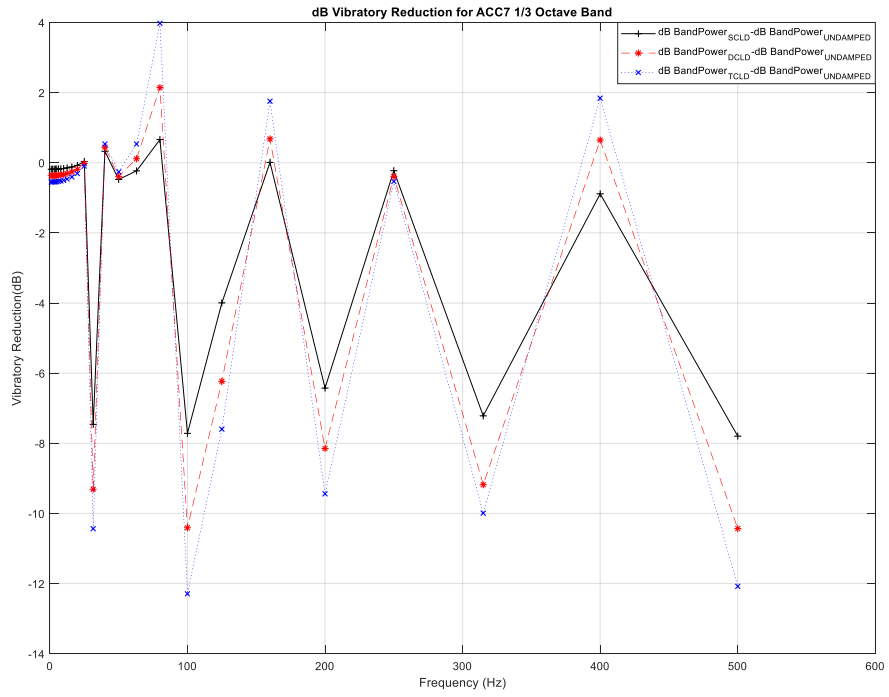


Figure 5.12. 1/3 Octave Band dB Band Power Reduction Point 7

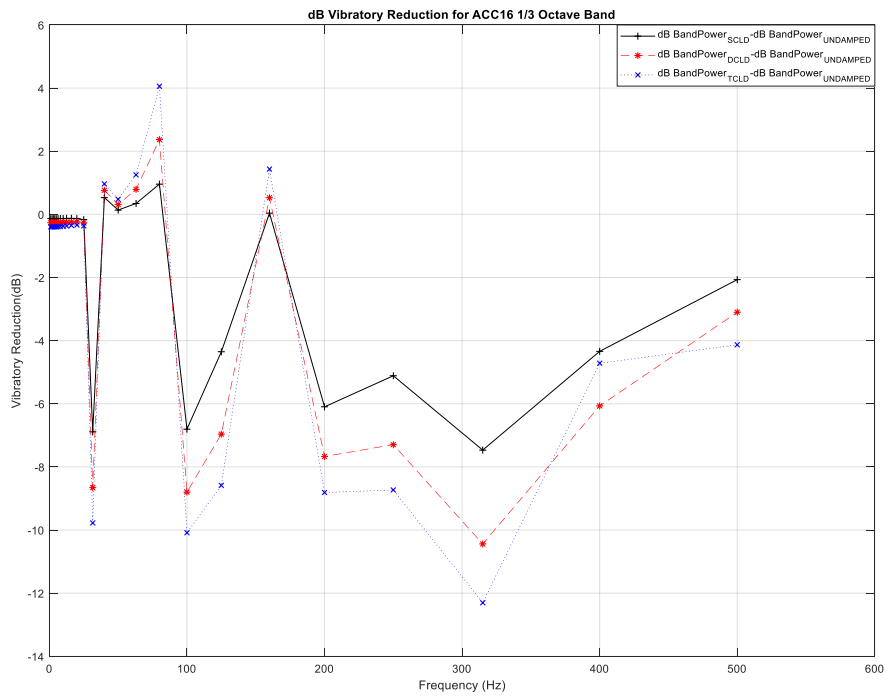


Figure 5.13. 1/3 Octave Band dB Band Power Reduction Point 16

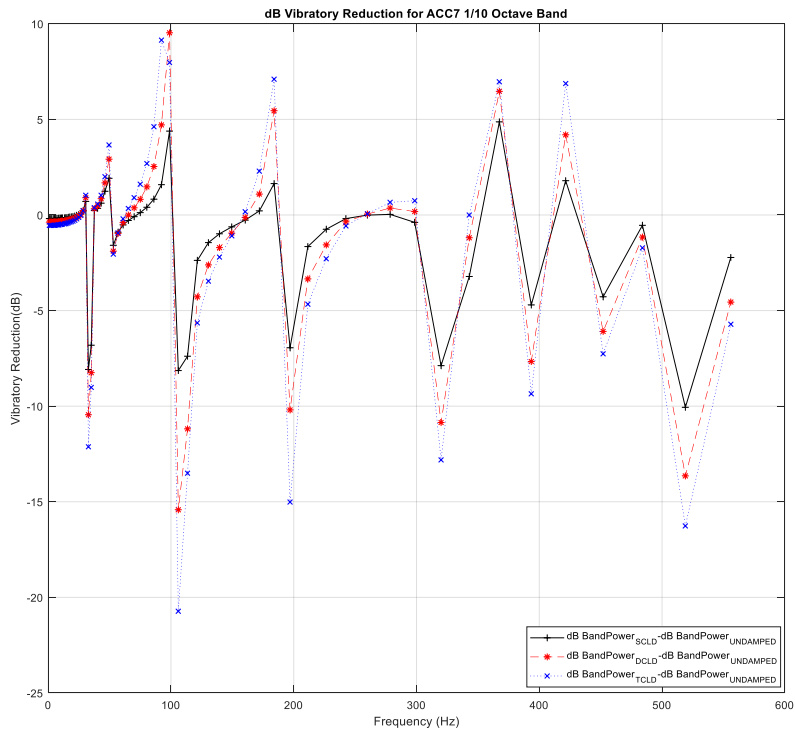


Figure 5.14. 1/10 Octave Band dB Band Power Reduction Point 7

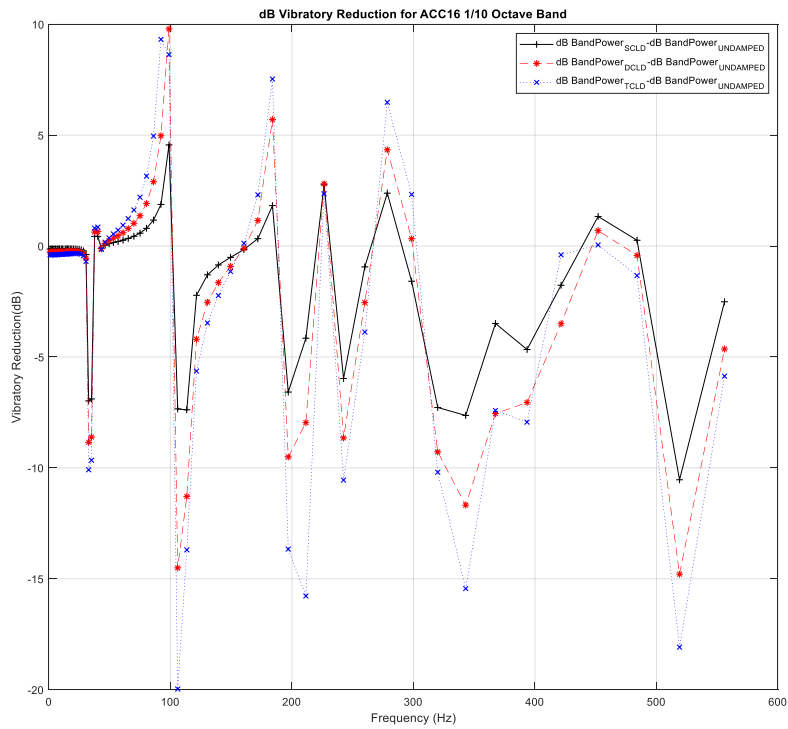


Figure 5.15. 1/10 Octave Band dB Band Power Reduction Point 16

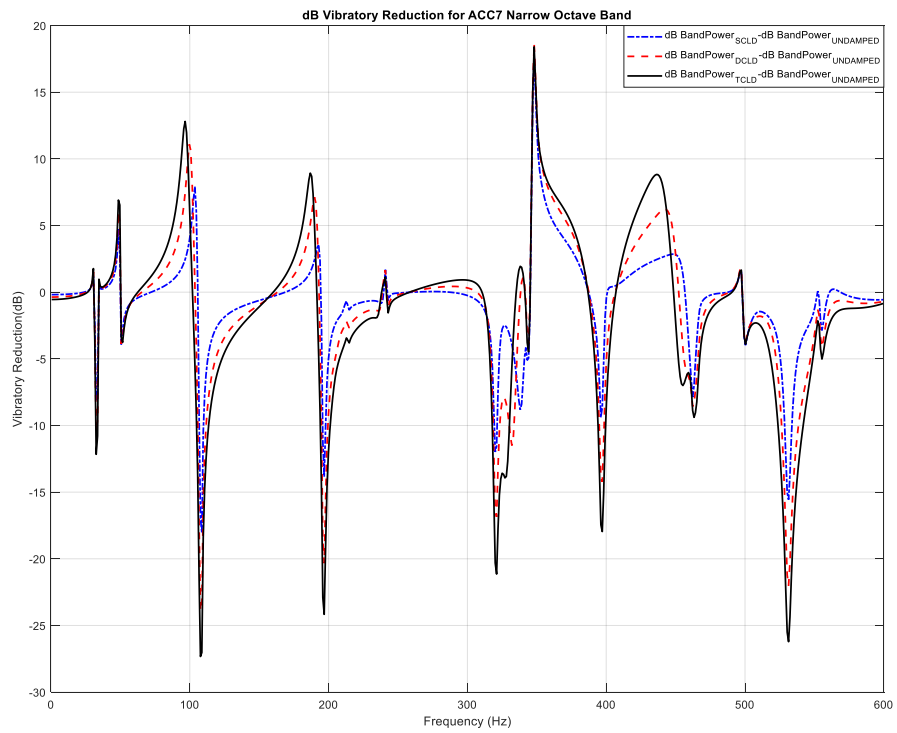


Figure 5.16. Narrow Octave Band dB Band Power Reduction Point 7

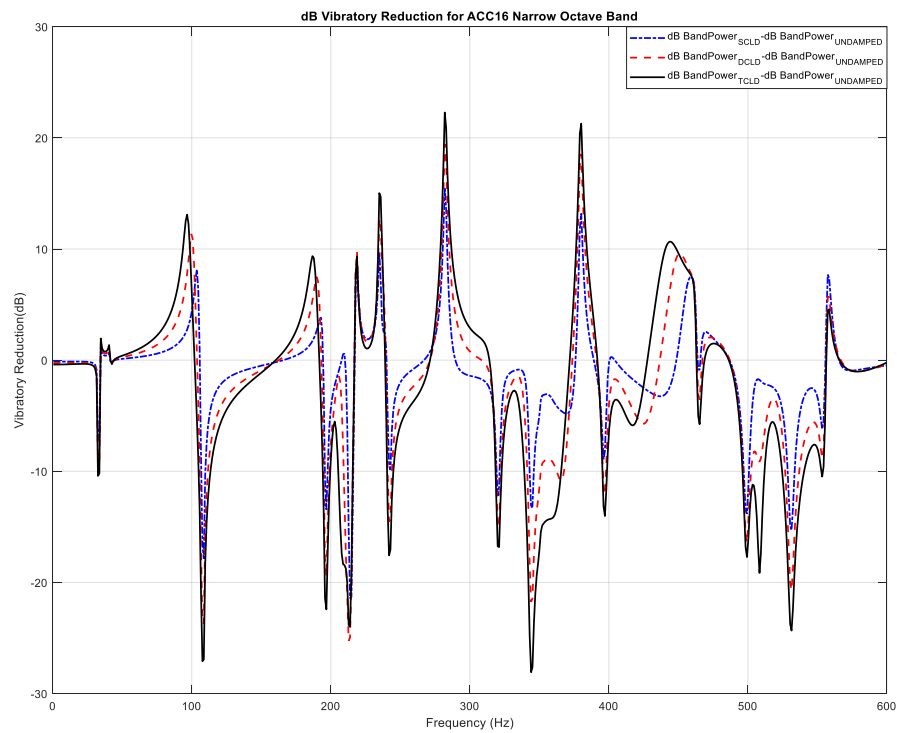


Figure 5.17. Narrow Octave Band dB Band Power Reduction Point 16

As found to be the best solution between multi-constrained layer damping treatments, TCLD was compared with uniform standoff layer treatment as follows. As expected due to shift in neutral axis, although the VEM material is one third of TCLD, the damping ratios on every mode is higher than the TCLD for uniform standoff. Due to added stiffness in the central region of fuselage, some modes are nearly vanished for uniform treatment. Due to coverage area and mode shape, in first mode the effect of spacer cannot be measured enough since the first mode of fuselage is the twisting from frames and stringers and the centre region is mostly stationary where spacer is located. In higher modes, the increase in damping ratios can be seen from FRFs and dB reduction graph. Also shifts in mode frequencies observed in TCLD treatment is less in the uniform standoff treatment which also can be clearly seen from the FRF plots given below.

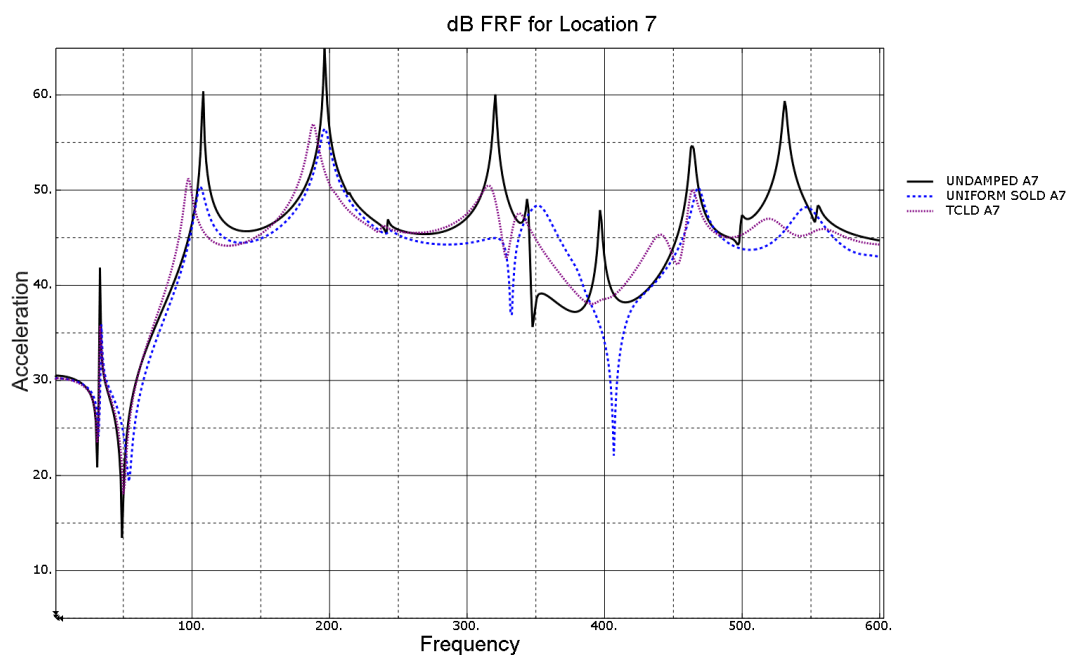


Figure 5.18. Bare Plate vs Triple CLD vs Uniform Spacer Point 7

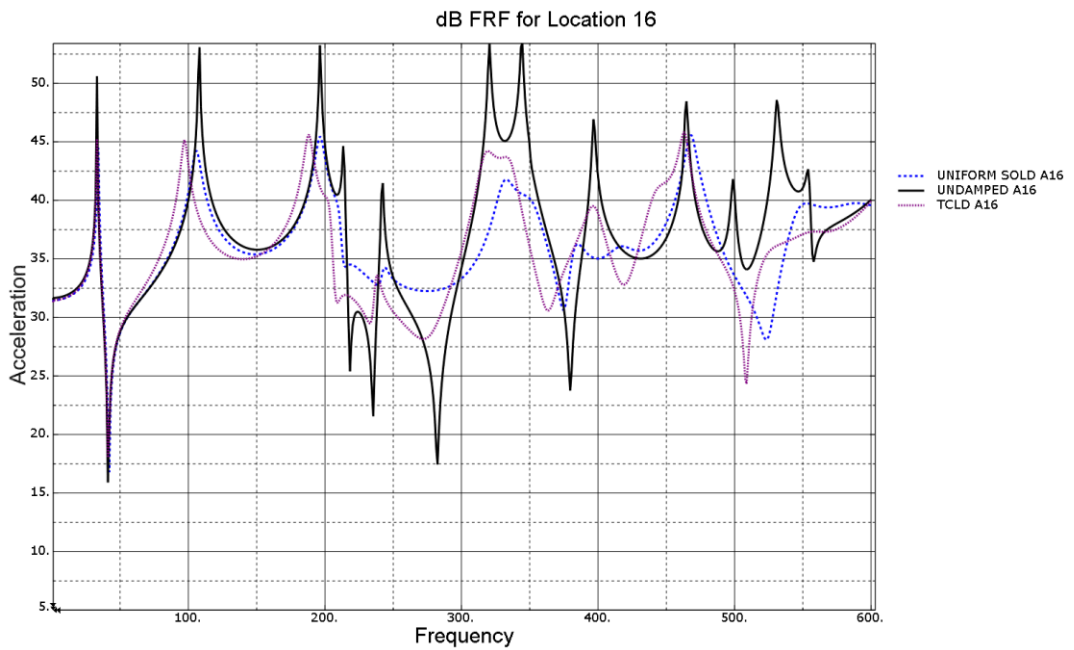


Figure 5.19. Bare Plate vs Triple CLD vs Uniform Spacer Point 16

Table 5.6. Input point 10 Output point 7 damping Ratios

ACC7	Mode1 Damping Ratio	Frequency (Hz)	Mode2 Damping Ratio	Frequency (Hz)	Mode3 Damping Ratio	Frequency (Hz)
Bare	0.0098	33.06	0.0051	108.18	0.0028	196.33
TCDL	0.0172	33.06	0.0226	97.16	0.0147	188.31
UNIFORM	0.0131	34.06	0.0287	106.18	0.0154	196.33
ACC7	Mode4 Damping Ratio	Frequency (Hz)	Mode5 Damping Ratio	Frequency (Hz)	Mode6 Damping Ratio	Frequency (Hz)
Bare	0.0025	320.53	0.0037	343.57	0.0026	396.66
TCDL	N/A	315.53	0.0177	337.56	N/A	N/A
UNIFORM	N/A	N/A	0.0251	351.59	N/A	N/A

ACC7	Mode7 Damping Ratio	Frequency (Hz)	Mode8 Damping Ratio	Frequency (Hz)	Mode9 Damping Ratio	Frequency (Hz)
Bare	N/A	N/A	0.0041	463.77	N/A	N/A
TCDL	0.0178	440.74	0.0069	463.77	N/A	N/A
UNIFORM	N/A	N/A	0.0081	467.78	N/A	N/A
ACC7	Mode10 Damping Ratio	Frequency (Hz)	Mode11 Damping Ratio	Frequency (Hz)	Mode12 Damping Ratio	Frequency (Hz)
Bare	0.0025	530.89	0.0012	554.93		
TCDL	N/A	518.87	N/A	558.93		
UNIFORM	N/A	N/A	0.0195	546.91		

Table 5.7. Input point 10 Output point 16 damping Ratios

ACC16	Mode1 Damping Ratio	Frequency (Hz)	Mode2 Damping Ratio	Frequency (Hz)	Mode3 Damping Ratio	Frequency (Hz)
Bare	0.0097	33.06	0.0052	108.18	0.0028	196.33
TCDL	0.0129	33.06	0.0222	97.16	0.0148	188.31
UNIFORM	0.0129	34.06	0.0285	106.18	0.0156	196.33
ACC16	Mode4 Damping Ratio	Frequency (Hz)	Mode5 Damping Ratio	Frequency (Hz)	Mode6 Damping Ratio	Frequency (Hz)
Bare	0.0036	213.36	0.0038	242.40	0.0024	320.53
TCDL	N/A	N/A	0.0130	238.40	N/A	319.53
UNIFORM	N/A	N/A	N/A	N/A	0.0328	332.55

ACC16	Mode7 Damping Ratio	Frequency (Hz)	Mode8 Damping Ratio	Frequency (Hz)	Mode9 Damping Ratio	Frequency (Hz)
Bare	0.0033	344.57	0.0026	396.66	0.0023	464.78
TCDL	N/A	332.55	0.0161	396.66	0.0069	462.77
UNIFORM	N/A	N/A	N/A	385.64	0.0077	467.78
ACC16	Mode10 Damping Ratio	Frequency (Hz)	Mode11 Damping Ratio	Frequency (Hz)	Mode12 Damping Ratio	Frequency (Hz)
Bare	0.0026	498.83	0.0026	530.89	0.0042	553.92
TCDL	N/A	N/A	N/A	N/A	N/A	N/A
UNIFORM	N/A	N/A	N/A	N/A	N/A	552.92

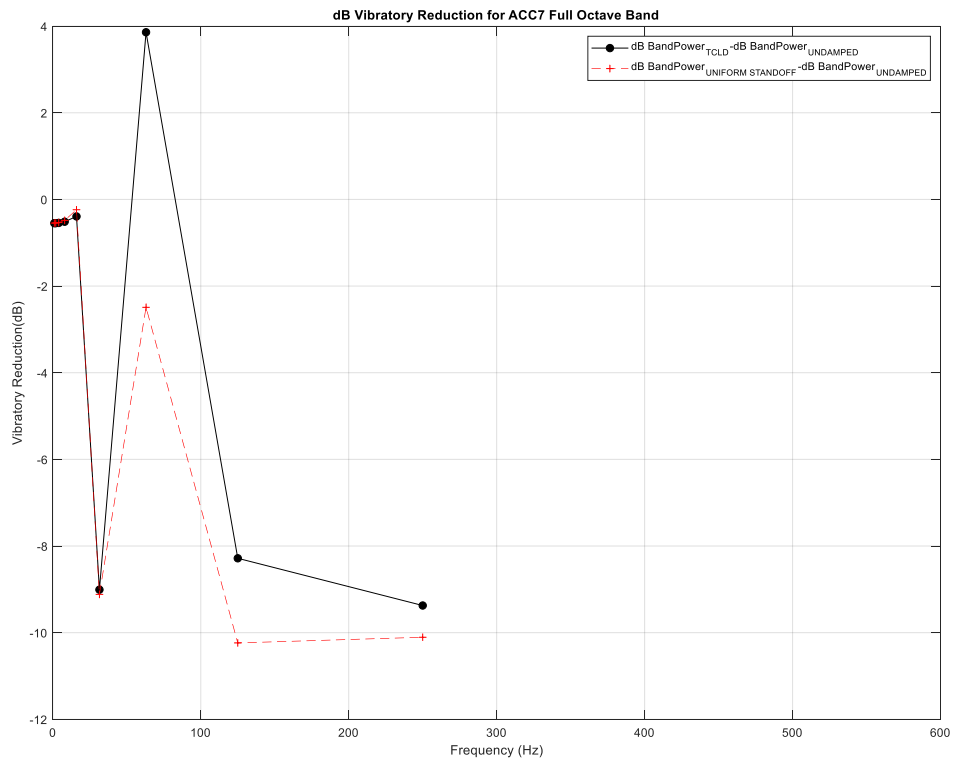


Figure 5.20. Full Octave Band dB Band Power Reduction Point 7

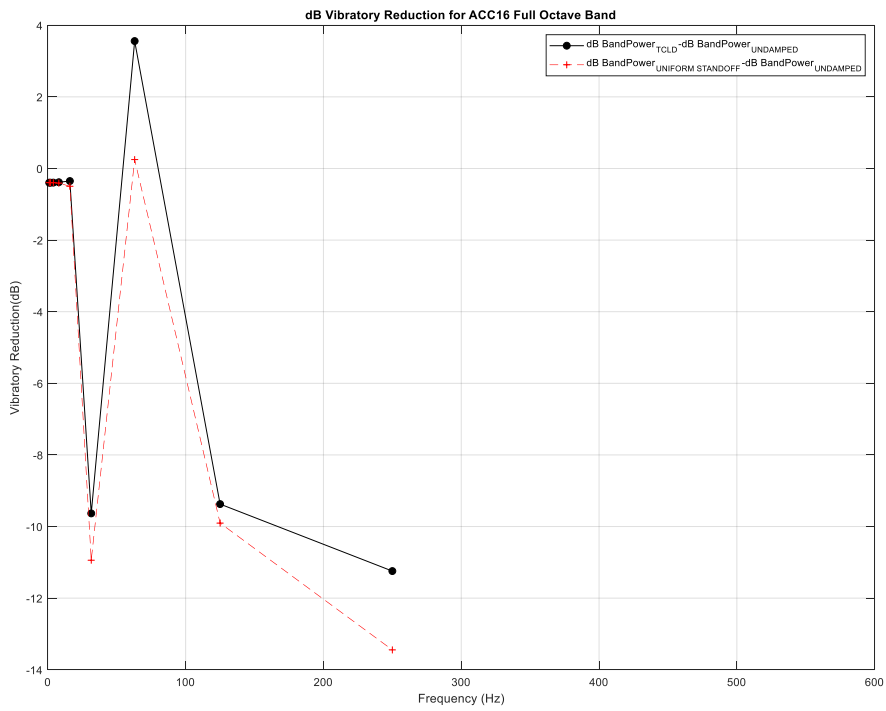


Figure 5.21. Full Octave Band dB Band Power Reduction Point 16

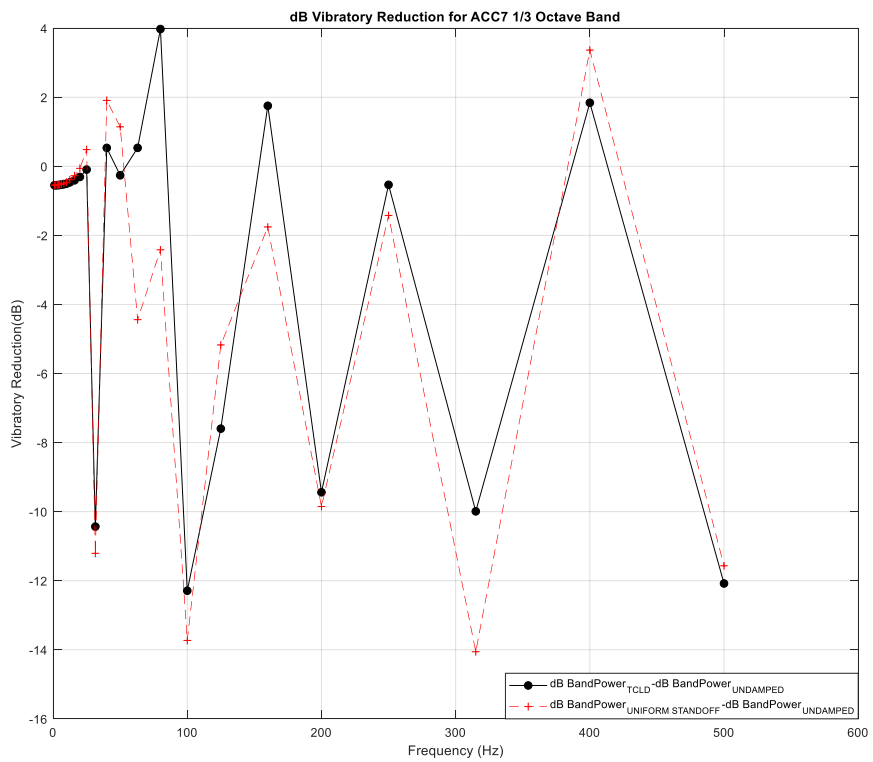


Figure 5.22. 1/3 Octave Band dB Band Power Reduction Point 7

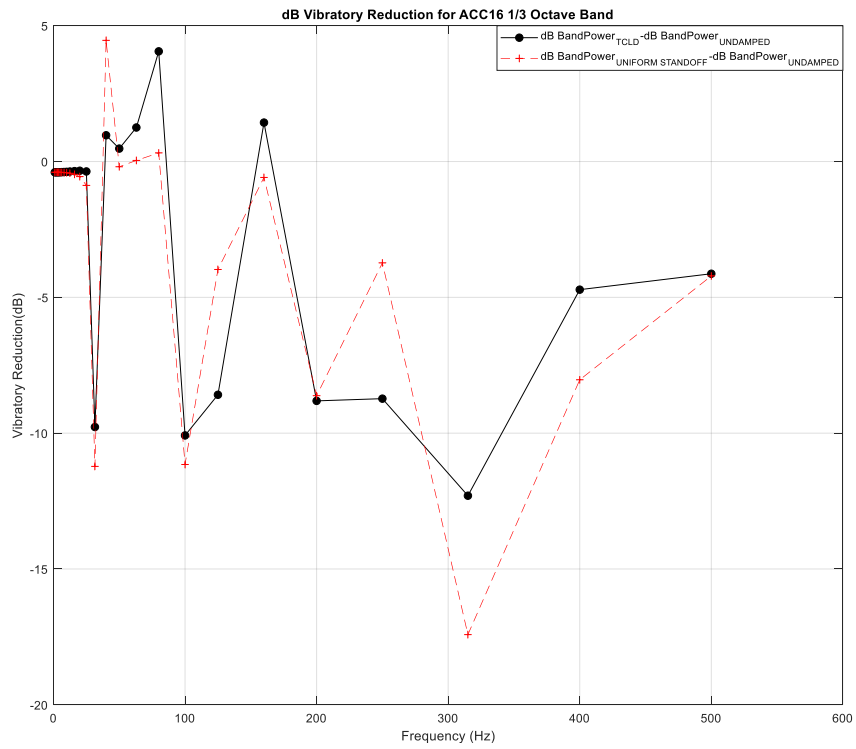


Figure 5.23. 1/3 Octave Band dB Band Power Reduction Point 16

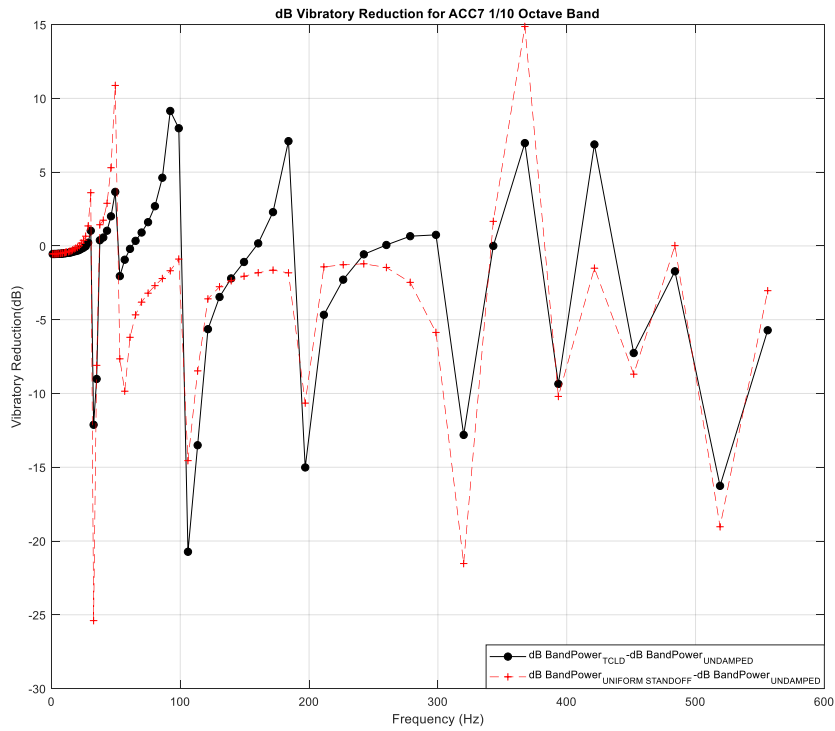


Figure 5.24. 1/10 Octave Band dB Band Power Reduction Point 7

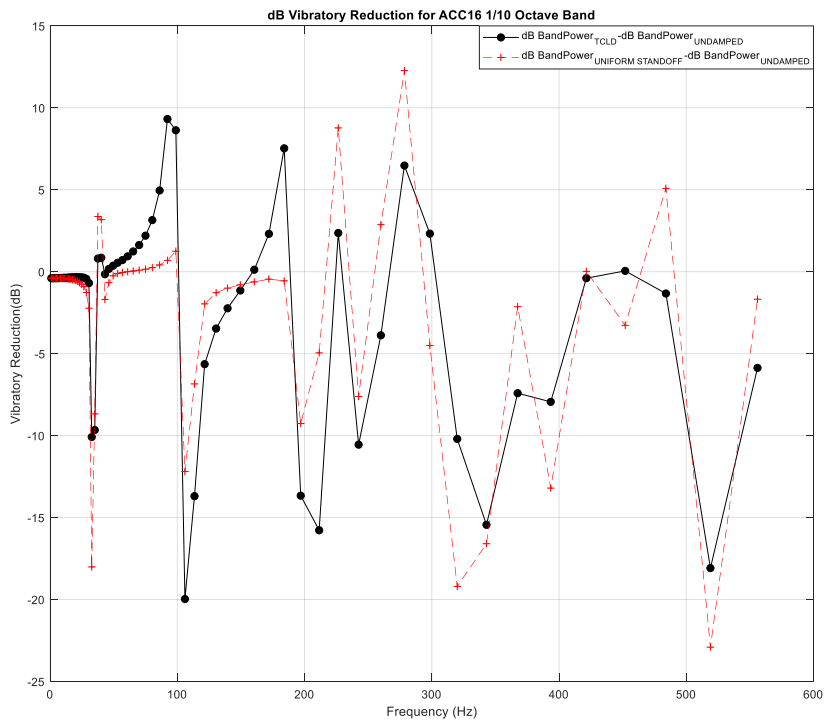


Figure 5.25. 1/10 Octave Band dB Band Power Reduction Point 16

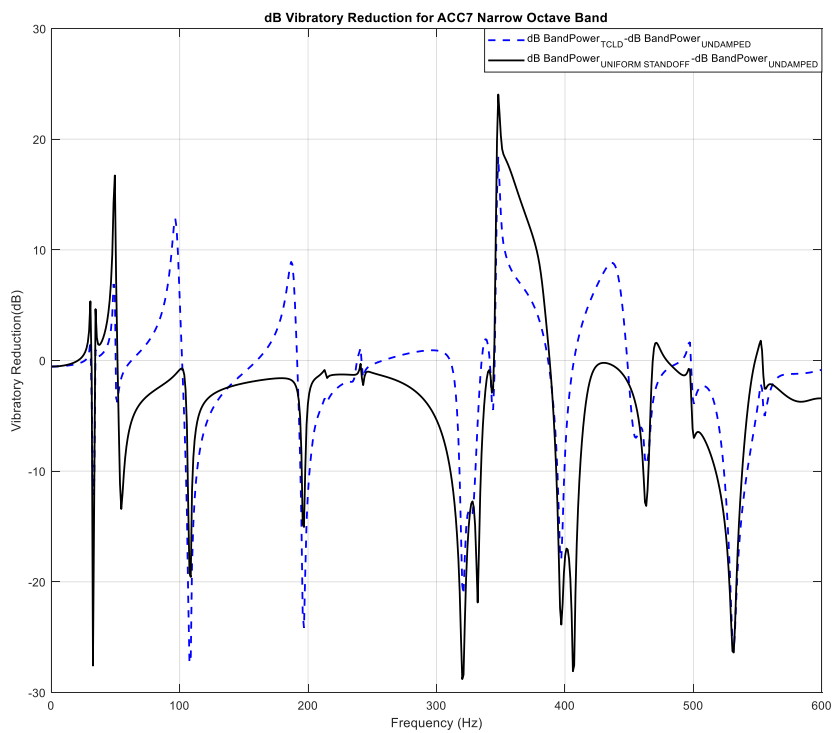


Figure 5.26. Narrow Octave Band dB Band Power Reduction Point 7

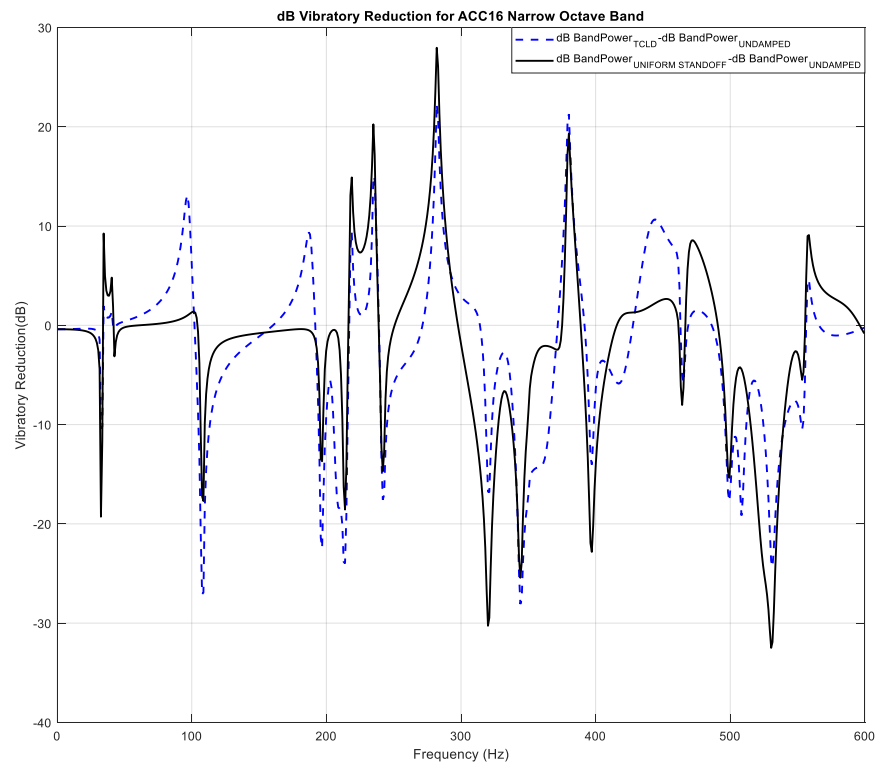


Figure 5.27. Narrow Octave Band dB Band Power Reduction Point 16

### 5.3. Optimized Spacer Geometry Modeling

#### 5.3.1. Optimized Spacer Geometry Using Literature Knowledge

Seeing that neutral axis shift increases the damping performance, increasing the tower height in a cost of reduced coverage contact area has to be studied for optimum width and height of the slotted towers. The slotted designs geometries are designed as periodic in parametric length which is changed between baselines and for each fixed length two different tower to gland ratio is used to simulate the height versus tower height effect of the solution. A basic scaled figure is shown below to visualize the change of design aspect between slotted designs. Although it is not a novel design, the parametric slotted design study is a design process for finding the optimal design for a fuselage like structure.

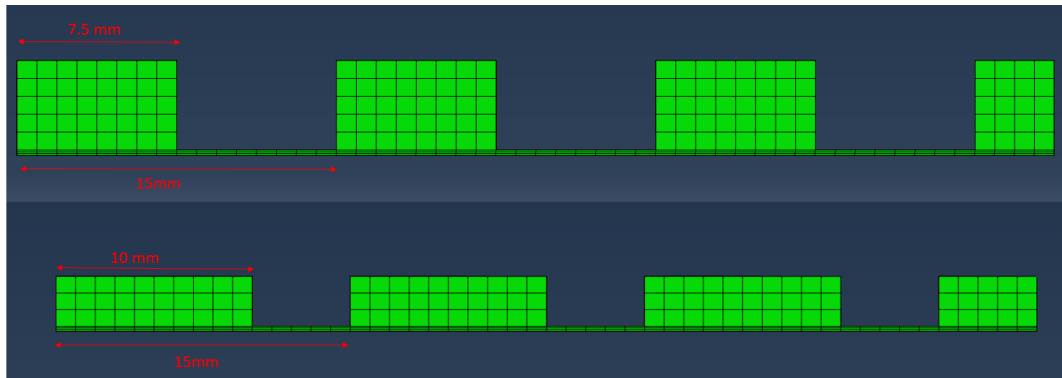


Figure 5.28. 15mm Periodic Slotted Spacer Design for equal and twice tower length

Also the spacer geometry was selected to be manufactured with 3D printing machine which has a fixed minimum thickness value of 0.254mm per layer and the height a values are adjusted to be times of this minimum thickness value. In the following table the weight, height and coverage area values of the baseline study solutions along with spacer designs can be found. For each slotted design the tower height is adjusted in order to maintain the same weight in each solution and increase the neutral axis shift to increase the shear deformation induced in VEM layer.

Table 5.8. Additional Mass with respect to Configurations

Configuration	Weight Added (g)	Weight Added (%)	Thickness (mm)	Contact Area (mm <sup>2</sup> )	Contact Area Percent (%)
SCLD	8.001	1%	0.127+0.254	10000	100%
DCLD	16.002	3%	2x(0.127+0.254)	2x10000	200%
TCLD	24.003	4%	3x(0.127+0.254)	3x10000	300%
UNIFORM	23.8506	4%	1.524	10000	100%
Slotted 10mm 1v1	23.975	4%	5.588	2500	25%

Slotted 10mm 2v1	23.557	4%	3.048	4444.4	44%
Slotted 15mm 1v1	23.641	4%	4.572	2899.82	29%
Slotted 15mm 2v1	23.587	4%	2.794	4900	49%
Slotted 20mm 1v1	23.851	4%	5.334	2500	25%
Slotted 20mm 2v1	23.557	4%	3.048	4444.448	44%

The slot width and tower height is summarized in the following table for clarification. The uniform spacer is compared with slotted spacer designs only, since it is selected to be the best solution among baseline designs, to find the optimal height and spacing of the spacer geometry for plate structure.

Table 5.9. Additional Mass with respect to Configurations

Slotted Designs	Tower Height	Tower Width	Slot Width
10 mm 1v1	5.588	5	5
10 mm 2v1	3.048	6.66666667	3.333333
15 mm 1v1	4.572	7.5	7.5
15 mm 2v1	2.794	10	5
20 mm 1v1	5.334	10	10
20 mm 2v1	3.048	13.3333333	6.666667

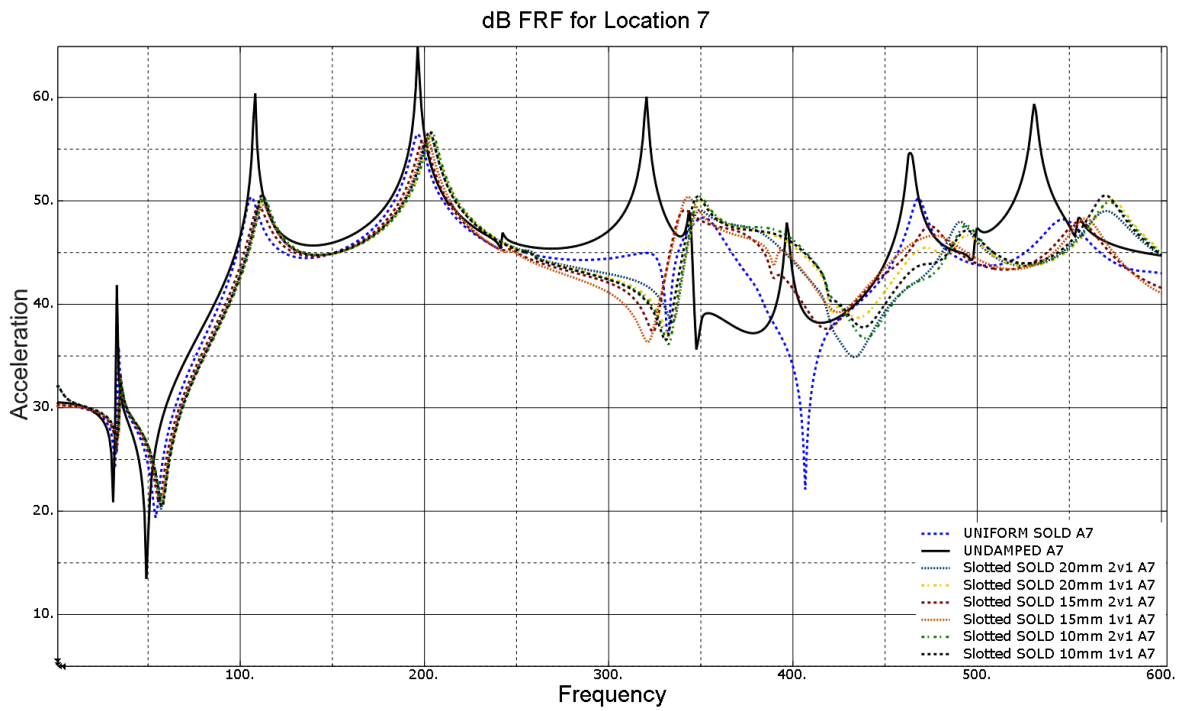


Figure 5.29. Uniform vs Slotted Spacers Point 7

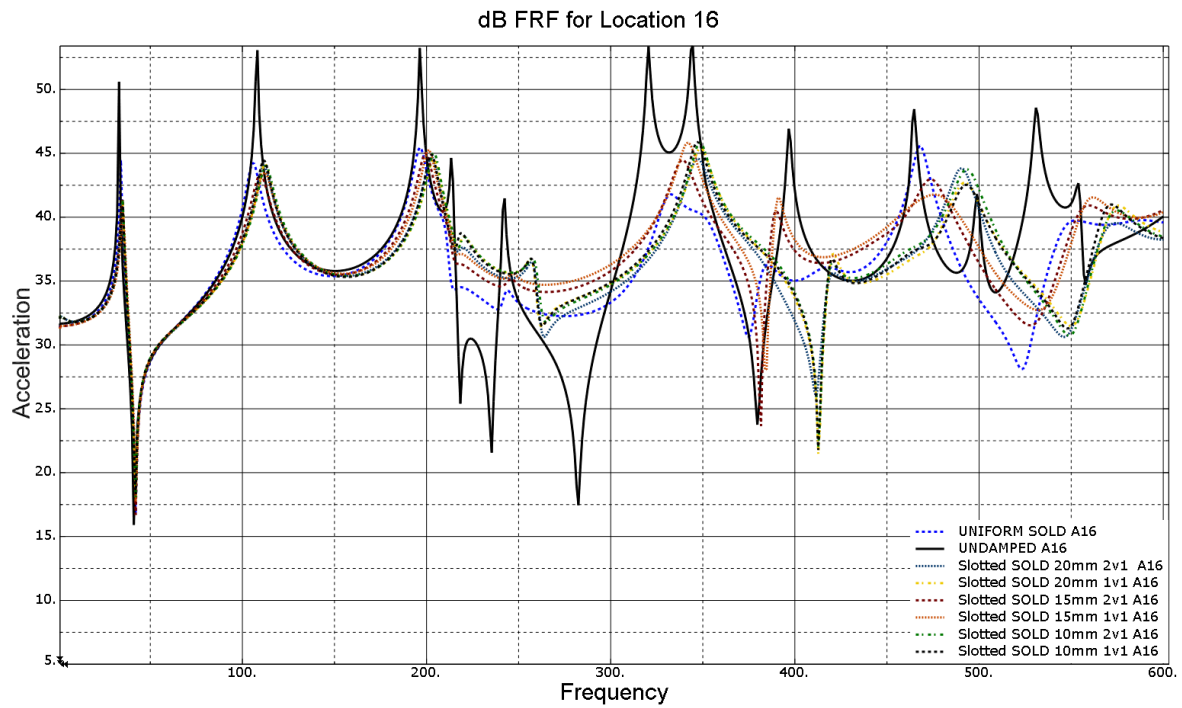


Figure 5.30. Uniform vs Slotted Spacers Point 16

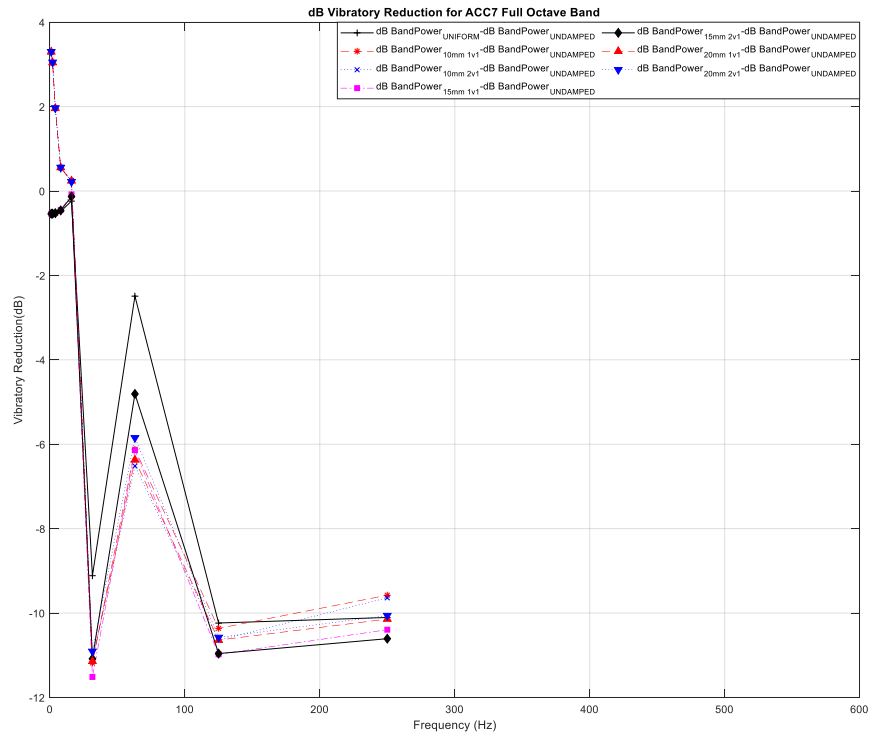


Figure 5.31. Full Octave Band dB Band Power Reduction Point 7

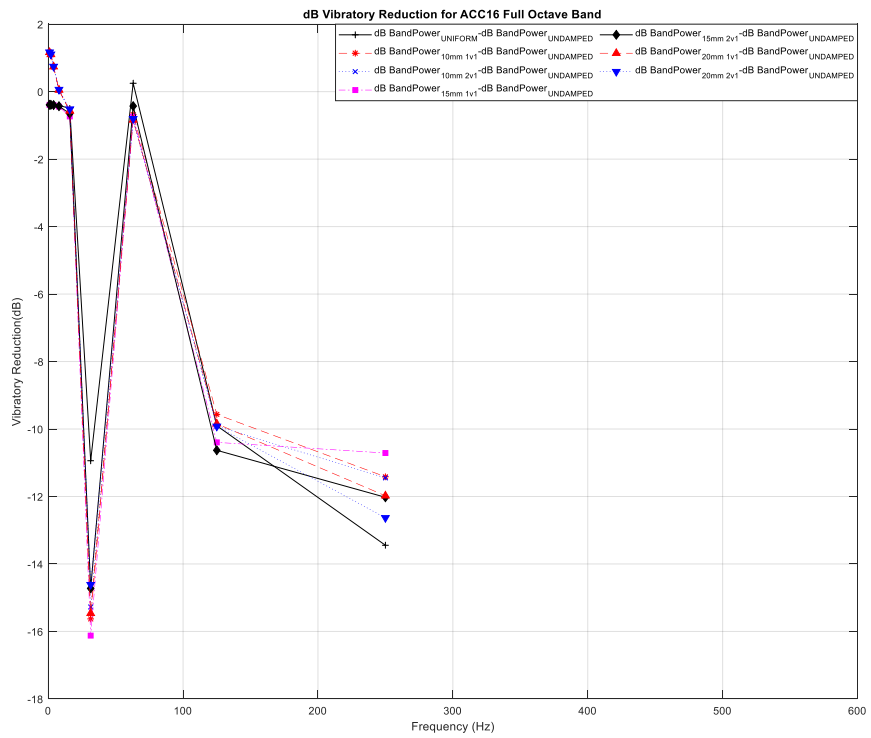


Figure 5.32. Full Octave Band dB Band Power Reduction Point 16

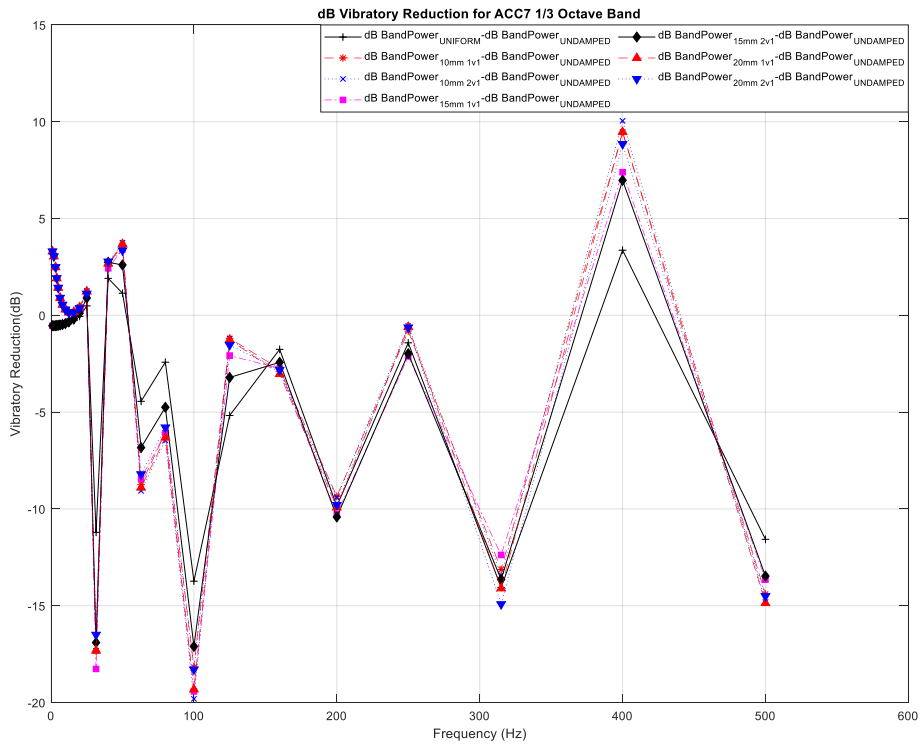


Figure 5.33. 1/3 Octave Band dB Band Power Reduction Point 7

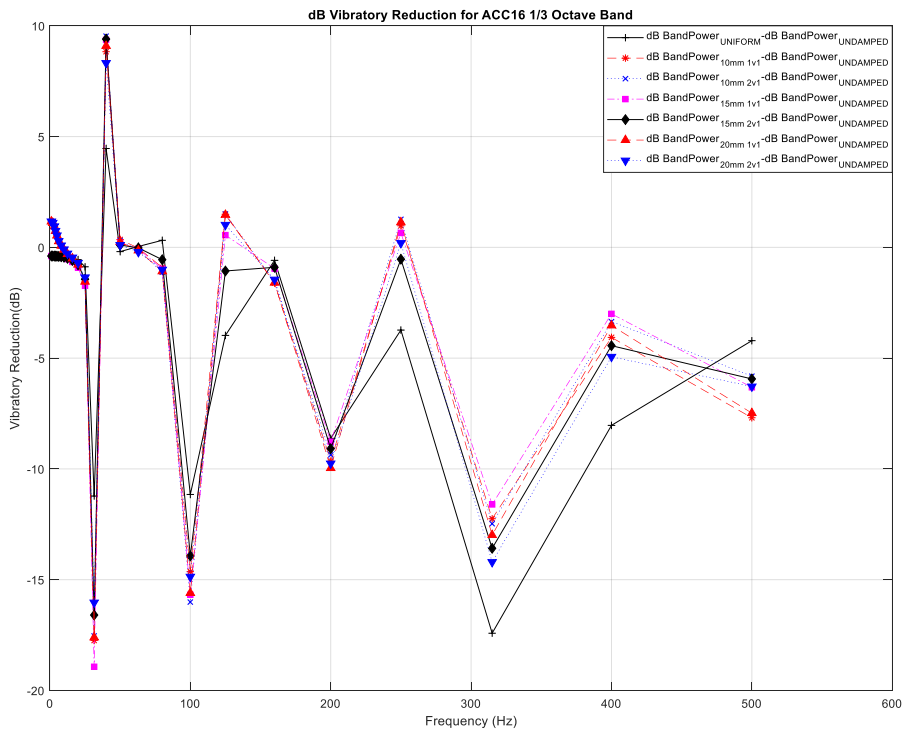


Figure 5.34. 1/3 Octave Band dB Band Power Reduction Point 16

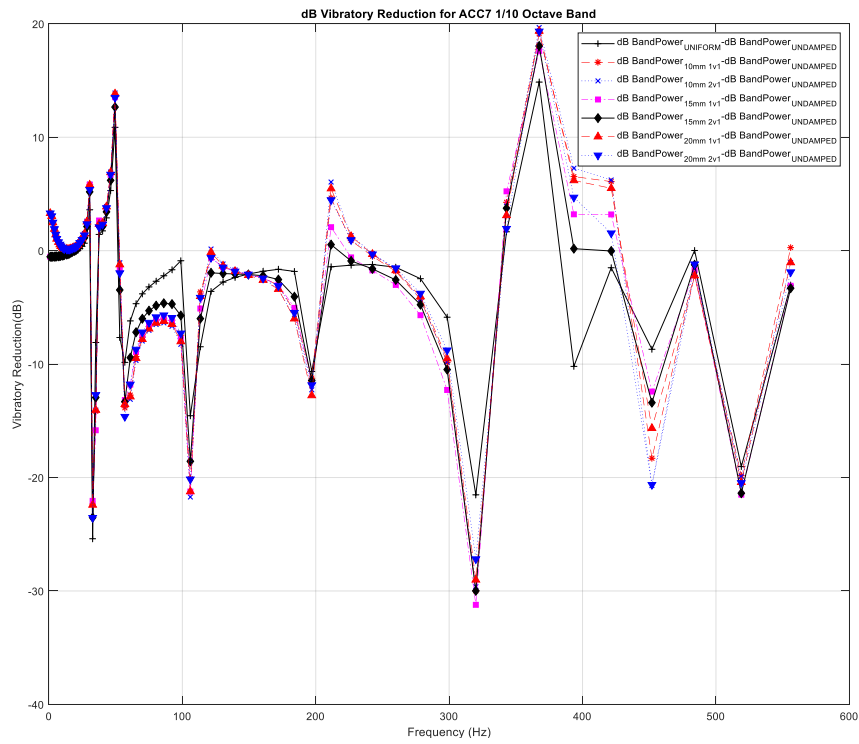


Figure 5.35. 1/10 Octave Band dB Band Power Reduction Point 7

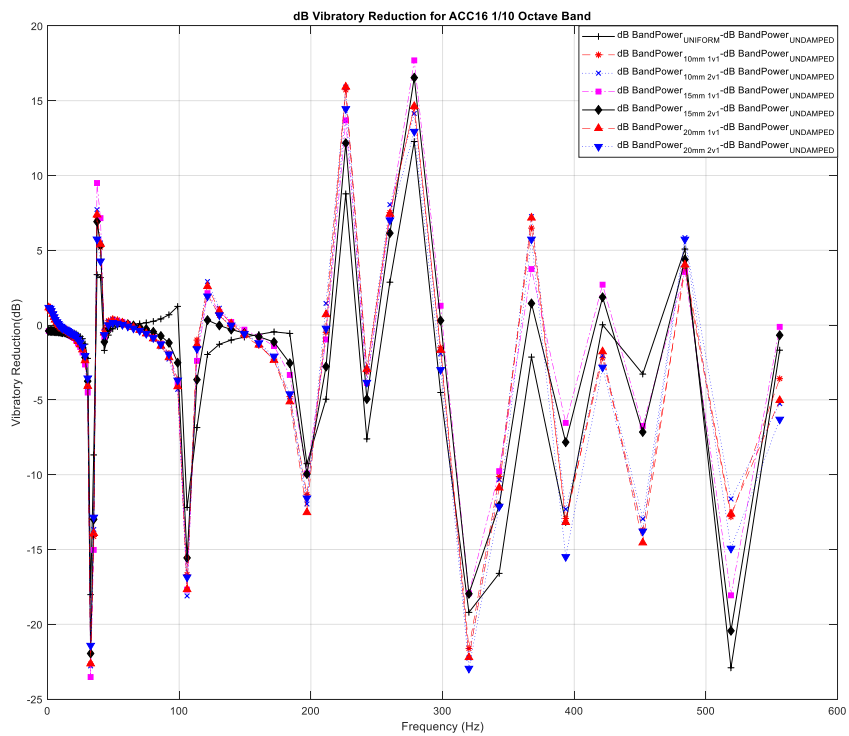


Figure 5.36. 1/10 Octave Band dB Band Power Reduction Point 16

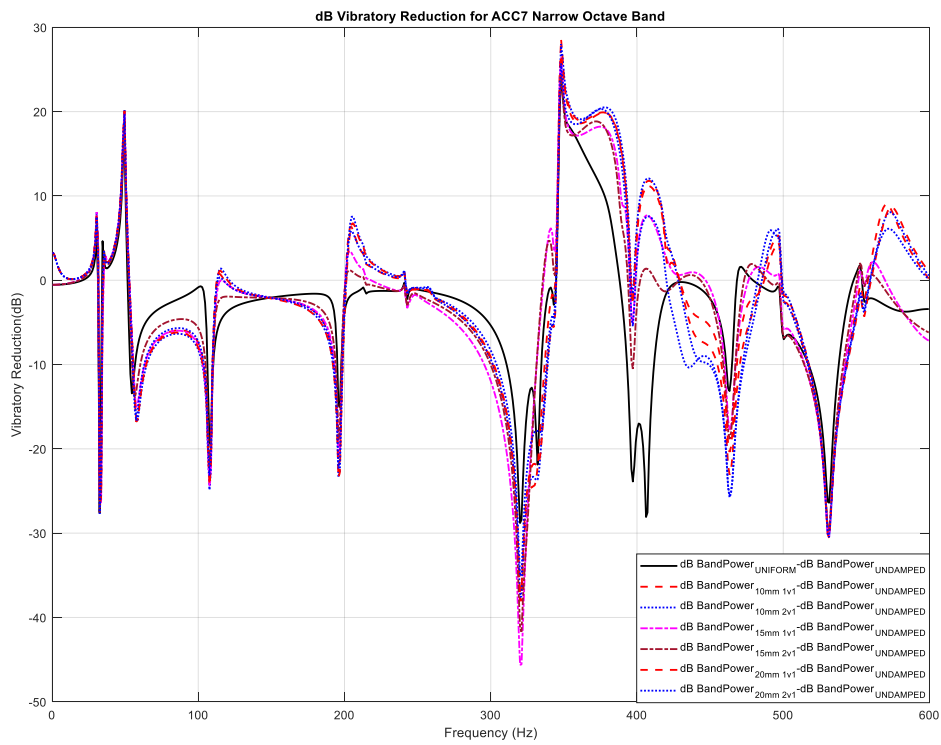


Figure 5.37. Narrow Octave Band dB Band Power Reduction Point 7

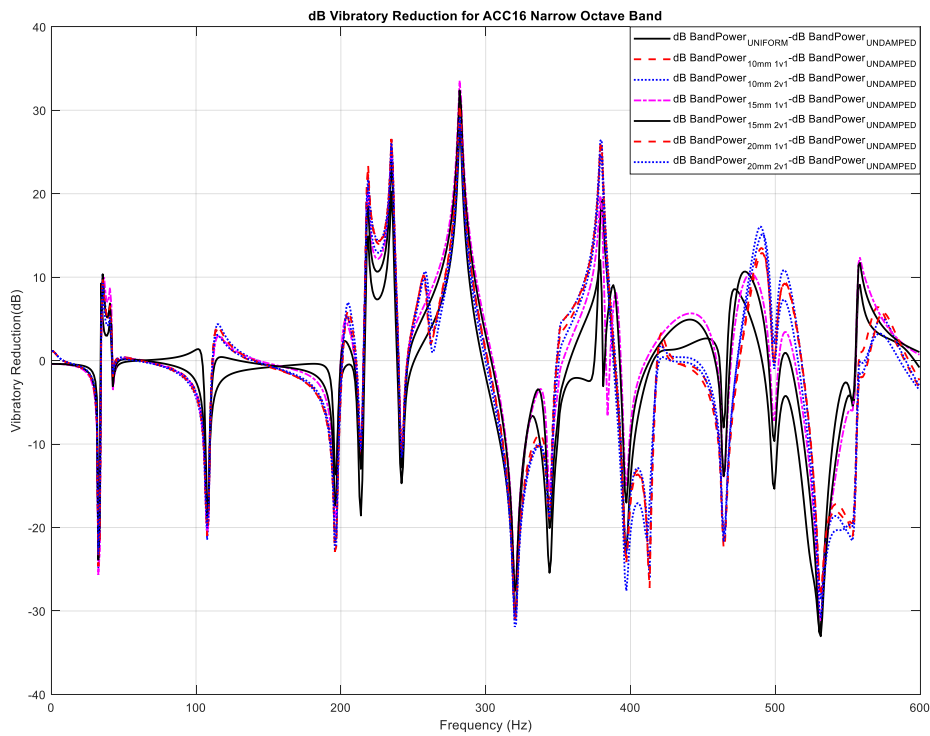


Figure 5.38. Narrow Octave Band dB Band Power Reduction Point 16

Table 5.10. Input point 10 Output point 7 damping Ratios

ACC7	Mode1 Damping Ratio	Frequency (Hz)	Mode2 Damping Ratio	Frequency (Hz)	Mode3 Damping Ratio	Frequency (Hz)
Bare	0.0098	33.06	0.0051	108.18	0.0028	196.33
UNIFORM	0.0131	34.06	0.0287	106.18	0.0154	196.33
SLOTTEDSOLD 10 1-1	0.0318	35.06	0.0280	112.19	0.0151	202.34
SLOTTEDSOLD 10 2-1	0.0310	35.06	0.0310	113.19	0.0150	204.34
SLOTTEDSOLD 15 1-1	0.0410	36.06	0.0359	112.19	0.0160	201.34
SLOTTEDSOLD 15 2-1	0.0200	35.06	0.0369	110.18	0.0169	199.33
SLOTTEDSOLD 20 1-1	0.0309	35.06	0.0308	112.19	0.0166	204.34
SLOTTEDSOLD 20 2-1	0.0205	35.06	0.0308	112.19	0.0165	203.34
ACC7	Mode4 Damping Ratio	Frequency (Hz)	Mode5 Damping Ratio	Frequency (Hz)	Mode6 Damping Ratio	Frequency (Hz)
Bare	0.0025	320.53	0.0037	343.57	0.0026	396.66
UNIFORM	N/A	N/A	0.0251	351.59	N/A	N/A
SLOTTEDSOLD 10 1-1	N/A	N/A	0.0145	348.58	N/A	N/A
SLOTTEDSOLD 10 2-1	N/A	N/A	0.0148	349.58	N/A	N/A
SLOTTEDSOLD 15 1-1	N/A	N/A	0.0159	342.57	0.0170	393.66
SLOTTEDSOLD 15 2-1	N/A	N/A	0.0303	341.57	N/A	N/A

SLOTTEDSOLD 20 1-1	N/A	N/A	0.0173	350.58	N/A	N/A
SLOTTEDSOLD 20 2-1	N/A	N/A	0.0371	349.58	N/A	N/A
ACC7	Mode7 Damping Ratio	Frequency (Hz)	Mode8 Damping Ratio	Frequency (Hz)	Mode9 Damping Ratio	Frequency (Hz)
Bare	N/A	N/A	0.0041	463.77	N/A	N/A
UNIFORM	N/A	N/A	0.0081	467.78	N/A	N/A
SLOTTEDSOLD 10 1-1	N/A	N/A	N/A	N/A	0.0183	494.83
SLOTTEDSOLD 10 2-1	N/A	N/A	N/A	N/A	0.0150	493.82
SLOTTEDSOLD 15 1-1	N/A	N/A	0.0355	476.80	N/A	N/A
SLOTTEDSOLD 15 2-1	N/A	N/A	0.0180	474.79	N/A	N/A
SLOTTEDSOLD 20 1-1	N/A	N/A	N/A	N/A	0.0285	494.83
SLOTTEDSOLD 20 2-1	N/A	N/A	N/A	N/A	0.0135	490.82
ACC7	Mode10 Damping Ratio	Frequency (Hz)	Mode11 Damping Ratio	Frequency (Hz)	Mode12 Damping Ratio	Frequency (Hz)
Bare	0.0025	530.89	0.0012	554.93		
UNIFORM	N/A	N/A	0.0195	546.91		
SLOTTEDSOLD 10 1-1	N/A	N/A	0.0131	569.95		
SLOTTEDSOLD 10 2-1	N/A	N/A	0.0151	571.95		
SLOTTEDSOLD 15 1-1	N/A	N/A	0.0149	558.93		

SLOTTEDSOLD 15 2-1	N/A	N/A	0.0174	555.93		
SLOTTEDSOLD 20 1-1	N/A	N/A	0.0141	572.96		
SLOTTEDSOLD 20 2-1	N/A	N/A	0.0188	569.95		

Table 5.11. Input point 10 Output point 16 damping Ratios

ACC16	Mode1 Damping Ratio	Frequency (Hz)	Mode2 Damping Ratio	Frequency (Hz)	Mode3 Damping Ratio	Frequency (Hz)
Bare	0.0097	33.06	0.0052	108.18	0.0028	196.33
UNIFORM	0.0129	34.06	0.0285	106.18	0.0156	196.33
SLOTTEDSOLD 10 1-1	0.0216	35.06	0.0281	111.19	0.0149	202.34
SLOTTEDSOLD 10 2-1	0.0188	35.06	0.0305	113.19	0.0151	204.34
SLOTTEDSOLD 15 1-1	0.0231	35.06	0.0344	112.19	0.0160	201.34
SLOTTEDSOLD 15 2-1	0.0237	35.06	0.0359	110.18	0.0170	199.33
SLOTTEDSOLD 20 1-1	0.0207	35.06	0.0294	112.19	0.0166	204.34
SLOTTEDSOLD 20 2-1	0.0297	34.06	0.0303	111.19	0.0165	202.34
ACC16	Mode4 Damping Ratio	Frequency (Hz)	Mode5 Damping Ratio	Frequency (Hz)	Mode6 Damping Ratio	Frequency (Hz)
Bare	0.0036	213.36	0.0038	242.40	0.0024	320.53
UNIFORM	N/A	N/A	N/A	N/A	0.0328	332.55
SLOTTEDSOLD 10 1-1	N/A	219.37	N/A	256.43	N/A	N/A

SLOTTEDSOLD 10 2-1	N/A	220.37	N/A	257.43	N/A	N/A
SLOTTEDSOLD 15 1-1	N/A	N/A	N/A	N/A	N/A	N/A
SLOTTEDSOLD 15 2-1	N/A	N/A	N/A	N/A	0.0166	338.56
SLOTTEDSOLD 20 1-1	N/A	220.37	N/A	256.43	N/A	N/A
SLOTTEDSOLD 20 2-1	N/A	N/A	N/A	257.43	N/A	N/A
ACC16	Mode7 Damping Ratio	Frequency (Hz)	Mode8 Damping Ratio	Frequency (Hz)	Mode9 Damping Ratio	Frequency (Hz)
Bare	0.0033	344.57	0.0026	396.66	0.0023	464.78
UNIFORM	N/A	N/A	N/A	385.64	0.0077	467.78
SLOTTEDSOLD 10 1-1	0.0121	347.58	0.0105	420.70	N/A	N/A
SLOTTEDSOLD 10 2-1	0.0121	348.58	N/A	420.70	N/A	N/A
SLOTTEDSOLD 15 1-1	0.0138	341.57	0.0070	390.65	0.0319	475.79
SLOTTEDSOLD 15 2-1	N/A	N/A	0.0084	389.65	0.0166	473.79
SLOTTEDSOLD 20 1-1	0.0134	348.58	0.0090	420.70	N/A	N/A
SLOTTEDSOLD 20 2-1	0.0148	347.58	N/A	420.70	N/A	N/A
ACC16	Mode10 Damping Ratio	Frequency (Hz)	Mode11 Damping Ratio	Frequency (Hz)	Mode12 Damping Ratio	Frequency (Hz)
Bare	0.0026	498.83	0.0026	530.89	0.0042	553.92
UNIFORM	N/A	N/A	N/A	N/A	N/A	552.92

SLOTTEDSOLD 10 1-1	0.0141	492.82	N/A	N/A	0.0167	571.95
SLOTTEDSOLD 10 2-1	0.0131	493.82	N/A	N/A	0.0201	574.96
SLOTTEDSOLD 15 1-1	N/A	N/A	N/A	N/A	0.0339	561.94
SLOTTEDSOLD 15 2-1	N/A	N/A	N/A	N/A	N/A	559.93
SLOTTEDSOLD 20 1-1	0.0144	491.82	N/A	N/A	0.0189	575.96
SLOTTEDSOLD 20 2-1	0.0115	490.82	N/A	N/A	N/A	573.96

From the above given results it is clearly seen that addition of slots in the design increased the damping performance for almost every mode in the interested frequency range as expected and literature results suggested. The results show that, for the selected 0-600Hz range, the periodic 15mm slotted design with twice width of tower to slot gives the highest damping ratios mostly. Due to small frequency range and closely spaced modes in this region, octave band solutions to estimate damping performance cannot clearly define the best solution due to mode shift in the range. If the solutions were such shifted and overdamped as full sixty-seven percent coverage with 5mm uniform spacer, that is tried in the initial base study and eliminated to be in the baseline geometries, the dB reduction solutions should have been clearly define the best solution among the spacer designs because it has broadband reduction in the FRF curves rather than improvement in several modes. However, due to weight limitations and coverage area selection this solution is not listed as explained above.

### 5.3.2. Optimized Spacer Geometry Using Novel Designs for Beams

The slotted designs are further investigated by using the outcomes of the thesis studies carried out by Sun [7] and Eyyüpoğlu [8] in 2015. They both carried out optimal spacer design for cantilevered beam in their study as summarized in literature review chapter. The solutions and designs of their studies should be adapted to free-free plate case by some assumptions. Their solutions will be used as starting points and modifications according to geometry and finite element solution simplifications will be made. Due to manufacturing capabilities available, some features cannot be adapted directly onto spacer geometry developed such as circular pockets, fillets and spherical objects. Each layer and thickness values are selected as multiple of minimum layer thickness 0.254mm.

#### 5.3.2.1. Enhanced Genetic Algorithm Solution Targeting Low Frequency Modes Results of Eyyüpoğlu [8]

Starting from the first three mode enhanced genetic algorithm study carried out by Eyyüpoğlu [8], the suggested solution is given in Figure 5.39.

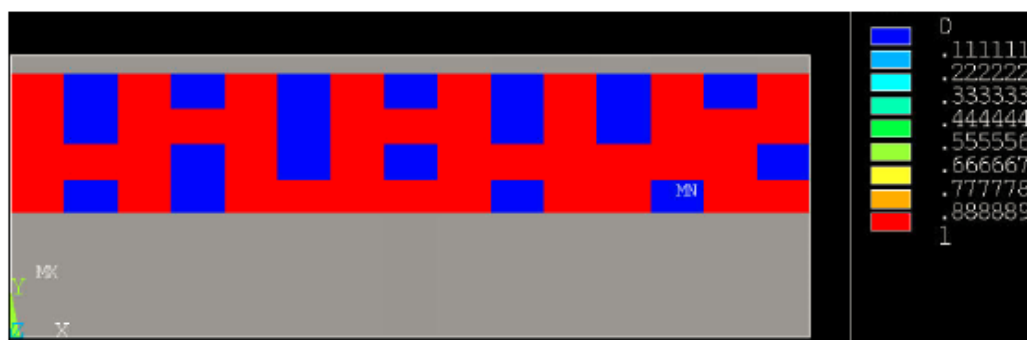


Figure 5.39. Enhanced Genetic Algorithm Material Distribution Optimized for First Three Mode [8]

The solution is as mentioned before is for cantilevered beam with 150mm length. Our fuselage skin itself is 300mm length and depth in x and y direction respectively and the frames restrict the body from edges of bare plates and give a resultant area of 275mm x 275mm. The solution suggested by Eyyüpoğlu [8] is mirrored in the free end and modelled as double cantilevered beam case as given in Figure 5.40.

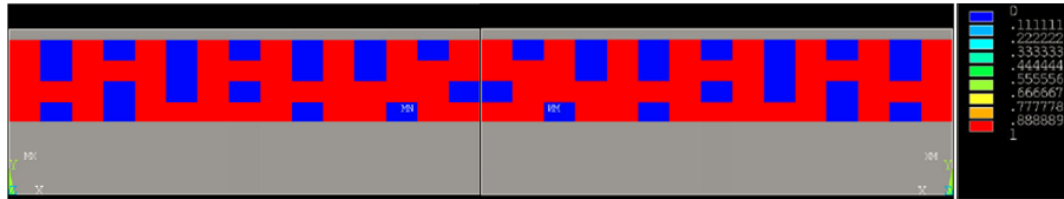


Figure 5.40. Enhanced Genetic Algorithm Material Distribution Double Cantilevered Beam

Since this solution becomes 2 x 150mm domain solution we only interest in the region where we can cover that is the central 100 mm region located symmetrically as given in Figure 5.41. The pattern in the small portion is symmetric from the mid axis and applied in the x and y plane similarly in order to design a sample slotted spacer given in Figure 5.42.

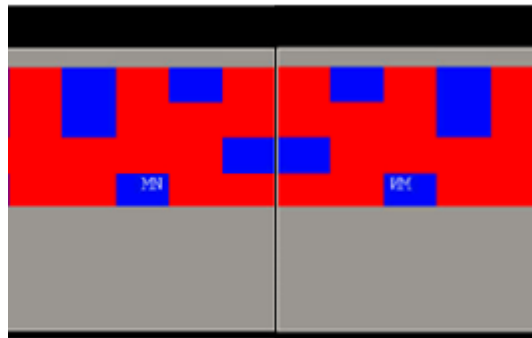


Figure 5.41. Enhanced Genetic Algorithm Material Distribution Double Cantilevered Beam 100mm coverage

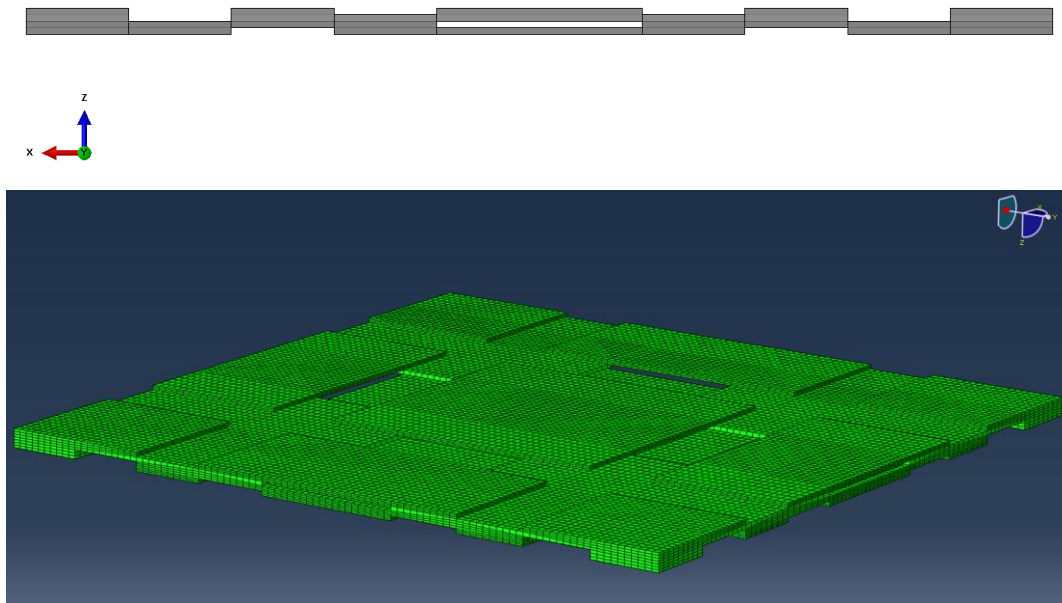


Figure 5.42. Enhanced Genetic Algorithm Material Distribution Double Cantilevered Beam 100mm coverage Designed Part and Mesh Generated

### 5.3.2.2. Global Response Surface Method Targeting Low Frequency Modes Results of Sun [7]

Similar approach was also carried out by Sun [7], targeting increase in damping ratio for first three mode using Global Response Surface Method (GRSM), and achieves increase in first five mode considering hundreds of solutions for given parameters. The main purpose of the GRSM method is to adjust the height and slot intervals with given initial parameters such as interval number and lower upper bounds for parameters and generates the best optimal solution among the results. This study also uses cantilevered beam of length 250mm and adjust slot locations according to response of the system with given parameters. The solution of GRSM is given in Figure 5.43. The design is done with 2mm fixed tower width with an addition of 10mm design space which sums to 250mm of full length.

H2	p1	p2	p3	p4	p5	p6	p7	p8	p9	p10	p11	p12	p13	p14	p15	p16	p17	p18	p19	p20	p21
2.51	8.73	8.13	9.27	2.97	9.50	3.15	7.20	2.91	6.09	1.22	8.59	2.45	2.25	3.99	7.72	8.77	8.74	8.41	8.87	2.86	2.04

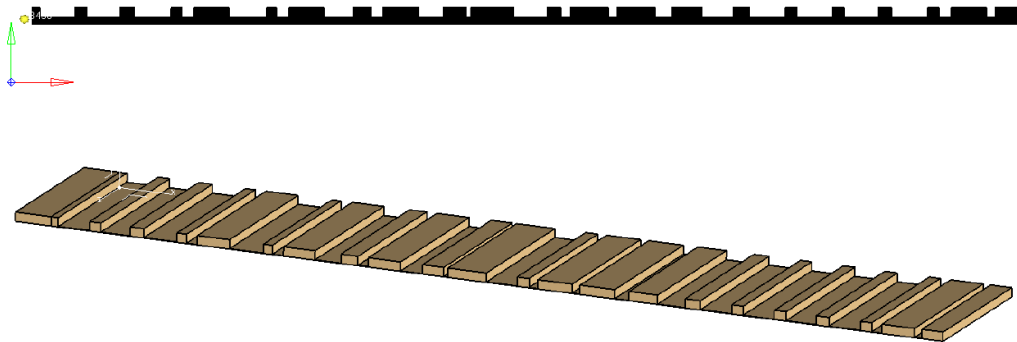


Figure 5.43. GRSM Optimum Solution for 250mm Cantilevered Beam [7]

With similar approach carried out on enhanced genetic algorithm design adaptation the design is mirrored about the plane located at the free end and scaled to 300mm total length for full coverage of fuselage surface. The length parameters given in Figure 5.43 are multiplied with 0.6 scale factor which comes from 300/500 length ratio of design space. The height of the slotted design is adjusted such that it will be same as the previous suggested solution. The generated slotted spacer model is shown below Figure 5.44, for better understanding of the proposed solution and adaptation procedure above mentioned.

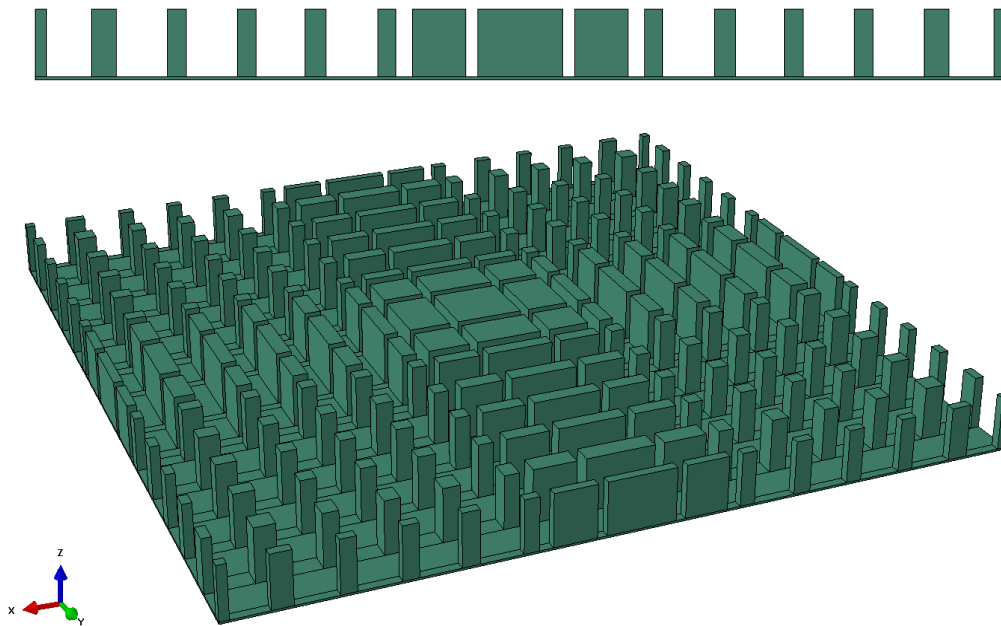


Figure 5.44. GRSM Optimum Solution for 250mm Cantilevered Beam

### 5.3.2.3. Spacer Design Using Topology Results of Sun [7]

Other than using brute slotted designs, the best solutions found by Sun [7], are also adapted to plates in this study. The beam optimized solution, which are symmetric in their own design space are taken into account and only best three novel design suggested by Sun [7] is used in the novel design study in this chapter. The used solutions are summarized below. These results were found to be the optimum designs for cantilever beam considered in the study and has the maximum damping ratios increase with less additional weight to the system. From the figure it is clearly seen that each of the topology solution given has a considerable increase compared to uniform spacer design of higher thickness. They have similar design points given below;

- Partial coverage
- Angled design on contact areas
- Pockets for weight reduction
- Symmetrical design criteria

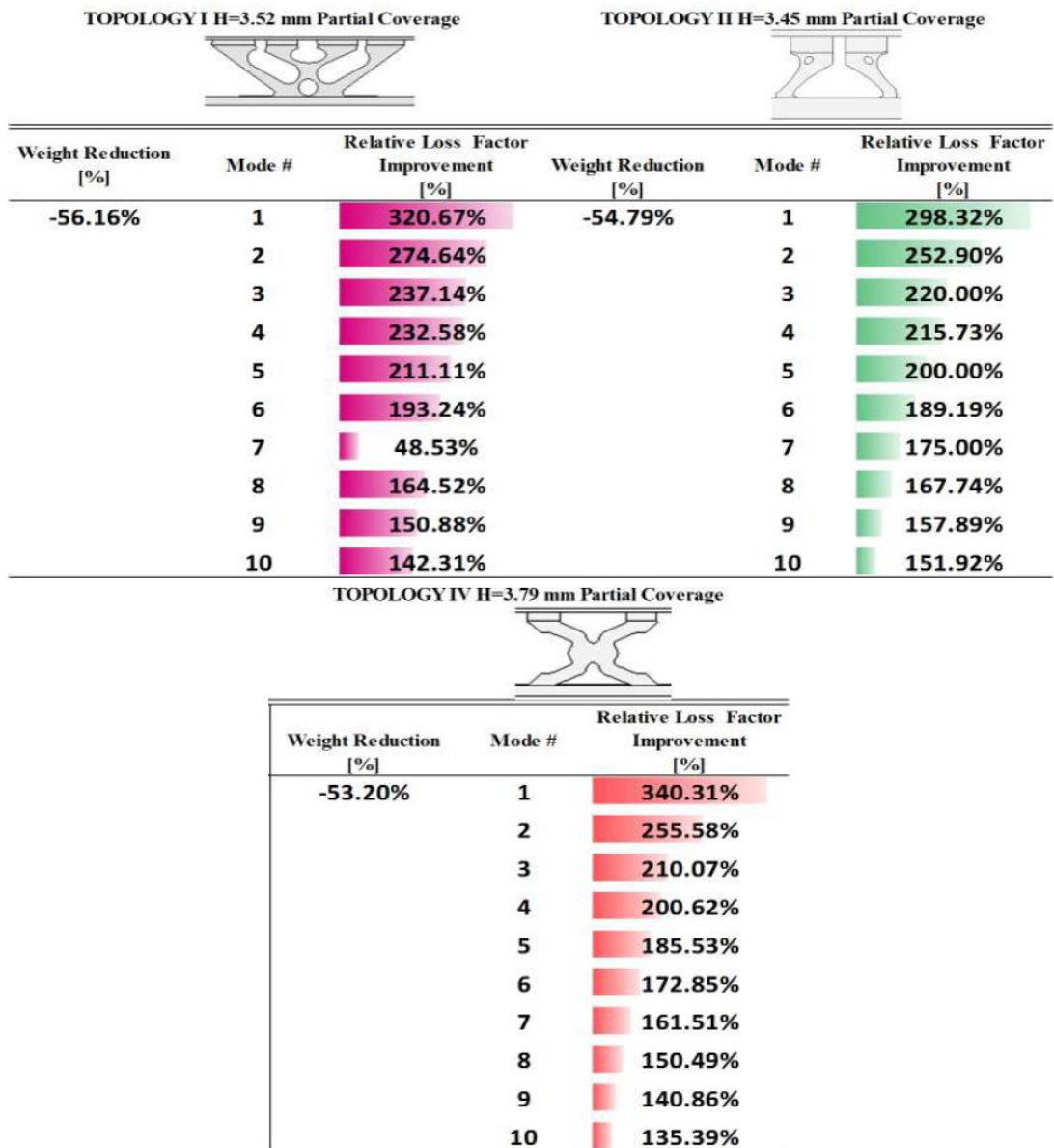


Figure 5.45. Topology Optimization Results for Cantilevered Beam suggested by Sun [7]

These suggested solutions are modelled in CATIA software for simplicity and modelled as connected to each other at base structure surface for ease of handling while bonding. The designed solutions are given in following figures.

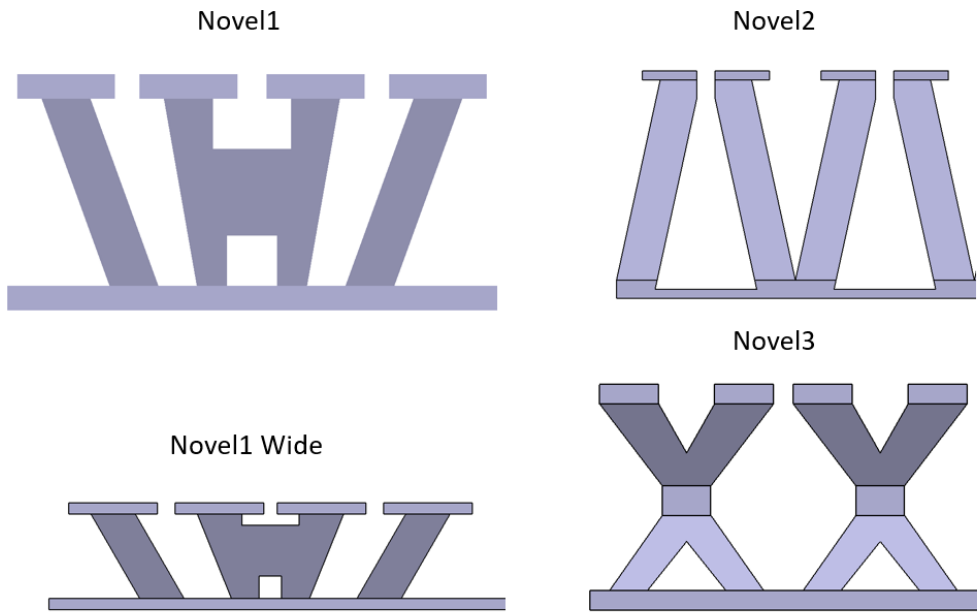


Figure 5.46. Topology Optimization Adapted Suggested Solutions Side View

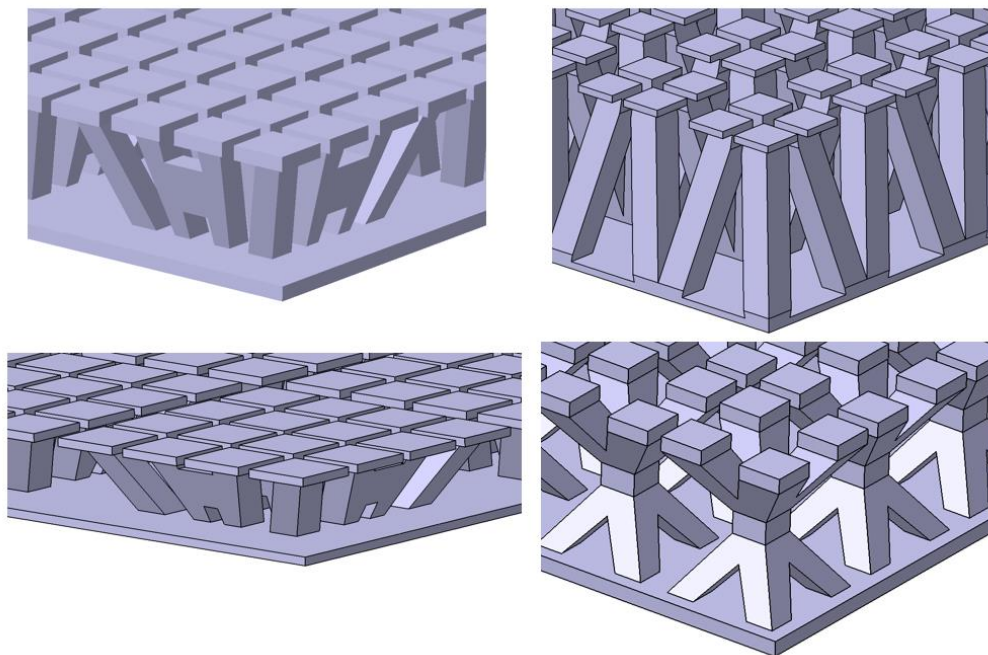


Figure 5.47. Topology Optimization Adapted Suggested Solutions Isometric View

From the figures it can be seen that for first topology optimization result of Sun [7], two different type of suggestions had been made. The difference between two of the design is that they have different length of design in x and y plane such that the second suggestion given in the bottom of the figure is much wider than the first suggestion. They have the same height in order to keep the neutral axis shift same between them but they have different heights for the second and third topology suggestions. Below the height, contact area and the mass ratio table is given for all suggested design until now.

Table 5.12. Designed Solution Parameters

Configuration	Weight Added (g)	Weight Added (%)	Thickness (mm)	Contact Area (mm <sup>2</sup> )	Contact Area Percent (%)
SCLD	8.001	1%	0.127+0.254	10000	100%
DCLD	16.002	3%	2x(0.127+0.254)	2x10000	200%
TCLD	24.003	4%	3x(0.127+0.254)	3x10000	300%
UNIFORM	23.8506	4%	1.524	10000	100%
Slotted 10mm 1v1	23.975	4%	5.588	2500	25%
Slotted 10mm 2v1	23.557	4%	3.048	4444.4	44%
Slotted 15mm 1v1	23.641	4%	4.572	2899.82	29%
Slotted 15mm 2v1	23.587	4%	2.794	4900	49%
Slotted 20mm 1v1	23.851	4%	5.334	2500	25%
Slotted 20mm 2v1	23.557	4%	3.048	4444.448	44%
Novel1	23.943	4%	4.826	6400	64%

Novel1 Wide	23.853	4%	4.826	6400	64%
Novel2	24.02	4%	6.35	3716.8	37%
Novel3	24.353	5%	5.842	3600	36%
Novel4 (Enhanced Genetic)	23.058	4%	2.54	3600	36%
Novel5 (GRMS)	23.897	4%	7.112	1858.3	19%

While designing of the topology optimized novel designs of Sun [7], some simplifications had to be done in design due to manufacturing capabilities and finite element solver capacities. Since 3D printer is capable of printing the spacer layer by layer with a thickness of 0.254 mm, the spherical and fillets in the design will not be as modelled in the manufactured part so these design features are changed to more rectangular sections for ease of manufacturing. Also due to finite element mesh capabilities, these rectangular sections can be mesh with coarser element that has higher aspect ratios for better results and increased solving time.

#### **5.3.2.4. Finite Element Results of the Novel Designs**

This chapter is dedicated for the finite element results obtained for the novel spacer designs and compared with the best slotted spacer mentioned in chapter 5.3.1, which is 15mm slotted design with 2vs1 tower to slot ratio.

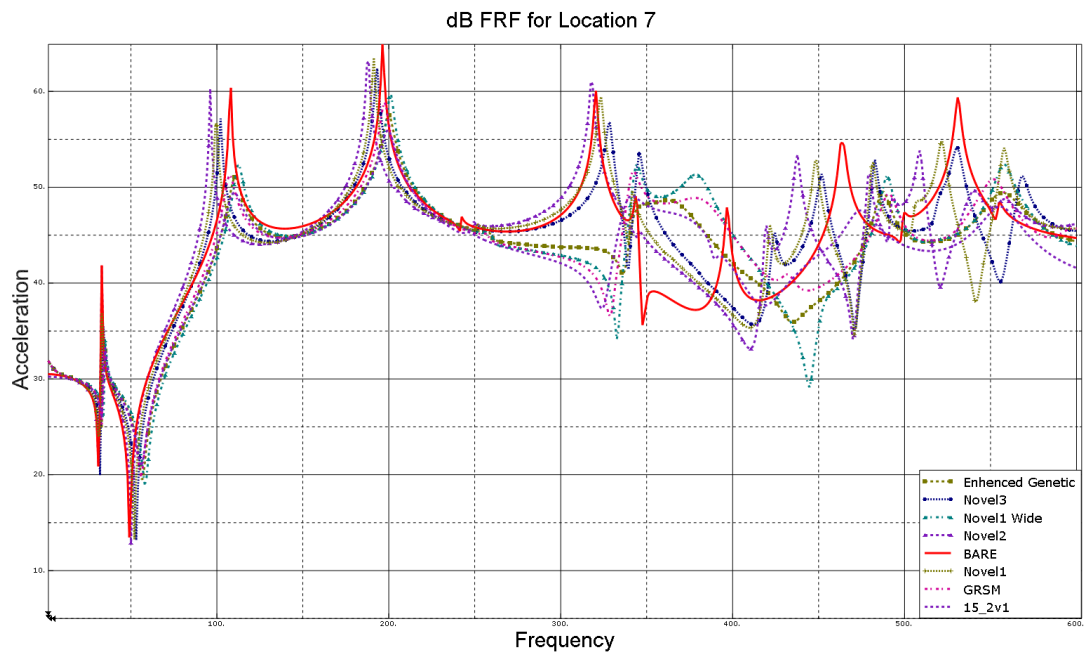


Figure 5.48. FRF Results for Novel Results Point 7

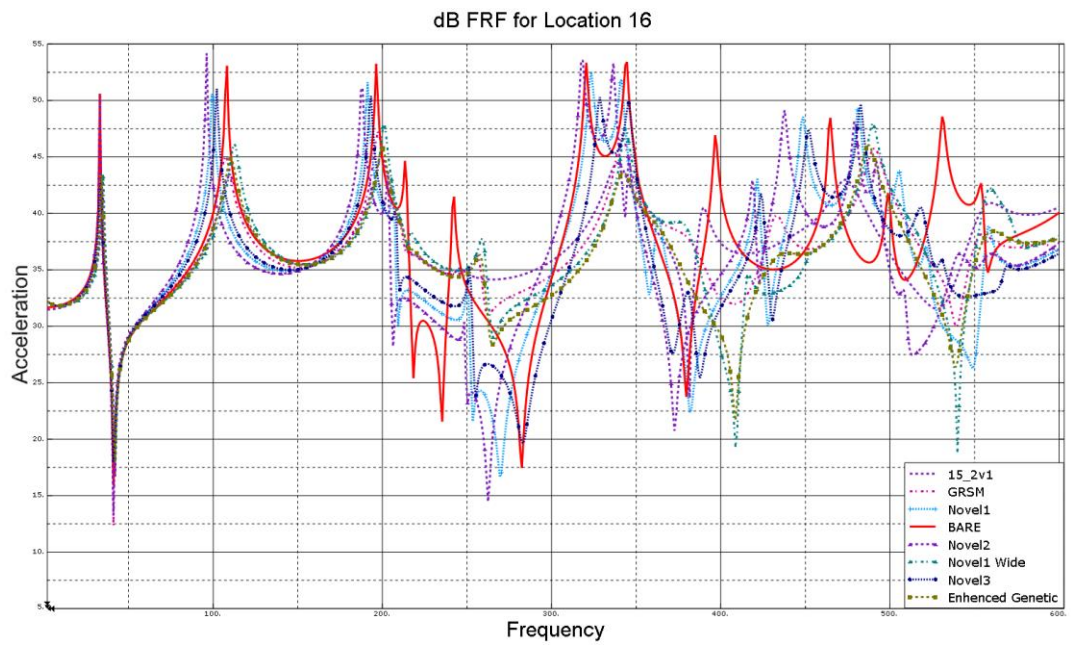


Figure 5.49. FRF Results for Novel Results Point 16

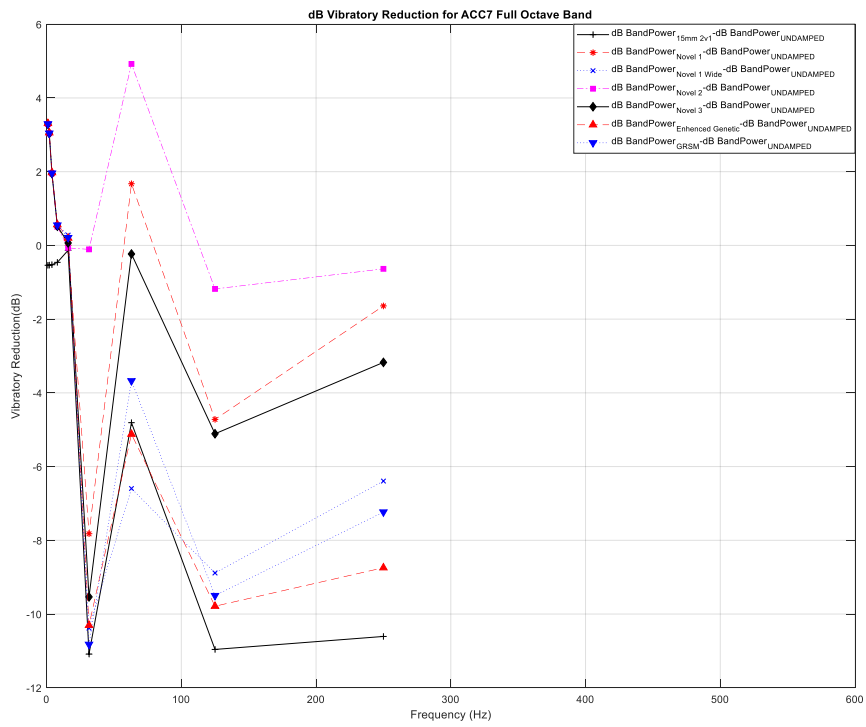


Figure 5.50. Full Octave Band dB Band Power Reduction Point 7

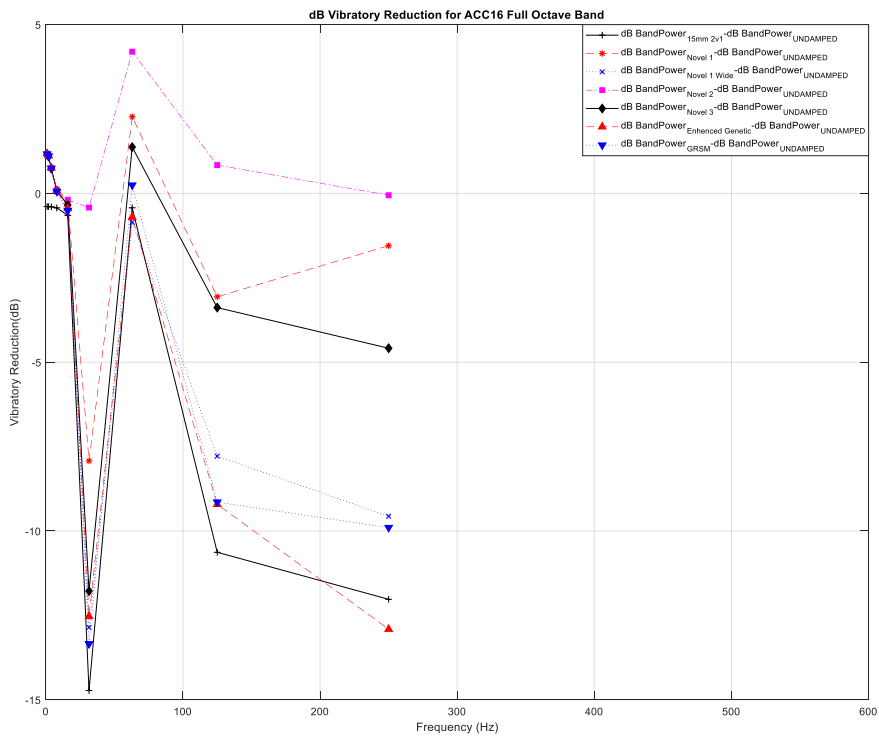


Figure 5.51. Full Octave Band dB Band Power Reduction Point 16

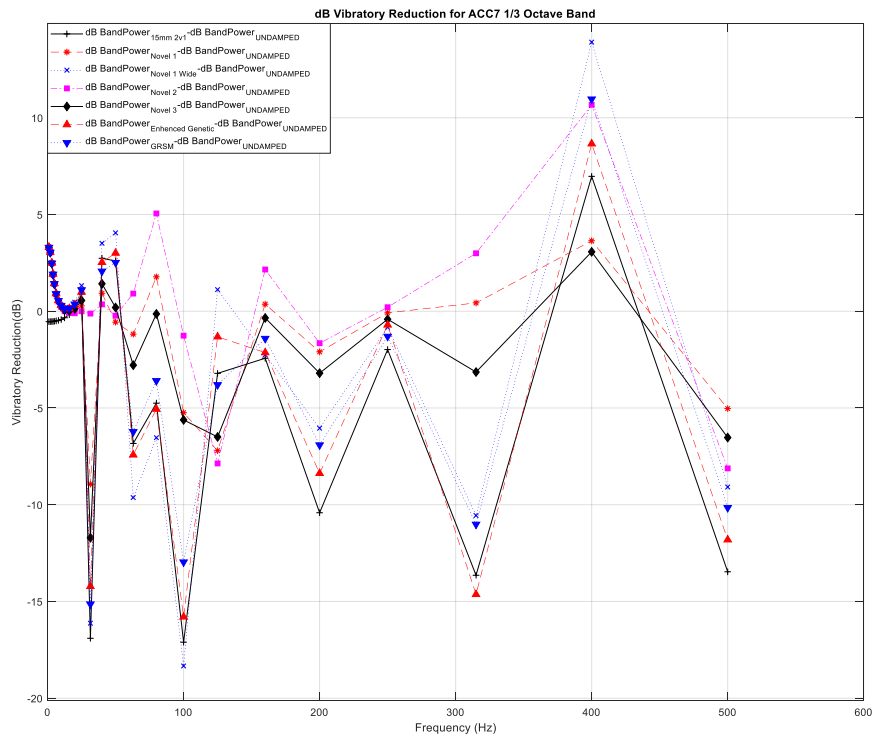


Figure 5.52. 1/3 Octave Band dB Band Power Reduction Point 7

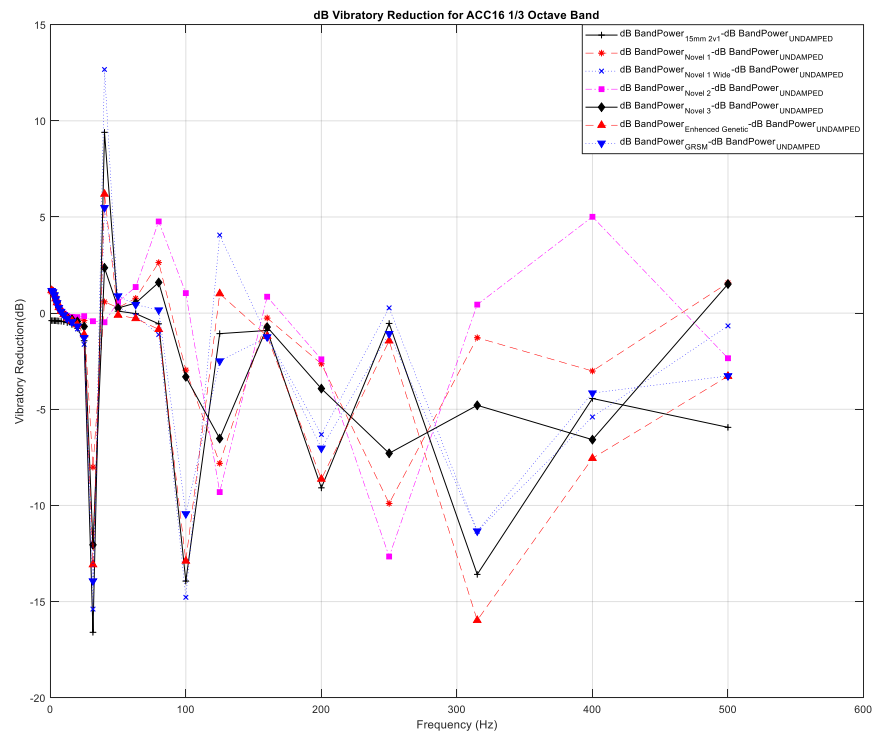


Figure 5.53. 1/3 Octave Band dB Band Power Reduction Point 16

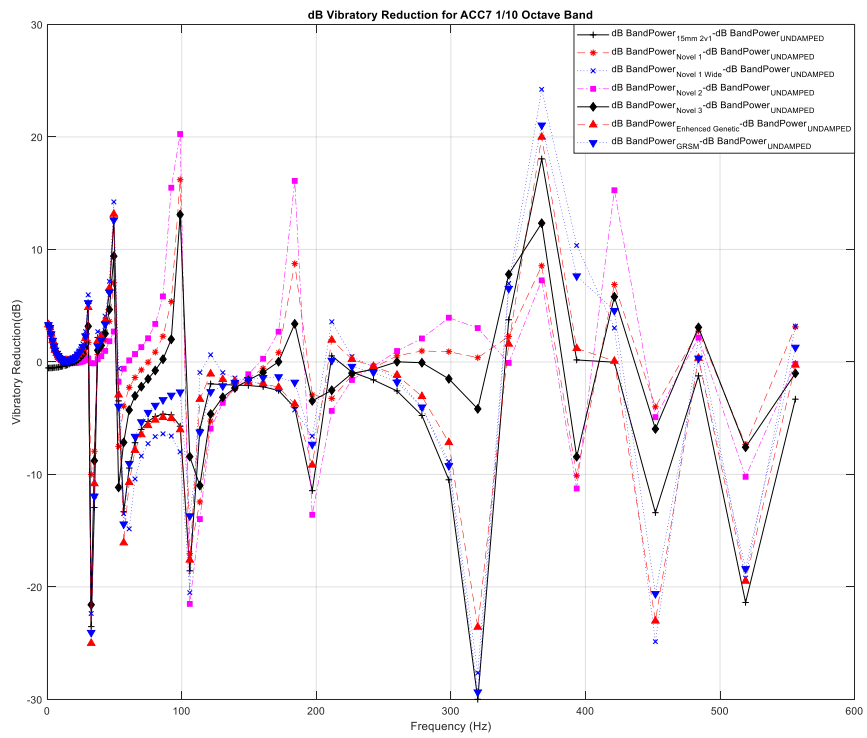


Figure 5.54. 1/10 Octave Band dB Band Power Reduction Point 7

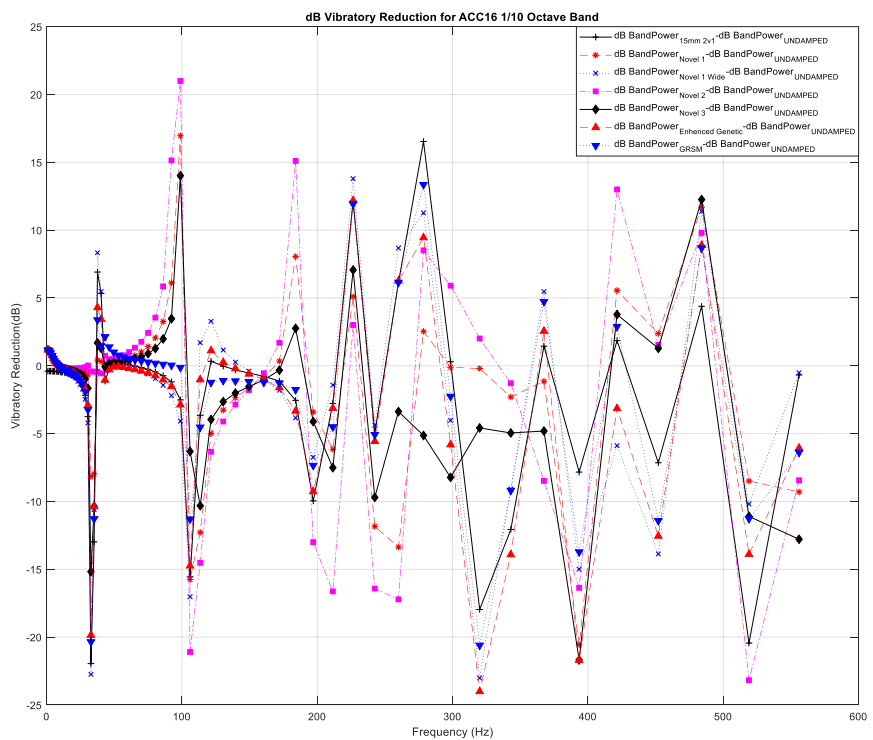


Figure 5.55. 1/10 Octave Band dB Band Power Reduction Point 16

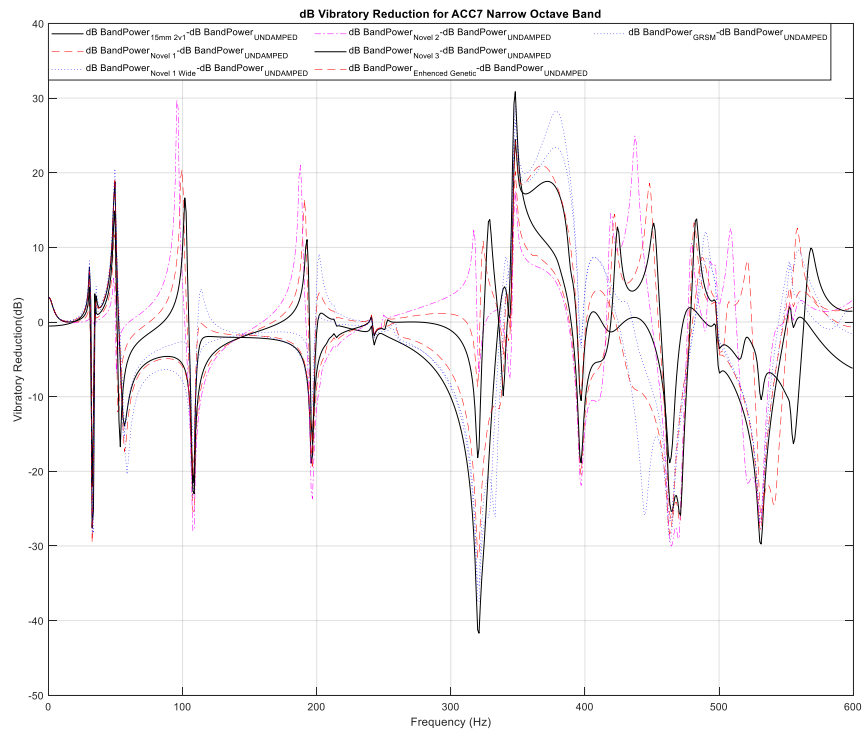


Figure 5.56. Narrow Octave Band dB Band Power Reduction Point 7

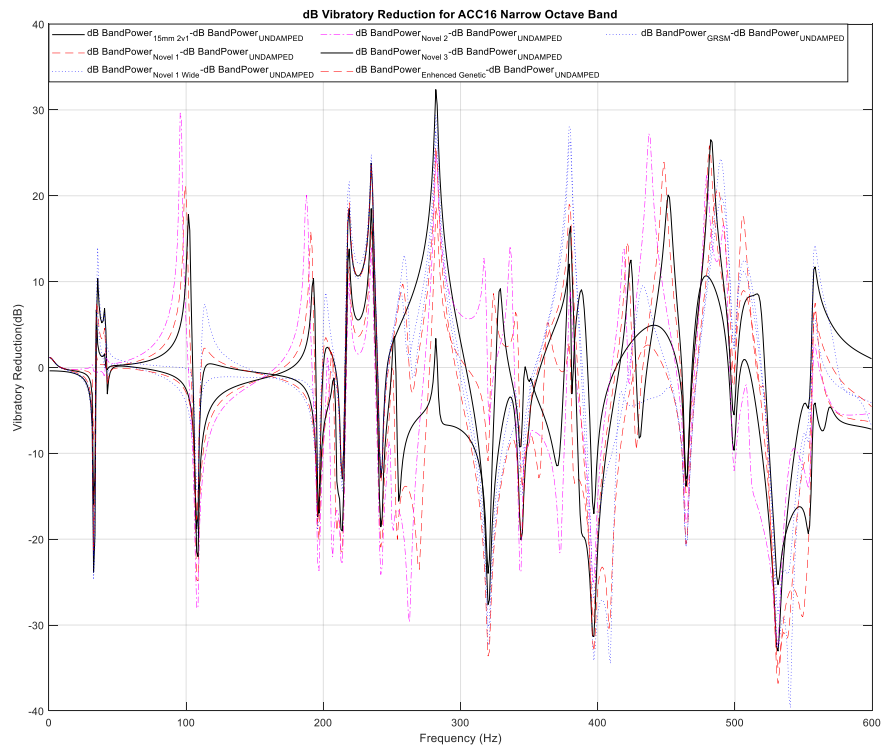


Figure 5.57. Narrow Octave Band dB Band Power Reduction Point 16

Table 5.13. Damping Ratio Comparison for Point 7

ACC7	Mode1 Damping Ratio	Frequency (Hz)	Mode2 Damping Ratio	Frequency (Hz)	Mode3 Damping Ratio	Frequency (Hz)
SLOTTEDSOLD 15 2-1	0.0200	35.06	0.0369	110.18	0.0169	199.33
Genetic	0.0282	34.06	0.0262	110.18	0.0126	200.33
GRSM	0.0329	34.06	0.0240	107.18	0.0096	197.33
Novel 1	0.0134	33.06	0.0099	99.17	0.0033	191.32
Novel 2	0.0097	33.06	0.0041	96.16	0.0052	188.31
Novel 3	0.0144	34.06	0.0058	102.17	0.0047	193.32
Novel 1 Wide	0.0163	35.06	0.0194	112.19	0.0078	201.34
ACC7	Mode4 Damping Ratio	Frequency (Hz)	Mode5 Damping Ratio	Frequency (Hz)	Mode6 Damping Ratio	Frequency (Hz)
SLOTTEDSOLD 15 2-1	N/A	N/A	0.0303	341.57	N/A	N/A
Genetic	N/A	N/A	N/A	362.60	N/A	N/A
GRSM	N/A	N/A	0.0094	342.57	N/A	N/A
Novel 1	N/A	N/A	0.0038	323.54	0.0141	332.00
Novel 2	0.0035	317.53	N/A	N/A	N/A	N/A
Novel 3	0.0045	328.55	N/A	N/A	0.0046	345.58
Novel 1 Wide	N/A	N/A	0.0073	344.57	0.0228	378.63
ACC7	Mode7 Damping Ratio	Frequency (Hz)	Mode8 Damping Ratio	Frequency (Hz)	Mode9 Damping Ratio	Frequency (Hz)
SLOTTEDSOLD 15 2-1	N/A	N/A	0.0180	474.79	N/A	N/A
Genetic	N/A	N/A	N/A	N/A	0.0078	487.81
GRSM	0.0100	431.72	N/A	N/A	0.0089	490.82

Novel 1	0.0029	421.70	N/A	N/A	0.0034	448.75
Novel 2	0.0032	419.70	0.0030	437.73	0.0029	479.80
Novel 3	0.0040	424.71	0.0042	451.75	0.0028	482.81
Novel 1 Wide	N/A	N/A	N/A	N/A	0.0054	489.82
ACC7	Mode10 Damping Ratio	Frequency (Hz)	Mode11 Damping Ratio	Frequency (Hz)	Mode12 Damping Ratio	Frequency (Hz)
SLOTTEDSOLD 15 2-1	N/A	N/A	0.0174	555.93		
Genetic	N/A	N/A	0.0183	556.93		
GRSM	N/A	N/A	0.0124	551.92		
Novel 1	0.0036	521.87	0.0034	557.93		
Novel 2	0.0030	508.85	0.0111	540.90		
Novel 3	0.0051	530.89	0.0053	567.95		
Novel 1 Wide	N/A	N/A	0.0082	557.93		

Table 5.14. Damping Ratio Comparison for Point 16

ACC16	Mode1 Damping Ratio	Frequency (Hz)	Mode2 Damping Ratio	Frequency (Hz)	Mode3 Damping Ratio	Frequency (Hz)
SLOTTEDSOLD 15 2-1	0.0237	35.06	0.0359	110.18	0.0170	199.33
Genetic	0.0144	34.06	0.0251	110.18	0.0127	200.33
GRSM	0.0149	34.06	0.0235	107.18	0.0096	197.33
Novel 1	0.0116	33.06	0.0097	99.17	0.0033	191.32
Novel 2	0.0098	33.06	0.0041	96.16	0.0052	188.31
Novel 3	0.0237	34.06	0.0058	102.17	0.0047	193.32
Novel 1 Wide	0.0133	35.06	0.0188	112.19	0.0078	201.34

ACC16	Mode4 Damping Ratio	Frequency (Hz)	Mode5 Damping Ratio	Frequency (Hz)	Mode6 Damping Ratio	Frequency (Hz)
SLOTTEDSOLD 15 2-1	N/A	N/A	N/A	N/A	0.0166	338.56
Genetic	N/A	N/A	0.0521	257.43	0.0146	342.57
GRSM	N/A	N/A	0.0221	256.43	0.0081	341.57
Novel 1	0.0193	206.34	0.0037	323.54	0.0037	341.57
Novel 2	0.0031	203.34	0.0037	317.53	0.0026	336.56
Novel 3	0.0040	251.42	N/A	N/A	0.0046	328.55
Novel 1 Wide	0.0108	259.43	N/A	N/A	0.0064	343.57
ACC16	Mode7 Damping Ratio	Frequency (Hz)	Mode8 Damping Ratio	Frequency (Hz)	Mode9 Damping Ratio	Frequency (Hz)
SLOTTEDSOLD 15 2-1	N/A	N/A	0.0084	389.65	0.0166	473.79
Genetic	N/A	N/A	N/A	438.73	N/A	N/A
GRSM	N/A	N/A	0.0120	432.72	N/A	N/A
Novel 1	0.0053	362.60	0.0027	421.70	N/A	N/A
Novel 2	0.0028	345.58	0.0028	418.70	0.0030	437.73
Novel 3	0.0046	345.58	0.0036	423.71	0.0044	451.75
Novel 1 Wide	N/A	374.62	N/A	N/A	N/A	N/A
ACC16	Mode10 Damping Ratio	Frequency (Hz)	Mode11 Damping Ratio	Frequency (Hz)	Mode12 Damping Ratio	Frequency (Hz)
SLOTTEDSOLD 15 2-1	N/A	N/A	N/A	N/A	N/A	559.93
Genetic	0.0078	486.81	N/A	N/A	N/A	560.94
GRSM	0.0087	490.82	N/A	N/A	0.0451	554.93
Novel 1	0.0034	448.75	0.0029	481.80	0.0041	557.93

Novel 2	0.0028	478.80	0.0033	491.82	N/A	N/A
Novel 3	0.0028	482.81	0.0072	517.86	N/A	N/A
Novel 1 Wide	0.0054	489.82	N/A	N/A	0.0102	558.93

### 5.3.2.5. Comparison of the Novel Designs

Until now, we have adapted the topology, enhanced genetic and parametric optimized beam solution on to plates and tested on plates whether they can be used on plates as an optimized damping performance solution. The damping vibration reduction is mainly considered through modal damping ratio since a broadband reduction cannot be observed for the suggested solutions and dB band power reduction estimates cannot point out a best solution directly for this frequency range of considered. In this chapter, best solutions suggested will be summarized for sake of comparison of their vibration characteristic. From the results it can be concluded that the slotted design with 15mm period with 2vs1 tower to slot ratio gives the best damping ratio increase in almost every mode but Genetic and GRMS methods close up and even pass the slotted spacer model in some modes. Also from the novel topology adapted designs, the best solution suggested is the wide version of the Novel 1 design since it is much closer in design parameter to suggested solution of Sun [7].

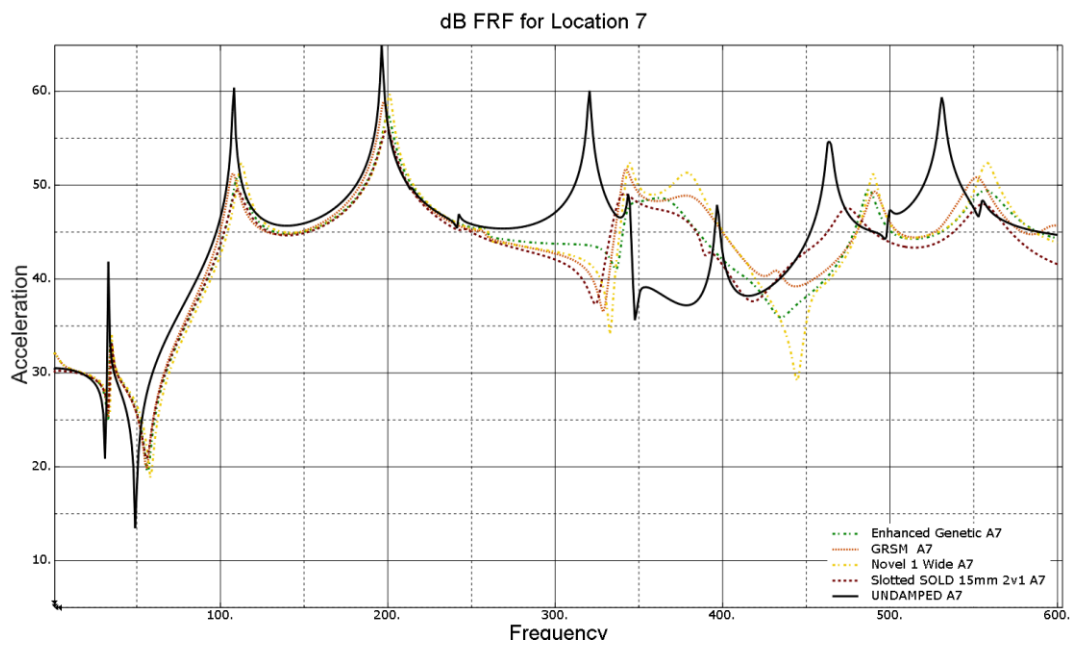


Figure 5.58. FRF Results for Best Novel Results Point 7

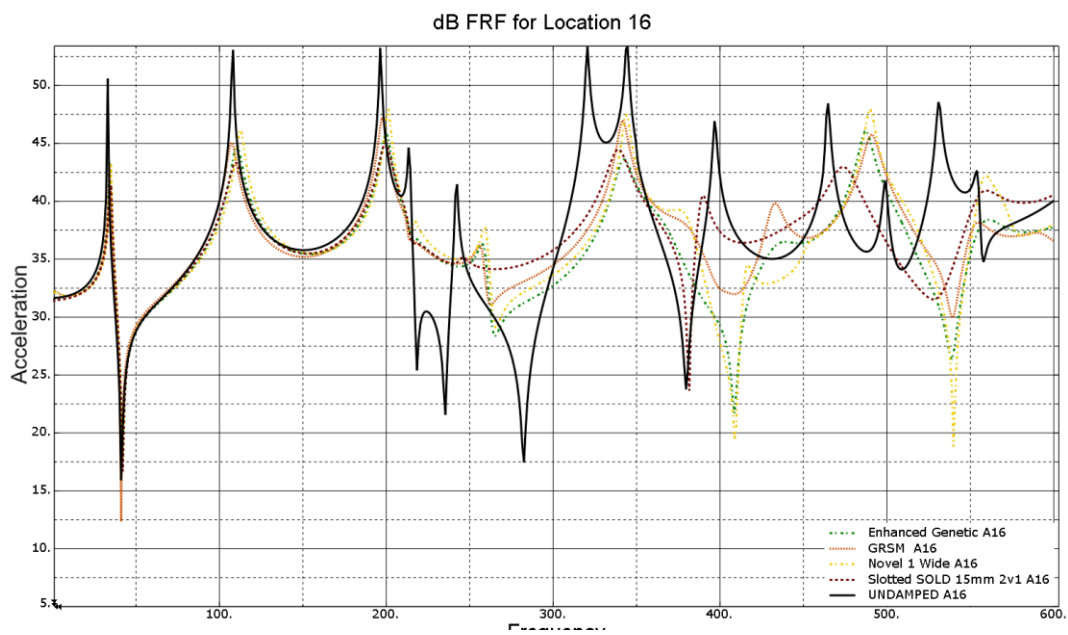


Figure 5.59. FRF Results for Best Novel Results Point 16

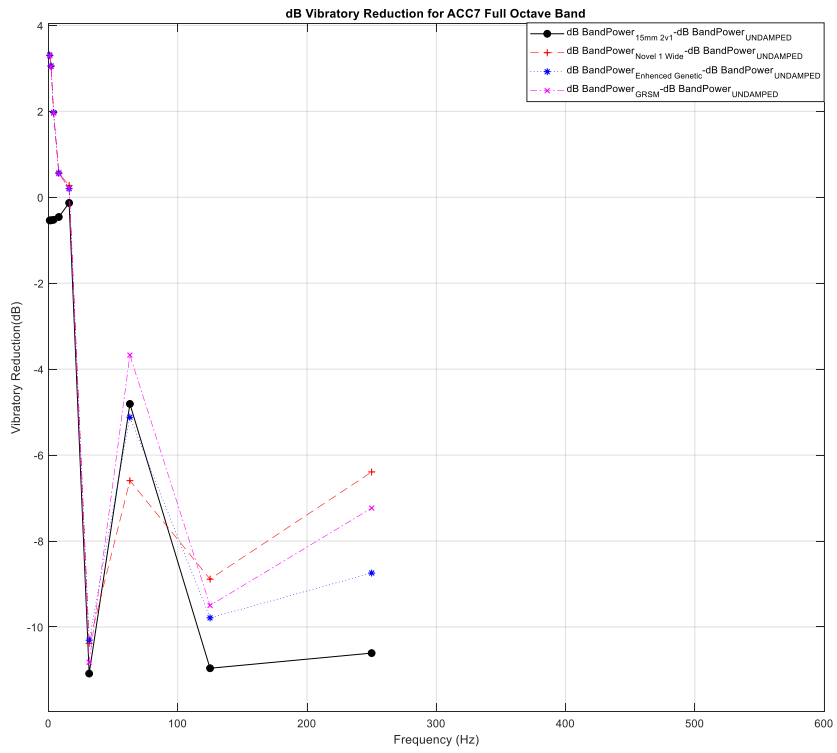


Figure 5.60. Full Octave Band dB Band Power Reduction Point 7

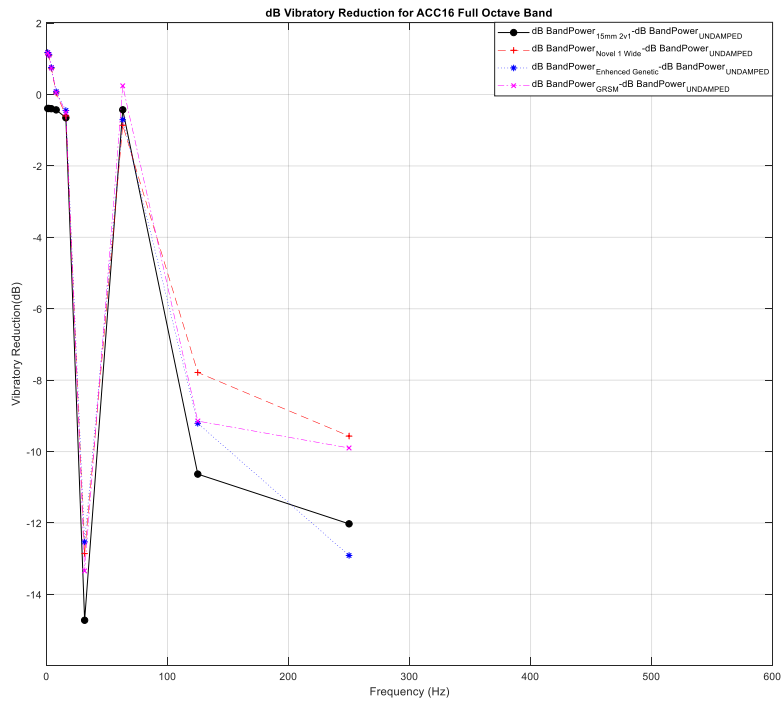


Figure 5.61. Full Octave Band dB Band Power Reduction Point 16

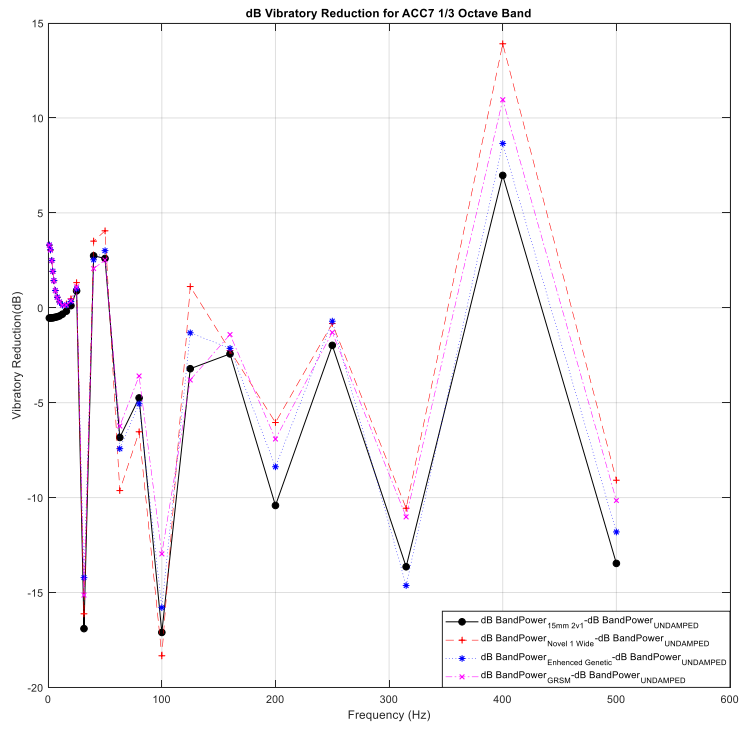


Figure 5.62. 1/3 Octave Band dB Band Power Reduction Point 7

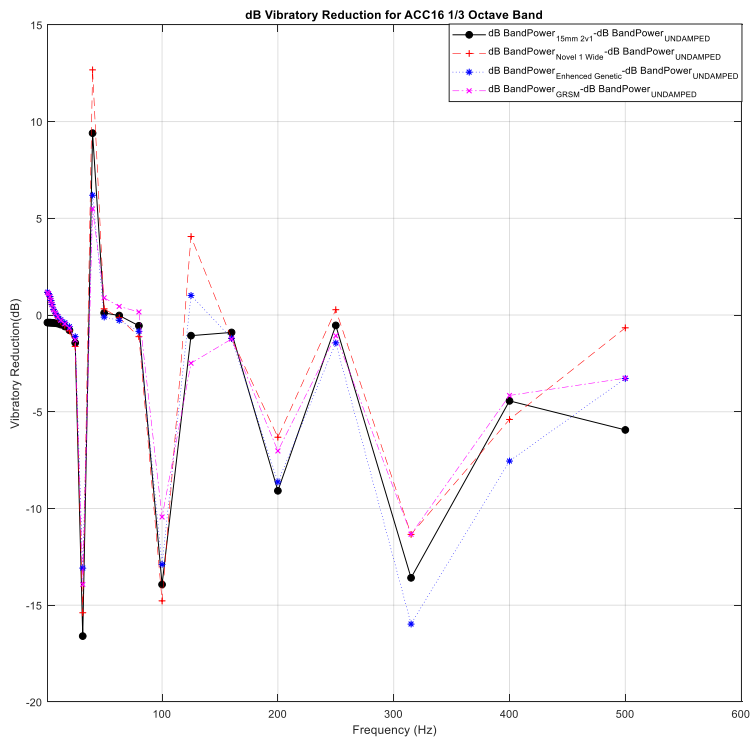


Figure 5.63. 1/3 Octave Band dB Band Power Reduction Point 16

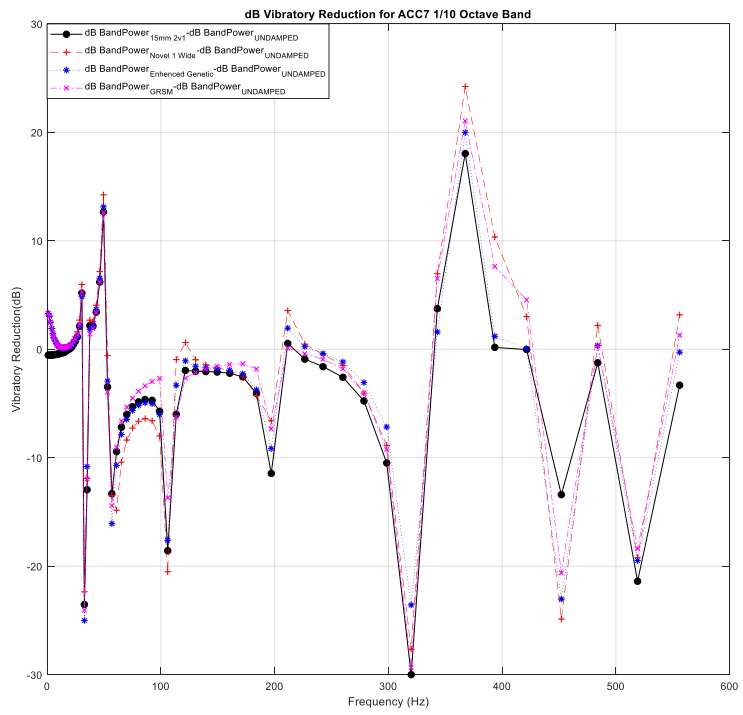


Figure 5.64. 1/10 Octave Band dB Band Power Reduction Point 7

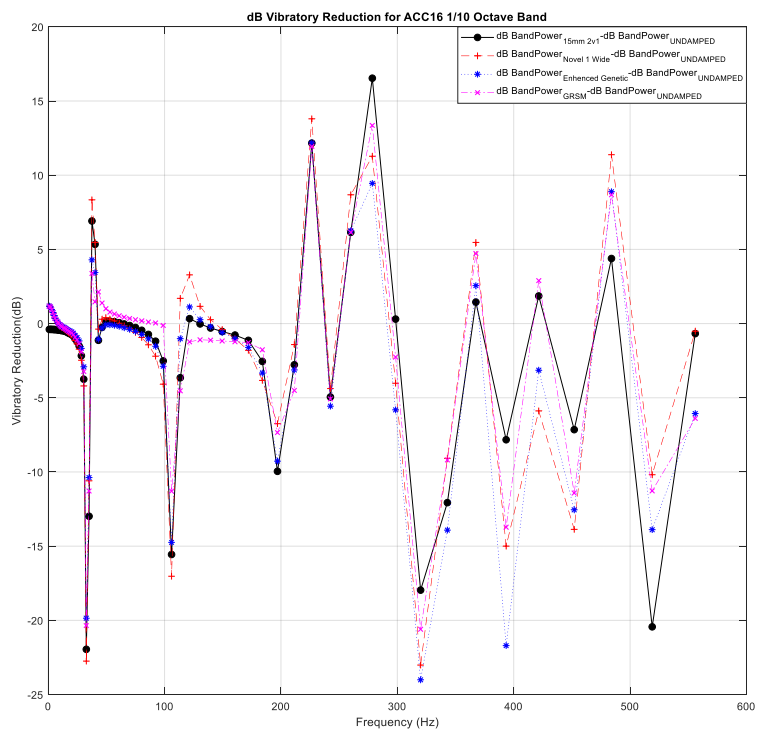


Figure 5.65. 1/10 Octave Band dB Band Power Reduction Point 16

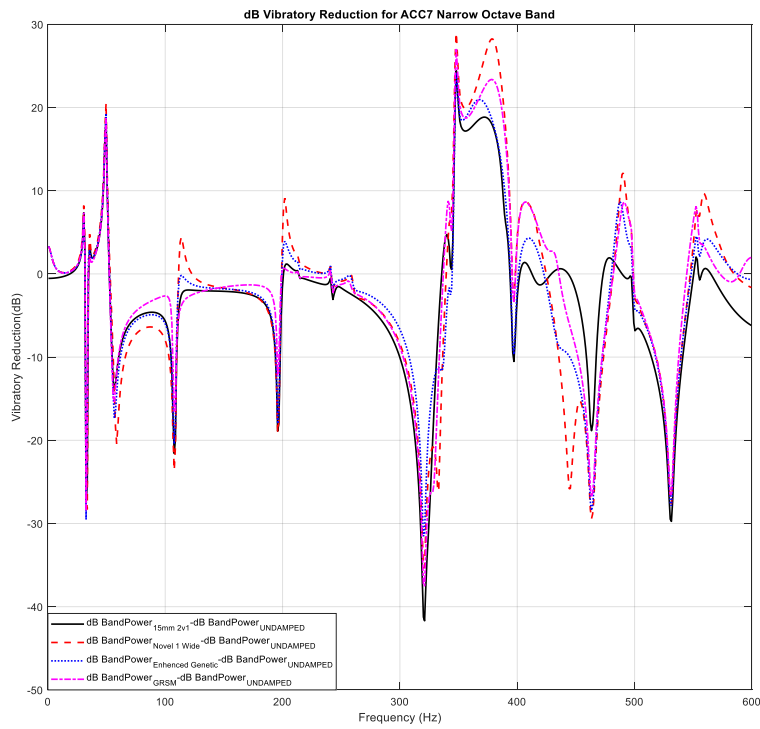


Figure 5.66. Narrow Octave Band dB Band Power Reduction Point 7

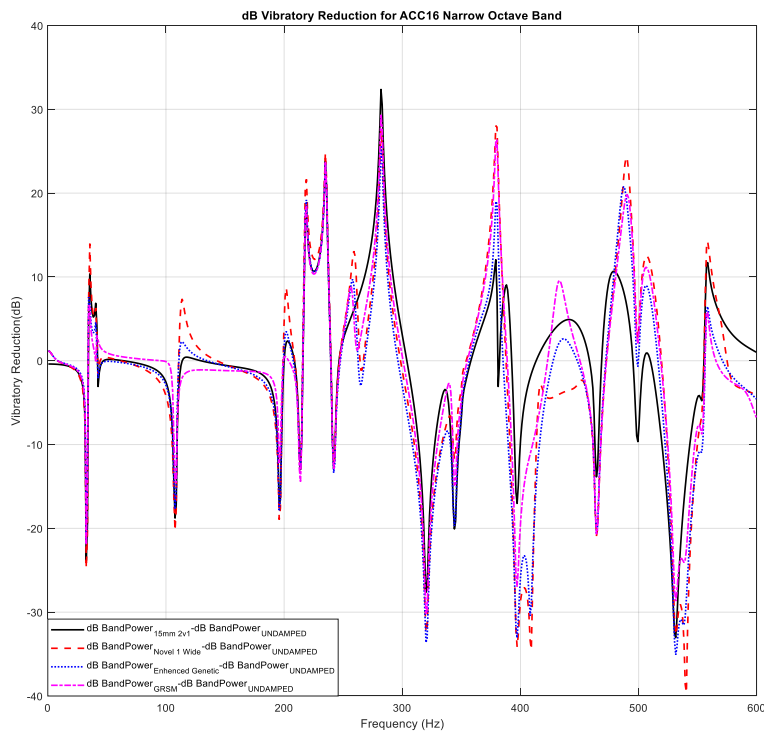


Figure 5.67. Narrow Octave Band dB Band Power Reduction Point 16

#### 5.4. Experimental Results of the Designed Surface Damping Treatments

In this chapter, the simulation results will be compared with experimental studies carried in METU Mechanical Engineering Vibration Laboratory. The tests were performed by supervisor Gökhan Osman Özgen and the departments equipment are used throughout the testing.

In order to manufacture the spacer geometries, as mentioned before, 3D printing technique is used for fast prototyping and low density material capability. Due to manufacturing restrictions, each spacer height is adjusted to be multiple of the minimum layer thickness value which is 0.254mm. after manufacturing processes, the damping treatments are bonded to fuselage layer using strong adhesive between spacer layer and bare skin plate of the fuselage.

In following figures; experimental setup and manufactured damping solutions are given.

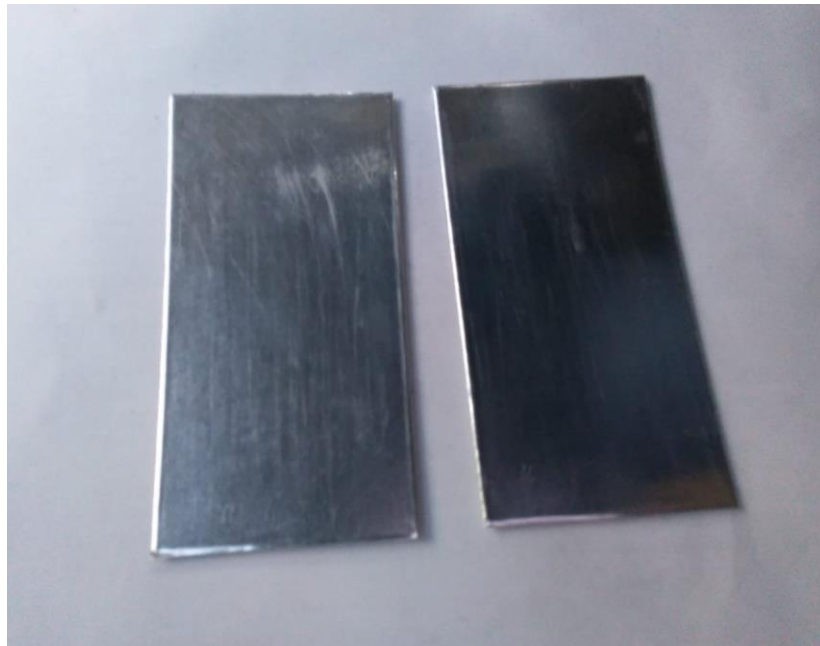


Figure 5.68. Constrained Layer Damping Treatment Patches

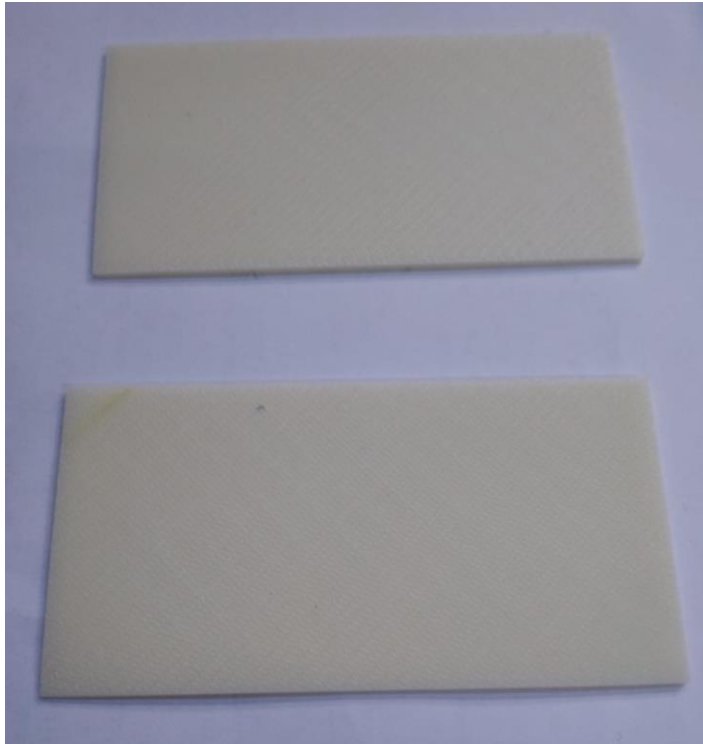


Figure 5.69. Uniform Spacer Layer Manufactured

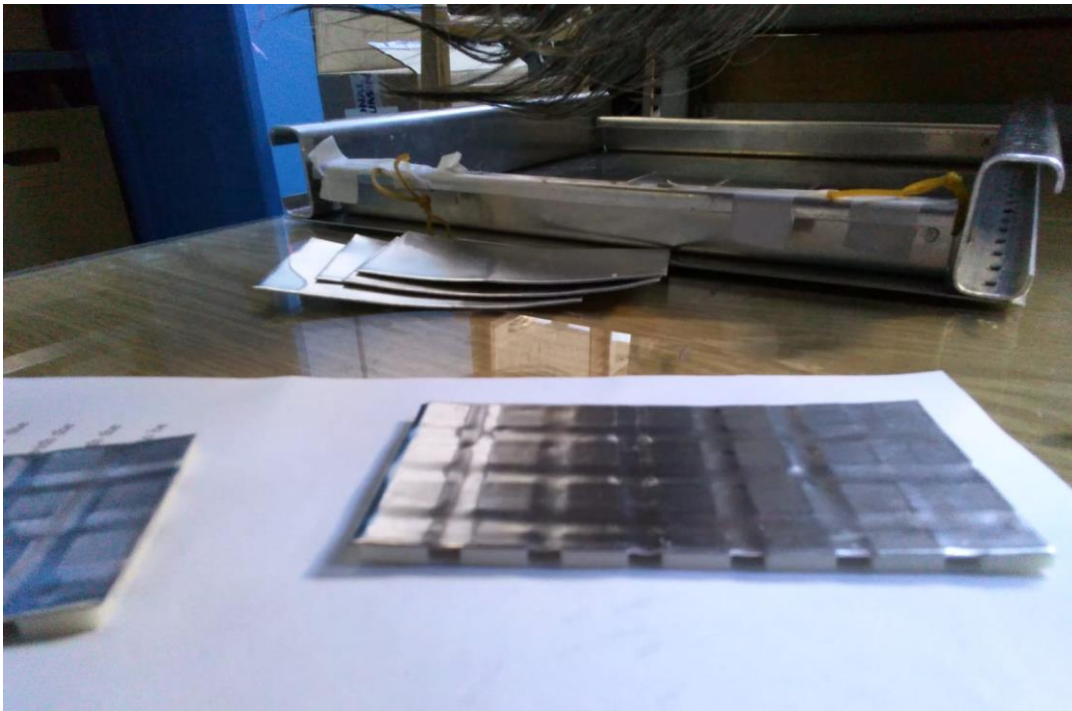


Figure 5.70. Standoff Layer Damping Treatment (Slotted Spacer)

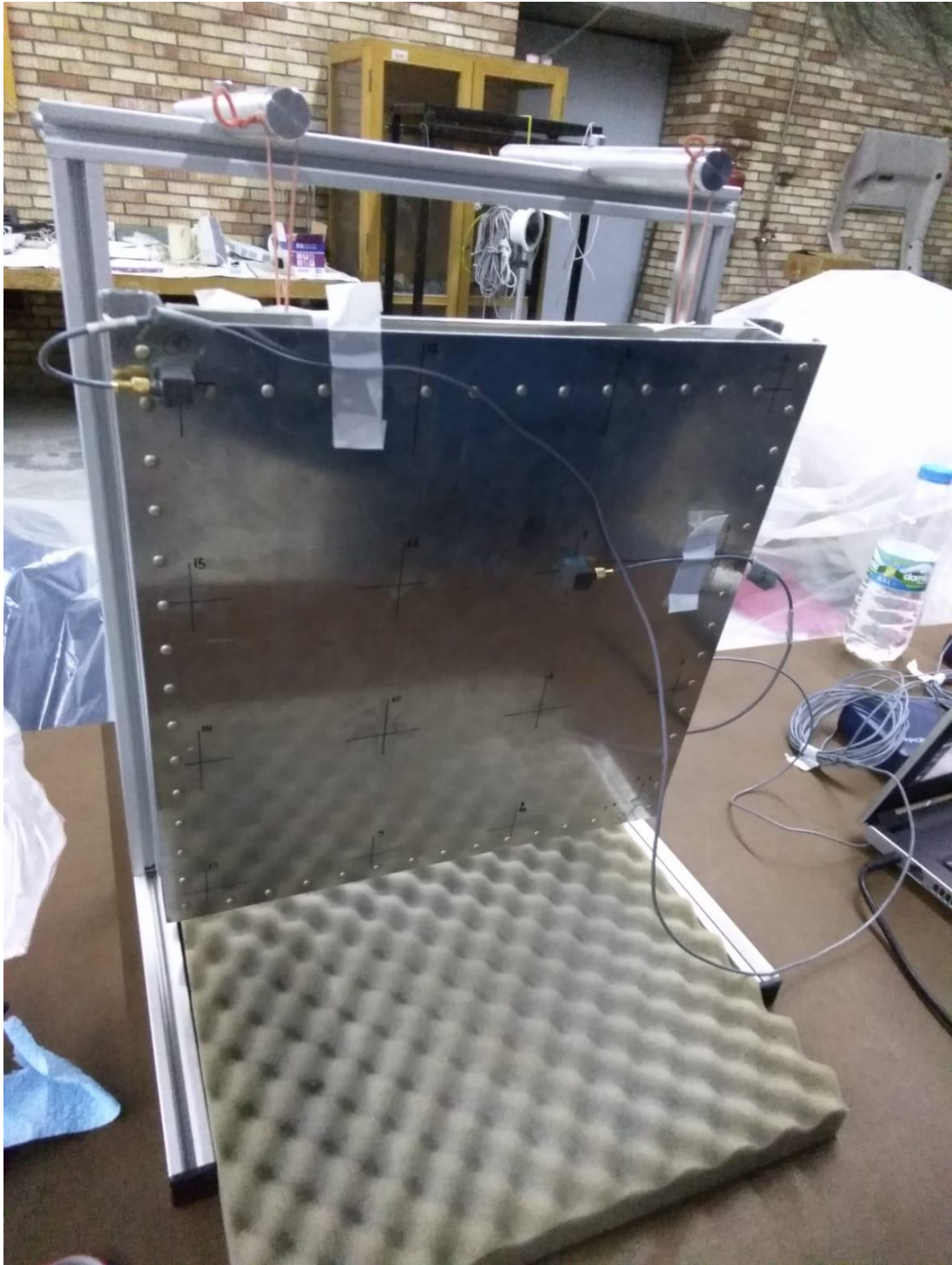


Figure 5.71. Experimental Setup for Fuselage Geometry

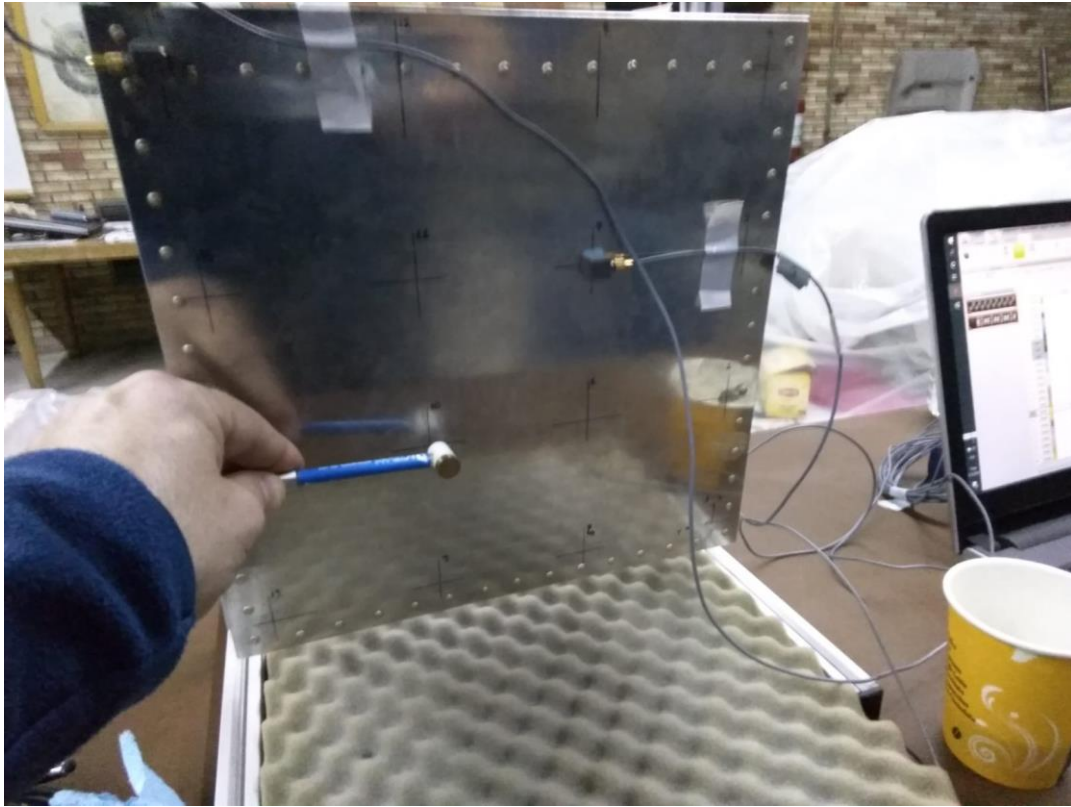


Figure 5.72. Bare Fuselage Experimental Setup

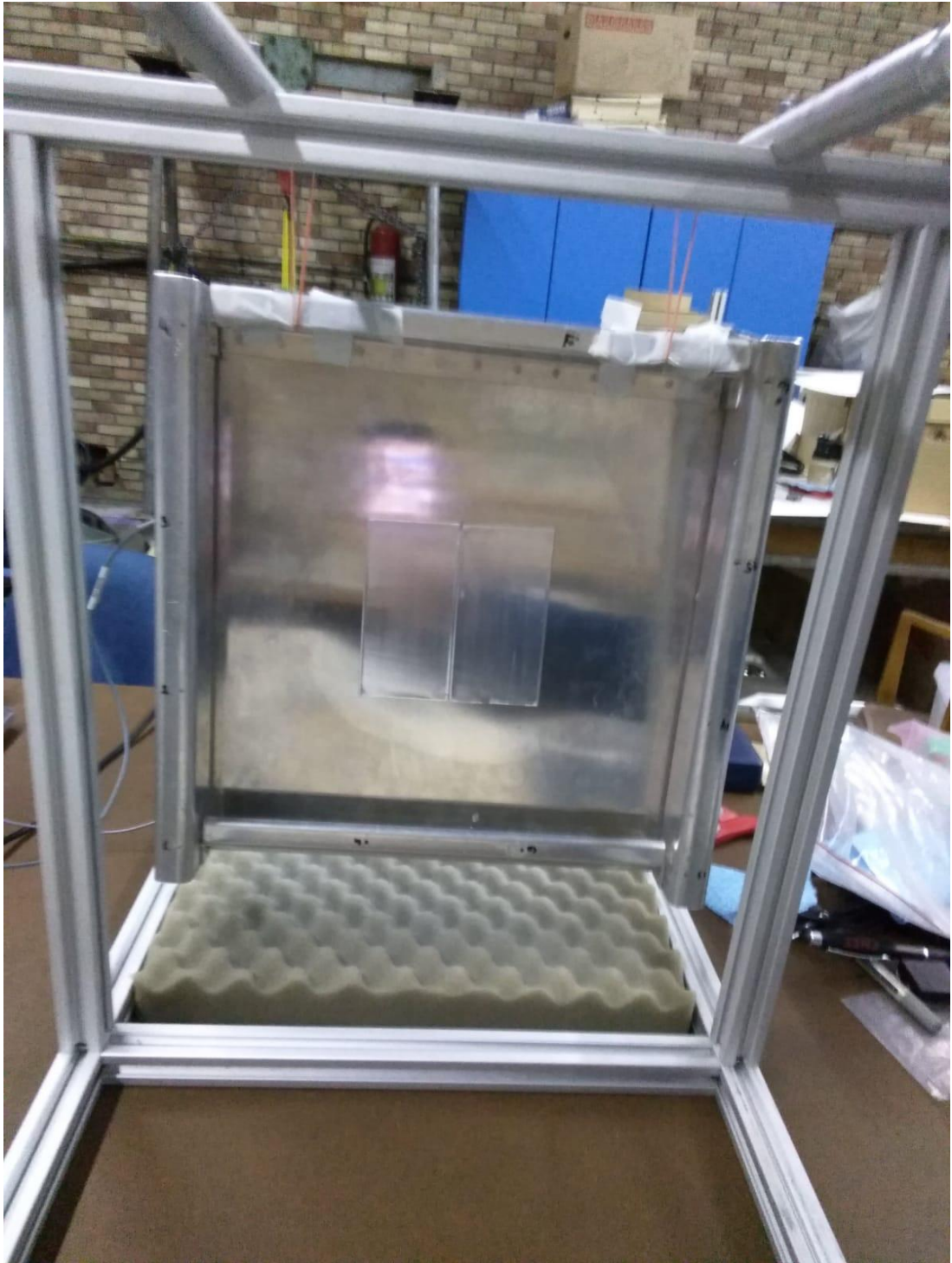


Figure 5.73. Multiple Constrained Layer Experimental Setup

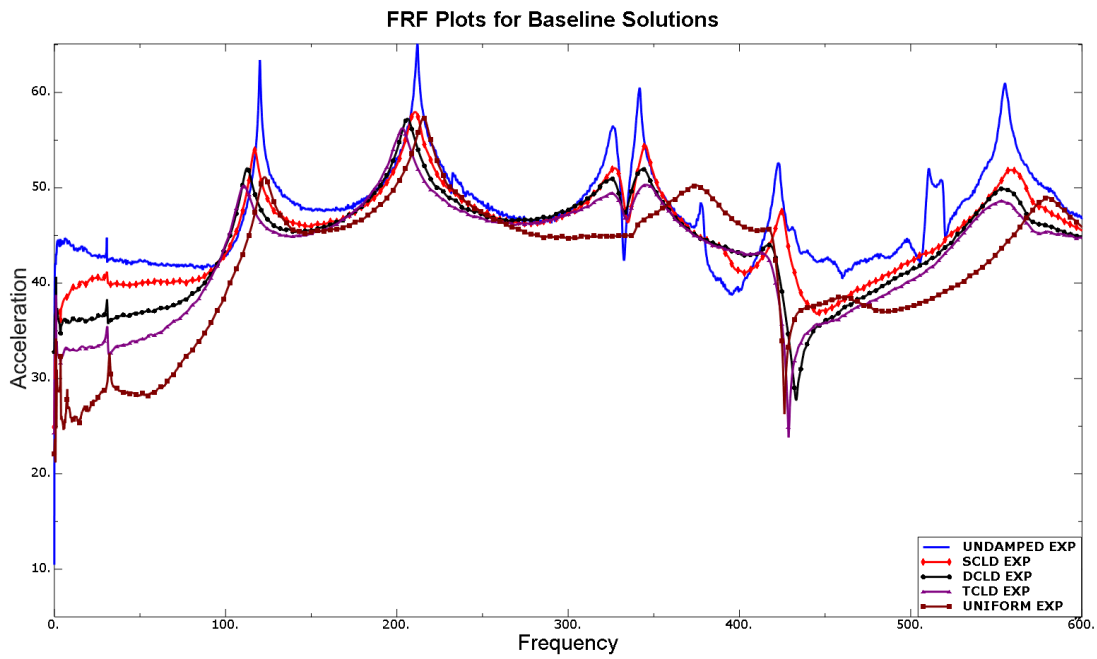


Figure 5.74. FRF Results for Experimental Results Point 7

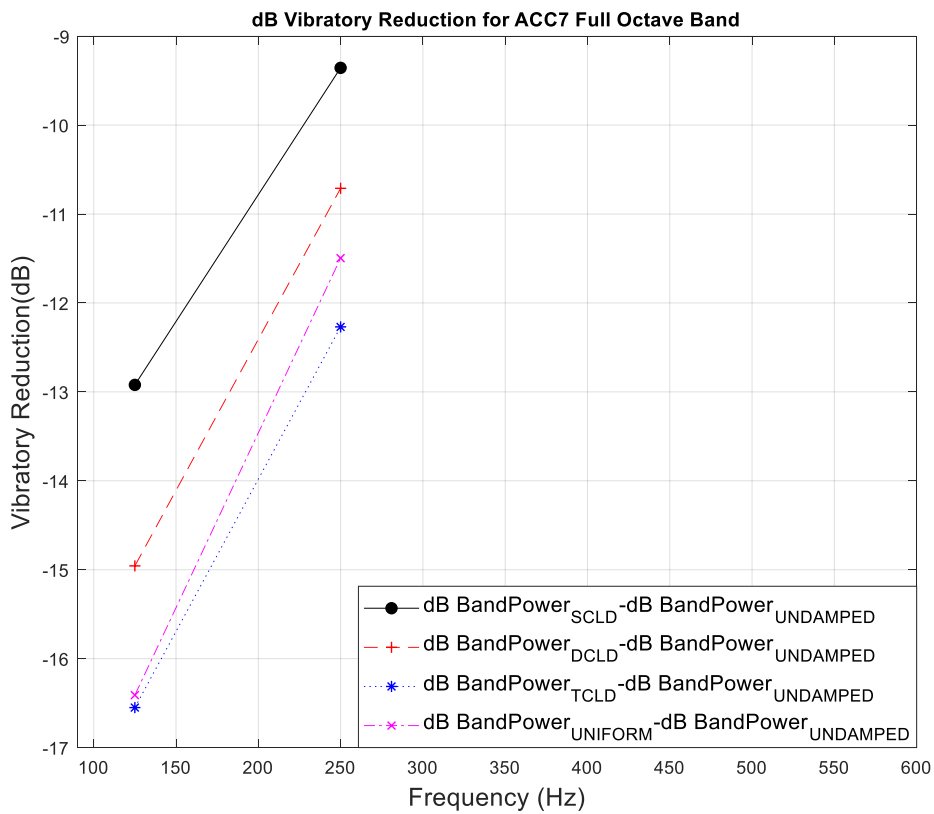


Figure 5.75. Full Octave Scale dB Band Power Reduction Results

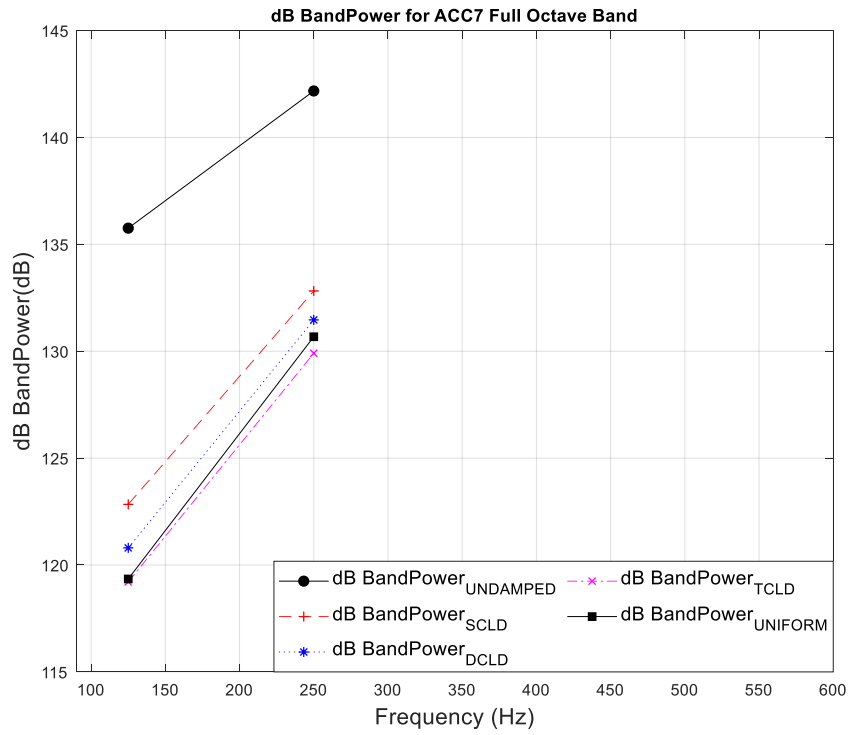


Figure 5.76. Full Octave Scale dB Band Power Results

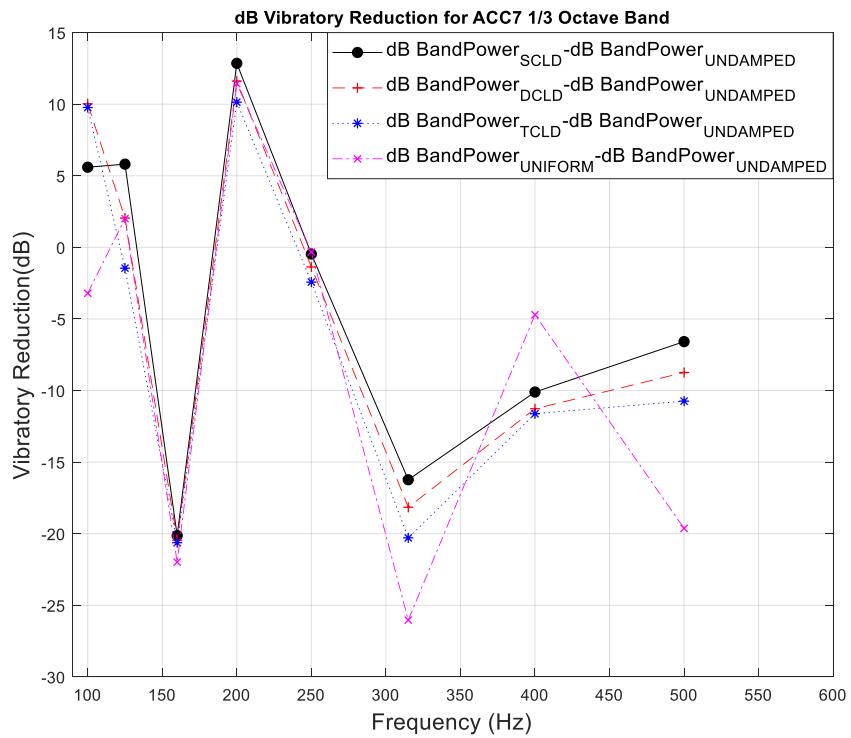


Figure 5.77. 1/3 Octave Scale dB Band Power Reduction Results

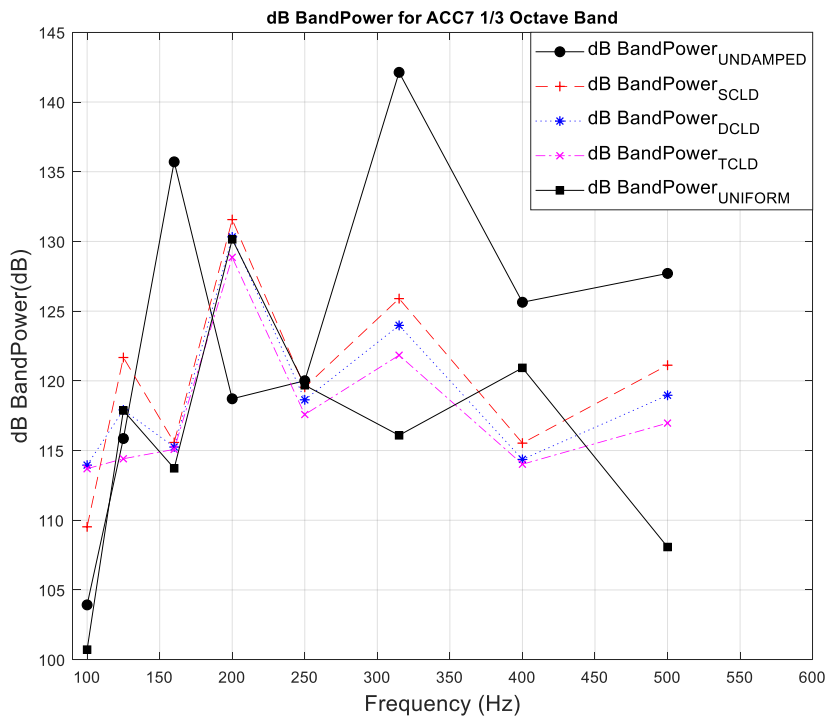


Figure 5.78. 1/3 Octave Scale dB Band Power Results

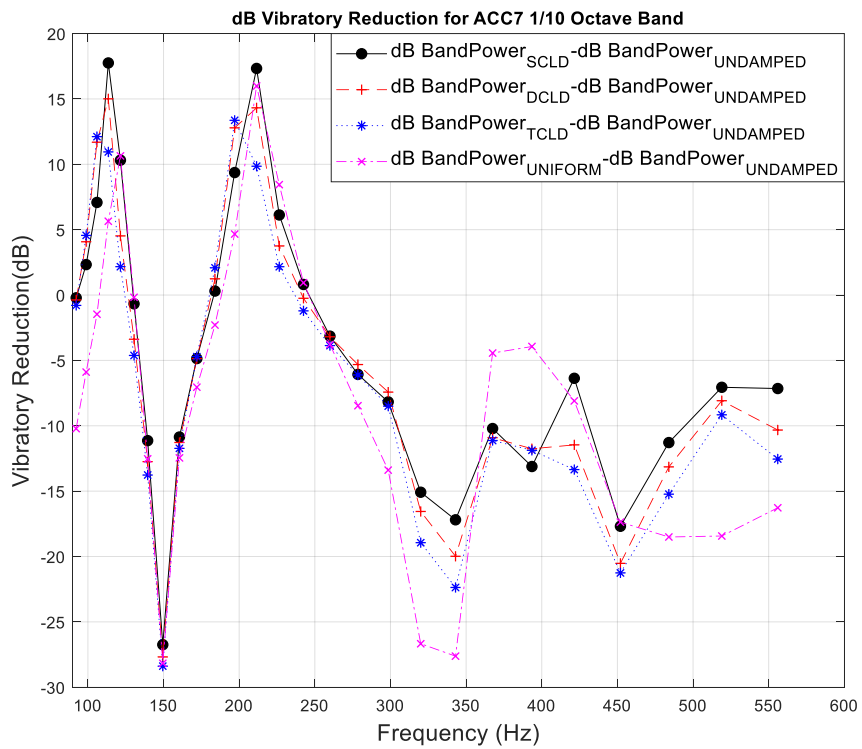


Figure 5.79. 1/10 Octave Scale dB Band Power Reduction Results

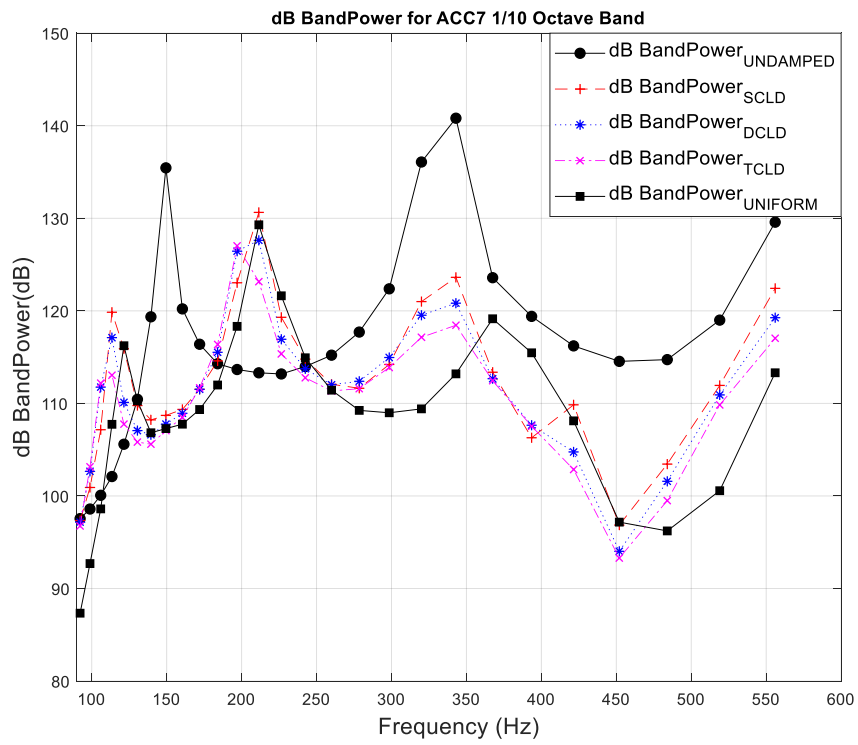


Figure 5.80. 1/10 Octave Scale dB Band Power Results

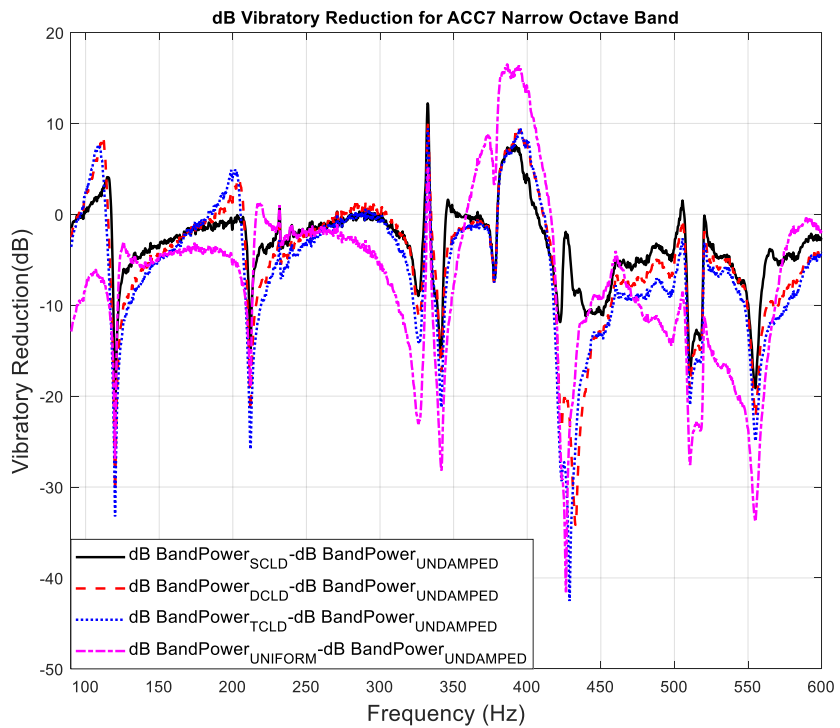


Figure 5.81. Narrow dB Band Power Reduction Results

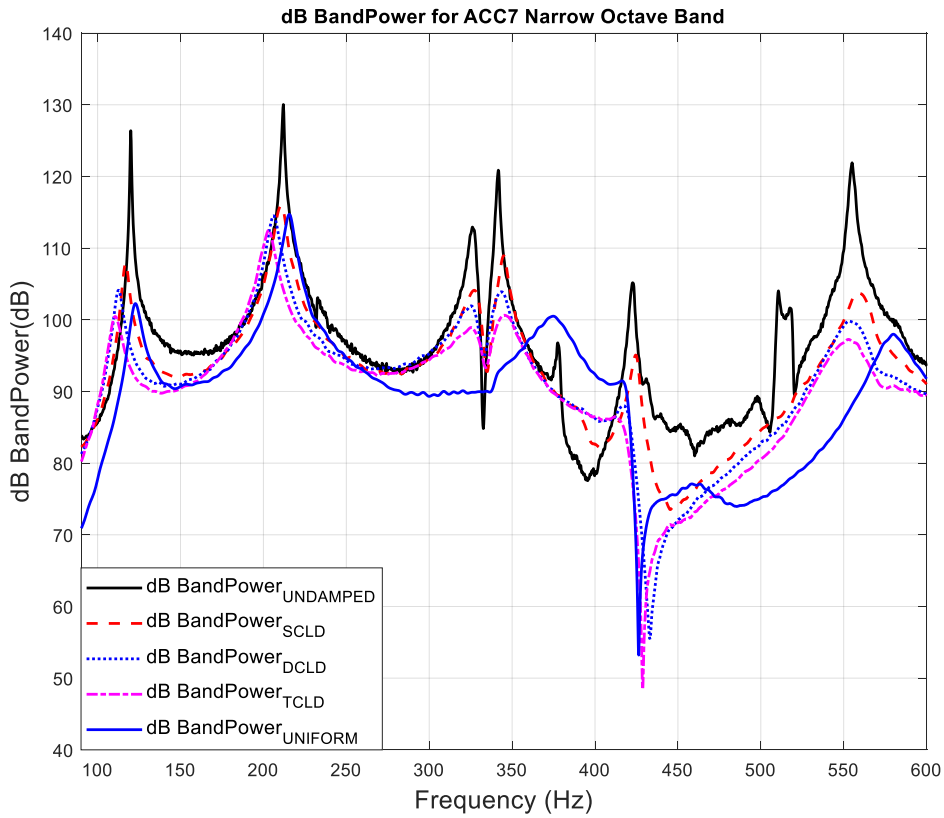


Figure 5.82. Narrow dB Band Power Results

Table 5.15. Calculated Experimental Damping Ratios

	Mode 1		Mode 2		Mode 3		Mode 4	
	F	Zeta	F	Zeta	F	Zeta	F	Zeta
Bare EXP	30.64	0.0058	120	0.0025	212.04	0.0027	326.05	0.0069
SCLD EXP	30.762	-	116.94	0.0165	210.69	0.0155	327.15	0.0164
DCLD EXP	30.762	0.0262	112.55	0.0226	206.06	0.0158	325.44	0.0209
TCLD EXP	31.006	0.0323	110.6	0.0324	203.13	0.0183	325.2	0.0328
UNIFORM EXP	32.227	0.0174	122.8	0.0259	215.58	0.0139	-	-
	Mode 5		Mode 6		Mode 7		Mode 8	
	F	Zeta	F	Zeta	F	Zeta	F	Zeta
Bare EXP	341.8	0.0025	377.44	0.0039	422.61	0.0034	510.62	0.0026
SCLD EXP	344.97	0.0077	-	-	424.56	0.006	-	-
DCLD EXP	343.51	0.0151	-	-	417.24	-	-	-
TCLD EXP	345.22	0.0213	-	-	412.11	-	-	-

UNIFORM EXP	-	-	374.76	0.0311	-	-	458.5	0.0526
	Mode 9		Mode 10		Mode 11		Mode 12	
	F	Zeta	F	Zeta	F	Zeta	F	Zeta
Bare EXP	517.46	-	555.05	0.0027				
SCLD EXP	-	-	558.35	0.0136				
DCLD EXP	-	-	553.22	0.0185				
TCLD EXP	-	-	552.98	0.0216				
UNIFORM EXP	-	-	579.83	0.0172				

From the above given results, one can see that the frequency response functions are not reliable until 82 Hz. Due to this reason the band power reduction calculations are performed after 82 Hz. Also there exist an unexpected behavior for uniform spacer layer configuration, where; the expected results were to be higher damping performance when compared with TCLD configuration; however, the damping performance results show that the TCLD has a better damping performance against uniform spacer configuration.

#### **5.4.1. Comparison of the Experimental and Simulation Results of the Designed Surface Damping Treatments**

This chapter is dedicated for comparison of the frequency response functions of the simulation results and the experimental results. The graphs show that, the trend of the system is well simulated but there exist frequency shifts among the solutions. Although, the modal frequencies of the simulation and experimental results shift, the trend of modal shifts between configurations are in accordance with each other. In addition, although the experimental result of the uniform spacer configuration is unexpected, the simulation of the uniform configuration is as expected and given in graphs below.

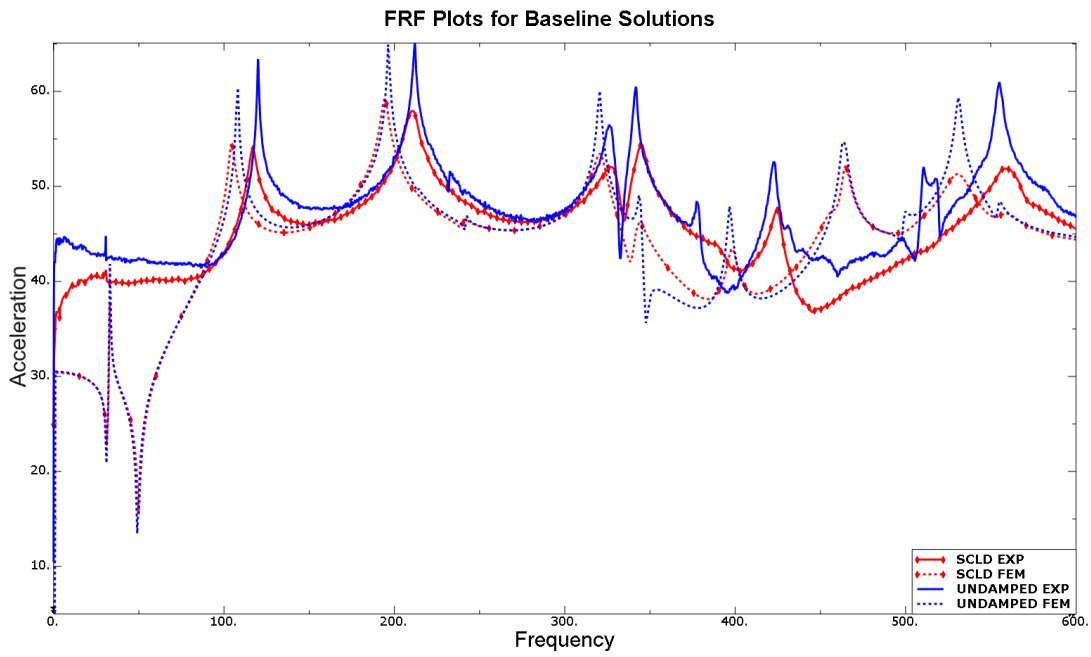


Figure 5.83. FRF Results Comparison for Experimental vs Simulation Results Point 7

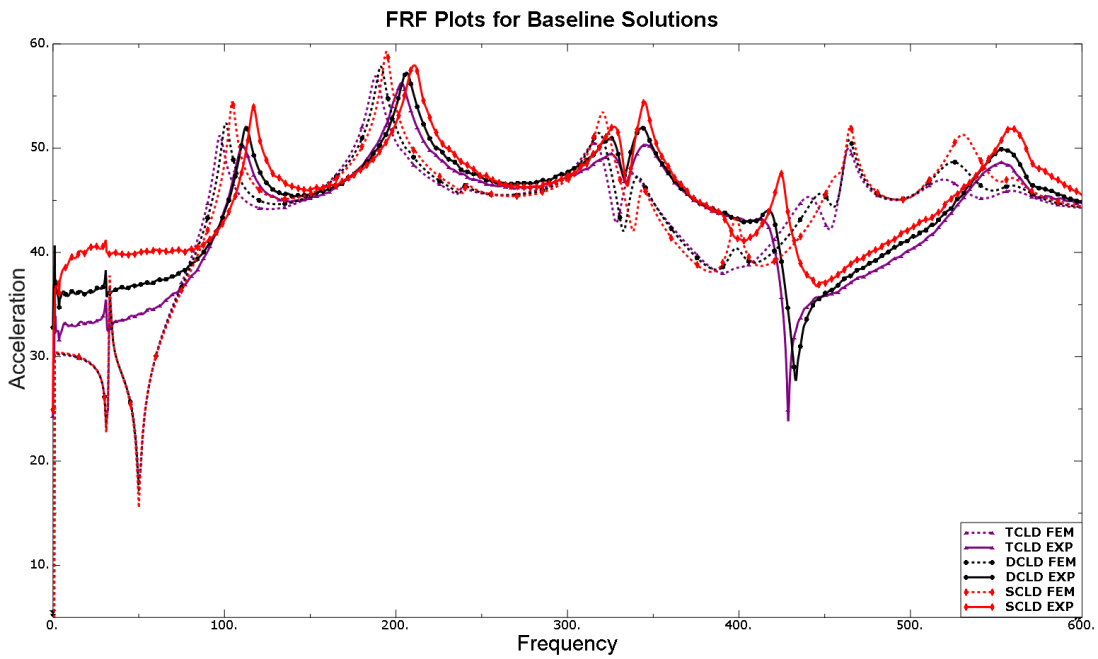


Figure 5.84. FRF Results Comparison for Multilayer CLDs Experimental vs Simulation Results Point

7

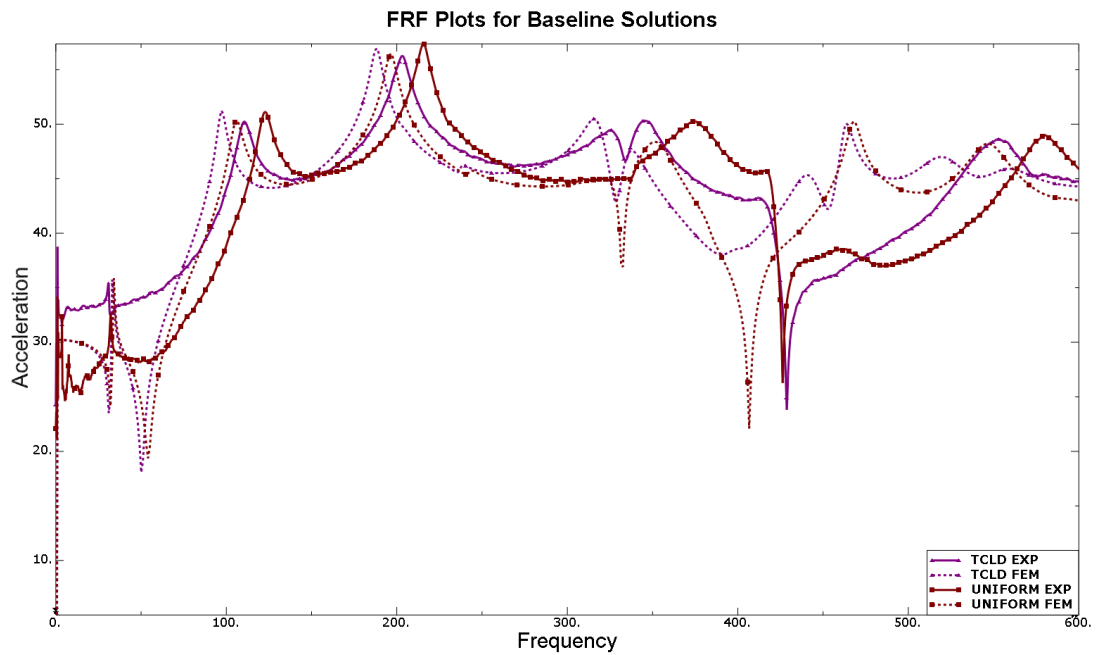


Figure 5.85. FRF Results Comparison of TCLD vs Uniform Spacer Experimental vs Simulation Results Point 7

The total band power reduction values calculated for experimental and simulation results are given below and the trend between configurations are again in accordance with each other with increased reduction values due to FRF plot shifts on higher frequencies. Also the dB band power reduction values are calculated after 82 Hz due to bad coherence values until 82 Hz.

Table 5.16. dB Band Power Reductions on full Frequency Range

Configuration	Total dB Reduction 7	Configuration	Total dB Reduction 7
SCLD	-6.575166215	SCLD Experiment	-11.08952041
DCLD	-8.33764061	DCLD Experiment	-12.61576457
TCLD	-9.46482205	TCLD Experiment	-14.17572345
UNIFORM	-10.19380949	UNIFORM Experiment	-13.22843491



## CHAPTER 6

### CONCLUSION AND FUTURE WORK

#### 6.1. Conclusion

The concept of this thesis study was to adapt the knowledge of optimized standoff solutions for beams to plates. While doing that, the purpose was to simulate the performance of the damping treatment on a structure that can be used in aerospace solutions where the vibration induced fatigue problems are important. In order to simulate the damping performance in usage area, a fuselage like structure is developed and verified. In addition, additional weight is limited in aerospace structures, which makes this study much more important where performance per weight added was tried to be maximized. Throughout this study, the outcomes of Sun and Eyyüpoğlu [7-8], was used for plate optimized spacer geometry design. The split edge effect on VEM layer significantly increases the damping performance and due to slots the reduced weight can be added to peaks of slots for much more neutral axis shift that also increases the damping performance as given in chapter six.

The developed and suggested damping treatment solutions are manufactured using fast prototyping method by using 3D printer and the solutions are experimentally tested to verify the simulation results. The tests show that the simulations have the same trend as experiments but due to experimental errors and modelling simplifications, some difference in the estimated FRF plots and experimental results.

Furthermore, in order to estimate the damping performance of the designed damping treatments, new method for estimating the output energy by using PSD relations is suggested. This method can be used to see the effects where the broadband reduction in the vibration levels are critical such as acoustic noise reduction for passenger comfort in aircraft applications or even luxury car industry.

## 6.2. Future Work

As a future work, necessary experimental work must be performed with improved manufacturing capabilities and increased simulation methods to observe the validity and applicability of the possible solutions. In addition, different spacer materials along with different off the shelf damping solutions (viscoelastic material and constraining layer) can be tried with different temperatures for better frequency coverage and performance improvement.

Also from the results it is visible that the selected frequency range 0-600Hz is not suitable for damping optimization due to high contribution of modes and measurement through mean square estimation gives faulty results due to peak shift with stiffness addition to system. Furthermore, the real life fuselage geometries will be fixed from frames in contrary to our fuselage case which is free-free condition for ease of experimentation, the wide frequency spectrum analysis such as 0-5000 Hz shall be performed for selected designs shall be investigated in order to simulate dB reduction estimation with fixed BCs from frames in order to shift modes apart from each other. This method will also be beneficial since the sinusoidal inputs on fuselage will mostly covered until 500 Hz but the acoustic noise problems due to random excitation will continue until 4000 Hz and clearly audible inside of the fuselage where passengers are seated. The wide spectrum analysis will also show the acoustic noise dampening performance of the design which will affect the passenger comfort, that is very important thing in commercial and VIP aerospace application and on premium automotive industry.

## REFERENCES

1. DIG Jones, Handbook of viscoelastic vibration damping, Wiley (2001).
2. J.M. Yellin, I.Y. Shen, Analytical model for a passive stand-off layer damping treatment applied to an Euler-Bernoulli beam, Proceedings of SPIE 3327, Smart Structures and Materials (1998), 349-357.
3. J.M. Yellin, I.Y. Shen, P.G. Reinhall, P.Y.H. Huang, Experimental investigation of a passive stand-off layer damping treatment applied to an Euler-Bernoulli beam, Proceedings of SPIE 3672, Smart Structures and Materials (1999), 228-233.
4. J.M. Yellin, I.Y. Shen, P.G. Reinhall, P.Y.H. Huang, An analytical and experimental analysis for a one-dimensional passive stand-off layer damping treatment, ASME Journal of Vibration and Acoustics 122 (2000), 440-447.
5. J.M. Yellin, I.Y. Shen, P.G. Reinhall, Analytical model for a one-dimensional slotted stand-off layer damping treatment, Proceedings of SPIE 3989, Smart Structures and Materials (2000), 132-141.
6. J.M. Yellin, I.Y. Shen, P.G. Reinhall, Experimental and finite element analysis of stand-off layer damping treatments for beams, Proceedings of SPIE 5760, Smart Structures and Materials (2005), 89-99.
7. E. Sun, Design and analysis of radar antenna structure with optimum dynamic behavior, Thesis (M.S.) -- Middle East Technical University, Ankara (2016).
8. K.O. Eyyüpoğlu, Development of a novel surface damping treatment, Thesis (M.S.) -- Middle East Technical University, Ankara (2016).
9. ABAQUS Analysis User's Manual (6.14), 2014
10. B.C. Nakra, Vibration control in machines and structures using viscoelastic damping, Journal of Sound Vibration 211 (1998), 449-465.
11. M.D. Rao, Recent applications of viscoelastic damping for noise control in automobiles and commercial airplanes. Journal of Sound Vibration 262(3) (2003), 457-474.

12. G. Lepoittevin and G. Kress, Optimization of segmented constrained layer damping with mathematical programming using strain energy analysis and modal data, *Journal of Materials and Design* 31 (2010), 14–24.
13. E.M. Kerwin, Damping of flexural waves by a constrained viscoelastic layer, *Journal of the Acoustical Society of America* 32 (1959), 952–962.
14. J.S. Whittier, The effect of configurational additions using interfaces on the damping of a cantilever beam, Wright Air Development Center WADC Technical Report (1959), 58-568.
15. R.A. DiTaranto, Theory of vibratory bending for elastic and viscoelastic layered finite-length beams, *ASME Journal of Applied Mechanics* 32 (1965), 881–886.
16. D.J. Mead and S. Markus, The forced vibration of a three-layer, damped sandwich beam with arbitrary boundary conditions, *Journal of Sound Vibration* 10 (1969), 163–75.
17. D.F. Golla and P.C. Hughes, Dynamics of Viscoelastic Structures-A time-domain finite element formulation, *ASME Journal of Applied Mechanics* 52 (1985), 897–906.
18. M.D. Rao and S. He, Dynamic analysis and design of laminated composite beams with multiple damping layers, *AIAA Journal* 31 (1993), 736–745.
19. M.A. Trindade, A. Benjeddou and R. Ohayon, Modelling of frequency-dependent viscoelastic materials for active-passive vibration damping, *ASME Journal of Vibration and Acoustics* 122 (2000), 169–174.
20. S.A. Hambric, A.W. Jarret, G.F. Lee and J.J Fedderly, Inferring viscoelastic dynamic material properties from finite element and experimental studies of beams with constrained layer damping, *ASME Journal of Vibration and Acoustics* 129 (2007), 158–168.
21. I.Y. Shen, Hybrid damping through intelligent constrained layer treatments, *ASME Journal of Vibration and Acoustics* 116 (1994), 341–349.
22. A. Baz, Robust control of active constrained layer damping, *Journal of Sound Vibration* 211 (1998), 467–480.

23. M.A. Trindade, Optimization of active-passive damping treatments using piezoelectric and viscoelastic materials, *Journal of Smart Materials and Structures* 16 (2007), 2159-2168.
24. M.R. Garrison, R.N. Miles, J.Q. Sun and W. Bao, Random response of a plate partially covered by a constrained layer damper, *Journal of Sound Vibration* 172(2) (1994), 231-245.
25. R.S. Masti and M.G. Sainsbury, Vibration damping of a cylindrical shells partially coated with a constrained viscoelastic treatment having a standoff layer, *Journal of Thin-Walled Structures* 43 (2005), 1355-1379.
26. Y.C. Chen and S.C. Huang, An optimal placement of CLD treatment for vibration suppression of plates, *International Journal of Mechanical Science* 44 (2002), 1801–1821.
27. S.Y. Kim, C.K. Mechefske and I.Y. Kim, Optimal damping layout in a shell structure using topology optimization, *Journal of Sound and Vibration* 332 (2013), 2873-2883.
28. Z. Kang, X. Zhang, S. Jiang and G. Cheng, On topology optimization of damping layer in shell structures under harmonic excitations, *Journal of Structural and Multidisciplinary Optimization* 46 (2012), 51-67.
29. W. Zheng, Y. Lei, S. Li and Q. Huang, Topology optimization of passive constrained layer damping with partial coverage on plate, *Journal of Shock and Vibration* 20 (2013), 199-211.
30. K. Svanberg, The method of moving asymptotes-a new method for structural optimization, *International Journal for Numerical Methods in Engineering* 24 (1987), 359–373.
31. C.M.A. Vasques, R.A.S. Moreira and J.D. Rodrigues, Viscoelastic Damping Technologies–Part I: Modeling and Finite Element Implementation, *Journal of Advanced Research in Mechanical Engineering* (2) (2010), 76-95.
32. C.M.A. Vasques, R.A.S. Moreira and J.D. Rodrigues, Viscoelastic Damping Technologies–Part II: Experimental Identification Procedure and, *Journal of Advanced Research in Mechanical Engineering* (2) (2010), 96-110.

33. Y. Xiong and O.K. Bedair, Analytical and Finite Element Modeling of Riveted Lap Joints in Aircraft Structure, *AIAA Journal* 37 (1999), 93–99.
34. Ç. Karaoğlu and N.S. Kuralay, Stress analysis of a truck chassis with riveted joints, *Journal of Finite Elements in Analysis and Design* 38 (2002) 1115–1130.
35. J. Mackerle, Finite element analysis of fastening and joining: A bibliography (1990–2002), *International Journal of Pressure Vessels and Piping* 80 (2003) 253–271.
36. A. Atre, A finite element and experimental investigation on the fatigue of riveted lap joints in aircraft, Thesis (Ph.D.) -- Georgia Institute of Technology, (2006).
37. John D. Ferry, *Viscoelastic Properties of Polymers*, Wiley, London, 1980
38. MDM 525 Vibration Control and Isolation Asst.Prof. Gökhan O. ÖZGEN  
Lecture Notes
39. Mead, D. J., 1999, *Passive Vibration Control*, Wiley, London.
40. J. Soovere, M.L. Drake, “Aerospace Structures Technology Damping Design Guide Volume III – Damping Material Data”, AFWAL-TR-84-3089, Vol. III, 1985
41. DIN LN 9415:1996-05, *Aerospace – Wrought aluminum alloy folded profiles, Z-section with one lipped flange – Dimensions, masses, static values*
42. DIN LN 9414:1996-05, *Aerospace – Wrought aluminum alloy folded profiles, channel section with internally lipped flanges – Dimensions, masses, static values*
43. DIN LN 9411:1996-05, *Aerospace – Wrought aluminum alloy folded profiles, angle – Dimensions, masses, static values*
44. CATIA v5-R22 (n.d.), Dassault Systèmes
45. R. D. Blevins, *Formulas for Natural Frequency and Mode Shape*, Krieger (2001)
46. G. B. Warburton, CHAPTER 5 - Vibrations of Plates and Shells, In *Structures and Solid Body Mechanics Series, The Dynamical Behavior of Structures*

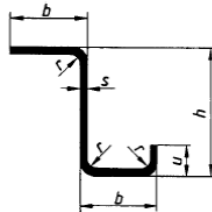
(Second Edition), Pergamon,1976, Pages 220-282

47. MIL-STD-810G Military Specification, *Environmental Engineering Considerations and Laboratory Tests*, Department of Defense Test Method Standard, January 2000
48. ME520 Analysis and Measurement Procedures for Random Vibrations and Noise Prof. Mehmet ÇALIŞKAN Lecture Notes
49. T.Yamaguchi, Y. Kurosawa and H. Enomoto, Damped vibration analysis using finite element method with approximated modal damping for automotive double walls with a porous material, *Journal of Sound and Vibration* 325 (2009), 436-450.
50. A. D. Nashif, D. I. G. Jones, J. P. Henderson, *Vibration Damping*, Wiley (1985)
51. G. Agnes, M. Ahmadian, A. K. W. A. Ahmed, *Encyclopedia of Vibration*, Elsevier (2001)



## APPENDICES

### A. DIN-LN-9415 [41]



Maße in Millimeter  
(Dimensions in millimetres)

**Bild 1**  
(Figure 1)

#### 3.1 Normbezeichnung

#### 3.1 Standard designation

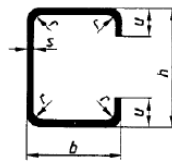
Z-Profil LN 9415 – 3.1364T3 – 30 15 10  
(Z section LN 9415 – 3.1364T3 – 30 15 10)

Benennung (Description)	_____	_____	_____	_____	_____	_____
Norm-Nummer (Standard number)	_____	_____	_____	_____	_____	_____
Werkstoff-Kennzahl (Material code)	_____	_____	_____	_____	_____	_____
Genauigkeitsgrad B: "-" oder K: "K" (Grade of accuracy B: "-" or K: "K")	_____	_____	_____	_____	_____	_____
Höhe $h$ in mm (Height $h$ in mm)	_____	_____	_____	_____	_____	_____
Breite $b$ in mm (Width $b$ in mm)	_____	_____	_____	_____	_____	_____
Dicke $s$ in $\frac{1}{10}$ mm (Thickness $s$ in $\frac{1}{10}$ mm)	_____	_____	_____	_____	_____	_____

Frühere Bezeichnung: Z-Profil 30 × 15 × 1 LN 9415 – 3.1364.5  
(Former designation: Z section 30 × 15 × 1 LN 9415 – 3.1364.5)



## B. DIN-LN-9414 [42]



Maße in Millimeter  
(Dimensions in millimetres)

Bild 1  
(Figure 1)

### 3.1 Normbezeichnung<sup>1)</sup>

### 3.1 Standard designation<sup>1)</sup>

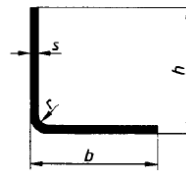
U-Profil LN 9414 – 3.1364T3 – 30 20 12  
(Channel LN 9414 – 3.1364T3 – 30 20 12)

Benennung (Description)	_____	_____	_____	_____	_____
Norm-Nummer (Standard number)	_____	_____	_____	_____	_____
Werkstoff-Kennzahl (Material code)	_____	_____	_____	_____	_____
Genauigkeitsgrad B: "–" oder K: "K" (Grade of accuracy B: "–" or K: "K")	_____	_____	_____	_____	_____
Höhe $h$ in mm (Height $h$ in mm)	_____	_____	_____	_____	_____
Breite $b$ in mm (Width $b$ in mm)	_____	_____	_____	_____	_____
Dicke $s$ in $1/10$ mm (Thickness $s$ in $1/10$ mm)	_____	_____	_____	_____	_____

Frühere Bezeichnung: U 30 × 20 × 1,2 LN 9414 – 3.1364.5  
(Former designation: Channel 30 × 20 × 1,2 LN 9414 – 3.1364.5)



## C. DIN-LN-9411 [43]



Maße in Millimeter  
(Dimensions in millimetres)

Bild 1  
(Figure 1)

### 3.1 Normbezeichnung

### 3.1 Standard designation

L-Profil LN 9411 – 3.1364T3 – 20 15 10  
(Angle LN 9411 – 3.1364T3 – 20 15 10)

Benennung (Description)	_____	_____	_____	_____	_____	_____
Norm-Nummer (Standard number)	_____	_____	_____	_____	_____	_____
Werkstoff-Kennzahl (Material code)	_____	_____	_____	_____	_____	_____
Genauigkeitsgrad B: "-" oder K: "K" (Grade of accuracy B: "-" or K: "K")	_____	_____	_____	_____	_____	_____
Höhe $h$ in mm (Height $h$ in mm)	_____	_____	_____	_____	_____	_____
Breite $b$ in mm (Width $b$ in mm)	_____	_____	_____	_____	_____	_____
Dicke $s$ in $1/10$ mm (Thickness $s$ in $1/10$ mm)	_____	_____	_____	_____	_____	_____

Frühere Bezeichnung: L 20 × 15 × 1 LN 9411 – 3.1364.5  
(Previous designation: L 20 × 15 × 1 LN 9411 – 3.1364.5)